UNIVERSIDAD COMPLUTENSE DE MADRID

FACULTAD DE CIENCIAS QUÍMICAS
DEPARTAMENTO DE QUÍMICA ORGÁNICA

TESIS DOCTORAL

Síntesis, estructura y propiedades electrónicas de nuevos sistemas push-pull basados en complejos de metales de transición

MEMORIA PARA OPTAR AL GRADO DE DOCTOR

PRESENTADA POR

Gong Ming Chu Zhu

DIRECTORES

Miguel Ángel Sierra Rodríguez
Israel Fernández López

Madrid, 2017

UNIVERSIDAD COMPLUTENSE DE MADRID

FACULTAD DE CIENCIAS QUÍMICAS

DEPARTAMENTO DE QUÍMICA ORGÁNICA

Síntesis, Estructura y Propiedades Electrónicas de Nuevos Sistemas Push-Pull Basados en Complejos de Metales de Transición

MEMORIA que para optar al grado de

DOCTOR EN CIENCIAS QUÍMICAS

presenta

GONG MING CHU ZHU

朱共鸣

Madrid, 2016

Miguel Ángel Sierra Rodríguez, Catedrático de Química Orgánica de la Facultad de Ciencias Químicas de la Universidad Complutense de Madrid e **Israel Fernández López**, Profesor contratado Doctor en el Departamento de Química Orgánica de la Facultad de Ciencias Químicas de la Universidad Complutense de Madrid,

CERTIFICAN:

Que la presente Memoria, titulada: **SÍNTESIS, ESTRUCTURA Y PROPIEDADES ELECTRÓNICAS DE NUEVOS SISTEMAS *PUSH-PULL* BASADOS EN COMPLEJOS DE METALES DE TRANSICIÓN**, se ha realizado bajo su dirección en el Departamento de Química Orgánica I de la Facultad de Ciencias Químicas de la Universidad Complutense de Madrid por el Licenciado en Química **Gong Ming Chu Zhu**, y autorizan su presentación para ser calificada como Tesis Doctoral.

Madrid, 3-Diciembre-2015

Fdo. Miguel A. Sierra Fdo. Israel Fernández

El trabajo recogido en esta Memoria ha sido financiado por los proyectos del Ministerio de Ciencia e Innovación (CTQ2010-20714-C0-01-BQU), Ministerio de Economía y Competitividad (CTQ2013-46459-C2-1-P), MEC-Consolider-Ingenio (2010-CSD2007-00006) y la Comunidad Autónoma de Madrid (CAM-S2009/PPQ-1634). Asimismo, Gong Ming Chu Zhu agradece al Ministerio de Ciencia e Innovación por la Beca de Formación de Personal Investigador (FPI) concedida (Ref: BES-2011-047607).

A mi familia

A Alicia

“La travesía de mil millas empieza con un paso”

Lao-Zi

“Quien cede el paso ensancha el camino”

Proverbio chino

“Poca gente es capaz de prever hacia dónde les lleva el camino hasta que llegan a su fin”

J. R. R. Tolkien

A lo largo de todos estos años mi camino ha sido una espiral de locura que ha derivado en ramificaciones infinitas, recodos desesperantes, pendientes empinadas, cambios de sentido y hasta caminos sin salida. Sin embargo, aunque agotado sigo avanzando, sigo luchando y sigo aprendiendo. Este afán de crecer y mejorar, no sólo como químico sino como persona, no hubiera sido posible sin la preciada ayuda de todas aquellas personas a las que he tenido el placer de conocer.

En primer lugar, quisiera agradecer a mis dos guías en esta enrevesada senda de los que he tenido el gusto de aprender. A mi director de tesis, el profesor Miguel A. Sierra, por haber confiado desde el principio en mí y por haberme llevado tan lejos cuando ni siquiera yo me veía capaz. Y a mi codirector de tesis, el profesor Israel Fernández, quien me ha enseñado no sólo a levantarme tras caer sino que además me ha inculcado la sabia costumbre de preguntarme: ¿Por qué caigo? Y ¿por qué debería volver a levantarme?

En segundo lugar, me gustaría agradecer a los profesores Gómez, de la Torre y Casarrubios por su interés en mi formación como investigador y a las discusiones productivas que hemos mantenido. Al doctor Guerrero por su colaboración en este trabajo. A Lola, Elena y Ángel del CAI de RMN por sus horas extras. Y al profesor Santiago Romano por su perenne buen humor.

I would like to thank Prof. Miguel García-Garibay at the University of California Los Angeles and all members of his research group for the opportunity to introduce me to the exciting chemistry of molecular rotors. I also want to express my gratitude in particular to Dr. Salvador, Tim and Geeta for their kindness during my short stay in the US.

También deseo expresar mi más sincero agradecimiento a todos esos caminantes con los que he compartido este maravilloso periplo. A Martiña y a Bea que me enseñaron a trabajar en el laboratorio. A toda la gente que ha ido dejando huella en el laboratorio, a Mamen, César, Nina, Pacheco, Alberto, Marta y Daiann. Y así, como yo he aprendido de los pasos de otros espero que los que vinieron después hayan aprendido de los míos, a Elena, Alba, Pablo, Yago, Marta e Irene. Sobre todo a Frutos y a los ya doctores Jaime y Carolina con los que he compartido sueños, ilusiones, dudas y, por supuesto, muchas risas. Por último, no me quiero olvidar de aquella persona con la que he compartido esta aventura y de la cual hemos aprendido y disfrutado enormemente, desde que aprendimos a gatear hasta que, por fin, desplegamos las alas para emprender un nuevo viaje, ¡muchas gracias, Sandra!

Todo buen camino que se precie ha de tener una posada donde descansar, quitarse el polvo del viaje y tomarse una buena jarra de cerveza en buena compañía. A Jaime, Alberto, Sara, Mario, Sergio, Ainhoa, María Jesús y Antonio por esos innumerables momentos que hemos compartido desde que nos conocimos en la carrera de químicas. A Diego por su inestimable amistad. A mis amigos del Fénix y a mis compañeros de wushu por su apoyo incondicional.

Como he dicho anteriormente mi camino ha tomado muchas formas, pero nunca hubiera imaginado que se uniera al de otra persona. No me refiero a que ambos caminos se cruzaran momentáneamente, ni que los dos caminos fueran paralelamente a un mismo destino, ni que un camino devorase sin dejar el menor rastro a otro, sino que fueran uno al lado del otro, se entrelazaran y se unieran para formar otro camino mucho más amplio, mucho más bonito y mucho más valioso. A Alicia por permitirme caminar a su lado.

Por último, quisiera dar las gracias a mi familia por su ánimo y preocupación por mí. En especial a mis hermanos por su apoyo y comprensión y por auparme siempre para que otee más allá del horizonte. A mis padres que sin su constante esfuerzo, sacrificio y valor durante tantos años, yo no habría llegado tan lejos. 最后，我想感谢我的家人对我的关心和鼓励。尤其是我的兄弟姐妹们，他们的理解和支持，总是让我看得更远，走得更远。而我的父母，没有你们这么多年的不断付出和努力，我是不会成功的！谢谢你们！

Los resultados aquí presentados se encuentran recogidos en las siguientes publicaciones:

Control over the E/Z Selectivity of the Catalytic Dimerization of Group 6 (Fischer) Metal Carbene Complexes.

Gong M. Chu, Israel Fernández, Miguel A. Sierra. *J. Org. Chem.* **2013**, *78*, 865-871.

Synthesis, Structure, and Electronic Properties of Extended π-Conjugated Group 6 Fischer Alkoxy-Bis(carbene) Complexes.

Gong M. Chu, Israel Fernández, Miguel A. Sierra. *Chem. Eur. J.* **2013**, *19*, 5899-5908.

Tuning the Photophysical Properties of BODIPY Molecules by π-Conjugation with Fischer Carbene Complexes.

Gong M. Chu, Andrés Guerrero-Martínez, Israel Fernández, Miguel A. Sierra. *Chem. Eur. J.* **2014**, *20*, 1367-1375.

Remote Control by π-Conjugation of the Emissive Properties of Novel Fischer Carbene-BODIPY Dyads.

Gong M. Chu, Andrés Guerrero-Martínez, Carmen Ramírez de Arellano, Israel Fernández, Miguel A. Sierra. *Enviado*.

Fluorescence Quenching in BODIPYs Having Ir- and Rh- Tethered Complexes.

Gong M. Chu, Israel Fernández, Andrés Guerrero-Martínez, Carmen Ramírez de Arellano, Miguel A. Sierra. *Eur. J. Inorg. Chem.,* doi: 10.1002/ejic.201501283. *En prensa*.

La presente memoria de la Tesis Doctoral se ha escrito siguiendo el formato de publicaciones. Incluye una introducción general detallada sobre el estado actual del área de investigación en la que se enmarca este trabajo y una discusión integradora de los resultados obtenidos. Los capítulos principales se han dividido según las distintas publicaciones, incluyendo un artículo enviado para su publicación en el momento de la redacción de la memoria. Los capítulos publicados conservan su formato original en inglés. Sin embargo, la introducción, discusión, objetivos y conclusiones se han escrito en castellano de acuerdo a la normativa para este formato de tesis. Con el fin de respetar al máximo las diferentes publicaciones, se han mantenido la bibliografía y numeración originales de las mismas, aunque se ha modificado el formato a fin de homogeneizar todas las referencias contenidas en la presente tesis.

La memoria adjunta un CD en el que se han incluido todas las coordenadas cartesianas y energías totales de todos los puntos estacionarios mencionados en esta memoria, obtenidos mediante métodos computacionales. El CD incluye también una recopilación de espectros de resonancia magnética nuclear de todos los compuestos no descritos previamente sintetizados a lo largo de esta tesis, y un archivo .pdf con la memoria completa.

Abreviaturas utilizadas en esta Memoria:

A	Aceptor/*Acceptor*
Ac	*Acetyl*
ADN	Ácido Desoxirribonucleico
ATR	*Attenuated Total Reflectance*
BODIPY	*Boron Dipyrromethene*
calcd	*Calculated*
cod	*Cyclooctadienyl*
CT	*Charge Transfer*
CV	*Cyclic Voltammetry*
D	Dador/*Donor*
dba	*Dibenzylidenacetone*
DDQ	*2,3-Dichloro-5,6-Dicyano-1,4-Benzoquinone*
DFT	*Density Functional Theory*
DIPEA	*N,N-Diisopropylethylamine*
dppe	*1,2-Bis(diphenylphosphino)ethane*
DSSC	*Dye Sensitized Solar Cell*
E_{pa}	*Anodic Potential Energy*
ESI	*Electrospray Ionization*
f	*Oscillator Strength*
Fc	*Ferrocenyl*
FMO	*Frontier Molecular Orbital*
FRET	*Förster Resonance Energy Transfer*
HOMO	*Highest Occupied Molecular Orbital*
HRMS	*High Resolution Mass Spectroscopy*
IC	*Internal Conversion*
ICT	*Intramolecular Charge Transfer*
ISC	*Intersystem Crossing*
LF	*Ligand Field*
LP	*Lone Pair*
LUMO	*Lowest Unoccupied Molecular Orbital*

MLCT	*Metal to Ligand Charge Transfer*
MMLL'CT	*Mixed Metal Ligand to Ligand' Charge Transfer*
MOF	*Metal Organic Framework*
NBO	*Natural Bond Orbital*
NHC	*N-Heterocyclic Carbene*
NLO	*Non-Linear Optics*
o-DCB	*Ortho-Dichlorobenzene*
OFET	*Organic Field-Effect Transistor*
OLED	*Organic Light-Emitting Diode*
OPVC	*Organic Photovoltaic Cell*
ORTEP	*Oak Ridge Thermal Ellipsoid Plot*
PCM	*Polarisable Continuum Model*
PET	*Photoinduced Electron Transfer*
SEnT	*Singlet Energy Transfer*
SOPT	*Second Order Perturbation Theory*
TD-DFT	*Time Dependent-Density Functional Theory*
TEnT	*Triplet Energy Transfer*
THF	*Tetrahydrofurane*
TLC	*Thin Layer Chromatography*
TM	*Transition Metal*
TMSCl	*Trimethylsilyl Chloride*
WBI	*Wiberg Bond Indices*

Índice

I. INTRODUCCIÓN Y ANTECEDENTES

I.1. Aspectos generales de los sistemas *push-pull*

Los sistemas *push-pull* son sistemas orgánicos con conjugación π-extendida que contienen en su estructura un grupo electrodador (D) y un grupo electroaceptor (A) unidos entre sí por un espaciador π-conjugado (D-π-A). Estos sistemas se caracterizan por mostrar una transferencia de carga intramolecular (ICT) desde la unidad dadora a la unidad aceptora. Dicha polarización se produce a través del espaciador con la consiguiente separación de cargas y generación del correspondiente dipolo. La ICT se suele representar mediante las dos formas resonantes extremas mostradas en la Figura 1.[1]

Figura 1. Representación esquemática de un sistema *push-pull*.

Los compuestos orgánicos π-conjugados tienen interesantes propiedades electrónicas, optoelectrónicas,[2] conductoras[3] y fotovoltaicas.[4] Actualmente se están desarrollando dispositivos orgánicos análogos a los sistemas inorgánicos tradicionales, como transistores orgánicos de efecto campo (OFET),[5] diodos orgánicos de emisión de luz (OLED),[6] células orgánicas fotovoltaicas (OPVC)[7] y células solares sensibilizadas por colorante (DSSC).[8] La química orgánica ofrece una gama más amplia de compuestos que la química inorgánica debido a que los compuestos orgánicos π-conjugados son relativamente fáciles de sintetizar y poseen propiedades fácilmente modulables.

En un sistema *push-pull* la interacción electrónica entre el dador y el aceptor reduce la energía del gap HOMO-LUMO. Por esta razón, la banda de

[1] Liang, M.; Chen, J. *Chem. Soc. Rev.* **2013**, *42*, 3453.
[2] (a) Para una edición especial sobre propiedades electrónicas y optoelectrónicas en materiales orgánicos, véase: ed. Forrest, S. R.; Thompson, M. E. *Chem. Rev.* **2007**, *107*, 923-1386. (b) Para una edición especial sobre materiales para la electrónica, véase: ed. Miller, R. D.; Chandross, E. A. *Chem. Rev.* **2010**, *110*, 1-574. (c) Para una edición especial sobre electrónica molecular, véase: ed. Mayor, M. *Chimia* **2010**, *64*, 348-420.
[3] Para una edición especial sobre conductores moleculares, véase: ed. Batail, P. *Chem. Rev.* **2004**, *104*, 4887-5782.
[4] (a) Para una edición especial sobre compuestos orgánicos fotovoltaicos, véase: ed. Brédas, J.-L.; Durrant, J. R. *Acc. Chem. Res.* **2009**, *42*, 1689-1857. (b) Lin, Y.; Li Y.; Zhan, X. *Chem. Soc. Rev.* **2012**, *41*, 4245.
[5] Allard, S.; Forster, M.; Souharce, B.; Thiem, H.; Scherf, U. *Angew. Chem., Int. Ed.* **2008**, *47*, 4070.
[6] Ohmori, Y. *Laser Photonics Rev.* **2009**, *4*, 300.
[7] Hains, A. W.; Liang, Z.; Woodhouse, M. A.; Gregg, B. A. *Chem. Rev.* **2010**, *110*, 6689.
[8] Para una edición especial sobre DSSC, véase: Burford, N.; King, R. B.; Lever, A. B. P. *Coord. Chem. Rev.* **2004**, *248*, 1161-1530.

absorción se desplaza a mayores longitudes de onda con respecto a sus análogos sin interacción electrónica y, como consecuencia, son generalmente coloreados.

En la actualidad se han diseñado y caracterizado una gran cantidad sistemas *push-pull* de tipo orgánico[9] con el fin de encontrar relaciones estructura-propiedad adecuadas para posibles aplicaciones ópticas y electrónicas. En principio, las propiedades optoelectrónicas, las propiedades ópticas no lineales (NLO), la ICT y la correspondiente diferencia entre los niveles de energía de los correspondientes orbitales frontera pueden modularse mediante varios factores,[10]

- naturaleza electrónica del dador y el aceptor
- interacción eficiente entre el dador y el aceptor
- extensión, composición y disposición espacial del sistema π
- planaridad de la molécula

En la Figura 2 se muestran varios ejemplos de sistemas *push-pull* con conjugación lineal, donde se pueden observar los grupos dadores, aceptores y espaciadores π más representativos presentes en este tipo de compuestos.

[9] Robertson, N. *Angew. Chem., Int. Ed.* **2006**, *45*, 2338.
[10] Bureš, F. *RSC Advances* **2014**, *4*, 58826.

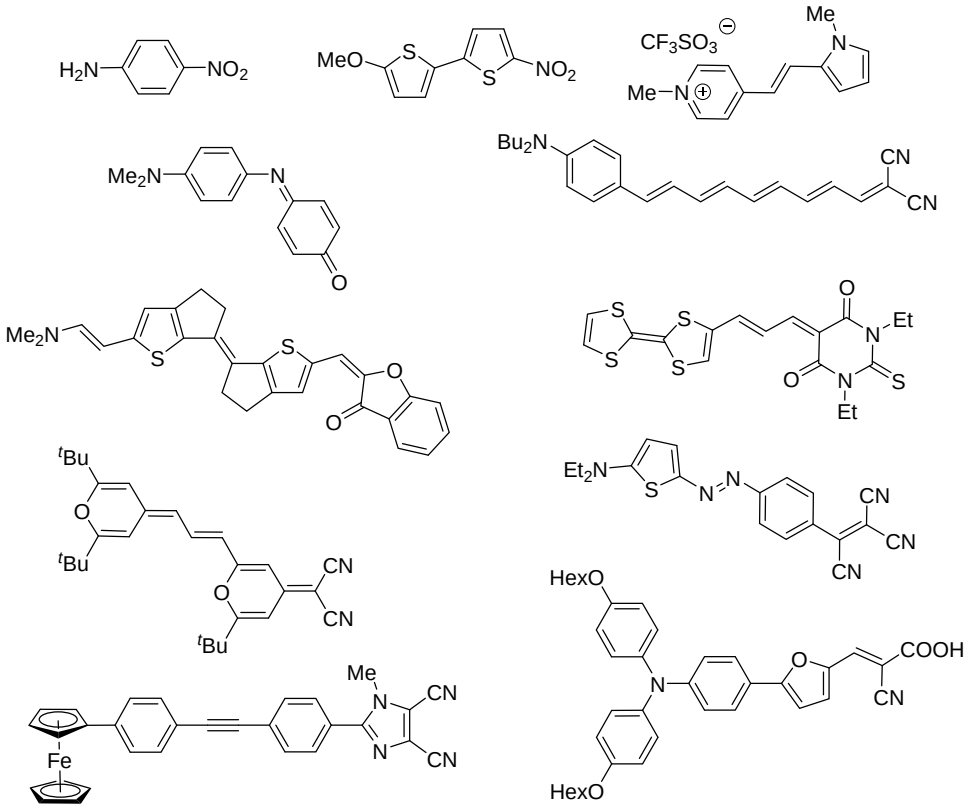

Figura 2. Estructuras representativas de sistemas *push-pull* con conjugación lineal.

Aunque los sistemas *push-pull* lineales y dipolares (D-π-A) son los más comunes, también se han estudiado sistemas cuadrupolares (A-π-D-π-A[11] y D-π-A-π-A)[12] y octupolares ((D-π)$_3$-A, **a**)[13] y (A-π)$_3$-D)).[14] De igual manera, se han sintetizado sistemas *push-pull* con forma de V- (**b**),[15] Y- (**c**),[13] H- (**d**)[16] y X- (**e**),[17] radialenos (**f**)[18] y radialenos expandidos (**g**),[19] todos ellos con interesantes propiedades NLO (Figura 3).

[11] Ren, J.; Wang, S.-M.; Wu, L.-F.; Xu, Z.-X.; Dong, B.-H. *Dyes and Pigments* **2008**, *76*, 310.
[12] Moylan, C. R.; Ermer, S.; Lovejoy, S. M.; McComb, I.-H.; Leung, D.; Wortmann, R.; Krdmer, P.; Twieg, R. *J. Am. Chem. Soc.* **1996**, *118*, 12950.
[13] Martin, F. A.; Baudequin, C.; Fiol-Petit, C.; Darabantu, M.; Ramondec, Y.; Plé, N. *Tetrahedron*, **2014**, *70*, 2546.
[14] Vivas, M. G.; Silva, D. L.; Malinge, J.; Boujtita, M.; Zalesny, R.; Bartkowiak, W.; Agren, H.;Canuto, S.; De Boni, L.; Ishow, E. *Sci. Rep.* **2014**, *4*, 4447.
[15] Ramírez, M. A.; Cuadro, A. M.; Álvarez-Builla, J.; Castaño, O.; Andrés, J. L.; Mendicuti, F.; Clays, K.; Asselberghs, I.; Vaquero, J. J. *Org. Biomol. Chem.* **2012**, *10*, 1659.
[16] Wu, W.; Wang, C.; Zhong, C.; Ye, C.; Qui, G.; Qin, J.; Li, Z. *Polym. Chem.* **2013**, *4*, 378.
[17] (a) Kato, S.-i.; Diederich, F. *Chem. Commun.* **2010**, *46*, 1994. (b) Zucchero, A. J.; McGrier, P. L.; Bunz, U. H. F. *Acc. Chem. Res.* **2010**, *43*, 397. (c) Kivala, M.; Diederich, F. *Acc. Chem. Res.* **2009**, *42*, 235.
[18] Wu, Y.-L.; Tancini, F.; Schweizer, W. B.; Paunescu, D.; Boudon, C.; Gisselbrecht, J.-P.; Jarowski, P. D.; Dalcanale, E.; Diederich, F. *Chem. Asian J.* **2012**, *7*, 1185.
[19] Ramsaywack, S.; Karaca, S.; Gholami, M.; Murray, A. H.; Hampel, F.; McDonald, R.; Elmaci, N.; Lüthi, H. P.; Tykwinski, R. R. *J. Org. Chem.* **2014**, *79*, 10013.

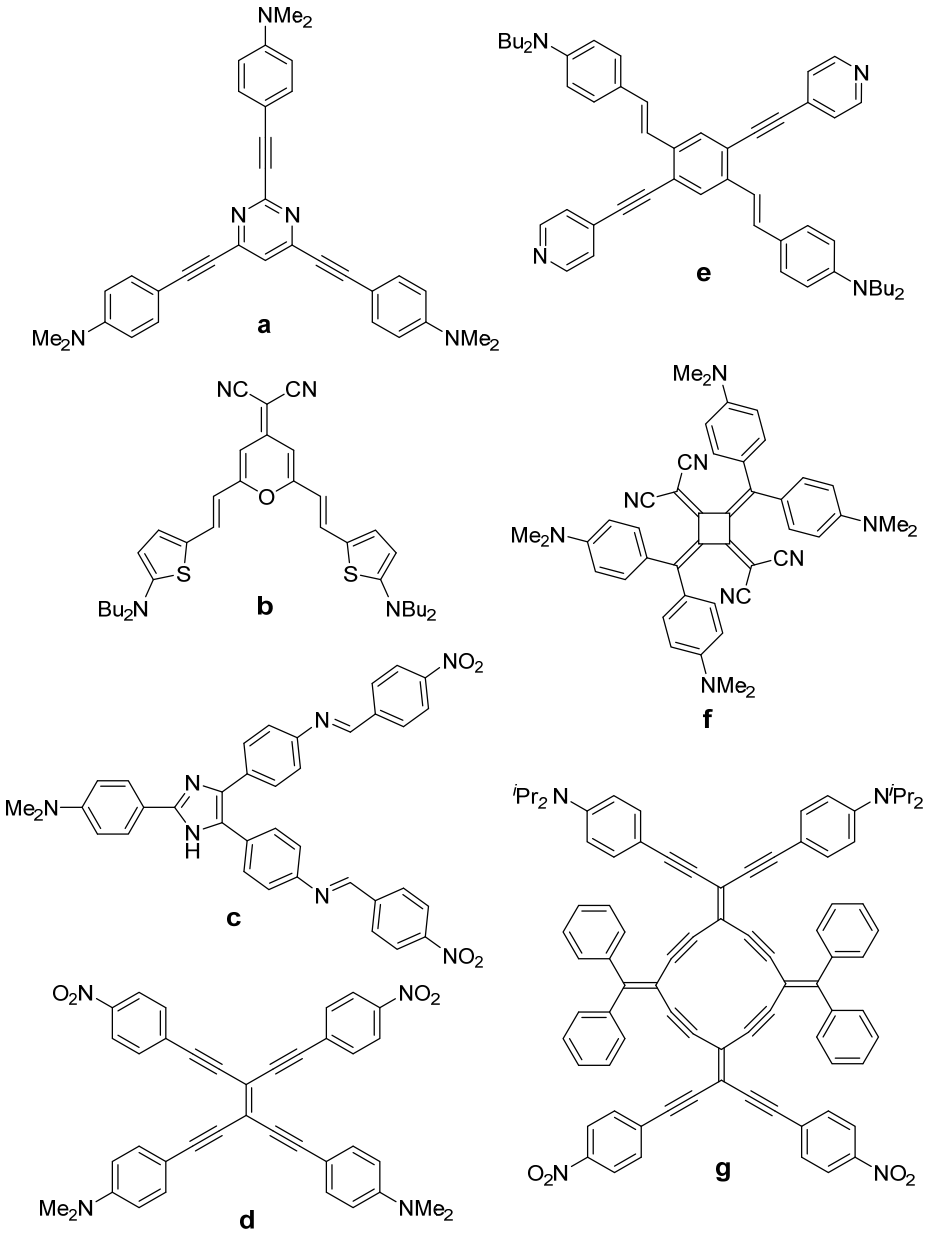

Figura 3. Sistemas *push-pull* con distintos tipos de conjugación.

Por otro lado, se han desarrollado sistemas *push-pull* sin conjugación π directa. Estos cromóforos no planos contienen en su estructura diversos puentes que permiten una deslocalización electrónica no convencional. Así, en la Figura 4 se representan sistemas como cumulenos (**h**),[20] ciclofanos (**i**),[21] biciclos saturados (**j**),[22] sistemas helicoidales (**k**),[23] sistemas homoconjugados como los 7,7-difenil-

[20] Gawel, P.; Wu, Y.-L.; Finke, A. D.; Trapp, N.; Zalibera, M.; Boudon, C.; Gisselbrecht, J.-P.; Schweizer, W. B.; Gescheidt, G.; Diederich, F. *Chem. Eur. J.* **2015**, *21*, 6215.

[21] (a) Rotzler, J.; Gsellinger, H.; Neuburger, M.; Vonlanthen, D.; Häussinger, D.; Mayor, M. *Org. Biomol. Chem.* **2011**, *9*, 86. (b) Tsuji, Y.; Yoshizawa, K. *J. Phys. Chem. C* **2012**, *116*, 26625.

[22] Kato, S.-i.; Beels, M. T. R.; La Porta, P.; Schweizer, W. B.; Boudon, C.; Gisselbrecht, J.-P.; Biaggio, I.; Diederich, F. *Angew. Chem., Int. Ed.* **2010**, *49*, 6207.

norbornanos (**l**),[24] espiro-compuestos (**m**),[25] tripticenos (**n**)[26] y compuestos con conjugación a través un camino ramificado (**ñ**, *branched conjugation pathway*).[27]

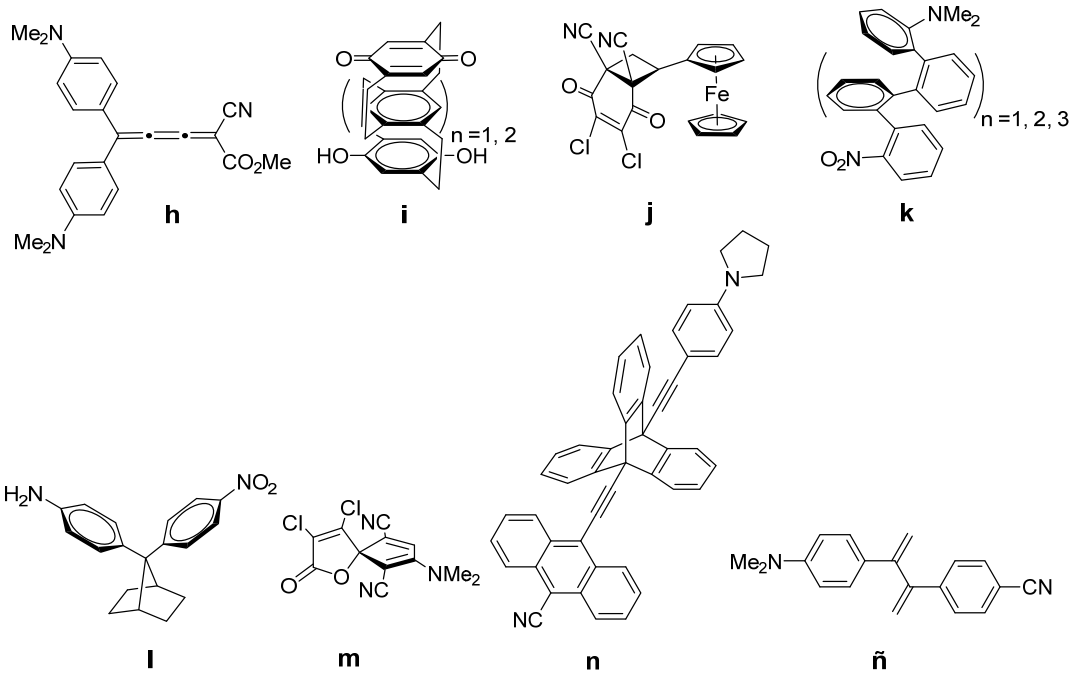

Figura 4. Ejemplos de sistemas *push-pull* con deslocalización electrónica no convencional.

Por último, cabe mencionar la existencia de sistemas de valencia mixta dadores de un único electrón.[28] Estos compuestos se caracterizan por la formación de aniones-radicales o cationes-radicales y se clasifican según la localización o la deslocalización de la carga en los centros rédox presentes en el sistema.[29] En la Figura 5 se muestran varios ejemplos de compuestos *push-pull* de valencia mixta.

[23] He, J.; Mathew, S. M.; Cornett, S. D.; Grundy, S. C.; Hartley, C. S. *Org. Biomol. Chem.* **2012**, *10*, 3398.
[24] (a) Herrero García, N.; Fernández, I.; Osío Barcina, J. *Chem. Eur. J.* **2011**, *17*, 7327. (b) Herrero-García, N.; Colorado Heras, M. R.; Torres, M. R.; Fernández, I.; Osío Barcina, J. *Eur. J. Org. Chem.* **2012**, 2643.
[25] (a) Jayamurugan, G.; Gisselbrecht, J.-P.; Boudon, C.; Schoenebeck, F.; Schweizer, W. B.; Bernet, B.; Diederich, F. *Chem. Commun.* **2011**, *47*, 4520. (b) Dengiz, C.; Dumele, O.; Kato, S.-i.; Zalibera, M.; Cias, P.; Schweizer, W. B.; Boudon, C.; Gisselbrecht, J.-P.; Gescheidt, G.; Diederich, F. *Chem. Eur. J.* **2014**, *20*, 1279. (c) Rizzo, F.; Cavazzini, M.; Righetto, S.; De Angelis, F.; Fantacci, S.; Quici, S. *Eur. J. Org. Chem.* **2010**, 4004.
[26] Goldsmith, R. H.; Vura-Weis, J.; Scott, A. M.; Borkar, S.; Sen, A.; Ratner, M. A.; Wasielewski, M. R. *J. Am. Chem. Soc.* **2008**, *130*, 7659.
[27] Van Walree, C. A.; van der Wiel, B. C.; Williams, R. M. *Phys. Chem. Chem. Phys.* **2013**, *15*, 15234.
[28] Para revisiones recientes sobre compuestos orgánicos de valencia mixta, véase: (a) Heckmann, A.; Lambert, C. *Angew. Chem., Int. Ed.* **2012**, *51*, 326. (b) Hankache, J.; Wenger, O. S. *Chem. Rev.* **2011**, *111*, 5138.
[29] Robin, M. B.; Day, P. *Adv. Inorg. Chem. Radiochem.* **1967**, *9*, 247.

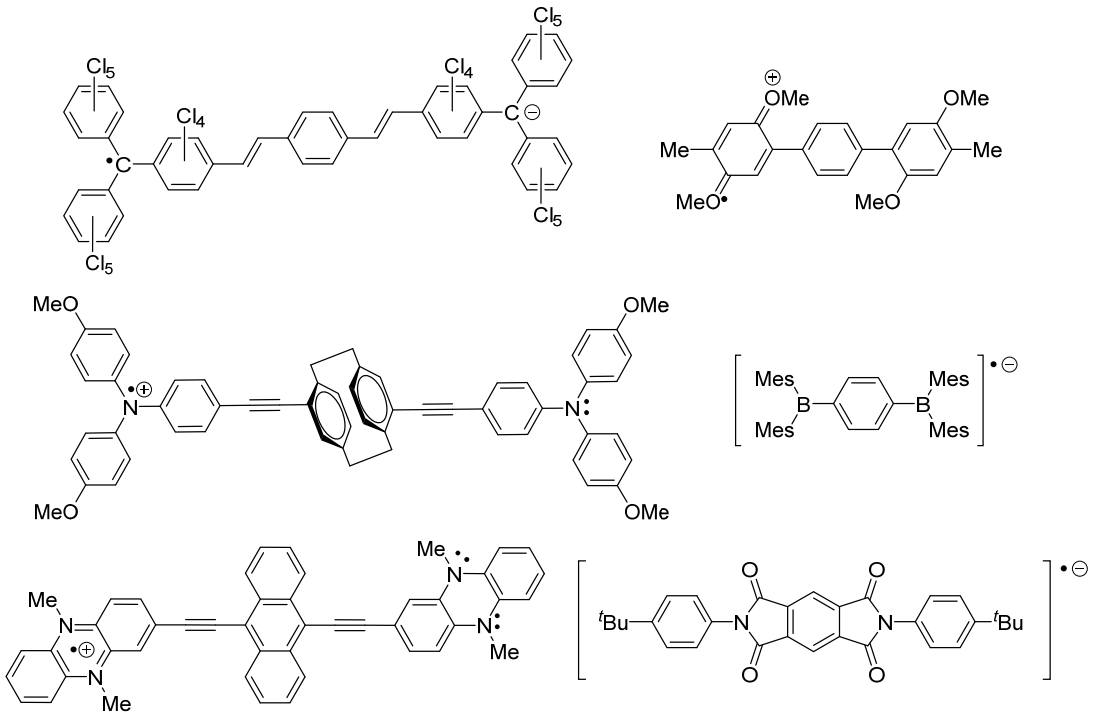

Figura 5. Ejemplos representativos de sistemas de valencia mixta.

Si bien los complejos de coordinación son una herramienta fundamental dentro de la síntesis orgánica actual, no se debe olvidar que presentan de manera adicional propiedades ópticas y electrónicas modulables. Por ello, la elección razonada tanto del metal y su esfera de coordinación como del espaciador permite modificar de manera controlada las propiedades optoelectrónicas del complejo así formado. Como consecuencia, la literatura está repleta de ejemplos de sistemas *push-pull* basados en distintos complejos de metales de transición (Ru,[30] Os,[31] Pt,[32] Cu,[33] Re[34], Zn[35] y Fe)[36] junto con la extensa bibliografía sobre

[30] (a) Chitumalla, R. K.; Gupta, K. S. V.; Malapaka, C.; Fallahpour, R.; Islam, A.; Han, L.; Kotamarthi, B.; Singh, S. P. *Phys. Chem. Chem. Phys.* **2014**, *16*, 2630. (b) De Sousa, S.; Ducasse, L.; Kauffmann, B.; Toupance, T.; Olivier, C. *Chem. Eur. J.* **2014**, *20*, 7017.

[31] Swetha, T.; Reddy, K. R.; Singh, S. P. *Chem. Rec.* **2015**, *15*, 457.

[32] (a) Geary, E. A. M.; Yellowlees, L. J.; Jack, L. A.; Oswald, I. D. H.; Parsons, S.; Hirata, N.; Durrant, J. R.; Robertson, N. *Inorg. Chem.* **2005**, *44*, 242. (b) Scarpaci, A.; Monnereau, C.; Hergue, N.; Blart, E.; Legoupy, S.; Odobel, F.; Gorfo, A.; Pérez-Moreno, J.; Clays, K.; Asselberghs, I. *Dalton Trans.* **2009**, 4538.

[33] Hewat, T. E.; Yellowlees, L. J.; Robertson, N. *Dalton Trans.* **2014**, *43*, 4127.

[34] Coe, B. J.; Foxon, S. P.; Pilkington, R. A.; Sánchez, S.; Whittaker, D.; Clays, K.; Depotter, G.; Brunschwig, B. S. *Organometallics* **2015**, *34*, 1701.

[35] Yi, C.; Giordano, F.; Cevey-Ha, N.-L.; Tsao, H. N.; Zakeeruddin, S. M.; Grätzel, M. *ChemSusChem* **2014**, *7*, 1107.

[36] (a) Coe, B. J.; Fielden, J.; Foxon, S. P.; Asselberghs, I.; Clays, K.; Van Cleuvenbergen, S.; Brunschwig, B. S. *Organometallics* **2011**, *30*, 5731. (b) Jayaweera, P. M.; Palayangoda, S. S.; Tennakone, K. *J. Photochem. Photobiol. A* **2001**, *140*, 173.

complejos metálicos de valencia mixta (Figura 6).[37]

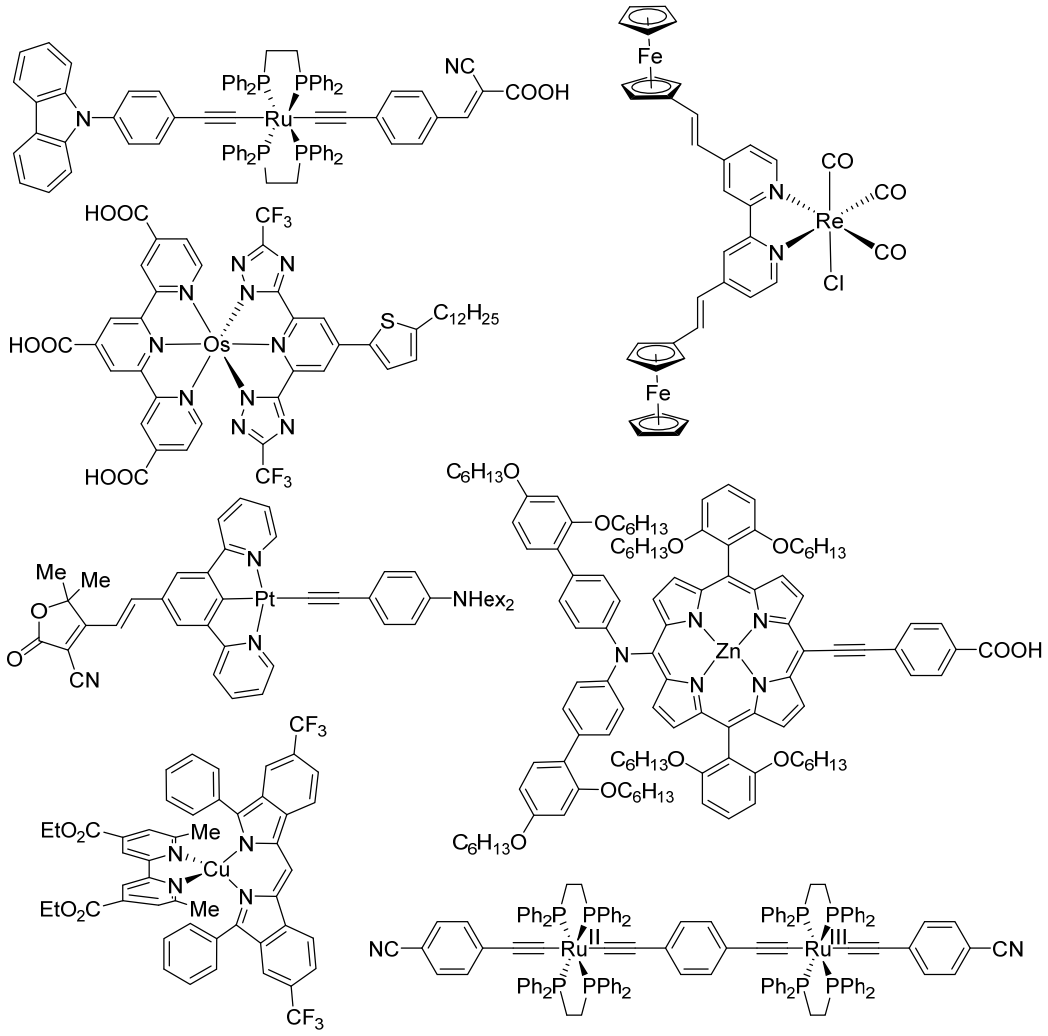

Figura 6. Diferentes ejemplos de sistemas *push-pull* basados en complejos metales de transición.

Un tipo particular de complejos de metales de transición usados en sistemas *push-pull* se basa en complejos metal-carbeno de tipo Fischer (Figura 7).[38] Estos compuestos presentan unas propiedades optoelectrónicas muy interesantes, como altos valores de hiperpolarizabilidad β.[39]

[37] Para una revisión reciente sobre especies homo-bimetálicas de valencia mixta, véase: (a) Aguirre-Etcheverry, P.; O'Hare, D. *Chem. Rev.* **2010**, *110*, 4839. Para una revisión sobre especies hetero-bimetálicas de valencia mixta, véase: (b) Ceccon, A.; Santi, S.; Orian, L.; Bisello, A. *Coord. Chem. Rev.* **2004**, *248*, 683. Para una revisión sobre especies trimetálicas de valencia mixta, véase: (c) D'Alessandro, D.; Keene, F. R. *Chem. Rev.* **2006**, *106*, 2270. Para una revisión de complejos de Ru de valencia mixta, véase: (d) Kaim, W.; Sarkar, B. *Coord. Chem. Rev.* **2007**, *251*, 584.

[38] (a) Maiorana, S.; Papagni, A.; Licandro, E.; Persoons, A.; Clays, K.; Houbrechts, S.; Porzio, W. *Gazz. Chim. It.* **1995**, *125*, 377. (b) Licandro, E.; Maiorana, S.; Papagni, A.; Hellier, P.; Capella, L.; Persoons, A.; Houbrechts, S. *J. Organomet. Chem.* **1999**, *583*, 111. (c) Jayaprakash, K. N.; Ray, P. C.; Matsuoka, I.; Bhadbhade, M. M.; Puranik, V. G.; Das, P. K.; Nishihara, H.; Sarkar, A. *Organometallics* **1999**, *18*, 3851. (d) Faux, N.; Caro, B.;

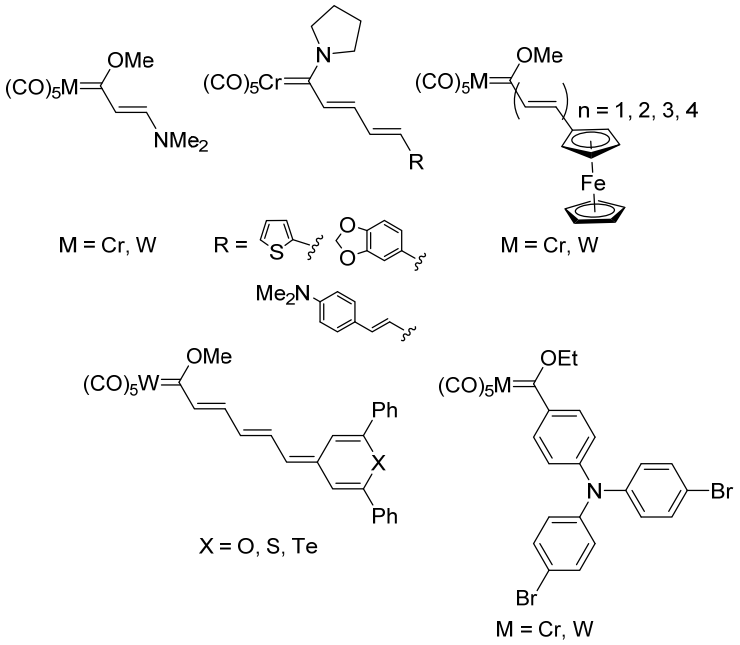

Figura 7. Sistemas dador-aceptor basados en complejos metal-carbeno de tipo Fischer.

En estas especies, el fragmento $M(CO)_5$, donde M es Cr, Mo o W, se comporta como un grupo fuertemente electroaceptor debido a la presencia de los cinco ligandos CO π-aceptores.[40] Además, los complejos organometálicos metal-carbeno de tipo Fischer, descritos inicialmente por Fischer y Maasböl en 1964,[41] son fácilmente modulables debido a la rica y variada reactividad que pueden experimentar.[42]

Robin-Le Guen, F.; Le Poul, P.; Nakatani, K.; Ishow, E. *J. Organomet. Chem.*, **2005**, *690*, 4982. (e) Weststrate, N.-A.; Fernández, I.; Liles, D. C.; van Jaarsveld, N.; Lotz, S. *Organometallics* **2015**, *34*, 696.

[39] Kanis, D. R.; Ratner, M. A.; Marks, T. J. *Chem. Rev.* **1994**, *94*, 195.

[40] (a) Fernández, I.; Sierra, M. A.; Cossío, F. P. *J. Org. Chem.* **2006**, *71*, 6178. (b) Fernández, I.; Sierra, M. A.; Cossío, F. P. *J. Org. Chem.* **2008**, *73*, 2083. (c) Andrada, D. M.; Granados, A. M.; Solà, M.; Fernández, I. *Organometallics* **2011**, *30*, 466. (d) Raubenheimer, H. G. *Dalton Trans.* **2014**, *43*, 16959.

[41] Fischer, E. O.; Maasböl, A. *Angew. Chem. Int. Ed. Engl.* **1964,** *3,* 580.

[42] Para revisiones recientes, véase: (a) Dötz, K. H. en *Metal Carbenes in Organic Synthesis*; Springer: Berlin, **2004**; Topics in Organometallic Chemistry, Vol. 13. (b) Barluenga, J.; Santamaría, J.; Tomás, M. *Chem. Rev*. **2004**, *104*, 2259. (c) Barluenga, J.; Fernández-Rodríguez, A. M.; Aguilar, E. *J. Organomet. Chem.* **2005**, *690*, 539. (d) Wu, Y.-T.; Kurahashi, T.; de Meijere, A. *J. Organomet. Chem.* **2005**, *690*, 5900. (e) Herndon, J. W. *Coord. Chem. Rev*. **2006**, *250*, 1889. (f) Sierra, M. A.; Gómez-Gallego, M.; Martínez-Álvarez, R. *Chem. Eur. J.* **2007**, *13*, 736. (g) Sierra, M. A.; Fernández, I.; Cossío, F. P. *Chem. Commun.* **2008**, *39*, 4671. (h) Dötz, K. H.; Stendel, J. *Chem. Rev*. **2009**, *109*, 3227. (i) Herndon, J. W. *Coord. Chem. Rev*. **2010**, *254*, 103. (j) Fernández-Rodríguez, M. A.; García-García, P.; Aguilar, E. *Chem. Commun*. **2010**, *46*, 7670. (k) Fernández, I.; Cossío, F. P.; Sierra, M. A. *Acc. Chem. Res*. **2011**, *44*, 479; (l) Fernández, I.; Sierra, M. A. *Top. Heterocycl. Chem*. **2013**, *30*, 65.

I.2. Estructura de complejos metal-carbeno de tipo Fischer

Los complejos metal-carbeno de tipo Fischer contienen en su estructura metales de los grupos 6 a 8 en un bajo estado de oxidación unidos a ligandos fuertemente electroaceptores (generalmente de tipo CO). En estos complejos, el ligando carbeno es de tipo singlete y se considera que el carbono carbénico presenta una hibridación sp^2. Además, se encuentran generalmente estabilizados por un heteroátomo (oxígeno, azufre o nitrógeno) unido al carbono carbénico, capaz de compensar la deficiencia de carga del mismo por conjugación.

El enlace metal-carbeno en complejos de tipo Fischer, aplicando el modelo de Dewar-Chatt-Duncanson,[43] se puede considerar como un doble enlace formal metal-carbeno (M=C). Esta unión entre el metal y el ligando carbeno consiste en un enlace dador de tipo σ del ligando carbeno a un orbital *d* vacío del metal y un enlace π débil, que se establece por retrodonación desde un orbital *d* ocupado del metal hacia el orbital p_z vacío del ligando carbeno (Figura 8).[44]

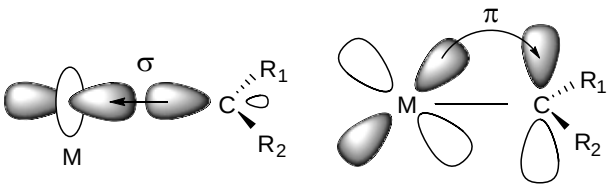

Figura 8. Enlace M=C en complejos metal-carbeno de tipo Fischer según el modelo de Dewar-Chatt-Duncanson.

El solapamiento débil entre los orbitales del metal y del ligando carbeno y la presencia de ligandos π-aceptores en la esfera de coordinación del metal, disminuyen la capacidad retrodonadora del mismo, hecho que justifica el fuerte carácter electrófilico del carbono carbénico. Esta deficiencia de carga se compensa en parte por la cesión del par de electrones sin compartir del heteroátomo directamente unido al carbono carbénico. En consecuencia, la electrofilia de los carbenos de Fischer aumenta al disminuir la capacidad de cesión de electrones del heteroátomo (orden de reactividad: O > S > N).

[43] (a) Dewar, M. J. S. *Bull. Soc. Chim. Fr*. **1951**, *18*, C79. (b) Chatt, J.; Duncanson, *J. Chem. Soc.* **1953**, 2929.
[44] Frenking, G.; Solà, M.; Vyboishchikov, S. F. *J. Organomet. Chem.* **2005**, *690*, 6178.

Tanto los resultados obtenidos por difracción de rayos-X como por las estimaciones realizadas mediante cálculos teóricos, indican que el orden de enlace entre el carbeno y el heteroátomo corresponde a un valor intermedio entre un enlace sencillo y uno doble.[45] Por lo tanto, estos complejos metal-carbeno pueden describirse como un híbrido de resonancia entre las estructuras mostradas en la Figura 9.

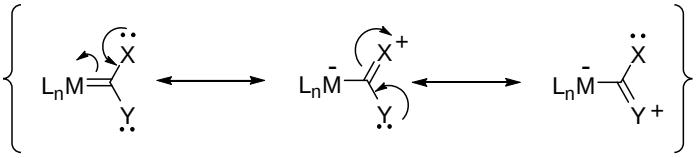

Figura 9. Formas resonantes de un complejo metal-carbeno de tipo Fischer.

I.3. Procesos de transmetalación catalizados por paladio en complejos metal-carbeno de tipo Fischer

Aunque la transmetalación es probablemente uno de los procesos más importantes en química organometálica,[46] la transferencia de un ligando carbeno desde un complejo metal-carbeno a otro centro metálico no es un proceso frecuente. La dificultad para llevar a cabo dicha transferencia se debe probablemente a la baja capacidad de estabilización del ligando carbeno por el nuevo centro metálico sobre el cual tiene lugar la transmetalación.[47] Sin embargo, en los últimos años el estudio de procesos que implican la transferencia de ligandos carbeno desde complejos metal-carbeno inducida por catalizadores derivados de metales de transición ha dado lugar a un nuevo campo de investigación, el cual ha abierto las puertas a nuevas formas de reactividad para este tipo de compuestos.

[45] (a) Nakatsuji, H.; Ushio, J.; Han, S.; Yonezawa, T. *J. Am. Chem. Soc.* **1983**, *105*, 426. (b) Jacobsen, H.; Ziegler, T. *Organometallics* **1995**, *14*, 224. (c) Wang, C.-C.; Wang, Y.; Liu, H.-J.; Lin, K.-J.; Chou, L.-K.; Chan, K.-S. *J. Phys. Chem. A* **1997**, *101*, 8887. (d) Cases, M.; Frenking, G.; Durán, M.; Solà, M. *Organometallics* **2002**, *21*, 4182.

[46] (a) Collman, J. P.; Hegedus, L. S.; Norton, J. R.; Finke, R. G. en *Principles and Applications of Organotransition Metal Chemistry*; University Science Books: Mill Valley, CA, **1987**. (b) Boudier, A.; Bromm, L. O.; Lotz, M.; Knochel, P. *Angew. Chem., Int. Ed.* **2000**, *39*, 4414. (c) de Meijere, A.; Diederich, F. en *Metal Catalyzed Cross-Coupling Reactions*; Wiley-VCH: Weinheim, **2004**.

[47] Lui, S. T.; Reddy, K. R. *Chem. Soc. Rev.* **1999**, *28*, 315.

La transferencia térmica, no catalizada, de ligandos carbeno para dar productos de dimerización intermolecular es una reacción que se realiza a temperaturas próximas a 130°C. La descomposición térmica de los carbenos de tipo Fischer da lugar a dos isómeros olefínicos cuya relación *E/Z* depende de la naturaleza del complejo inicial metal-carbeno.[48]

Nuestro grupo de investigación describió a finales del siglo XX, la transferencia de ligandos carbeno catalizada por paladio desde complejos metal-carbeno del grupo 6 (Esquema 1).[49] Estos procesos de transmetalación a temperatura ambiente se realizaron con los complejos metal-carbeno **1**, un 10% de $Pd(OAc)_2$, en presencia de Et_3N y utilizando THF como disolvente, obteniendo una mezcla de isómeros *E*/*Z* de 1,2-difenil-1,2-dimetoxieteno **2** en proporción 1:2.

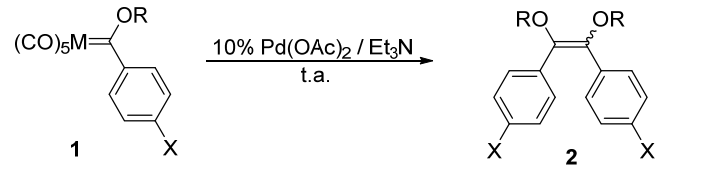

1a, M = Cr, R = Me, X = H
1b, M = Cr, R = Me, X = Br
1c, M = W, R = Et, X = H

2a, R = Me, X = H (53%)
2b, R = Me, X = Br (62%)
2c, R = Et, X = H (46%)

Esquema 1. Dimerización de complejos metal-carbeno catalizada por Pd.

Los resultados iniciales demostraron que la transferencia del ligando carbeno era posible en condiciones de reacción catalíticas a temperatura ambiente. Esta reacción se llevó a cabo con distintos catalizadores de paladio, con cargas muy bajas de catalizador, en diversos disolventes y en rangos de temperatura variables. Tanto estos factores como el uso de ciertos aditivos ejercen una escasa influencia en la relación de isómeros *E/Z* en el doble enlace que se obtiene en la reacción de dimerización.[50]

De esta manera, la dimerización catalizada por paladio resulta muy eficaz para la síntesis de sistemas poliénicos conjugados **3**, compuestos endiínicos **4**, así

[48](a) Fischer, E. O.; Heckl, B.; Dötz, K. H.; Muller, J.; Werner, H. *J Organomet. Chem.* **1969**, *16*, P29. (b) Fischer, E. O.; Dötz, K. H. *J. Organomet. Chem.* **1972**, *36*, C4-C6.
[49] Sierra, M. A.; Mancheño, M. J.; Sáez, E.; del Amo, J. C. *J. Am. Chem. Soc*. **1998**, *120*, 6812.
[50] Sierra, M. A.; del Amo, J. C.; Mancheño, M. J.; Gómez-Gallego, M. *J. Am. Chem. Soc.* **2001**, *123*, 851.

como productos cíclicos insaturados **5** o especies bimetálicas conjugadas **6** (Esquema 2).[50,51]

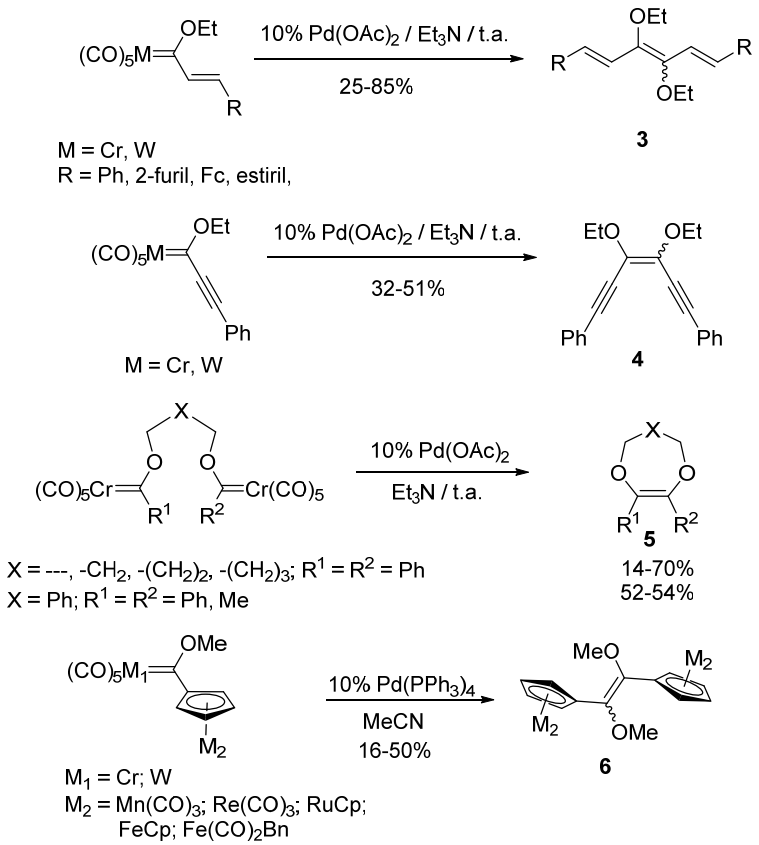

Esquema 2. Diferentes ejemplos de dimerización de complejos metal-carbeno.

Los resultados experimentales obtenidos en las diferentes reacciones catalizadas por Pd, han llevado a proponer el ciclo catalítico mostrado en el Esquema 3 para la reacción de dimerización. El complejo metal-carbeno **7** reacciona con el catalizador de paladio generando el complejo palada-carbeno **9**. Esta reacción de transmetalación ocurre probablemente a través del intermedio ciclopropánico heterobimetálico **8** que evoluciona a **9** por extrusión de la especie "$M(CO)_5$". A continuación, se produce un nuevo proceso de transmetalación desde otra molécula del complejo metal-carbeno **7** para dar lugar al complejo bis-palada-carbeno **10**, que conduce después a la regeneración del catalizador Pd^0 y a la formación del producto de dimerización, como mezcla de isómeros *E/Z* **11**.

[51] Lage, M. L.; Curiel, D.; Fernández, I.; Mancheño, M. J.; Gómez-Gallego, M.; Molina, P.; Sierra, M. A. *Organometallics* **2011**, *30*, 1794.

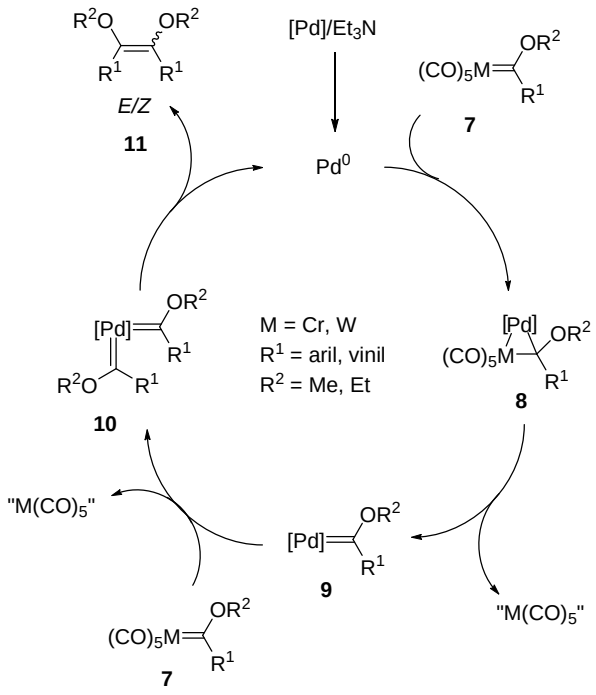

Esquema 3. Mecanismo propuesto para la transmetalación catalizada por Pd.

Este mecanismo es consistente con el aislamiento y caracterización de palada-carbenos[52] y bis-palada-carbenos.[53] Además, se sustenta en los cálculos teóricos realizados en nuestro grupo de investigación.[54] Así, la última etapa del ciclo catalítico que conecta el complejo de partida **12** con el producto de dimerización final **17**, termina con la formación del enlace C=C en el complejo **13**. La adición de una molécula de ligando fosfina al complejo **13** da lugar al complejo de 18 electrones **14**, el cual forma el complejo **15** a través del estado de transición **TS1-Pd**. Finalmente, el producto de dimerización coordinado a paladio **15** es intercambiado por otra molécula de ligando fosfina para cerrar el ciclo catalítico y liberar la olefina **17**. De forma alternativa, el enlace C=C se puede formar desde el bis-palada-carbeno **13**. En este caso, el complejo **17** se genera a través del estado de transición **TS2-Pd**, donde una molécula de PH_3 puede coordinarse al centro metálico para formar **15** o puede sustituir al ligando alqueno para formar $[Pd(PH_3)_2]$ y la olefina **17** (Esquema 4).

[52] Albéniz, A. C.; Espinet, P.; Manrique, R.; Pérez-Mateo, A. *Angew. Chem., Int. Ed.* **2002**, *41*, 2363.
[53] (a) López-Alberca, M. P.; Mancheño, M. J.; Fernández, I.; Gómez-Gallego, M.; Sierra, M. A.; Torres, R. *Org. Lett*. **2007**, *9*, 1757. (b) Para un estudio de transferencia estequiométrica de carbenos de cromo a paladio, platino y oro, véase: Kessler, F.; Sznesni, N.; Maass, C.; Hohberger, C.; Weibert, B.; Fischer, H. *J. Organomet. Chem*. **2007**, *692*, 3005.
[54] Fernández, I.; Mancheño, M. J.; Vicente, R.; López, L. A.; Sierra, M. A. *Chem. Eur. J.* **2008**, *14*, 11222.

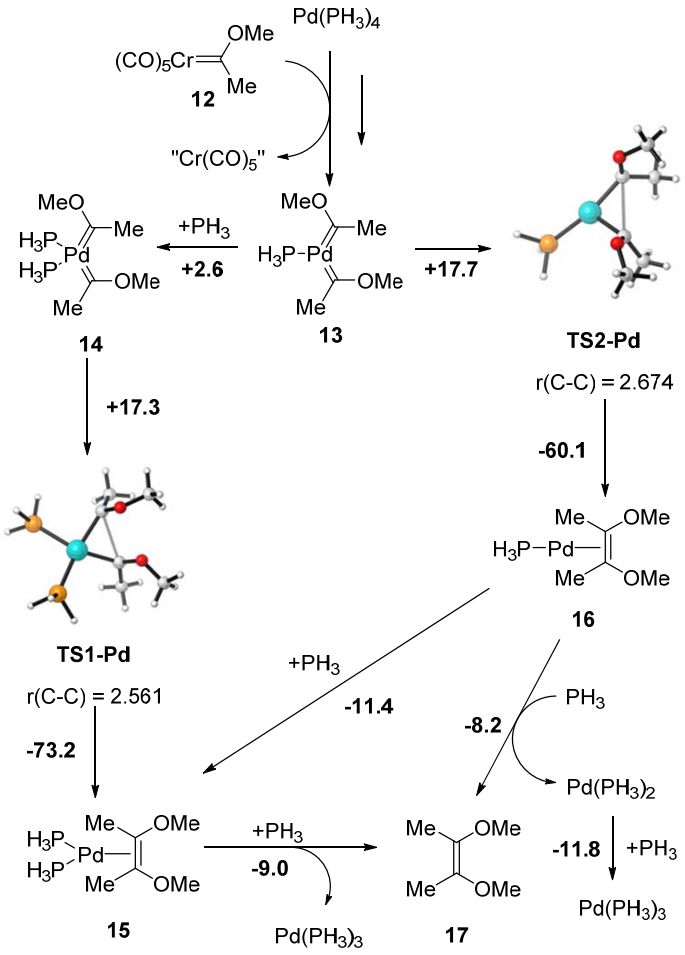

Esquema 4. Última etapa de la transmetalación. Las distancias interatómicas se muestran en Å y las energías relativas en kcal·mol^{-1}.[54]

Por tanto, la última etapa del mecanismo propuesto es la que determina la relación *E*/*Z* de los dímeros y por ello el efecto del ligando va a ser crucial en los complejos bis-palada-carbeno **13** y **14** a la hora de obtener un isómero de manera mayoritaria frente al otro.

I.4. Estructura electrónica de complejos metal-carbeno de tipo Fischer

Los complejos metal-carbeno de tipo Fischer son fuertemente coloreados. El espectro de UV-visible de estos complejos presenta tres bandas bien diferenciadas: una banda débil en torno a 500 nm correspondiente a la transferencia de carga metal-ligando (MLCT), una banda de intensidad moderada alrededor de 350-450 nm debida a una transición de campo del ligando de baja energía (LF) y una banda débil entre 300-350 nm, que en muchas ocasiones se

encuentra solapada con la anterior y que corresponde a una transición LF de mayor energía.

Las bandas MLCT y LF se asignaron originalmente[55] a la promoción de un electrón desde el orbital no enlazante centrado en el metal (HOMO) a un orbital *p* centrado en el carbeno (LUMO) (banda MLCT), mientras que la banda LF se asignó a la transición vertical al orbital (LUMO+1) centrado en el metal. Sin embargo, cálculos TD-DFT recientes realizados en nuestro grupo de investigación[56] demuestran que la banda MLCT resulta de la promoción de un electrón desde el orbital HOMO-1 (centrado en el metal) al orbital LUMO (orbital π-extendido que contiene al orbital átomico p_z del carbono carbénico). En cambio, la banda LF corresponde a la transición vertical HOMO-3 (centrado en el sistema π del carbeno) al LUMO (Figura 10).

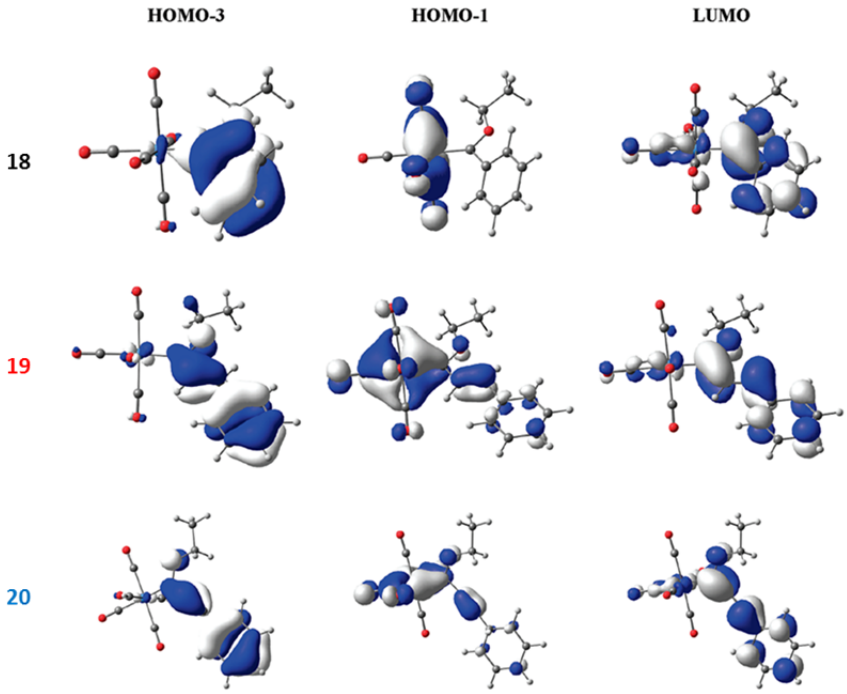

Figura 10. Orbitales moleculares calculados para los complejos **18**, **19** y **20**.[56]

Por tanto, ambas transiciones tienen un marcado carácter π-π* y por esta razón, la posición de las bandas de absorción de los complejos metal-carbeno de

[55] La asignación de las transiciones se realizó inicialmente en base a cálculos teóricos: (a) Block, T.J.; Fenkse, R. F.; Casey, C. P. *J. Am. Chem. Soc.* **1976**, *98*, 441. (b) Nakatsuji, J.; Uskio, J.; Yonezawa, T. *J. Am. Chem. Soc.* **1983**, *105*, 426. (c) Foley, H.C.; Strubinger, L. M.; Targos, T. S.; Geoffroy, G. L. *J. Am. Chem. Soc.* **1983**, *105*, 3064.

[56] Lage, M. L.; Fernández, I.; Mancheño, M. J.; Sierra, M. A. *Inorg. Chem*. **2008**, *47*, 5253.

tipo Fischer está influenciada por la sustitución sobre el ligando carbeno. Así, la presencia de heteroátomos fuertemente π-dadores sobre el carbeno (por ejemplo, N frente a O) provoca desplazamientos hipsocrómicos en el espectro de absorción de dichos compuestos, mientras que la introducción de sustituyentes π-conjugados (PhCH=CH- (**19**) o PhC≡C- (**20**) frente a Ph- (**18**)) induce un claro desplazamiento batocrómico en la banda MLCT (Figura 11).[56]

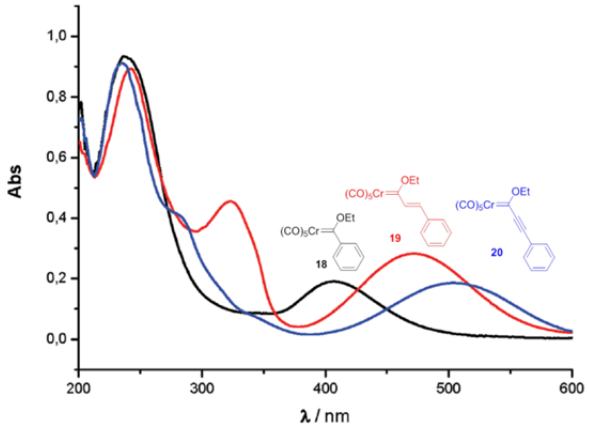

Figura 11. Espectro de UV/vis de los compuestos **18**, **19** y **20**.

Si bien la incorporación de complejos metal-carbeno de tipo Fischer como grupo electroaceptor en sistemas *push-pull* se llevó a cabo inicialmente en 1995,[38a] no fue hasta 2008 cuando se realizó un estudio sistemático sobre la influencia de los sutituyentes en las propiedades electrónicas de estos complejos (Figura 12).[56]

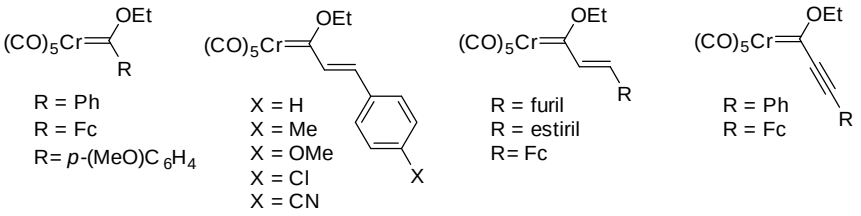

Figura 12. Estructuras estudiadas para determinar la influencia de distintos sustituyentes en las propiedades electrónicas.

Dichos sustituyentes claramente determinan la geometría de equilibrio de los complejos metal-carbeno α,β-insaturados de tipo Fischer. Así, complejos con sustituyentes π-dadores se describen mejor mediante la forma resonante **II** de la Figura 13. Como consecuencia directa, el enlace C1-C2 se acorta mientras que el

enlace Cr=C1 se alarga. El efecto opuesto ocurre en complejos con sustituyentes π-aceptores, en los que la forma resonante **II** apenas contribuye en la descripción de los mismos.

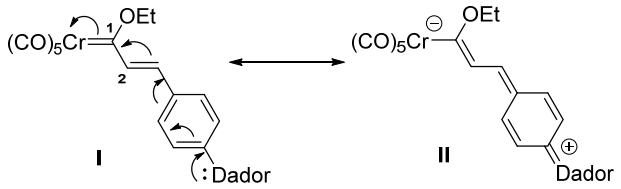

Figura 13. Posibles formas resonantes de los complejos α,β-insaturados de tipo Fischer.

Este trabajo concluye que si bien la posición de la banda MLCT depende ligeramente de la naturaleza electrónica del sustituyente en posición *para*- del grupo fenilo, la transición LF depende en gran medida de esta sustitución. Así, los sustituyentes π-dadores unidos al grupo fenilo provocan claros desplazamientos batocrómicos en la posición de la banda LF mientras que la banda MLCT apenas se ve afectada. En cambio, los grupos π-aceptores provocan un desplazamiento significativo de la banda LF hacia el azul y un pequeño desplazamiento hacia el rojo de la banda MLCT.

I.5. Complejos metal-BODIPY

I.5.1. Aspectos generales

La introducción del cromóforo 4,4-difluoro-4-bora-3a,4a-diaza-*s*-indaceno (BODIPY) en sistemas *push-pull* basados en complejos de metal de transición es de gran interés actualmente.[57] Esto es debido no sólo a las aplicaciones como

[57] (a) Collado, D.; Casado, J.; González, S. R.; Navarrete, J. T. L.; Suau, R.; Pérez-Inestrosa, E.; Pappenfus, T. M.; Raposo, M. M. M. *Chem. Eur. J.* **2011**, *17*, 498. (b) Burckstummer, H.; Kronenberg, N. M.; Meerholz, K.; Würthner, F. *Org. Lett.* **2010**, *12*, 3666. (c) Erten-Ela, S.; Yilmaz, M. D.; Icli, B.; Dede, Y.; Icli, S.; Akkaya, E. U. *Org. Lett.* **2008**, *10*, 3299. (d) Chu, T.-Y.; Lu, J.; Beaupré, S.; Zhang, Y.; Pouliot, J.-R. M.; Wakim, S.; Zhou, J.; Leclerc, M.; Li, Z.; Ding, J.; Tao, Y. *J. Am. Chem. Soc.* **2011**, *133*, 4250. (d) Ziessel, R.; Retailleau, P.; Elliott, K. J.; Harriman, A. *Chem. Eur. J.* **2009**, *15*, 10369. (e) Didier, P.; Ulrich, G.; Mely, Y.; Ziessel, R. *Org. Biomol. Chem.* **2009**, *7*, 3639. (f) Niu, S.; Ulrich, G.; Retailleau, P.; Ziessel, R. *Tetrahedron Lett.* **2011**, *52*, 4848. (g) Shi, W.-J.; Lo, P.-C.; Singh, A.; Ledoux-Rak, I.; Ng, D. K. P. *Tetrahedron* **2012**, *68*, 8712. (h) Ulrich, G.; Barsella, A.; Boeglin, A.; Niu, S.; Ziessel, R. *ChemPhysChem* **2014**, *15*, 2693.

fotosensibilizador de este fluoróforo sino también por su eficiencia en procesos de transferencia electrónica.[58]

Estas especies, descritas por primera vez por Treibs y Kreuzer en 1968,[59] han sido ampliamente estudiadas[60] y deben su valor a sus excepcionales propiedades ópticas: intensa absorción en el UV/Vis, emisión de fluorescencia con altos rendimientos cuánticos y elevada estabilidad (tanto química como fotoquímicamente).[61] Asimismo, pequeñas modificaciones en la estructura del BODIPY permiten modular las propiedades electrónicas de estos cromóforos. Otras ventajas adicionales son una buena solubilidad, su estabilidad en medios fisiológicos y su relativa insensibilidad a cambios en el pH del medio. Estas características convierten a los cromóforos basados en BODIPY en sistemas muy útiles para aplicaciones en biomedicina (marcaje de proteínas[62] y de ADN,[63] terapia fotodinámica[62b] e incluso tratamiento de cáncer)[64] y en ciencia de materiales (indicadores fluorescentes,[62a] OLED,[65] células solares,[66] interruptores moleculares,[67] fotosensores[68] y láseres).[69]

La unidad básica de BODIPY consta de un núcleo de dipirrometeno y un átomo de boro situados en el mismo plano. La numeración básica de este núcleo se indica en la Figura 14, donde R comúnmente es un átomo de flúor, aunque también se pueden encontrar grupos alcoxi, alquilo, arilo y alquinil derivados.

---

[58] Singh, S. P.; Gayathri, T. *Eur. J. Org. Chem.* **2014**, 4689.
[59] Treibs, A.; Kreuzer, F. H. *Justus Liebigs Ann. Chem.* **1968**, *718*, 208.
[60] Para revisions recientes, véase: (a) Boens, N.; Leen, V.; Dehaen W. *Chem. Soc. Rev.* **2012**, *41,* 1130. (b) Kamkaew, A.; Lim, S. H.; Lee, H. B.; Kiew, L. V.; Chung, L. Y.; Burgess K. *Chem. Soc. Rev.* **2013**, *42*, 77. (c) Shing, S. P.; Gayathri, T. *Eur. J. Org. Chem.* **2014**, *22*, 4689. (d) Frath, D.; Massue, J.; Ulrich, G.; Ziessel, R. *Angew. Chem., Int. Ed.* **2014**, *53*, 2290.
[61] Laudet, A.; Burgess K. *Chem. Rev.* **2007**, *107*, 4891.
[62] (a) Karolin, J.; Johansson, L. B.-A.; Strandberg, L.; Ny, T. *J. Am. Chem. Soc.* **1994**, *116*, 7801. (b) Tan, K.; Jaquinod, L.; Paolesse, R.; Nardis, S.; Di Natale, C.; Di Carlo, A.; Prodi, L.; Montalti, M.; Zaccheroni, N.; Smith, K. M. *Tetrahedron* **2004**, *60*, 1099. (c) Yee, M.-c.; Fas, S. C.; Stohlmeyer, M. M.; Wandless, T. J.; Cimprich, K. A. *J. Biol. Chem.* **2005**, *280*, 29053.
[63] Metzker, M. L. WO Patent WO/2003/066812, 2003.
[64] (a) Wang, F.; Zhu, Y.; Zhou, L.; Pan, L.; Cui, Z.; Fei, Q.; Luo, S.; Pan, D.; Huang, Q.; Wang, R.; Zhao, C.; Tian, H.; Fan, C. *Angew. Chem., Int. Ed.* **2015**, *54*, 7349. (b) Peña, B.; Barhoumi, R.; Burghardt, R. C.; Turro, C.; Dunbar, K. R. *J. Am. Chem. Soc.* **2014**, *136*, 7861.
[65] Owczarczyk, Z. R.; Brown, C. T.; Jarikov, V. V. US Patent 2005/0221120, 2005.
[66] Kubo, Y.; Eguchi, D.; Matsumoto, A.; Nishiyabu, R.; Yakushiji, H.; Shigaki, K.; Kaneko, M. *J. Mater. Chem. A* **2014**, *2*, 5204.
[67] (a) Golovkova, T. A.; Kozlov, D. V.; Neckers, D. C. *J. Org. Chem.* **2005**, *70*, 5545. (b) Trieflinger, C.; Rurack, K.; Daub, J. *Angew. Chem., Int. Ed.* **2005**, *44*, 2288.
[68] Daly, B.; Ling, J.; de Silva, A. P. *Chem. Soc. Rev.* **2015**, *44*, 4203.
[69] Pérez-Ojeda, M. E.; Thivierge, C.; Martin, V.; Costela, A.; Burgess, K.; García-Moreno, I. *Opt. Mater. Express* **2011**, *1*, 243.

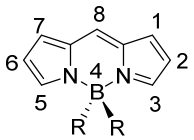

Figura 14. Estructura básica del fluoróforo BODIPY y su correspondiente numeración.

Una característica de estos fluoróforos es que la modificación sencilla del esqueleto permite una infinidad de oportunidades para modular sus propiedades ópticas (Figura 15).

Finalmente, el número de complejos metal-BODIPY ha ido creciendo a lo largo de los últimos años, puesto que la introducción de un complejo metálico en el sistema BODIPY permite modular las propiedades optoelectrónicas de los productos resultantes (Figura 16). No obstante, la introducción de un metal en el BODIPY generalmente desactiva su fluorescencia. En función del mecanismo de desactivación de la emisión por parte del metal de transición, se pueden obtener diversas propiedades optoelectrónicas y en consecuencia, aplicaciones distintas a las observadas en sistemas puramente orgánicos.

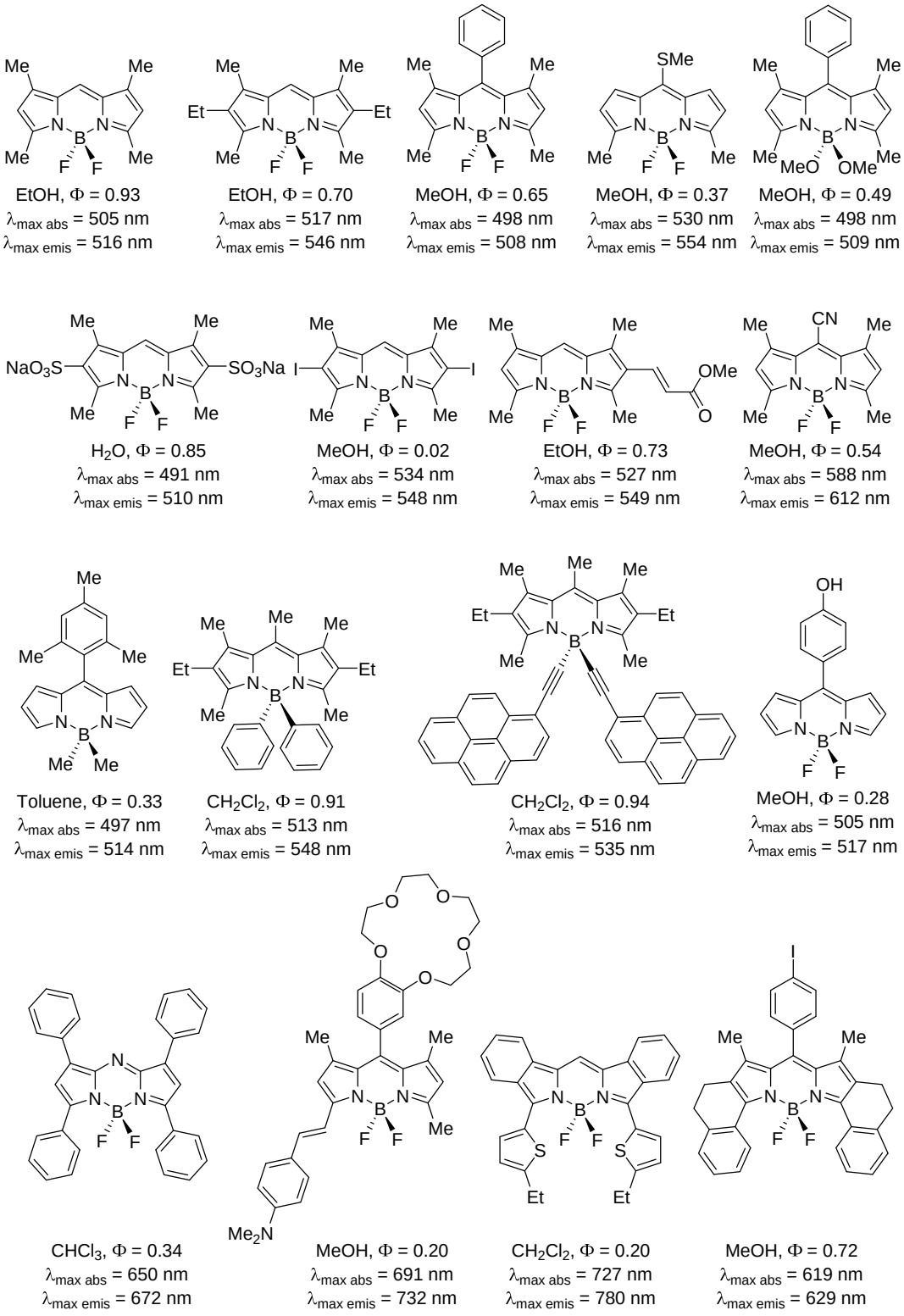

Figura 15. Ejemplos de distintos BODIPY.

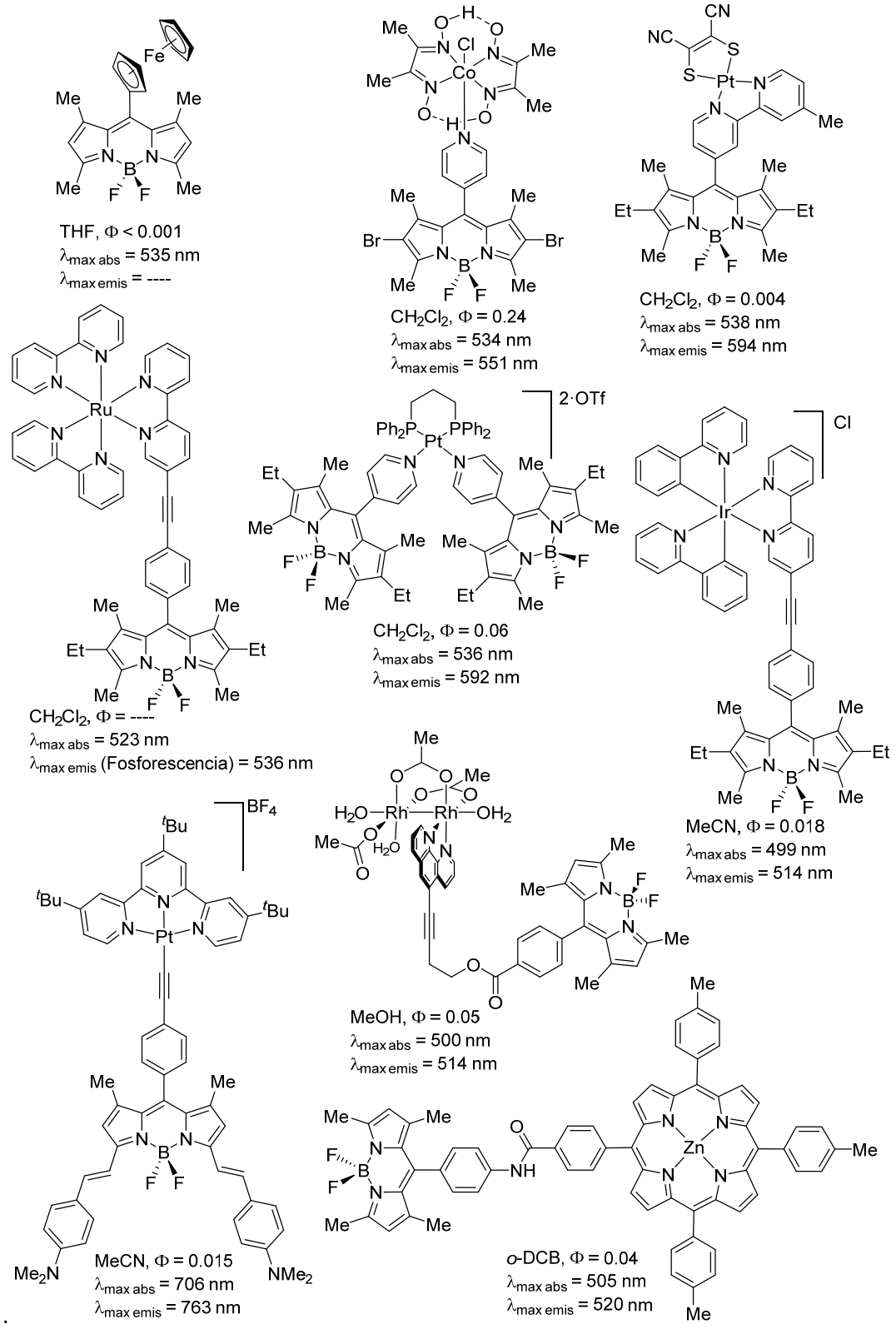

Figura 16. Ejemplos de complejos metal-BODIPY.

I.5.2. Mecanismos de desactivación de la fluorescencia en complejos metal-BODIPY[70]

Por desactivación de la fluorescencia se entiende cualquier proceso que disminuya la intensidad de emisión de un fluoróforo. En esta memoria se recogen los mecanismos más comunes de disminución y/o supresión de la fluorescencia para complejos metal-BODIPY. La desactivación se puede, por tanto, producir por los siguientes mecanismos:

- transferencia de energía de resonancia de Förster (FRET)
- cruce intersistémico (ISC)
- transferencia electrónica o interacción Dexter
- transferencia de electrones fotoinducida (PET)
- conversión interna (IC)

Es muy importante resaltar que muchas veces la desactivación de la fluorescencia no se debe a un único mecanismo sino que varios mecanismos pueden operar a la vez.

En cualquier caso, todos los mecanismos de desactivación son dependientes de la distancia entre el fluoróforo y el desactivador. Así, el valor de la transferencia de energía vía FRET viene dada por la siguiente ecuación:[70]

$$k_T(r) = \frac{1}{\tau_D}\left(\frac{R_0}{r}\right)^6 \qquad \text{(Ec.1)}$$

donde τ_D es el tiempo de vida del dador en ausencia del aceptor, *r* es la distancia entre el dador y el aceptor y R_0 es la distancia Förster, definida como la distancia a la cual la transferencia de energía tiene un 50% de eficiencia. Por otro lado, el valor de la transferencia electrónica se expresa mediante la siguiente ecuación:[70]

$$k_E(r) = A\, e^{[-\beta(r-r_c)]} \qquad \text{(Ec. 2)}$$

siendo *r* la distancia entre el fluoróforo y el desactivador, r_c, la distancia de la aproximación más cercana al contacto molecular y *A*, un factor preexponencial. El

[70] Para estudiar detenidamente los mecanismos de desactivación de la fluorescencia, véase: Lakowicz, J. R. *Principles of Fluorescence Spectroscopy*, 3rd ed.; Springer, **2006**.

ISC, la interacción Dexter y la PET se encuentran regidas por esta última ecuación, que depende exponencialmente de la distancia.

Un claro ejemplo de esta dependencia es el caso que describen Blum y colaboradores,[71] donde el rendimiento cuántico de fluorescencia de los complejos de paladio y zirconio es muy alto ya que el complejo metálico se encuentra relativamente alejado del fluoróforo BODIPY (Figura 17).

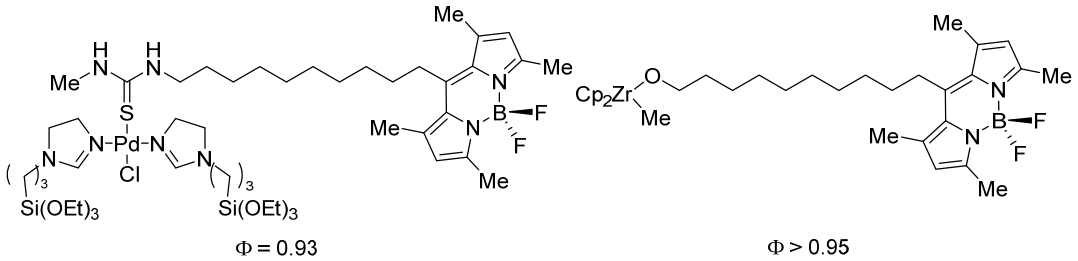

Figura 17.

I.5.2.1. Transferencia de energía de resonancia Förster

El mecanismo de FRET consiste en una interacción D-A a través del espacio que puede ocurrir a grandes distancias. Así, un dador en estado excitado transfiere la energía al fragmento aceptor, el cual se excita pudiendo emitir o no en función de la naturaleza del aceptor (Figura 18). Para que se produzca esta transferencia de energía la banda de emisión del dador y la banda de absorción del aceptor deben solapar en mayor o menor medida y no es necesario que haya un contacto molecular directo entre el dador y el aceptor. Por estas razones la FRET no depende de factores estéricos ni electrostáticos.

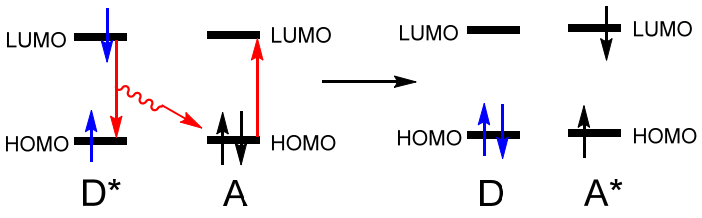

Figura 18. Diagrama de FRET.

[71] Canham, S. M.; Bass, J. Y.; Navarro, O.; Lim, S.-G.; Das, N.; Blum, S. A. *Organometallics* **2008**, *27*, 2172.

Un claro ejemplo de mecanismo FRET lo encontramos en díadas BODIPY-metaloporfirina. Se puede encontrar una extensa variedad de ejemplos en la bibliografía sobre antenas BODIPY-porfirina con diferentes cationes como Zn, Ni, Ru, Sn, Pt, Ga, Yb, Sb y Mg.[72] En la Figura 19 se muestran dos ejemplos representativos de complejos BODIPY-porfirina, uno basado en Ru[73] y otro en Zn.[74] Ambas especies tienen desactivada su fluorescencia mediante una transferencia de energía del BODIPY a la unidad de porfirina metalada de tipo FRET.

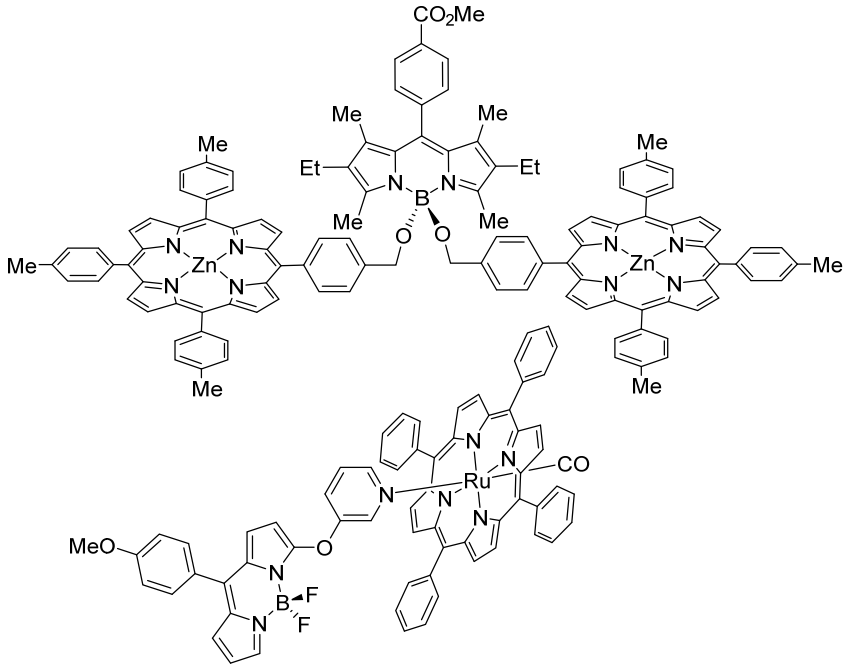

Figura 19.

Las tríadas supramoleculares BODIPY-porfirina de Zn-fullereno se han estudiado como sistemas de captación de luz artificiales.[75] El compuesto de la Figura 20 es capaz de captar un fotón provocando eficientemente la transferencia de energía desde el BODIPY excitado a la porfirina metalada. A continuación, se produce la transferencia electrónica al fullereno, con la correspondiente

[72] Khan, T. K.; Broering, M.; Mathur S.; Ravikanth, M. *Coord. Chem. Rev.* **2013**, *257*, 2348.
[73] Khan, T. K.; Ravikanth, M. *Tetrahedron* **2012**, *68*, 830.
[74] Brizet, B.; Eggenspiller, A.; Gros, C. P.; Barbe, J.-M; Goze, C.; Denat, F.; Harvey, P. D. *J. Org. Chem.* **2012**, *77*, 3646.
[75] (a) D'Souza, F.; Smith, P. M.; Zandler, M. E.; McCarty, A. L.; Itou, M.; Araki, Y.; Ito, O. *J. Am. Chem. Soc.* **2004**, *126*, 7898. (b) Bandi, V.; Gobeze, H. B.; Karr, P. A.; D'Souza, F. *J. Phys. Chem. C* **2014**, *118*, 18969.

separación de cargas. De esta manera, se sugiere que dichas tríadas actúan como mímicos de la fotosíntesis

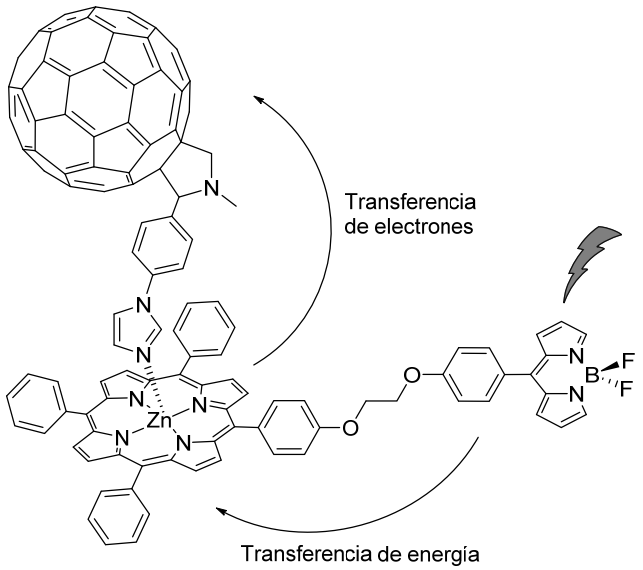

Figura 20.

I.5.2.2. Cruce intersistémico

El cruce entre sistemas se puede definir como un proceso en el que un electrón en el estado excitado pasa a un estado de menor energía con diferente multiplicidad.

Aunque los BODIPY se caracterizan por una formación del estado triplete prácticamente despreciable, es posible obtener fosforescencia con distintos sensibilizadores metálicos. De esta manera, Ziessel y colaboradores[76] describieron el primer BODIPY fosforescente (Figura 21). La estrategia utilizada por estos autores se basa en la población del estado triplete mediante el efecto del átomo pesado del metal de transición.[77] Para ello, se emplean metales de transición que poseen un tiempo de vida media elevado en el estado triplete.[78]

[76] Galletta, M.; Campagna, S.; Quesada, M.; Ulrich, G.; Ziessel, R. *Chem. Commun.* **2005**, *33*, 4222.

[77] Se entiende por efecto del átomo pesado al fenómeno observado en moléculas que poseen átomos con altos números atómicos. El aumento de electrones conlleva un aumento de las transiciones prohibidas por espín y de transiciones no emisivas. Koziar, J. C.; Cowan, D. O. *Acc. Chem. Res.* **1978**, *11*, 334.

[78] (a) Harriman, A.; Rostron, J. P.; Cesario, M.; Ulrich, G.; Ziessel, R. *J. Phys. Chem. A* **2006**, *110*, 7994. (b) Galletta, M.; Puntoriero, F.; Campagna, S.; Chiorboli, C.; Quesada, M.; Goeb, S.; Ziessel, R. *J. Phys. Chem. A* **2006**, *110*, 4348.

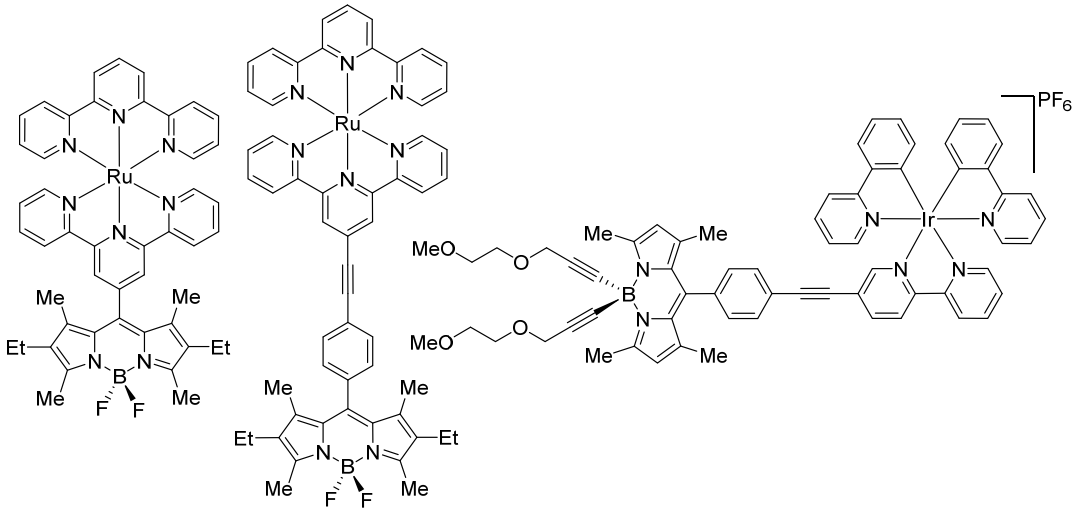

Figura 21.

Así, los sistemas metal-BODIPY pueden generar el estado triplete del BODIPY a baja temperatura. La excitación selectiva de la subunidad del metal provoca que la transferencia de energía triplete sea intramolecular (^{3}MLCT* → ^{3}BODIPY*) o que se genere el cruce intersistémico directo (^{1}BODIPY* → ^{3}BODIPY*) debido a la presencia del centro metálico (Figura 22).

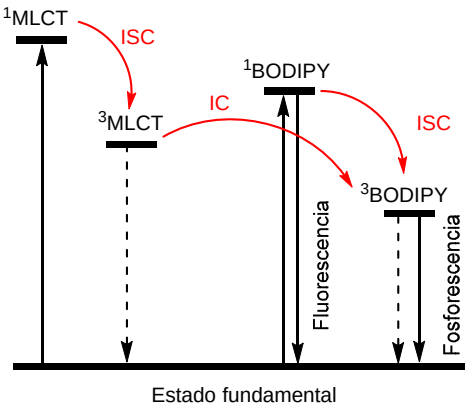

Figura 22.

A pesar de este precedente, no fue hasta el año 2013 en el que Zhao y colaboradores[79] describieron el primer metal-BODIPY con fosforescencia a temperatura ambiente (Figura 23). Estos sistemas Ir-BODIPY han sido estudiados como fotosensibilizadores triplete para aplicaciones como la fotooxidación con oxígeno singlete.

[79] Sun, J.; Zhong, F.; Yi, X.; Zhao, J. *Inorg. Chem.* **2013**, *52*, 6299.

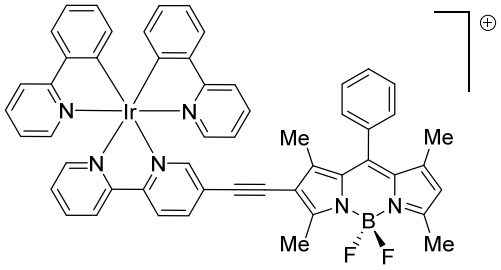

Figura 23. Primer metal-BODIPY fosforescente a temperatura ambiente.

I.5.2.3. Interacción Dexter

La interacción Dexter consiste en la transferencia de electrones a través de enlaces y depende del solapamiento efectivo de orbitales en sistemas conjugados. En el mecanismo Dexter, el fluoróforo excitado transfiere un electrón al LUMO del aceptor mientras que el aceptor transfiere a su vez otro electrón de su HOMO al HOMO del dador. Este proceso puede ocurrir de manera concertada o por etapas (Figura 24). Al igual que en el caso de la FRET, es necesario el solapamiento en mayor o menor medida entre la banda de emisión del dador y la banda de absorción del aceptor.

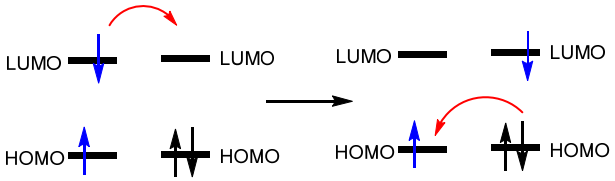

Figura 24. Diagrama de interacción Dexter.

Lindsey y colaboradores proponen que la eficiencia de la transferencia de energía a través de enlaces depende fundamentalmente de tres factores principales:[80]

- factores estéricos entre el dador y el aceptor
- energías relativas y características de los orbitales frontera
- naturaleza del espaciador que conecta el dador y el aceptor

[80] Holten, D.; Bocian, D.; Lindsey, J. S. *Acc. Chem. Res.* **2002**, *35*, 57.

En la Figura 25 se puede apreciar un cable molecular lineal diseñado por Lindsey y Wagner.[81] En este sistema, la transferencia de energía mediante la interacción Dexter desde el BODIPY a la porfirina no metalada se produce a través de porfirinas metaladas con una eficiencia muy alta.

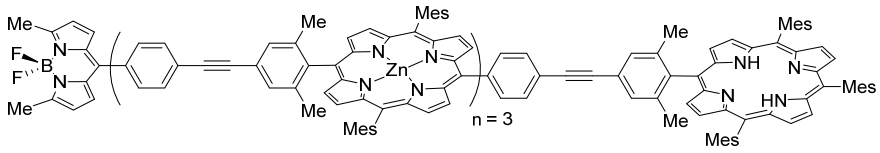

Figura 25.

No todos los mecanismos estudiados de desactivación son simples. En la literatura se encuentran ejemplos en los que varios mecanismos de desactivación actúan a la vez. Así Eisenberg y colaboradores[82] describieron una especie multicromofórica Pt-BODIPY con completa supresión de la emisión (Figura 26).

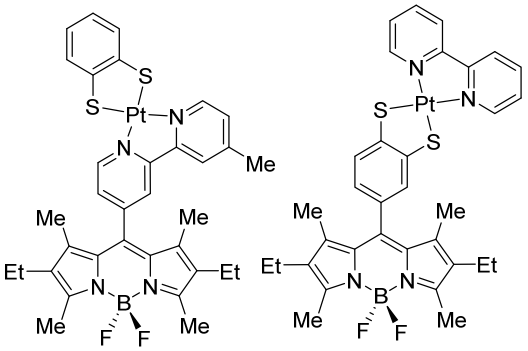

Figura 26.

En estas díadas se produce la excitación del BODIPY a su estado fotoexcitado singlete, seguido de una transferencia de energía singlete (SEnT) al singlete MMLL'CT del metal. Tras un ISC del singlete del metal al triplete, se produce una transferencia de energía triplete (TEnT) del metal al estado triplete del BODIPY. Estas dos transferencias de energía son atribuidas a un mecanismo Dexter. Por último, se produce el decaimiento no radiativo desde el estado triplete del BODIPY según se muestra en el diagrama de la Figura 27.

[81] Wagner, R. W.; Lindsey, J. S. *J. Am. Chem. Soc.* **1994**, *116*, 9759.
[82] Lazarides, T.; McCormick, T. M.; Wilson, K. C.; Lee, S.; McCamant, D. W.; Eisenberg, R. *J. Am. Chem. Soc.* **2010**, *133*, 350.

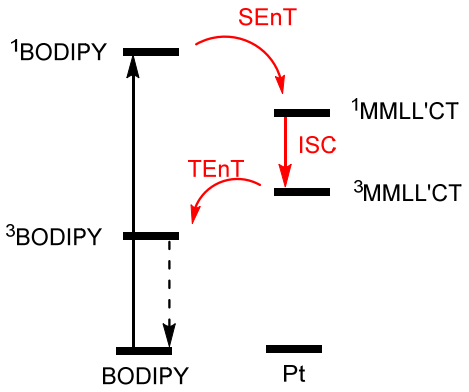

Figura 27.

I.5.2.4. Transferencia electrónica fotoinducida

La transferencia electrónica fotoinducida es el mecanismo más usual de desactivación de la fluorescencia en los sistemas metal-BODIPY. Este mecanismo de PET (del inglés, *Photoinduced Electron Transfer*) se basa en la fotoexcitación del fluoróforo que provoca una transferencia electrónica intramolecular. En la Figura 28 se representan los dos posibles mecanismos para este proceso: a) d-PET, donde el dador de electrones es el fluoróforo excitado, y b) a-PET, siendo el aceptor el fluoróforo fotoexcitado. En c) se representa al fluoróforo sin perturbación electrónica.

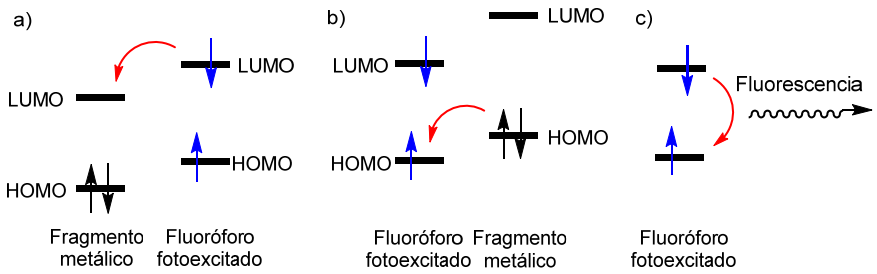

Figura 28. Diagrama PET.

Ravinkath y colaboradores[83] describieron varios sistemas ferroceno-BODIPY (Figura 29) en los que lograron modificar sus propiedades de emisión variando el estado de oxidación del metal. La oxidación del ferroceno al ión

[83] Rao, M. R.; Kumar, K. V. P.; Ravikanth, M. *J. Organomet. Chem.* **2010**, *695*, 863.

ferrocinio elimina el proceso de transferencia electrónica debido al catión Fe^{2+} responsable de la desactivación y, por tanto, restaura su fluorescencia.

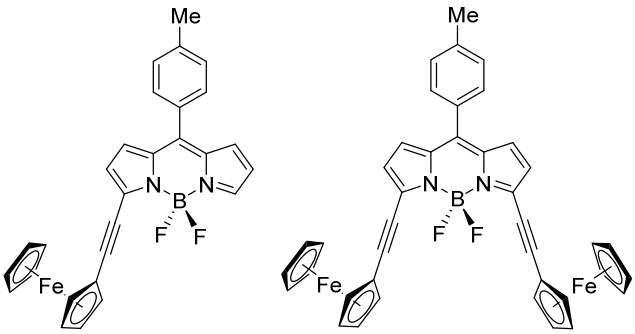

Figura 29.

Un estudio similar ha sido descrito por Lippard y Rosenthal.[84] Las díadas Cu(II)-BODIPY de la Figura 30 presentan una desactivación total de la fluorescencia como consecuencia de un mecanismo PET. Adicionalmente, la reducción a Cu(I) regenera las propiedades emisivas del fluoróforo.

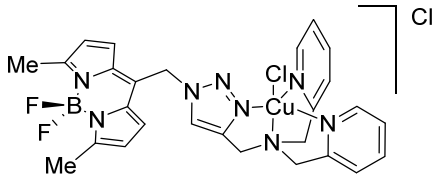

Figura 30.

Pryce y colaboradores[85] y Weare y colaboradores[86] describieron en el mismo año una díada muy parecida de Cobaloxima-BODIPY (Figura 31) para la generación electrocatalítica y fotocatalítica de hidrógeno, respectivamente. La fluorescencia de estos complejos Co-BODIPY se encuentra completamente suprimida debida a la transferencia electrónica desde el BODIPY fotoexcitado al complejo de cobalto. Este flujo de electrones se considera esencial a la hora de generar hidrógeno molecular.

[84] Rosenthal, J.; Lippard, S. J. *J. Am. Chem. Soc.* **2010**, *132*, 5536.
[85] Manton, J. C.; Long, C.; Vos, J. G.; Pryce, M. T. *Phys. Chem. Chem. Phys.* **2014**, *16*, 5229.
[86] Bartelmess, J.; Francis, A. J.; El Roz, K. A.; Castellano, F. N.; Weare, W. W.; Sommer, R. D. *Inorg. Chem.* **2014**, *53*, 4527.

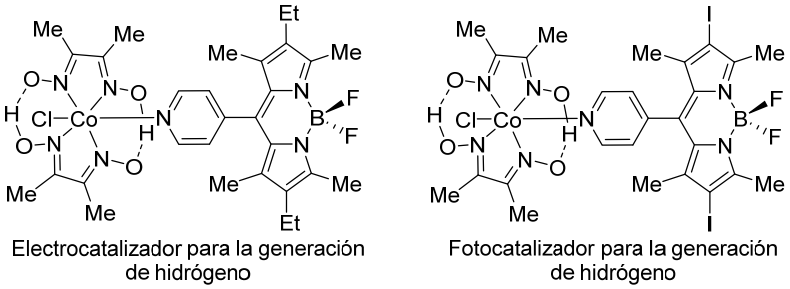

Figura 31.

El trabajo de Mirkin y colaboradores[87] demuestra que es posible modular la PET variando la esfera de coordinación del metal con ligandos hemilábiles (Esquema 5). Así, las propiedades de emisión de las díadas Pt-BODIPY se pueden modular mediante la variación de los ligandos unidos al metal (en este caso, cambio del S por el grupo NMe en el puente que une el Pt y el BODIPY).

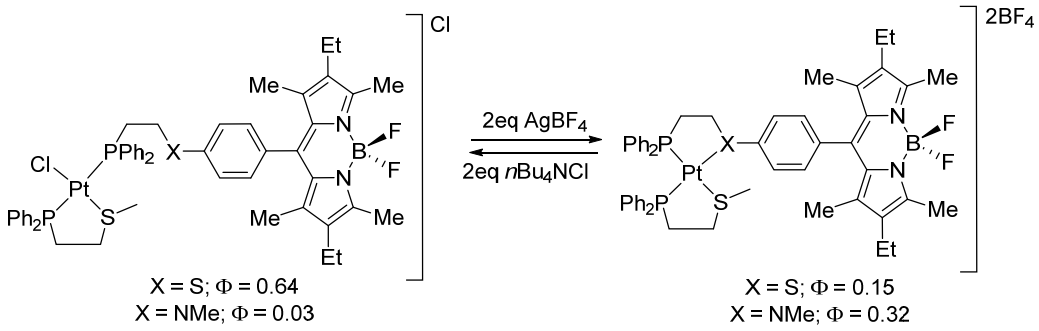

Esquema 5.

Plenio y Kos[88] han estudiado extensamente distintos complejos organometálicos conteniendo BODIPY funcionalizados con carbenos *N*-heterocíclicos (NHC) en su estructura (Figura 32). Este estudio demuestra que al reemplazar un ligando electrodador (cod) por un ligando electroaceptor (CO), un complejo completamente desactivado se puede convertir en uno con un rendimiento cuántico excelente. Además, se establece que el rendimiento cuántico depende claramente de la densidad electrónica sobre el metal de transición. Así, un metal rico en electrones provoca una disminución de la eficiencia de la desactivación por PET mientras un metal con menor densidad electrónica genera un incremento en la emisión de fluorescencia.

[87] Lifschitz, A. M.; Shade, C. M.; Spokoyny, A. M.; Mendez-Arroyo, J.; Stern, C. L.; Sarjeant, A. A.; Mirkin, C. A. *Inorg. Chem.* **2013**, *52*, 5484.
[88] Kos, P.; Plenio, H. *Chem. Eur. J.* **2015**, *21*, 1088.

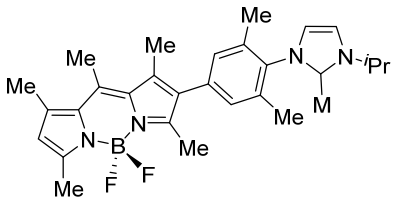

Figura 32.

I.5.2.5. Conversión interna

La conversión interna es un mecanismo por el cual un electrón excitado cae a un estado de menor energía con la misma multiplicidad sin emitir radiación. Suelen ser procesos indeseables debido a que compiten eficazmente con la emisión de la fluorescencia.

Un ejemplo de conversión interna es la rotación del grupo arilo en la posición C8 del BODIPY.[89] Mientras que en el BODIPY **21** existe una rotación libre de dicho grupo arilo, el BODIPY análogo **22** posee una rotación restringida debido a la presencia de los grupos metilo en posición *orto*- (Figura 33). Como consecuencia, las propiedades de emisión de estos compuestos son totalmente diferentes.

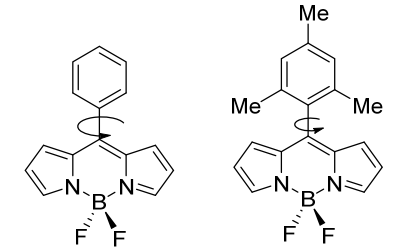

Figura 33.

Holten y colaboradores[89a] llevaron a cabo el estudio teórico de las superficies de energía potencial de los BODIPY **21** y **22** encontrando que la rotación del grupo arilo es clave para el proceso de emisión de los BODIPY. Por

[89] (a) Kee, H. L.; Kirmaier, C.; Yu, L.; Thamyongkit, P.; Youngblood, W. J.; Calder, M. E.; Ramos, L.; Noll, B. C.; Bocian, D. F.; Scheidt, W. R.; Birge, R. R.; Lindsey, J. S.; Holten, D.; *J. Phys. Chem. B* **2005**, *109*, 20433. (b) Hedley, G. J.; Ruseckas, A.; Harriman, A.; Samuel, I. D. W. *Angew. Chem., Int. Ed.* **2011**, *50*, 6634.

esta razón, se calculó la energía relativa del estado fundamental S_0 y de los estados excitados S_1 y T_1 frente al ángulo diedro definido por el plano del grupo arilo y el plano del BODIPY. El compuesto **21** posee una barrera rotacional a 180° en el estado fundamental S_0 de unos 50 kJ/mol. Además, posee mínimos de energía a 55° y 125° que concuerdan con los ≈ 60° determinados en la estructura de rayos-X.[89a] El estado triplete T_1 presenta una barrera rotacional de unos 25 kJ/mol y posee un mínimo local a 180°. En cambio, el estado singlete excitado de más baja energía (S_1) no posee una barrera rotacional sino que muestra un mínimo de energía en torno a los 180°. Esta conformación en el estado excitado se acopla eficientemente al estado fundamental por la conversión interna provocando un decaimiento no radiativo (Figura 34).

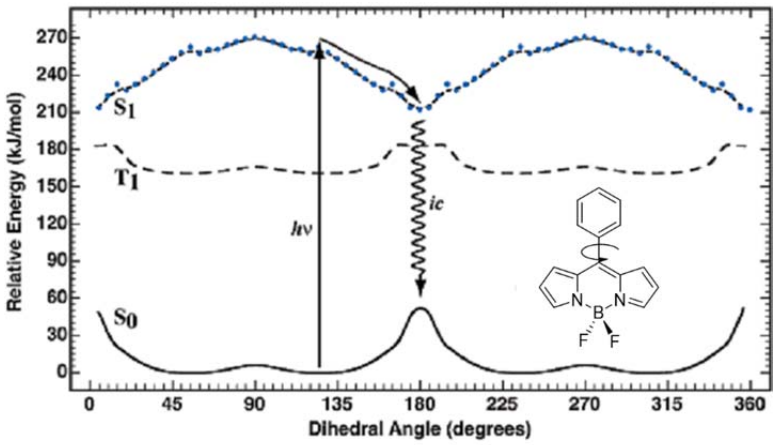

Figura 34. Superficies de energía potencial del estado fundamental y estados excitados S_1 y T_1 para el compuesto **21** (gráfico tomado de la referencia 89a).

El estudio de las superficies de energía del estado fundamental y el primer estado excitado del compuesto **22** es marcadamente diferente. En este caso, la rotación se encuentra impedida tanto en el estado S_0 como en el estado S_1 por una barrera más energética (≈ 150 kJ/mol y ≈ 60 kJ/mol, respectivamente). Por tanto, la orientación del grupo mesitilo apenas se modifica en ninguno de los dos estados singlete. Como consecuencia, la relajación del estado excitado al estado fundamental sólo se puede producir en forma de emisión radiativa eficiente (Figura 35).

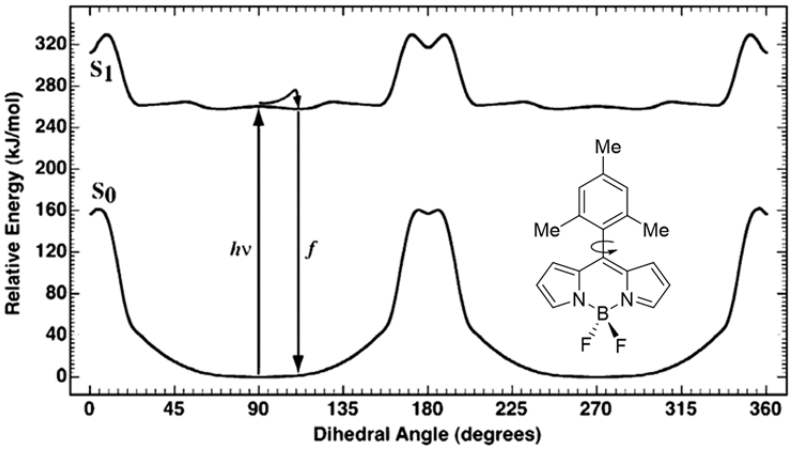

Figura 35. Superficie de energía potencial del estado fundamental y estado excitado S_1 para el compuesto **22** (gráfico tomado de la referencia 89a).

La fluorescencia de estos rotores moleculares se encuentra influenciada por la rotación libre del grupo arilo en posición C8 y éste, a su vez, es sensible a la viscosidad del medio, ya que limita su movimiento.[90] Zhu y colaboradores han descrito el comportamiento de las díadas metal-BODIPY frente a la viscosidad del medio[91] (Figura 36), demostrando que las propiedades de emisión del fluoróforo dependen en gran medida de dicha viscosidad.

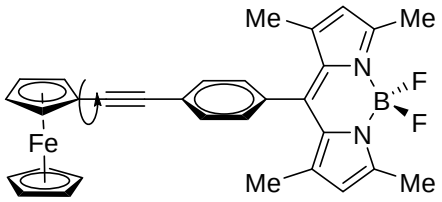

Figura 36.

[90] Kuimova, M. K.; Yahioglu, G.; Levitt, J. A.; Suhling, K. *J. Am. Chem. Soc.* **2008**, *130*, 6672.
[91] Yin, X.; Li, Y.; Zhu, Y.; Jing, X.; Li Y.; Zhu, D. *Dalton Trans.* **2010**, *39*, 9929.

II. *OBJETIVOS*

La presente tesis doctoral se centra en el estudio tanto teórico como experimental de nuevos sistemas *push-pull* basados en complejos organometálicos con el objeto de modular sus propiedades ópticas y electrónicas. A continuación, se detallan los objetivos particulares de este trabajo:

-Capítulo 1. El objetivo principal del primer capítulo de la memoria es el diseño de nuevos sistemas *push-pull* basados en complejos metal-carbeno de tipo Fischer. En concreto, se sintetizarán nuevas especies de tipo A-π-D-π-A donde se analizarán y estudiarán la influencia tanto del espaciador como del metal de transición sobre la geometría de equilibrio y las propiedades electrónicas de estos nuevos sistemas.

-Capítulo 2. El segundo capítulo presenta como objetivo principal el diseño de sistemas *push-pull* (D-π-A) empleando un complejo metal-carbeno de tipo Fischer (A) y un fluoróforo BODIPY (D) unidos mediante conjugación-π a través de un espaciador etileno. Asimismo, se modificará el heteroátomo unido directamente al carbono carbénico y se analizará su efecto sobre la estructura y las propiedades fotofísicas del fluoróforo.

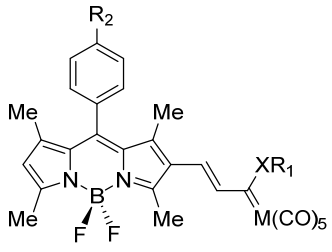

-Capítulo 3. El objetivo del tercer capítulo se centra en la síntesis y la caracterización de sistemas *push-pull* (D-π-A) de tipo BODIPY-metal carbeno de tipo Fischer con conjugación-π remota. Además, se evaluará la influencia que ejercen diversos factores, como el resto R y el par de electrones libre del

nitrógeno de la anilina en posición C8 del BODIPY sobre las propiedades electrónicas y emisivas de estas nuevas estructuras.

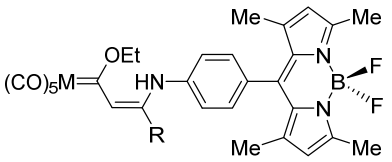

-Capítulo 4. El siguiente capítulo abordará el diseño de díadas metal-BODIPY unidas mediante diferentes unidades de grupo arilo. Así, se analizarán tanto la influencia que ejerce la naturaleza del metal como la distancia entre el fluoróforo y el fragmento metálico sobre las propiedades fotofísicas de estas díadas no coplanarias.

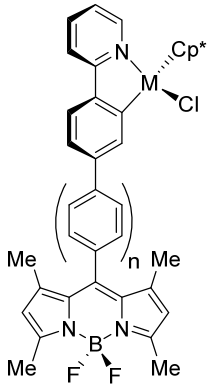

-**Capítulo 5**. Además, en el último capítulo se estudiará el efecto del ligando sobre la relación de isómeros *E/Z* obtenida en la reacción de dimerización catalítica de complejos metal-carbeno de tipo Fischer. Se buscarán las condiciones óptimas para obtener la mejor relación *E/Z* en la dimerización para su posterior aplicación en la síntesis de polienos altamente conjugados empleando otros complejos metal-carbeno de tipo Fischer.

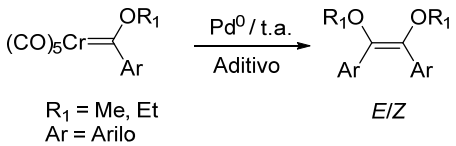

III. *CAPÍTULO 1*

III.1. *Synthesis, Structure, and Electronic Properties of Extended π-Conjugated Group 6 Fischer Alkoxy–Bis(carbene) Complexes*

Abstract: The synthesis, structure and electronic properties of novel Group 6 Fischer alkoxy–bis(carbene) complexes are reported. The UV/Vis spectra of these species display two main absorptions at approximately 350 and 550 nm attributable to a ligand-field (LF) and metal-to-ligand charge-transfer (MLCT) transitions, respectively. The planarity of the system and the cooperative effect of both pentacarbonyl metal moieties greatly enhance the conjugation between the group at the end of the spacer and the metal carbene fragment provoking dramatic changes in the LF and MLCT absorptions. This is in contrast to related push–pull Fischer monocarbenes, where the position of the MLCT band remains mostly unaltered regardless the substituent attached to the donor fragment. In addition, the MLCT maxima can be tuned with subtle modifications of the electronic nature of the central aryl fragment in the novel A-π-D-π-A (A=acceptor, D=donor) systems. DFT and time-dependent (TD)DFT quantum chemical calculations at the B3LYP/def2-SVP level have also been performed to determine the minimum-energy molecular structure of this family of compounds and to analyse the nature of the vertical one-electron excitations associated to the observed UV/Vis absorptions as well as to rationalise their electrochemical behaviour. The ability of tuning up the electronic properties of the compounds studied herein may be of future use in material chemistry.

Chem. Eur. J. **2013**, *19*, 5899.

III.2. Introduction

Fischer carbene complexes are attractive synthetic intermediates that are able to carry out a wide variety of organic transformations under mild reaction conditions.[1] Representative examples of the rich and versatile chemistry of this family of organometallic complexes are the useful Dötz benzannulation reaction,[2] which produces substituted phenols by reaction of the carbene with alkynes and carbon monoxide, different cycloaddition reactions,[3] the catalytic transmetalation to late transition metals,[4] which enhances the reactivity of the carbene complexes and the photochemical transformations[1h,5] (mainly the photocarbonylation reaction[6] but also photo-dyotropic rearrangements[7]).

Although these species have been mainly applied to organic and organometallic synthesis, nowadays their applications have been extended to other fields like bioorganometallics,[8] sugar-derived metal–carbene gelators,[9] and materials chemistry.[10] In the latter field, the well-known electronwithdrawing ability of the pentacarbonyl(metal) carbene moiety, which behaves similar to a Lewis acid complexed carbonyl function,[11] has been used in new push–pull molecules with interesting non-linear optical (NLO) properties. The good NLO behaviour of these complexes has been attributed to the polarisation of the π-electron system of the spacer connecting the carbene complex and the donor fragment produced by the strong electron-accepting character of the $(CO)_5M{=}C$ group.[10b]

On the other hand, we have studied the electronic structure of α,β-unsaturated Fischer carbenes **1**, where the $(CO)_5Cr{=}C$ group is connected to aryl groups, which have different substituents, through the simplest π-spacer moiety (i.e., HC=CH, Scheme 1).[12] It was found that π-donor groups lead to significant red shifts of the ligand-field (LF) band whereas π-acceptor groups provoke the opposite effect (λ_{max} ranging from 307 to 360 nm). However, this effect is not observed in the corresponding metal–ligand charge-transfer (MLCT) band, whose absorption maximum remains practically constant (λ_{max} ranging from 468 to 484 nm) and, therefore, it does not depend on the electronic nature of the

substituent. Moreover, the corresponding Cr-C bond lengths remain nearly constant as well, indicating that π conjugation between the metal fragment and the group attached to the spacer is not quite effective. Similar conclusion was drawn in previous reports on push–pull systems involving Fischer carbene complexes.[10b]

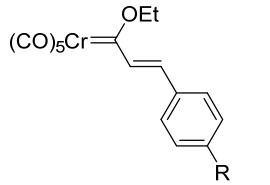

1: R = Ph, Me, OMe, Cl, CN, furyl, styryl, Fc

Scheme 1. α,β-Unsaturated Fischer carbenes studied previously (see Ref. (12)).

In order to gain a deeper understanding of the effect of π conjugation on Fischer carbene complexes, we have focused on a series of Fischer bis(carbene) complexes where the metal fragments are linked together through an aryl fragment by a conjugated spacer. Reported herein are the results of a combined experimental (structure, UV/Vis and electrochemistry)/computational study, which shows remarkable differences between the properties of these bis(carbene) complexes and their mononuclear counterparts.

III.3. Results and Discussion

Synthesis and structure of complexes 2: The Fischer bis(carbene) complexes **2** were prepared from the pentacarbonyl(ethoxy)methylchromium(0) or tungsten(0) carbene complexes **3a** or **3b** and the corresponding dialdehyde **4** in the presence of Et_3N and TMSCl following the reaction conditions reported by Aumann and Heinen.[13] Thus, to a solution of the dialdehyde (1 equiv) in anhydrous Et_2O, Et_3N (8 equiv), trimethylsilyl chloride (TMSCl, 6 equiv) and complex **3** (3 equiv) were added at room temperature and the mixture was stirred for 24 h. Removal of the solvent and purification of the residue by column chromatography allowed the isolation of the bis(carbene) complexes **2** in moderate to good yields (Scheme 2).

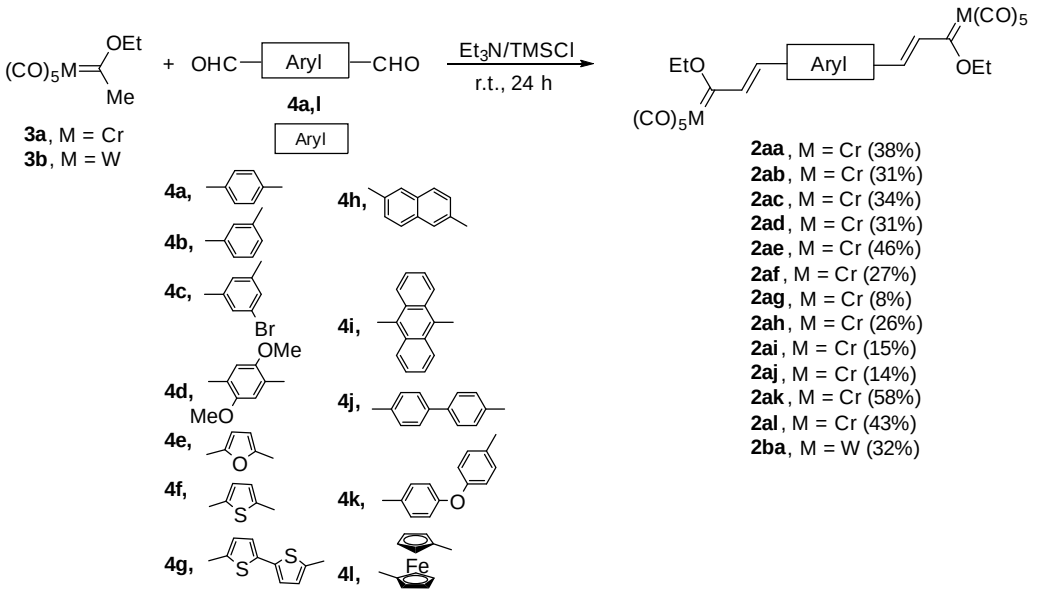

Scheme 2. Synthesis of the bis(carbene) complexes **2** through the Aumann reaction.

The structures of all bis(carbene) complexes were established by NMR experiments and by comparison with the data reported for complexes **2aa** and **2ac**,[13] and related species.[11,12,14] Thus, the carbene carbon atom directly attached to chromium(0) appears at $\delta \approx 330$ ppm in the corresponding ^{13}C-NMR spectrum, which is typical for α,β-unsaturated Fischer carbene complexes. Moreover, the olefinic hydrogen atoms exhibit a coupling constant of $J \approx 15$ Hz, attributable to the *E* stereochemistry of both double bonds. Furthermore, two possible isomers of bis(carbene) complexes **2**, which maintain the *E*–*E* stereochemistry on both double bonds and the *s-trans* conformation with the carbene fragment can be envisaged (Figure 1).

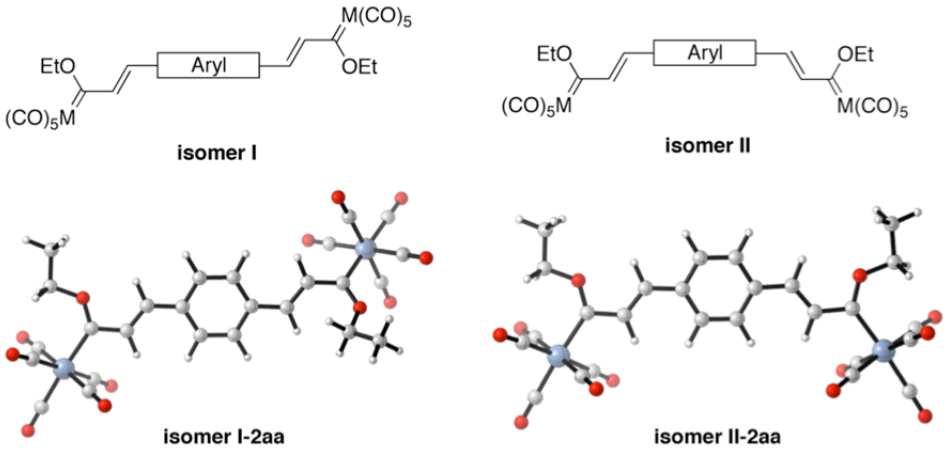

Figure 1. Schematic representation of the possible isomers of complexes **2** (top) and DFT-optimised geometries of both isomers of complex **2aa** (bottom).

Density functional theory (DFT) calculations carried out at the B3LYP/def2-SVP level (see Computational Details) on complexes **2aa**, **2ab**, **2ae**, **2af** and **2ba** clearly indicate that isomer **II** is invariably the most stable species (ΔE = 5.1, 4.5, 7.0, 7.4 and 8.5 kcal·mol^{-1}, respectively).[15] This computational prediction was experimentally confirmed with the help of a X-ray diffraction analysis on suitable crystals of the bis(carbene) complex **2af** (grown in pentane/ethyl acetate solution at 20°C).[16] The ORTEP diagram showed in Figure 2 indicates that isomer **II** is not only the preferred one in the gas phase but also in the solid state. This result suggests that the crystal packing has little influence, if any, in the conformation adopted by these species. Moreover and as expected, the ethoxy group directly attached to the carbene carbon atom adopts the so called *anti* conformation (i.e., the CH_2 group is oriented towards the CO wall of the metal fragment), which is the preferred conformation for most of the alkoxy Fischer carbene complexes in the gas phase and in the solid state.[17] Another important geometrical feature revealed by this experimental–computational study is the high planarity exhibited by these bis(carbene) complexes (see also Figure 1S in the Supporting Information), which plays a crucial role in their electronic structures (see below).

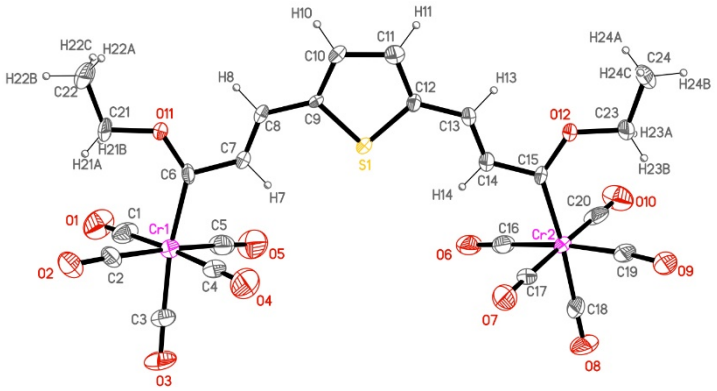

Figure 2. ORTEP diagram of compound **2af**. Ellipsoids are drawn at the 30 % probability level.

Electronic structure and optical properties: Figure 3 show the UV/Vis spectra of all chromium(0) bis(carbene) complexes **2aa–2al** recorded at room temperature in hexane with a concentration of approximately 1·10^{-5} mol·L^{-1} (see also Table 1). Similarly to related styryl monocarbene complexes,[12] the variation

of the π spacer leads to significant changes in the value of the wavelength of the absorption maxima of the LF band (λ_{max} ranging from 312 nm in **2ac** to 398 nm in **2af**). TD-DFT calculations were effected on complexes **1** and **2aa**–**2ai**, and the computed vertical excitation energies concur reasonably well with the experimental data (see Table 1). These calculations ascribe the LF absorption to the promotion of one electron from the HOMO-6 to the LUMO. As shown in Figure 4, these orbitals can be considered as π-extended molecular orbitals, which are delocalised in the carbene ligand and as a consequence, the LF band possesses a marked π–π* character. For this reason, it is not surprising that a modification of the electronic nature of the central aryl moiety is reflected in a significant change in the position of the LF band.

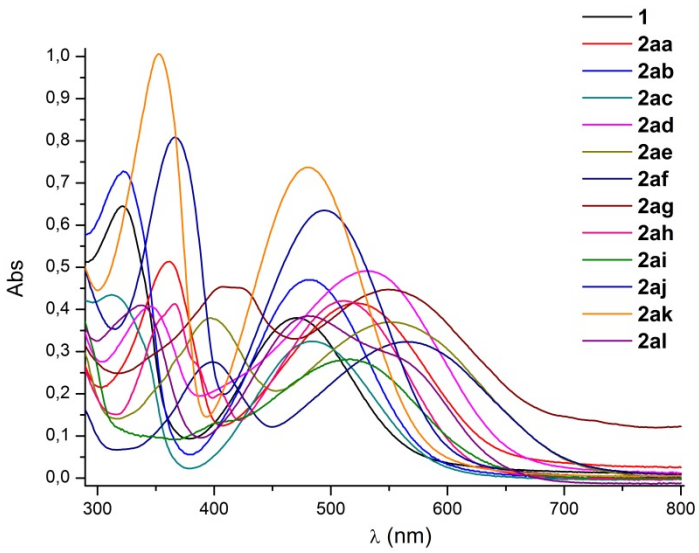

Figure 3. UV/Vis spectra of the bis(carbene) complexes **2**.

Table 1. Comparison of the main UV/Vis excitation energies, the oscillator strengths (*f*, in parenthesis) and the calculated bond lengths for complexes **1**, **2** and **5**.

	Complex	λ_1 (LF band) [nm][a]	Transition LF[b]	λ_2 (MLCT band) [nm][a]	Transition MLCT[b]	C_{ipso}-CH(=CH) [Å][c]	RCH=CHR' [Å][c]
1	**1**, R = H	323 (327, 0.59)	HOMO-3→LUMO	471 (453, 0.45)	HOMO-1→LUMO	1.460	
2	**2aa**	362 (383, 0.79)	HOMO-6→LUMO	523 (556, 0.98)	HOMO→LUMO	1.457 (1.135)	1.360 (1.675)
3	**2ab**	322 (327, 0.60)	HOMO-6→LUMO+1 (0.28) HOMO-7→LUMO (0.64)	482 (476, 0.28)	HOMO-3→LUMO (0.38) HOMO-2→LUMO+1 (0.58)	1.464 (1.114)	1.358 (1.700)
4	**2ac**	312 (333, 0.59)	HOMO-7→LUMO+1	485 (480, 0.26) (457, 0.46)	Combination band HOMO-3→LUMO HOMO-2→LUMO+1	1.465 (1.110)	1.357 (1.704)
5	**2ad**	356 (369, 0.60)	HOMO-6→LUMO	531 (579, 1.10)	HOMO→LUMO	1.453 (1.143)	1.362 (1.657)
6	**2ae**	397 (412, 0.40)	HOMO-6→LUMO	552 (604, 0.49)	HOMO→LUMO	1.429 (1.187)	1.364 (1.636)
7	**2af**	398 (413, 0.57)	HOMO-6→LUMO	565 (608, 0.76)	HOMO→LUMO	1.436 (1.191)	1.364 (1.638)
8	**2ag**			549			
9	**2ah**	366 (370, 0.39)	HOMO-7→LUMO	511 (546, 1.20)	HOMO→LUMO	1.460 (1.129)	1.360 (1.678)
10	**2ai**	404 (455, 0.08)	HOMO→LUMO+1	516 (494, 0.10)	HOMO-3→LUMO	1.465 (1.106)	1.360 (1.699)
11	**2aj**	366		494			
12	**2ak**	352		480			
13	**2al**	336		580			
14	**2ba**	357		489			
15	**5**	362		511			

[a] The first value corresponds to experimental data (recorded at room temperatura in hexane with a concentration ≈ 1 x 10^{-5} mol·L^{-1}). In prenthesis, the first value corresponds to the computed PCM (hexane)-TD-B3LYP/def2-SVP vertical excitation energy and the second value is the corresponding oscillator strength. [b] Time-dependent (TD) DFT vertical transition assigned to the observed band. [c] Computed bond lengths C_{ipso}-CH(=CH) and RCH=CHR'. Corresponding Wiberg bond índices are given in parenthesis.

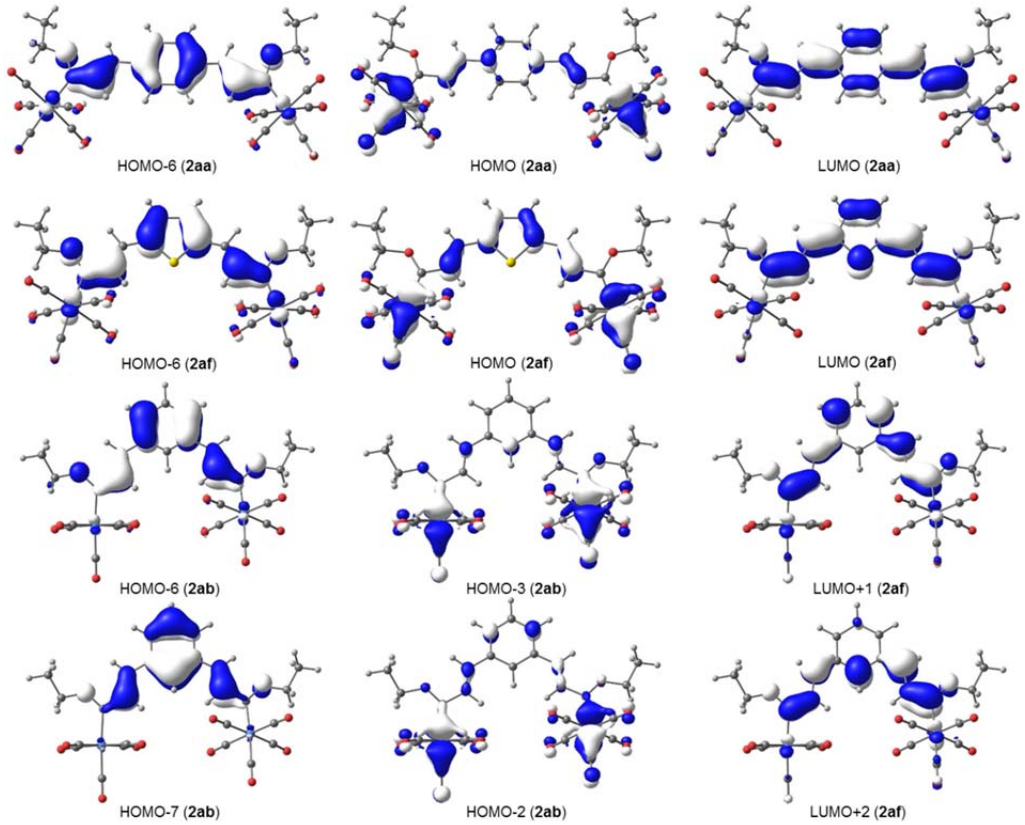

Figure 4. Computed molecular orbitals of complexes **2aa**, **2ab** and **2af** (isosurface value of 0.035au).

Strikingly, a remarkable dependence of the position of the wavelength of the absorption maximum of the MLCT band with the nature of the π connector is also observed in this family of bis(carbene) complexes. This behaviour is clearly different to that observed for their related monocarbene counterparts, where the position of the MLCT band remains practically constant and independent of the electronic nature of the substituent.[12] Indeed, a strong bathochromic shift is induced in the parent bis(carbene) complex **2aa** (λ_{max} = 523 nm) compared to its monocarbene counterpart **1a** (λ_{max} = 471 nm). This finding can be ascribed to the cooperative effect of both acceptor pentacarbonylmetal moieties, which greatly enhances the conjugation between the aryl group and the metal carbenes through the π spacer. This is confirmed in complexes **2ab** and **2ac** (where the *meta*-disubstituted phenyl group interrupts the conjugative path). Now the MLCT absorption maxima (λ_{max} = 482 and 485 nm, respectively) resemble that of monocarbene **1a**. A similar situation is found in complexes **2aj** and **2ak**, where the nonplanar biphenyl and biphenylether fragments, respectively, make the

electronic communication more difficult (λ_{max} = 490 and 484 nm, respectively). Likewise, in compound **2ai** the *ipso* hydrogen atoms of the adjacent phenyl rings enforce the non-planarity of the π system (see Figure 5) and as a result, λ_{max} (MLCT) is slightly blue shifted compared to the parent bis(carbene) **2aa**.

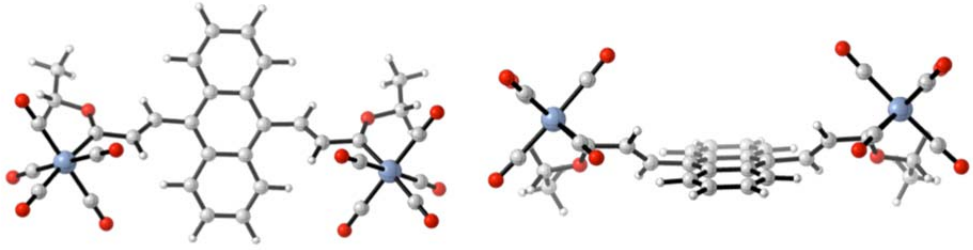

Figure 5. Different views of the DFT-optimised geometry of complex **2ai**.

From the data shown in Figure 3 and Table 1, it becomes obvious that the position of the MLCT band can be tuned with subtle modifications of the electronic nature of the central aryl fragment. Thus, the replacement of two hydrogen atoms in the parent complex **2aa** by two methoxy groups (complex **2ad**) leads to a slight red shift of the MLCT band (from 523 to 531 nm). This finding seems to indicate that an increase in the electronic density of the aryl group (by introducing good π donors like methoxy groups) results in a more effective conjugation in the A-π-D-π-A (A = acceptor, D = donor) system. This hypothesis is clearly confirmed by complexes **2ae** and **2af**, where the phenyl group is replaced by a stronger donor bridge like furyl and thienyl groups, respectively, whose MLCT bands are remarkably red shifted when compared to **2aa** (from 523 to 552 and 565 nm, respectively). A similar behaviour is observed in the bithienyl-substituted complex **2ag** (λ_{max} = 549 nm) and the ferrocenyl bis(carbene) complex **2al** (λ_{max} = 580 nm), thus confirming the reported donor character of the Cp_2Fe (Cp = cyclopentadienyl) group in this kind of complexes.[12] Therefore, it can be concluded that the introduction of the second carbene complex unit in these novel A-π-D-π-A species induces a quite significant bathochromic shift ($\Delta\lambda_{max} \approx$ 100 nm) in the position of the, otherwise invariable, MLCT band. This bathochromic shift strongly depends on, and therefore it can be tuned by, the electronic nature of the bridge. The effect is even more appealing when compared

with the position of the MLCT band in monocarbene complexes analogues to **1**, which is essentially invariable.

TD-DFT calculations ascribe the MLCTabsorption to the promotion of one electron from the HOMO to the LUMO (Table 1). Whereas the LUMO can be considered as a π-extended molecular orbital delocalised in the carbene ligand, which includes the p_z atomic orbital of both carbene carbon atoms, the HOMO is mainly centred in a d_π atomic orbital of both transition metals (Figure 4). Therefore, and similar to the LF band, the MLCT absorption can be viewed as a π-π* transition. In those cases where the conjugative path is interrupted (like in **2ab** or **2ac**, for instance), the involved orbitals resemble those of the monocarbene analogues. Thus, the MLCT band results of the combination of the HOMO-3 → LUMO and HOMO-2 → LUMO+1 vertical transitions.

The predominant π-π* character of both transitions should be reflected in a small solvatochromism.[18] Thus, the UV/Vis spectra of complex **2aa** were recorded in solvents with different polarity (i.e., hexane, CH_2Cl_2, MeOH and MeCN). Figure 6 shows that the LF absorption, which involves genuine π orbitals, is nearly independent of the polarity of the solvent ($\Delta\lambda_{max}$ = 4 nm). Similarly, a small solvatochromic effect in the MLCT absorption is observed ($\Delta\lambda_{max}$ in the range of 10–24 nm). Therefore, both results provide further experimental support to the π-π* computational predicted nature of both transitions.

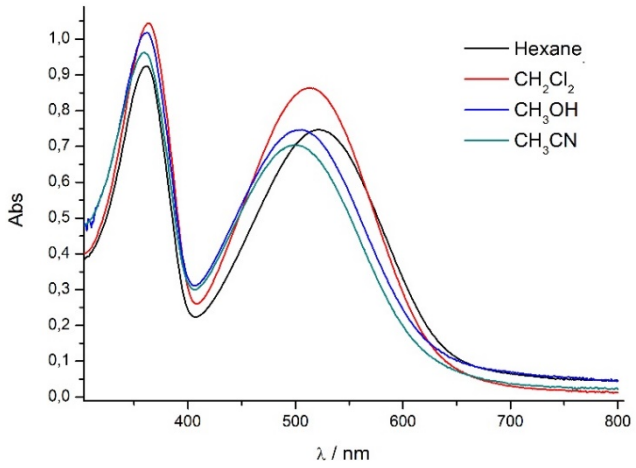

Figure 6. UV/Vis spectra of compound **2aa** conducted in different solvents.

The enhanced π conjugation in this novel A-π-D-π-A chromophores should be in addition reflected in measurable changes in the equilibrium geometry of the different compounds. Thus, the contribution of the resonance structure **II** (Scheme 3) should be higher in those compounds where the conjugation is more effective (i.e., those exhibiting MLCT bands at longer λ_{max}). As a result of the population of this resonance form, the C_{ipso}-CH (=CHR) bond becomes stronger (and the corresponding bond length shorter), whereas the ArylCH=CHR double bond becomes weaker (and the corresponding bond length longer). From the data in Table 1, it becomes obvious that the contribution of the resonance form **II** in complexes **2ab**, **2ac** and **2ai**, where the conjugative path is interrupted, is not important as they exhibit the longest C_{ipso}-C bond lengths (associated Wiberg bond indices (WBIs) ranging from 1.106 to 1.114 au) and the shortest C=C bonds (associated Wiberg bond indices ranging from 1.699 to 1.704 au). In contrast, for those systems where the π conjugation is more effective and their MLCT bands are significantly red shifted (**2aa**, **2ad**, **2ae** and **2af**), the opposite trend was found in the optimised equilibrium geometries. Thus, the latter species possess stronger C_{ipso}-C bonds (associated Wiberg bond indices ranging from 1.135 to 1.191 au) and weaker C=C bonds (associated Wiberg bond indices ranging from 1.636 to 1.675 au). As the extension of the π conjugation is the major factor controlling the position of the MLCT band and the equilibrium geometries of the bis(carbene) complexes **2**, it is not surprising that both parameters are correlated. Indeed, good linear relationships between the computed Wiberg bond indices of the C_{ipso}-C and the C=C bonds and the experimental wavelength of the MLCT absorption maxima have been found (Figure 7, λ_{max} vs. WBI (C_{ipso}-C): correlation coefficient = 0.93 and standard error = 0.01; λ_{max} vs. WBI (RHC=CHR): correlation coefficient = 0.90 and standard error = 0.02).

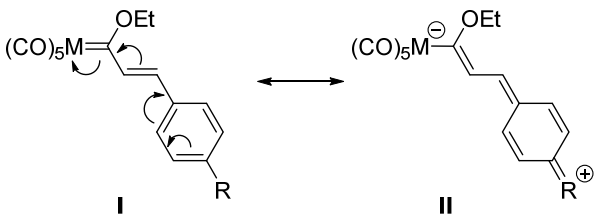

Scheme 3. Possible resonance forms of an α,β-unsaturated Fischer carbene complex.

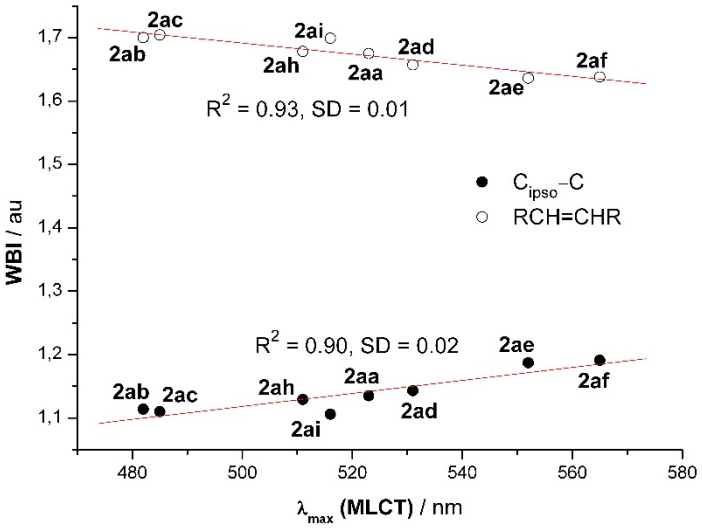

Figure 7. Plot of the experimental λ_{max} (MLCT) versus the computed Wiberg bond indices of the C_{ipso}-C (•) and the RCH=CHR' (◦) bonds.

Finally, the effect of the transition metal on the electronic structure of the bis(carbene) complexes was also addressed. To this end, we have analysed the UV/Vis spectra of the bischromium(0) carbene complex **2aa**, the bistungsten(0) carbene complex **2ba** and the mixed Cr^0–W^0 complex **5**, which is synthesised in a two-steps procedure from carbene complex **3a** through complex **6** (Scheme 4).

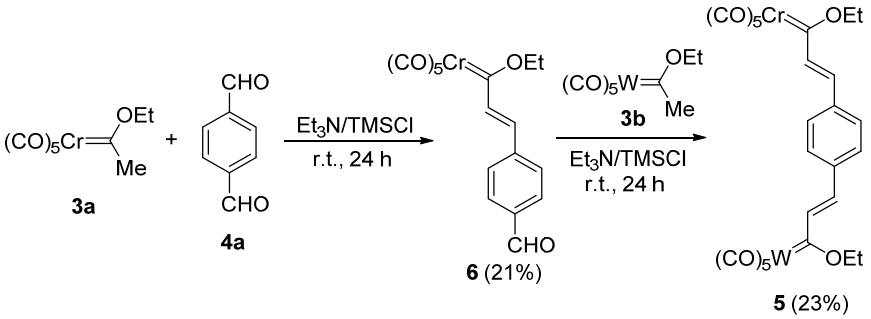

Scheme 4. Synthesis of mixed bis(carbene) complex **5**.

Figure 8 shows the UV/Vis spectra of complexes **2aa**, **2ba** and **5**. As the metal fragments are not directly involved in the LF absorption, no significant differences are observed in the corresponding wavelength of the absorption maxima (see data in Table 1). Differently, a remarkable change in the position of the MLCT band is found when replacing the chromium(0) in **2aa** by tungsten(0) in **2ba** (λ_{max} = 523 and 489 nm, respectively). According to the arguments discussed

above, this result indicates that the extension of the π conjugation in **2ba** is lower than in **2aa**. This finding nicely agrees with the well-known lower acceptor capacity of the pentacarbonyl tungsten(0) carbene fragment compared to its chromium(0) counterpart, which is the result of the higher π-backdonation ability of tungsten(0). Interestingly, the maximum of the MLCT band of the mixed complex **5** appears at an intermediate position of **2aa** and **2ba** (λ_{max} = 511 nm), which further supports the above-mentioned cooperative effect of both pentacarbonyl metal moieties to enhance the conjugation between the aryl group at the end of the spacer and the metal carbene fragment.

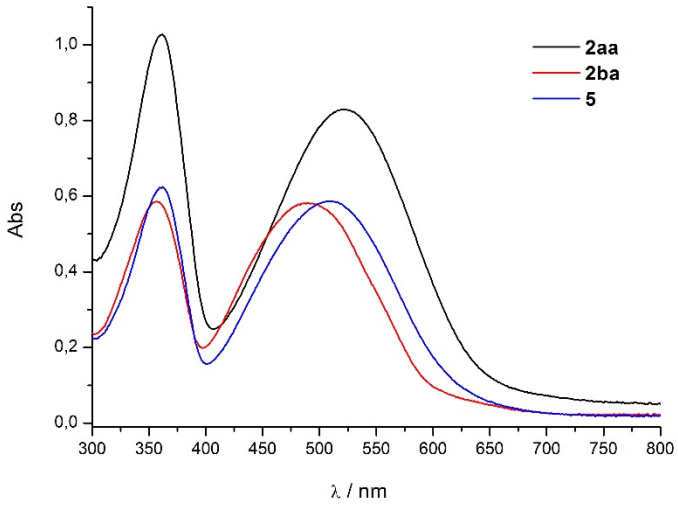

Figure 8. UV/Vis spectra of the bis(carbene) complexes **2aa**, **2ba** and **5**.

Electrochemistry: To gain more insight into the properties of this family of bis(carbene) complexes, their electrochemistry was also studied. The cyclic voltammograms of complexes **1**, **2** and **5** (those of complexes **2** are shown in Figure 9) were recorded (CH_2Cl_2 solutions with the addition of 0.1M NBu_4ClO_4, as the supporting electrolyte). Oxidation potentials were measured by using an Ag/AgCl reference electrode, a glassy carbon working electrode and a platinum counter electrode. Similar to related α,β-unsaturated alkoxy monocarbene complexes **1**[19] most of the considered bis(carbene) complexes **2** exhibit two irreversible oxidation waves in the range +0.99 to +1.54 V (Figure 9 and Table 2), which can be ascribed to the irreversible formation of the corresponding radical

cation and dication species, respectively. Although the differences in the first oxidation potential (1st E_{pa}) are small, they are significant. From the data given in Table 1, a correlation between the computed HOMO and the 1st E_{pa} can be found. Thus, computed higher (i.e., less negative) HOMO values should lead to lower 1st E_{pa} values, resulting in an easier formation of the corresponding radical cation. With the notable exception of complex **2ai** (Table 2, entry 10), the higher HOMO values were found, not surprisingly, for the species with enhanced π-conjugation (**2ad**, **2ae**, **2af** and **2ag**). These data are an additional proof of the effect of the second metal moiety in the bis(carbene) A-π-D-π-A system, and support the structural and electronic properties discussed above.

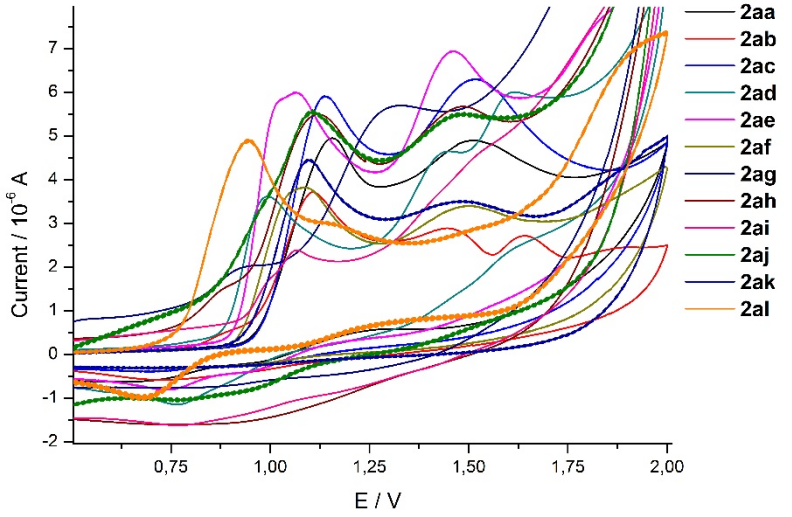

Figure 9. Cyclic voltammograms for complexes **2** in CH_2Cl_2 containing NBu_4ClO_4 (0.1 M) as supporting electrolyte (Ag/AgCl as a reference).

Table 2. Electrochemical data[a] and HOMO energies[b] of complexes **1**, **2** and **5**.

Entry	Complex	1st E_{pa} [V]	2nd E_{pa} [V]	3rd E_{pa} [V]	HOMO [eV]
1	**1**	1.12	1.46		-5.89
2	**2aa**	1.16	1.51		-5.98
3	**2ab**	1.11	1.44	1.64	-5.93
4	**2ac**	1.14	1.52		-5.99
5	**2ad**	0.99	1.45	1.61	-5.79
6	**2ae**	1.06	1.46		-5.83
7	**2af**	1.08	1.50		-5.89
8	**2ag**	0.92	1.32		
9	**2ah**	1.12	1.48		-5.93
10	**2ai**	0.99			-5.68
11	**2aj**	1.11	1.48		
12	**2ak**	1.09	1.50		
13	**2al**	0.96	1.24		
14	**2ba**	1.22	1.54		
15	**5**	1.11	1.39		

[a] Measured in CH_2Cl_2, with 3 M Ag/AgCl as a reference. [b] Data computed at the B3LYP/def2-SVP level.

III.4. Conclusions

Novel π-extended alkoxy Fischer bis(carbene) complexes have been prepared by the reaction of the corresponding dialdehydes with alkoxychromium(0) and alkoxytungsten(0) carbene complexes by using the standard conditions reported by Aumann.[13] The UV/Vis spectra of these species display two main absorptions at approximately 350 and 550 nm attributable to ligand-field (LF) and metal-to-ligand chargetransfer (MLCT) transitions, respectively. According to TD-DFT calculations, these absorptions are ascribed to the HOMO-6 → LUMO (LF) and the HOMO → LUMO (MLCT) vertical transitions and possess a remarkable π–π* character. The planarity of the system and the cooperative effect of both pentacarbonyl metal moieties greatly enhance the conjugation between the tether and the metal carbene fragment, which is reflected in dramatic changes in the LF and MLCTabsorptions. This behaviour is markedly different to that observed for the monocarbene counterparts **1**,[12] whose MLCT band is nearly indifferent to the nature of the substituent attached to the aryl fragment. This study shows that the MLCT maxima can be tuned with subtle

modifications of the electronic nature of the central aryl fragment connecting both metal moieties in the novel A-π-D-π-A systems. As a consequence of the extended π conjugation, a strong correlation between the equilibrium geometries of these bis(carbene) complexes and their optical properties is observed. The experimental electrochemical data (the first oxidation potential, 1st E_{pa}) also correlates with the computed HOMO energies of the different complexes. The ability of tuning up the electronic properties of the compounds studied herein may be of future use in material chemistry.

III.5. Computational Methods

Geometry optimisations without symmetry constraints were carried out by using the Gaussian 09 suite of programs[20] with the B3LYP[21] functional in combination with the double-ζ plus polarisation def2-SVP basis sets[22] for all atoms. This level is denoted B3LYP/def2-SVP. Stationary points were characterised as minima by calculating the Hessian matrix analytically at this level. Calculations of absorption spectra were accomplished by using the time-dependent density functional theory (TD-DFT)[23] method at the same level. TD-DFT calculations were performed in hexane as solvent by using the polarisable continuum model (PCM) method.[24] The assignment of the excitation energies to the experimental bands was performed on the basis of the energy values and oscillator strengths. The B3LYP Hamiltonian was chosen because it was proven to provide reasonable UV/Vis spectra for a variety of chromophores[25] including Fischer carbene complexes[17] and other organometallic species.[26] Despite that, the B3LYP functional sometimes underestimate the energy of the charge-transfer (CT) excited states. This shortcoming of standard global hybrid functionals has been reported for donor–acceptor compounds for which there is a negligible overlap between the molecular orbitals involved in the excitation.[27] To solve the problem, the use of a long-range corrected functional as, for example, the CAM-B3LYP functional,[28] is recommended. However, the CAM-B3LYP approach completely fails in reproducing the optical spectra of **2aa**. Wiberg bond indices were computed by using the natural bond orbital (NBO) method.[29]

III.6. Experimental Section

All reactions were carried out under an argon atmosphere. All solvents used in this work were purified by distillation and were freshly distilled immediately before use. Triethylamine (Et_3N) was distilled from calcium hydride, whereas diethyl ether (Et_2O) was purified by using a Pure Solv PS-MD-5 system. Flame-dried glassware was used for moisture-sensitive reactions. Silica gel (Merck: 230–400 mesh) was used as stationary phases for purification of crude reaction mixtures by flash column chromatography under Ar pressure. Identification of products was made by thin-layer chromatography (Kieselgel 60F-254). UV light (λ = 254 nm) and 5% phosphomolybdic acid solution in 95% EtOH were used to develop the plates. NMR spectra were recorded at 25°C in $CDCl_3$ on a Bruker Avance 300 (300 MHz for ^1H and 75 MHz for ^{13}C) or a Bruker AM-500 (500 MHz for ^1H and 125 MHz for ^{13}C) spectrometer. Chemical shifts are given in [ppm] relative to $CDCl_3$ ($\delta(^1H)$ = 7.27 ppm and $\delta(^{13}C)$ = 77.0 ppm). UV measures were recorded on a Varian (Cary 50) spectrometer. IR spectra were taken on a MIR (8000–400 cm^{-1}) spectrometer as solid films by slow evaporation of the solvent by using the ATR (attenuated total reflectance) technique. Cyclic voltammetry (CV) was performed at room temperature in CH_2Cl_2 solutions containing 0.1M NBu_4ClO_4 as supporting electrolyte. Electrochemical analyses were performed on a PG-STAT 302N potentiostat (Autolab) by using a Metrohm 6.084.010 glassy

carbon electrode (GCE) as the working electrode with a BAS MF 2063 Ag/AgCl (3M) reference electrode and a Pt wire counter electrode. The electrochemical software was General Purpose Electrochemical System (GPES; EcoChemie B.V.). HRMS was recorded on a QTOF 6520: HP-1200 (Agilent Technologies) or a FTMS Bruker APEX Q IV.

All commercially available products were used without further purification. The following dialdehydes were prepared according to literature: 9,10-diformylanthracene,[30] b,b'-*p*-phenylen-di-acrolein,[31] 2,6-naphthalenedi-carbaldehyde,[32] 5-bromoisophthalaldehyde,[33] 4,4'-diformyl-1,1'-biphenyl,[34] 4,4'-diformylphenyl ether,[35] 2,5-diformylfuran,[36] 2,5-diformylthiophene,[37] 5,5'-diformyl-2,2'bithiophene[38] and 1,1'-ferrocene dicarbaldehyde,[39] The following metal carbenes were prepared according to previously described methods: pentacarbonyl[(ethoxy)(methyl)carbene]chromium(0) (**3a**),[40] pentacarbonyl-[(ethoxy)(methyl)carbene]tungsten(0) (**3b**),[41] decacarbonyl-μ-[1,4-phenylenbis-(1ethoxy-2-propen-3-yl-1-yliden)]dichromium (**2aa**)[13] and decacarbonyl-μ-[1,3-phenylenbis(1-ethoxy-2-propen-3-yl-1-yliden)]dichromium (**2ab**).[13]

General procedure for the preparation of the Fischer bis(carbene) complexes 2: To a solution of the corresponding dialdehyde (**4**) (1 mmol) in anhydrous Et_2O (5 mL) were added Et_3N (8 mmol) and TMSCl (6 mmol). Immediately, a solution of pentacarbonyl[(ethoxy)(methyl)carbene]metal(0) (**3**) (3 mmol) in anhydrous Et_2O (1 mL) was added to the solution mixture at room temperature in a single portion. The reaction was stirred until total disappearance of the starting material (checked by TLC). The solvent was removed under reduced pressure and the product was purified by flash column chromatography on silica gel (*n*-hexane/AcOEt).

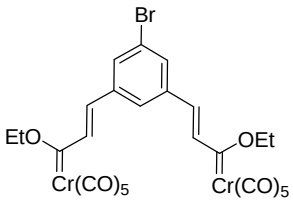

Synthesis of complex 2ac: Following the general procedure, with 5-bromoisophthalaldehyde (**4c**, 67 mg, 0.31 mmol), Et_3N (0.37 mL, 2.48 mmol) and TMSCl (0.24 mL, 1.86 mmol) in 1.6 mL of dry Et_2O and carbene complex **3a** (245 mg, 0.93 mmol) in 0.3 mL of dry Et_2O. The reaction mixture was stirred at room temperature for 24 h. The solvent was removed under reduced pressure and purified by flash chromatography to yield compound **2ac** as a dark red solid (74 mg, 34%). ^{1}H NMR (300 MHz, ppm): δ 7.90 (d, *J* = 15.4 Hz, 2H), 7.70 (d, *J* = 1.3 Hz, 2H), 7.62 (s, 1H), 6.78 (d, *J* = 15.4 Hz, 2H), 5.18 (q, *J* = 7.0 Hz, 4H), 1.73 (t, *J* = 7.0 Hz, 6H). ^{13}C NMR (75 MHz, ppm): δ 332.1, 224.2, 216.4, 140.7, 137.5, 132.8, 128.4, 125.5, 123.8, 76.6, 15.2. IR (CH_2Cl_2): ν 2056, 1923 cm^{-1}. HRMS (ESI): *m/z* calcd for $C_{26}H_{16}BrCr_2O_{12}$ [M - H] 702.8645, found 702.8630.

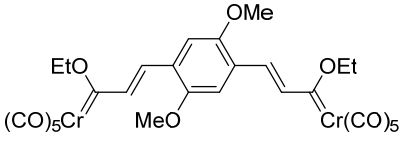

Synthesis of complex 2ad: Following the general procedure, with 2,5-dimethoxybenzene-1,4-dicarboxaldehyde (**4d**, 200 mg, 1.03 mmol), Et_3N (1.2 mL, 8.41 mmol) and TMSCl (0.75 mL, 6.18 mmol) in 5.2 mL of dry Et_2O and carbene complex **3a** (816 mg, 3.09 mmol) in 1 mL

of dry Et_2O. The reaction mixture was stirred at room temperature for 24 h. The solvent was removed under reduced pressure and purified by flash chromatography to yield compound **2ad** as a dark purple solid (217 mg, 31%). ^{1}H NMR (300 MHz, ppm): δ 8.07 (d, *J* = 15.4 Hz, 2H), 7.22 (d, *J* = 15.4 Hz, 2H), 7.05 (s, 2H), 5.15 (q, *J* = 7.0 Hz, 4H), 3.94 (s, 6H), 1.72 (t, *J* = 7.0 Hz, 6H). ^{13}C NMR (75 MHz, ppm): δ 330.8, 224.5, 216.8, 154.1, 141.2, 126.9, 124.4, 111.5, 76.2, 56.1, 15.2. IR (CH_2Cl_2): ν 2053, 1919 cm^{-1}. HRMS (ESI): *m/z* calcd for $C_{28}H_{21}Cr_2O_{14}$ [M - H] 684.9748, found 684.9743.

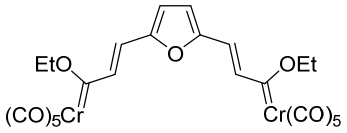

Synthesis of complex 2ae: Following the general procedure, with 2,5-diformylfuran (**2e**, 200 mg, 1.61 mmol), Et_3N (1.8 mL, 12.88 mmol) and TMSCl (1.2 mL, 9.66 mmol) in 8.1 mL of dry Et_2O and carbene complex **3a** (1.28 g, 4.83 mmol) in 1.6 mL of dry Et_2O. The reaction mixture was stirred at room temperature for 24 h. The solvent was removed under reduced pressure and purified by flash chromatography to yield compound **2ae** as a dark purple solid (450 mg, 46%). ^{1}H NMR (300 MHz, ppm): δ 7.93 (d, *J* = 15.1 Hz, 2H), 6.86 (s, 2H), 6.64 (d, *J* = 15.1 Hz, 2H), 5.12 (q, *J* = 7.0 Hz, 4H), 1.70 (t, *J* = 7.0 Hz, 6H). ^{13}C NMR (75 MHz, ppm): δ 328.5, 224.8, 216.6, 154.1, 138.0, 120.6, 113.2, 75.9, 15.2. IR (CH_2Cl_2): ν 2054, 1922 cm^{-1}. HRMS (ESI): *m/z* calcd for $C_{24}H_{15}Cr_2O_{13}$ [M - H] 614.9329, found 614.9326.

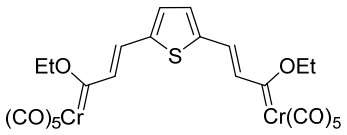

Synthesis of complex 2af: Following the general procedure, with 2,5-diformylthiophene (**4f**, 100 mg, 0.71 mmol), Et_3N (0.8 mL, 5.61 mmol) and TMSCl (0.54 mL, 4.26 mmol) in 3.6 mL of dry Et_2O and carbene complex **3a** (562 mg, 2.13 mmol) in 0.7 mL of dry Et_2O. The reaction mixture was stirred at room temperature for 24 h. The solvent was removed under reduced pressure and purified by flash chromatography to yield compound **2af** as a dark purple solid (120 mg, 27%). ^{1}H NMR (300 MHz, ppm): δ 7.73 (d, *J* = 14.8 Hz, 2H), 7.34 (s, 2H), 7.00 (d, *J* = 14.8 Hz, 2H), 5.11 (q, *J* = 7.1 Hz, 4H), 1.69 (t, *J* = 7.1 Hz, 6H). ^{13}C NMR (75 MHz, ppm): δ 328.5, 224.5, 216.6, 144.2, 139.1, 134.5, 121.2, 76.0, 15.2. IR (CH_2Cl_2): ν 2053, 1922 cm^{-1}. HRMS (ESI): *m/z* calcd for $C_{24}H_{15}Cr_2O_{12}S$ [M - H] 630.9101, found 630.9121.

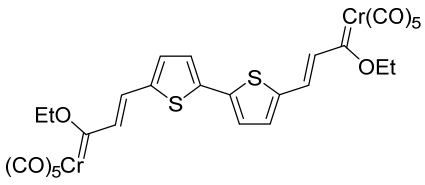

Synthesis of complex 2ag: Following the general procedure, with 5,5'-diformyl-2,2'bithiophene (**4g**, 100 mg, 0.45 mmol), Et_3N (0.53 mL, 3.6 mmol) and TMSCl (0.33 mL, 2.7 mmol) in 2.3 mL of dry Et_2O and carbene complex **3a** (356 mg, 1.35) in 0.5 mL of dry Et_2O. The reaction mixture was stirred at room temperature for 24 h. The solvent was removed under reduced pressure and purified by flash chromatography to yield compound **2ag** as a purple solid (26 mg, 8%). ^{1}H NMR (500 MHz, ppm): δ 7.69 (d, *J* = 14.9 Hz, 2H), 7.34-7.26 (m, 8H), 7.06 (d, *J* = 14.9 Hz, 2H), 5.11 (q, *J* = 7.0 Hz, 4H), 1.70 (t, *J* = 7.0 Hz, 6H). ^{13}C NMR (75 MHz, ppm): δ 327.3, 224.5, 216.7, 141.1, 140.3, 138.3, 135.3, 126.4, 121.9,

75.9, 15.2. IR (CH_2Cl_2): ν 2052, 1922 cm^{-1}. HRMS (ESI): *m/z* calcd for $C_{28}H_{17}Cr_2O_{12}S_2$ [M - H] 712.8979, found 712.9003.

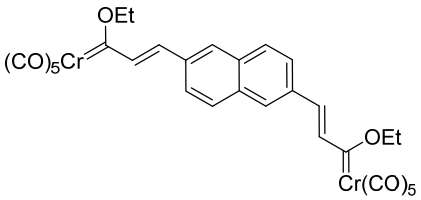

Synthesis of complex 2ah: Following the general procedure, with 2,6-naphthalenedicarbaldehyde (**4h**, 200 mg, 1.09 mmol), Et_3N (1.2 mL, 8.72 mmol) and TMSCl (0.79 mL, 6.54 mmol) in 5.5 mL of dry Et_2O and carbene complex **3a** (863 mg, 3.27 mmol) in 1.1 mL of dry Et_2O. The reaction mixture was stirred at room temperature for 24 h. The solvent was removed under reduced pressure and purified by flash chromatography to yield compound **2ah** as a dark red solid (194 mg, 26%). ^1H NMR (300 MHz, ppm): δ 8.07 (d, *J* = 15.3 Hz, 2H), 8.01 (s, 2H), 7.89 (d, *J* = 8.6 Hz, 2H), 7.77 (d, *J* = 8.6 Hz, 2H), 7.09 (d, *J* = 15.3 Hz, 2H), 5.18 (q, *J* = 7.0 Hz, 4H), 1.75 (t, *J* = 7.0 Hz, 6H). ^{13}C NMR (75 MHz, ppm): δ 330.8, 224.4, 216.7, 140.0, 134.3, 133.7, 131.8, 129.4, 128.8, 125.0, 80.1, 76.3, 15.2. IR (CH_2Cl_2): ν 2054, 1916 cm^{-1}. HRMS (ESI): *m/z* calcd for $C_{30}H_{19}Cr_2O_{12}$ [M - H] 674.9694, found 674.9708.

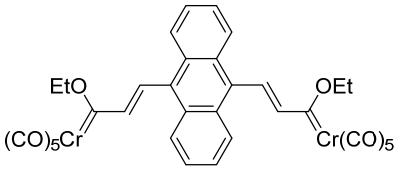

Synthesis of complex 2ai: Following the general procedure, with 9,10-diformylanthracene (**4i**, 116 mg, 0.50 mmol), Et_3N (0.56 mL, 4.0 mmol) and TMSCl (0.38 mL, 3.0 mmol) in 2.5 mL of dry Et_2O and carbene complex **3a** (396 mg, 1.5 mmol) in 0.5 mL of dry Et_2O. The reaction mixture was stirred at room temperature for 24 h. The solvent was removed under reduced pressure and purified by flash chromatography to yield **2ai** as a dark purple solid (56 mg, 15%). ^1H NMR (300 MHz, ppm): δ 8.32 (m, 4H), 7.90 (s, *J* = 1.3 Hz, 4H), 7.57 (m, 4H), 5.31 (q, *J* = 7.1 Hz, 4H), 1.84 (t, *J* = 7.1 Hz, 6H). ^{13}C NMR (75 MHz, ppm): δ 331.7, 224.2, 216.5, 148.5, 131.6, 129.8, 126.5, 126.0, 125.9, 76.6, 15.3. IR (CH_2Cl_2): ν 2057, 1922 cm^{-1}. HRMS (ESI): *m/z* calcd for $C_{34}H_{22}Cr_2O_{12}$ [M - H] 725.9928, found 725.9957.

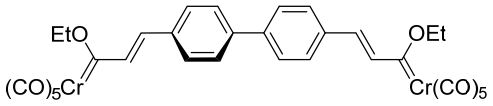

Synthesis of complex 2aj: Following the general procedure, with 4,4'-diformyl-1,1'-biphenyl (**4j**, 170 mg, 0.81 mmol), Et_3N (0.91 mL, 6.48 mmol) and TMSCl (0.61 mL, 4.86 mmol) in 4.1 mL of dry Et_2O and carbene complex **3a** (641 mg, 2.43 mmol) in 0.8 mL of dry Et_2O. The reaction mixture was stirred at room temperature for 24 h. The solvent was removed under reduced pressure and purified by flash chromatography to yield compound **2aj** as a dark red solid (79 mg, 14%). ^1H NMR (300 MHz, ppm): δ 7.99 (d, *J* = 15.2 Hz, 2H), 7.69 (s, 8H), 6.98 (d, *J* = 15.2 Hz, 2H), 5.16 (q, *J* = 7.1 Hz, 4H), 1.73 (t, *J* = 7.1 Hz, 6H). ^{13}C NMR (75 MHz, ppm): δ 330.9, 224.3, 216.7, 142.1, 139.6, 134.2, 130.0, 128.6, 127.6, 76.3, 15.2. IR (CH_2Cl_2): ν 2055, 1914 cm^{-1}. HRMS (ESI): *m/z* calcd for $C_{32}H_{21}Cr_2O_{12}$ [M - H] 700.9850, found 700.9858.

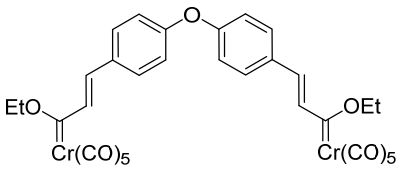

Synthesis of complex 2ak: Following the general procedure, with 4,4'-diformylphenylether (**4k**, 200 mg, 0.88 mmol), Et_3N (1.0 mL, 7.0 mmol) and TMSCl (0.7 mL, 5.28 mmol) in 4.4 mL of dry Et_2O and carbene complex **3a** (697 mg, 2.64 mmol) in 0.9 mL of dry Et_2O. The reaction mixture was stirred at room temperature for 24 h. The solvent was removed under reduced pressure and purified by flash chromatography to yield compound **2ak** as a dark red solid (368 mg, 58%). ^{1}H NMR (300 MHz, ppm): δ 7.89 (d, *J* = 15.3 Hz, 2H), 7.61 (d, *J* = 8.6 Hz, 2H), 7.07 (d, *J* = 8.6 Hz, 2H), 6.96 (d, *J* = 15.3 Hz, 2H), 5.13 (q, *J* = 7.1 Hz, 4H), 1.71 (t, *J* = 7.1 Hz, 6H). ^{13}C NMR (75 MHz, ppm): δ 330.2, 224.3, 216.7, 158.7, 139.0, 131.2, 130.0, 128.9, 119.5, 76.1, 15.1. IR (CH_2Cl_2): ν 2055, 1917 cm^{-1}. HRMS (ESI): *m/z* calcd for $C_{32}H_{21}Cr_2O_{13}$ [M - H] 716.9799, found 716.9793.

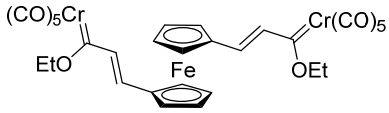

Synthesis of complex 2al: Following the general procedure, with 1,1'-ferrocene dicarbaldehyde (**4l**, 200 mg, 0.83 mmol), Et_3N (0.93mL, 6.64 mmol) and TMSCl (0.63 mL, 4.98 mmol) in 4.2 mL of dry Et_2O and carbene complex **3a** (657 mg, 2.49 mmol) in 0.8 mL of dry Et_2O. The reaction mixture was stirred at room temperature for 24 h. The solvent was removed under reduced pressure and purified by flash chromatography to yield compound **2al** as a dark red solid (263 mg, 43%). ^{1}H NMR (300 MHz, ppm): δ 7.47 (d, *J* = 15.2 Hz, 2H), 7.01 (d, *J* = 15.2 Hz, 2H), 5.02 (q, *J* = 7.1 Hz, 4H), 4.58 (s, 8H), 1.68 (t, *J* = 7.1 Hz, 6H). ^{13}C NMR (75 MHz, ppm): δ 326.1, 224.2, 217.1, 138.5, 135.2, 80.1, 75.4, 74.3, 71.3, 15.1. IR (CH_2Cl_2): ν 2053, 1915 cm^{-1}. HRMS (ESI): *m/z* calcd for $C_{30}H_{21}Cr_2FeO_{12}$ [M - H] 732.9201, found 732.9202.

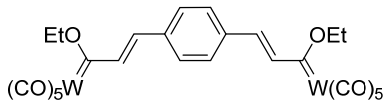

Synthesis of complex 2ba: Following the general procedure, with terephthalaldehyde (**4a**, 100 mg, 0.75 mmol), Et_3N (0.83 mL, 6 mmol) and TMSCl (0.55 mL, 4.5 mmol) in 3.8 mL of dry Et_2O and tungsten(0)-carbene complex **3b** (891 mg, 2.25 mmol) in 0.8 mL of dry Et_2O. The reaction mixture was stirred at room temperature for 24 h. The solvent was removed under reduced pressure and purified by flash chromatography to yield compound **2ba** as a dark brown solid (213 mg, 32%). ^{1}H NMR (300 MHz, ppm): δ 7.93 (d, *J* = 15.4 Hz, 2H), 7.64 (s, 4H), 7.13 (d, *J* = 15.4 Hz, 2H), 4.96 (q, *J* = 7.0 Hz, 4H), 1.70 (t, *J* = 7.0 Hz, 6H). ^{13}C NMR (75 MHz, ppm): δ 304.7, 203.8, 197.4, 144.2, 137.0, 131.7, 129.8, 79.0, 15.0. IR (CH_2Cl_2): ν 2064, 1917 cm^{-1}. HRMS (ESI): *m/z* calcd for $C_{26}H_{17}O_{12}W_2$ [M - H] 888.9754, found 888.9748.

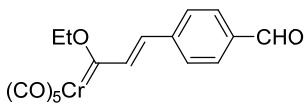

Synthesis of complex 6: Following the reported procedure,[12] with terephthalaldehyde (**4a**, 200 mg, 1.49 mmol), Et_3N (0.83 mL, 5.96 mmol) and TMSCl (0.54 mL, 4.47 mmol) in 7.6 mL of dry Et_2O and carbene complex **3a** (393 mg, 1.49) in 1.6 mL of dry Et_2O. The reaction mixture was stirred at room temperature for 24 h. The solvent was removed under reduced pressure and purified by flash chromatography to yield compound **6** as a dark red solid (120 mg, 21%). ^{1}H NMR

(300 MHz, ppm): δ 10.05 (s, 1H), 8.00 (d, *J* = 15.1 Hz, 2H), 7.92 (d, *J* = 7.0 Hz, 1H), 7.74 (d, *J* = 7.0, 2H), 6.87 (d, *J* = 15.1 Hz, 1H), 5.19 (br s, 2H), 1.74 (br s, 3H). ^{13}C NMR (75 MHz, ppm): δ 332.4, 224.3, 216.4, 191.4, 141.2, 140.6, 137.1, 130.1, 129.5, 126.1, 76.6, 15.1. IR (CH_2Cl_2): ν 2056, 1922 cm^{-1}. HRMS (ESI): *m/z* calcd for $C_{17}H_{12}CrO_7$ [M - H] 378.9915, found 378.9928.

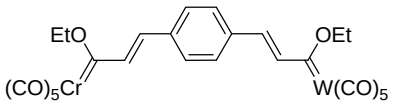

Synthesis of complex 5: Following the reported procedure,[12] with complex **6** (92 mg, 0.24 mmol), Et_3N (0.13 mL, 0.96 mmol) and TMSCl (0.1 mL, 0.72 mmol) in 1.2 mL of dry Et_2O was added the carbene complex (95 mg, 0.24 mmol) in 0.3 mL of dry Et_2O. The reaction mixture was stirred at room temperature for 24 h. The solvent was removed under reduced pressure and purified by flash chromatography to yield compound **5** dark red solid (41 mg, 23%). ^{1}H NMR (300 MHz, ppm): δ 7.98 (d, *J* = 15.4 Hz, 2H), 7.91 (d, *J* = 15.4 Hz, 2H), 7.64 (s, 4H), 7.14 (d, *J* = 15.4 Hz, 1H), 6.87(d, J =15.4 Hz, 1H), 5.16 (q, *J* = 7.0 Hz, 2H), 4.95 (q, *J* = 7.0 Hz, 2H), 1.72 (t, *J* = 15.4 Hz, 3H), 1.70 (t, *J* = 7.0 Hz, 6H). ^{13}C NMR (75 MHz, ppm): δ 331.2, 304.7, 224.4, 216.6, 203.8, 197.4, 144.2, 140.0, 137.0, 136.9, 131.7, 130.0, 129.7, 79.0, 76.4, 15.2, 14.9. IR (CH_2Cl_2): ν 2064, 2054, 1902 cm^{-1}. HRMS (ESI): *m/z* calcd for $C_{26}H_{17}CrO_{12}W$ [M - H] 756.9647, found 756.9655.

III.7. References

(1) For selected recent reviews on the chemistry and applications of Fischer carbenes, see: (a) Wu, Y.-T.; Kurahashi, T.; de Meijere, A. *J. Organomet. Chem*. **2005**, *690*, 5900. (b) Gómez-Gallego, M.; Mancheño, M. J.; Sierra, M. A. *Acc. Chem. Res*. **2005**, *38*, 44. (c) Sierra, M. A.; Gómez-Gallego, M.; Martínez-Álvarez, R. *Chem. Eur. J.* **2007**, *13*, 736. (d) Sierra, M. A.; Fernández, I.; Cossío, F. P. *Chem. Commun.* **2008**, 4671. (e) Dötz, K. H.; Stendel, J. *Chem. Rev.* **2009**, *109*, 3227. (f) Herndon, J. W. *Coord. Chem. Rev.* **2010**, *254*, 103. (g) Fernández-Rodríguez, M. A.; García-García, P.; Aguilar, E. *Chem. Commun.* **2010**, *46*, 7670. (h) Fernández, I.; Cossío, F. P.; Sierra, M. A. *Acc. Chem. Res.* **2011**, *44*, 479.

(2) (a) Dötz, K. H. *Angew. Chem*. **1975**, *87*, 672. *Angew. Chem. Int. Ed. Engl.* **1975**, *14*, 644. (b) Wulff W. D. in *Comprehensive Organic Synthesis, Vol. 5* (Eds.: B. M. Trost, I. Fleming), Pergamon, Oxford, **1991**, p. 1065. (c) Minatti, A.; Dötz, K. H. *Top. Organomet. Chem.* **2004**, *13*, 123. (d) Waters, M. L.; Wulff, W. D. *Org. React.* **2008**, *70*, 121. See also reference (1e).

(3) For representative examples, see: (a) Wulff, W. D.; Bauta, W. E.; Kaesler, R. W.; Lankford, P. J.; Miller, R. A.; Murray, C. K.; Yang, D. C. *J. Am. Chem. Soc.* **1990**, *112*, 3642. (b) Anderson, B. A.; Wulff, W. D.; Powers, T. S.; Tribbitt, S.; Rheingold, A. L. *J. Am. Chem. Soc.* **1992**, *114*, 10784. (c) Barluenga, J.; Aznar, F.; Barluenga, S. *J. Chem. Soc. Chem. Commun.* **1995**, 1973. (d) Barluenga, J.; Aznar, F.; Barluenga, S.; Fernández, M.; Martín, A.; García-Granda, S.; Piñera-Nicolás, A. *Chem. Eur. J.* **1998**, *4*, 2280. (e) Barluenga, J.; Fernández-Rodríguez, M. A.; Aguilar, E. *Org. Lett.* **2002**, *4*, 3659. (f) Granados, A. M.; Fracaroli, A. M.; De Rossi, R. H.; Fuertes, P.; Torroba, T. *Chem. Commun.* **2008**, 483. (g) Baeza, B.; Casarrubios, L.; Ramírez-López, P.; Gómez-Gallego, M.; Sierra, M. A. *Organometallics* **2009**, *28*, 956. (h) Luo, N.; Zheng, Z.; Yu, Z. *Org. Lett.* **2011**, *13*, 3384. (i) Rivero, A. R.; Fernández, I.; Sierra, M. A. *J. Org. Chem.* **2012**, *77*, 6648.

(4) (a) Sierra, M. A.; Mancheño, M. J.; Sáez, E.; del Amo, J. C. *J. Am. Chem. Soc.* **1998**, *120*, 6812. (b) Sierra, M. A.; del Amo, J. C.; Mancheño, M. J.; Gómez-Gallego, M. *J. Am. Chem. Soc.* **2001**, *123*, 851. (c) Fernández, I.; Mancheño, M. J.; Vicente, R.; López, L. A.; Sierra, M. A. *Chem. Eur. J.* **2008**, *14*, 11222. (d) López-Alberca, M. P.; Fernández, I.; Mancheño, M. J.; Gómez-Gallego, M.; Casarrubios, L.; Sierra, M. A. *Eur. J. Org. Chem*. **2011**, 3293. (e) Chu, G. M.; Fernández, I.; Sierra, M. A. *J. Org. Chem.* **2013**, *78*, 865. For a revision, see reference (1b).

(5) Hegedus, L. S. *Tetrahedron* **1997**, *53*, 4105.

(6) (a) Arrieta, A.; Cossío, F. P.; Fernández, I.; Gómez-Gallego, M.; Lecea, B.; Mancheño, M. J.; Sierra, M. A. *J. Am. Chem. Soc.* **2000**, *122*, 11509. (b) Fernández, I.; Sierra, M. A.; Mancheño, M. J.; Gómez-Gallego, M.; Cossío, F. P. *J. Am. Chem. Soc.* **2008**, *130*, 13892. (c) Fernández, I.; Sierra, M. A.; Gómez-Gallego, M.; Mancheño, M. J.; Cossío, F. P. *Chem. Eur. J.* **2005**, *11*, 5988. (d) Fernández, I.; Sierra, M. A. *Top. Heterocycl. Chem.* **2013**, *30*, 65.

(7) (a) Sierra, M. A.; Fernández, I.; Mancheño, M. J.; Gómez-Gallego, M.; Torres, M. R.; Cossío, F. P.; Arrieta, A.; Lecea, B.; Poveda, A.; Jiménez-Barbero, J. *J. Am. Chem. Soc.* **2003**, *125*, 9572. (b) Fernández, I.; Sierra, M. A.; Gómez-Gallego, M.; Mancheño, M. J.; Cossío, F. P. *Angew. Chem.* **2006**, *118*, 131; *Angew. Chem. Int. Ed.* **2006**, *45*, 125. For a recent revision on dyotropic reactions, see: Fernández, I.; Cossío, F. P.; Sierra, M. A. *Chem. Rev.* **2009**, *109*, 6687.

(8) (a) Salmain, M.; Licandro, E.; Baldoli, C.; Maiorana, S.; Tran-Huy, H.; Jaouen, G. C. *J. Organomet. Chem.* **2001**, *617–618*, 376. (b) Baldoli, C.; Cerea, P.; Giannini, C.; Licandro, E.; Rigamonti, C.; Maiorana, S. *Synlett* **2005**, 1984. (c) Llordes, A.; Sierra, M. A.; López-Alberca, M. P.; Molins, E.; Ricart, S. *J. Organomet. Chem.* **2005**, *690*, 6096. (d) Sierra, M. A.; Rodríguez-Fernández, M.; Casarrubios, L.; Gómez-Gallego, M.; Mancheño, M. J. *Eur. J. Org. Chem.* **2009**, 2998. (e) Dutta, P.; Sawoo, S.; Ray, N.; Bouloussa, O.; Sarkar, A. *Bioconjugate Chem.* **2011**, *22*, 1202.

(9) (a) Bühler, G.; Feiters, M. C.; Nolte, R. J. M.; Dötz, K. H. *Angew. Chem.* **2003**, *115*, 2599; *Angew. Chem., Int. Ed.* **2003**, *42*, 2494. (b) Tu, T.; Assenmacher, W.; Peterlik, H.; Weisbarth, R.; Nieger, M.; Dötz, K. H. *Angew. Chem.* **2007**, *119*, 6486; *Angew. Chem., Int. Ed.* **2007**, *46*, 6368. (c) Klawonn, T.; Gansäuer, A.; Winkler, I.; Lauterbach, T.; Franke, D.; Nolte, R. J. M.; Feiters, M. C.; Böner, H.; Hentschel, J.; Dötz, K. H. *Chem. Commun.* **2007**, 1894. (d) Gansäuer, A.; Winkler, I.; Klawonn, T.; Nolte, R. J. M.; Feiters, M. C.; Börner, H. G.; Hentschel, J.; Dötz, K. H. *Organometallics* **2009**, *28*, 1377.

(10) (a) Leroux, F.; Stumpt, R.; Fischer, H. *Eur. J. Inorg. Chem.* **1998**, 1225. (b) Licandro, E.; Maiorana, S.; Papagani, A.; Hellier, P.; Capella, L.; Persoons, A.; Houbrechts, S. *J. Organomet. Chem.* **1999**, *583*, 111. (c) Robin-Le Guen, F.; Le Poul, P.; Caro, B.; Pichon, R.; Kervarec, N. *J. Organomet. Chem.* **2001**, *626*, 37. (d) Faux, N.; Caro, B.; Robin-Le Guen, F.; Le Poul, P.; Nakatani, K.; Ishow, E. *J. Organomet. Chem.* **2005**, *690*, 4982.

(11) (a) Fernández, I.; Sierra, M. A.; Cossío, F. P. *J. Org. Chem.* **2008**, *73*, 2083. (b) Fernández, I.; Sierra, M. A.; Cossío, F. P. *J. Org. Chem.* **2006**, *71*, 6178. (c) Andrada, D. M.; Granados, A. M.; Solà, M.; Fernández, I. *Organometallics* **2011**, *30*, 466.

(12) Lage, M. L.; Fernández, I.; Mancheño, M. J.; Sierra, M. A. *Inorg. Chem.* **2008**, *47*, 5253.

(13) Aumann, R.; Heinen, H. *Chem. Ber.* **1987**, *120*, 537.

(14) Péron, V.; Porhiel, E.; Ferrand, V.; Le Bozec, H. *J. Organomet. Chem.* **1997**, *539*, 201.

(15) ΔE values computed as ΔE = E(isomer I) - E(isomer II). All energies, which include the corresponding zero-point vibrational energies, have been computed at the B3LYP/def2-SVP level (see Computational Details).

(16) CCDC-915792 contains the supplementary crystallographic data for this paper. These data can be obtained free of charge from The Cambridge Crystallographic Data Centre via www.ccdc.cam.ac.uk/data_request/cif.

(17) (a) Fernández, I.; Cossío, F. P.; Arrieta, A.; Lecea, B.; Mancheño, M. J.; Sierra, M. A. *Organometallics* **2004**, *23*, 1065. (b) Andrada, D. M.; Zoloff Michoff, M. E.; Fernández, I.; Granados, A. M.; Sierra, M. A. *Organometallics* **2007**, *26*, 5854. (c) Valyaev, D. A.; Brousses, R.; Lugan, N.; Fernández, I.; Sierra, M. A. *Chem. Eur. J.* **2011**, *17*, 6602. (d) Lugan, N.; Fernández, I.; Brousses, R.; Valyaev, D. A.; Lavigne, G.; Ustynyuk, N. A. *Dalton Trans.* **2013**, *42*, 898.

(18) Nemykin, V. N.; Makarova, E. A.; Grosland, J. O.; Hadt, R. G.; Koposov, A. Y. *Inorg. Chem.* **2007**, *46*, 9591.

(19) (a) Fernández, I.; Mancheño, M. J.; Gómez-Gallego, M.; Sierra, M. A. *Org. Lett.* **2003**, *5*, 1237. (b) López-Alberca, M. P.; Mancheño, M. J.; Fernández, I.; Gómez-Gallego, M.; Sierra, M. A.; Torres, R. *Chem. Eur. J.* **2009**, *15*, 3595. (c) Lage, M. L.; Fernández, I.; Mancheño, M. J.; Sierra, M. A. *Chem. Eur. J.* **2010**, *16*, 6616.

(20) Gaussian 09, Revision B.01, Frisch, M. J.; Trucks, G. W.; Schlegel, H. B.; Scuseria, G. E.; Robb, M. A.; Cheeseman, J. R.; Scalmani, G.; Barone, V.; Mennucci, B.; Petersson, G. A.; Nakatsuji, H.; Caricato, M.; Li, X.; Hratchian, H. P.; Izmaylov, A. F.; Bloino, J.; Zheng, G.; Sonnenberg, J. L.; Hada, M.; Ehara, M.; Toyota, K.; Fukuda, R.; Hasegawa, J.; Ishida, M.; Nakajima, T.; Honda, Y.; Kitao, O.; Nakai, H.; Vreven, T.; Montgomery, J. A., Jr.; Peralta, J. E.; Ogliaro, F.; Bearpark, M.; Heyd, J. J.; Brothers, E.; Kudin, K. N.; Staroverov, V. N.; Kobayashi, R.; Normand, J.; Raghavachari, K.; Rendell, A.; Burant, J. C.; Iyengar, S. S.; Tomasi, J.; Cossi, M.; Rega, N.; Millam, J. M.; Klene, M.; Knox, J. E.; Cross, J. B.; Bakken, V.; Adamo, C.; Jaramillo, J.; Gomperts, R.; Stratmann, R. E.; Yazyev, O.; Austin, A. J.; Cammi, R.; Pomelli, C.; Ochterski, J. W.; Martin, R. L.; Morokuma, K.; Zakrzewski, V. G.; Voth, G. A.; Salvador, P.; Dannenberg, J. J.; Dapprich, S.; Daniels, A. D.; Farkas, Ö.; Foresman, J. B.; Ortiz, J. V.; Cioslowski, J.; Fox, D. J. Gaussian, Inc., Wallingford CT, **2009**.

(21) (a) Becke, A. D. *J. Chem. Phys.* **1993**, *98*, 5648. (b) Lee, C.; Yang, W.; Parr, R. G. *Phys. Rev. B* **1988**, *37*, 785.

(22) Weigend, F.; Alhrichs, R. *Phys. Chem. Chem. Phys.* **2005**, *7*, 3297.

(23) (a) Casida, M. E. in *Recent Developments and Applications of Modern Density Functional Theory, Vol. 4* (Ed.: J. M. Seminario), Elsevier, Amsterdam, **1996**. (b) Casida, M. E. *Recent Advances in Density Functional Methods, Vol. 1* (Ed.: D. P. Chong), World Scientific, Singapore, **1995**, p. 155.

(24) (a) Miertuš, S.; Scrocco, E.; Tomasi, J. *Chem. Phys.* **1981**, *55*, 117. (b) Pascual-Ahuir, J. L.; Silla, E.; Tuñón, I. *J. Comput. Chem.* **1994**, *15*, 1127. (c) Barone, V.; Cossi, M. *J. Phys. Chem. A* **1998**, *102*, 1995.

(25) For a review, see: Dreuw, A.; Head-Gordon, M. *Chem. Rev.* **2005**, *105*, 4009.

(26) For some recent examples, see: Braunschweig, H.; Herbst, T.; Rais, D.; Ghosh, S.; Kupfer, T.; Radacki, K.; Crawford, A. G.; Ward, R. W.; Marder, T. B.; Fernández, I.; Frenking, G. *J. Am. Chem. Soc.* **2009**, *131*, 8989. See also reference (18).

(27) (a) Wiggins, P.; Williams, J. A. G.; Tozer, D. J. *J. Chem. Phys.* **2009**, *131*, 091101. (b) Peach, P.; Benfield, M. J. G.; Helgaker, T.; Tozer, D. J. *J. Chem. Phys.* **2008**, *128*, 044118.

(28) Yanai, T.; Tew, D. P.; Handy, N. C. *Chem. Phys. Lett.* **2004**, *393*, 51.

(29) (a) Foster, J. P.; Weinhold, F. *J. Am. Chem. Soc.* **1980**, *102*, 7211. (b) Reed, A. E.; Weinhold, F. *J. Chem. Phys.* **1985**, *83*, 1736. (c) Reed, A. E.; Weinstock, R. B.; Weinhold, F. *J. Chem. Phys.* **1985**, *83*, 735. (d) Reed, A. E.; Curtiss, L. A.; Weinhold, F. *Chem. Rev.* **1988**, *88*, 899.

(30) Lee, A. E.; Grace, M. R.; Meyer, A. G.; Tuck, K. L. *Tetrahedron Lett.* **2010**, *51*, 1161.

(31) Lüttringhaus, A.; Schill, G. *Chem. Ber.* **1960**, *93*, 3048.

(32) Gingras, M.; Collet, C. *Synlett* **2005**, 2337.

(33) Netzke, K.; Snatzke, G. *Chem. Ber.* **1989**, *122*, 1365.

(34) Helms, A.; Heiler, D.; McLendon, G. *J. Am. Chem. Soc.* **1992**, *114*, 6227.

(35) Kuhnert, N.; Burzlaff, N.; Patel, C.; López-Periago, A. *Org. Biomol. Chem.* **2005**, *3*, 1911.

(36) Yoon, D.-W.; Gross, D. E.; Lynch, V. M.; Sessler, J. L.; Hay, B. P.; Lee, C.-H. *Angew. Chem.* **2008**, *120*, 5116; *Angew. Chem., Int. Ed.* **2008**, *47*, 5038.

(37) Ping, L.; Guang, X. M. *J. Serb. Chem. Soc.* **2005**, *70*, 201.

(38) Chen, R.; Yang, X.; Tian, H.; Wang, X.; Hagfeldt, A.; Sun, L. *Chem. Mater.* **2007**, *19*, 4007.

(39) Balavoine, G. G. A.; Doisneau, G.; Filleben-Khan, T. *J. Organomet. Chem.* **1991**, *412*, 381.

(40) Hegedus, L. S.; McGuire, M. A.; Schultze, L. M. *Org. Synth.* **1987**, *65*, 140.

(41) Fischer, E. O.; Massböl, A. *Chem. Ber.* **1967**, *100*, 2445.

III.8. Supporting Information

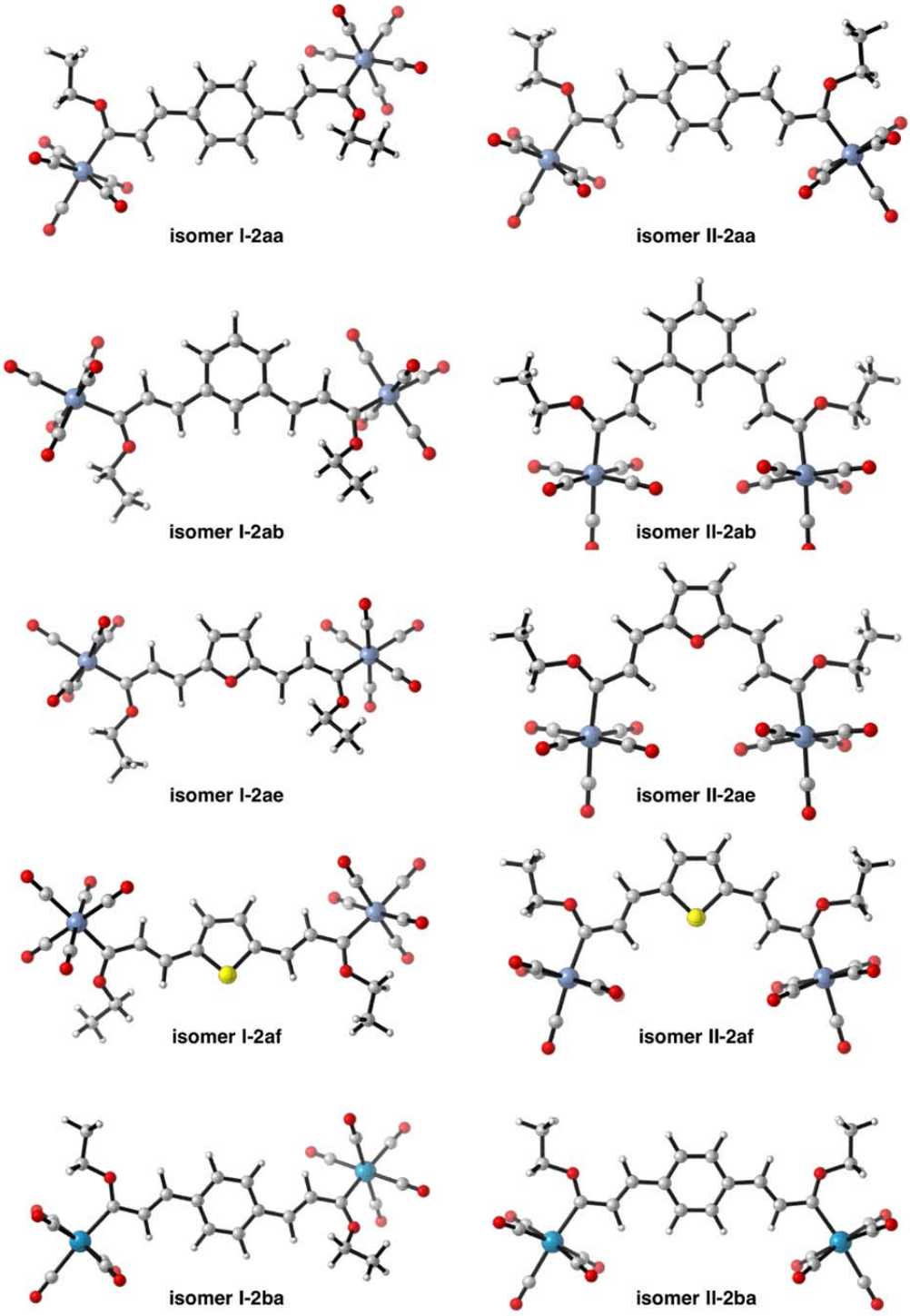

Figure 1S. Optimised geometries of compounds **2aa**, **2b**, **2ae**, **2af** and **2ba** at the B3LYP/def2-SVP level.

IV. *CAPÍTULO 2*

IV.1. *Tuning the Photophysical Properties of BODIPY Molecules by π-Conjugation with Fischer Carbene Complexes*

Abstract: The synthesis, structure, and photophysical properties of novel BODIPY–Fischer alkoxy-, thio-, and aminocarbene dyads are reported. The BODIPY chromophore is directly attached to the carbene ligand by an ethylenic spacer, thus forming donor–bridge–acceptor π-extended systems. The extension of the π-conjugation is decisive in the equilibrium geometries of the dyads and is clearly reflected in the corresponding absorption and emission spectra. Whereas the BODIPY fragment is mainly isolated in aminocarbene complexes, it is fully conjugated in alkoxycarbene derivatives. The former thus exhibit the characteristic photophysical properties of BODIPY units, whereas complete suppression of the BODIPY fluorescence emission is observed in the latter, as a direct consequence of the strong electron-accepting character of the $(CO)_5M{=}C$ moiety. As the π-acceptor character of the metal–carbene group can be modified, the electronic properties of the conjugated BODIPY can be tuned. Density functional calculations have been carried out to gain insight into the photophysical properties.

Chem. Eur. J. **2014**, *20*, 1367.

IV.2. Introduction

Since the synthesis of the first 4,4-difluoro-4-borata-3a-azonia-4a-aza-*s*-indacene in 1968 by Treibs and Kreuzer,[1] boradiazaindacenes (BODIPYs) have become highly useful molecular entities in fields such as materials science or medicinal chemistry.[2] This is mainly due to the fascinating optical properties associated with this family of compounds. Thus, their excellent thermal and photochemical stabilities, high fluorescence quantum yields, negligible triplet-state formation, and intense absorption profiles have transformed BODIPY species into quite attractive materials with applications in, for instance, biomolecules labeling, ion sensing and signaling, energy transfer cassettes, or light harvesting systems.[2] For these reasons, it is not surprising that numerous synthetic methods have been developed to produce new BODIPY derivatives with interesting and tunable photophysical properties.[2,3] In this sense, the attachment of BODIPY units to a transition-metal center to prepare a dyad is highly attractive. The great number of possible modifications (that is, variation of the transition metal and/or its coordination sphere) that can be effected in these systems may, in principle, allow the properties of the BODIPY–transitionmetal dyad to be tuned. However, in most of the reported dyads the metal centers were attached onto the peripheral moieties of the BODIPY fragment [4–6] rather than to its π-conjugated core.[7,8] As a result, the impact of the transition-metal fragment on the properties associated with the BODIPY chromophore is not that remarkable.

At this point, we turned our attraction to Group 6 Fischer carbene complexes because of their exceptional properties as electron-withdrawing groups.[9] The π-acceptor ability of these species has resulted not only in their wide use in organic synthesis (that is, Fischer carbene complexes behaving similarly to a Lewis acid complexed carbonyl function),[10] but also in their emerging role as building blocks in the field of new materials.[11]

As the modification of the electronic properties of the carbene ligand has proved to be relatively easy,[9] we hypothesized that the direct attachment by π-conjugation of a Group 6 Fischer carbene complex to the π-core of BODIPY could have a significant impact on the photophysical properties of the BODIPY moiety.

Herein we report the successful accomplishment of such hypothesis, which allows the preparation of new organometallic compound–BODIPY dyads possessing tunable photophysical properties.

IV.3. Results and Discussion

Synthesis and structure of the new BODIPY derivatives: Alkoxy-BODIPY–Fischer carbene complexes **3** were prepared from the pentacarbonyl[(ethoxy)(methyl)]carbene chromium(0) or tungsten(0) complexes **1a** or **1b** and the corresponding formyl-BODIPY **2a-c** in the presence of Et_3N and TMSCl following the reaction conditions reported by Aumann and Heinen.[12] Thus, Et_3N (4 equiv), trimethylsilyl chloride (TMSCl, 3 equiv), and complex **1** (1.5 equiv) were added to a solution of the aldehyde (1 equiv) in anhydrous Et_2O at room temperature and the mixture was stirred for 24 h. Removal of the solvent and purification of the residue by column chromatography allowed the isolation of the new BODIPY complexes **3** in moderate to good yields (Scheme 1). Furthermore, aminocarbenes **4** were prepared from alkoxycarbene complexes **3** by an aminolysis reaction using dimethylamine at -100°C in anhydrous tetrahydrofuran in excellent yields.

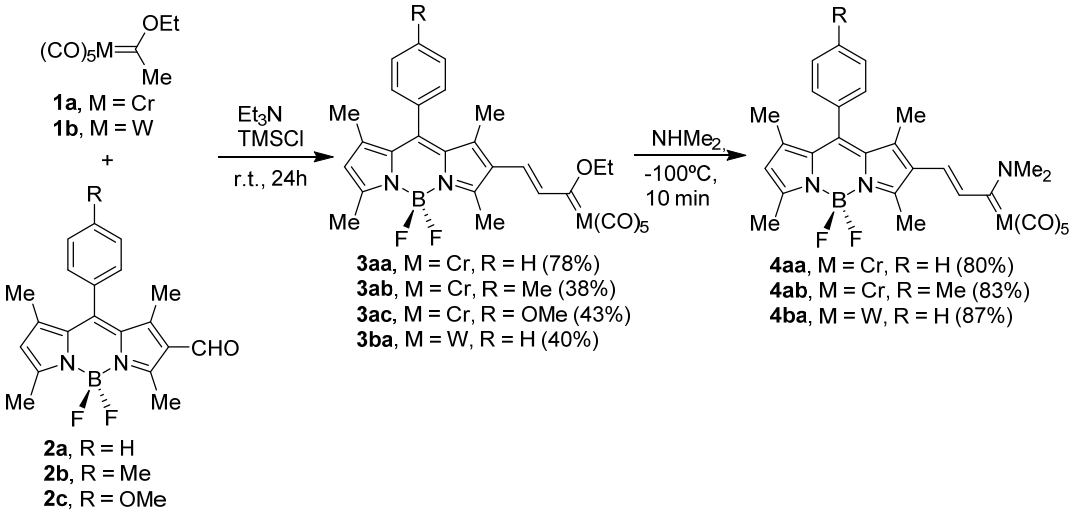

Scheme 1. Synthesis of carbene complexes **3** and **4**.

The structures of carbene complexes **3** and **4** were established by NMR experiments and by comparison with the data reported for related chromium(0) and tungsten(0) α,β-unsaturated Fischer carbene complexes.[12–14] Thus, the carbene carbon atom directly attached to chromium(0) in alkoxycarbenes **3** appears at δ ≈ 325 ppm in the corresponding ^{13}C NMR spectra, while a value of δ ≈270 ppm was found in aminocarbenes **4** as a result of the well-known higher π-donation of the NMe_2 group to the p_z atomic orbital of the carbene carbón atom compared to the OEt group. Moreover, the olefinic hydrogen atoms of the tether joining the BODIPY and the metal–carbene fragments exhibit a coupling constant of *J* = 15–17 Hz, which is attributable to an *E* stereochemistry of the double bond. With these characteristics, two possible isomers of the carbene complexes **3** and **4**, which maintain the *E*-stereochemistry and the *s-trans* arrangement but with a different relative orientation of the BODIPY and metal–carbene fragments, can be envisaged (Scheme 2).

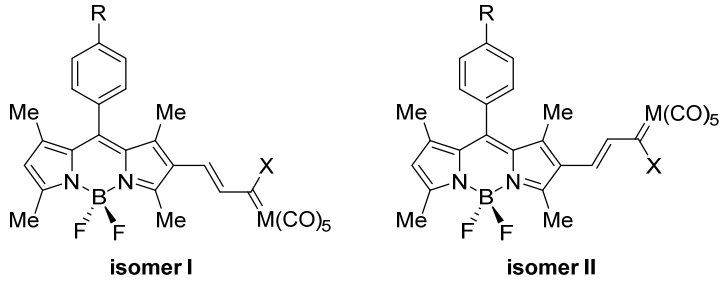

Scheme 2. Possible isomers of complexes **3** (X = OEt) and **4** (X = NMe_2).

Density functional theory (DFT) calculations carried out at the B3LYP/def2-SVP level (see the computational details in the Experimental Section) on complexes **3aa** (where the OEt group was replaced by a methoxy group) and **4aa** reveal that both isomers are nearly isoenergetic in the gas phase (ΔE(**3aaI–3aaII**) = 0.4 kcal·mol^{-1} and ΔE(**4aaI–4aaII**) = 0.1 kcal·mol^{-1}). Interestingly, a X-ray diffraction analysis of suitable crystals of carbene complex **3ba** (grown in pentane/ethyl acetate solution at -20°C) indicates that in the solid state, isomer I is preferred (Figure 1).[15] This suggests that the crystal packing has a strong influence on the conformation adopted by these species. Moreover, and as expected, the ethoxy group directly attached to the carbene carbon atom adopts the so-called *anti*

conformation (that is, the CH_2 group is oriented towards the CO wall of the metal fragment), which is the preferred conformation for most of the alkoxy Fischer carbene complexes not only in the gas phase but also in the solid state.[16]

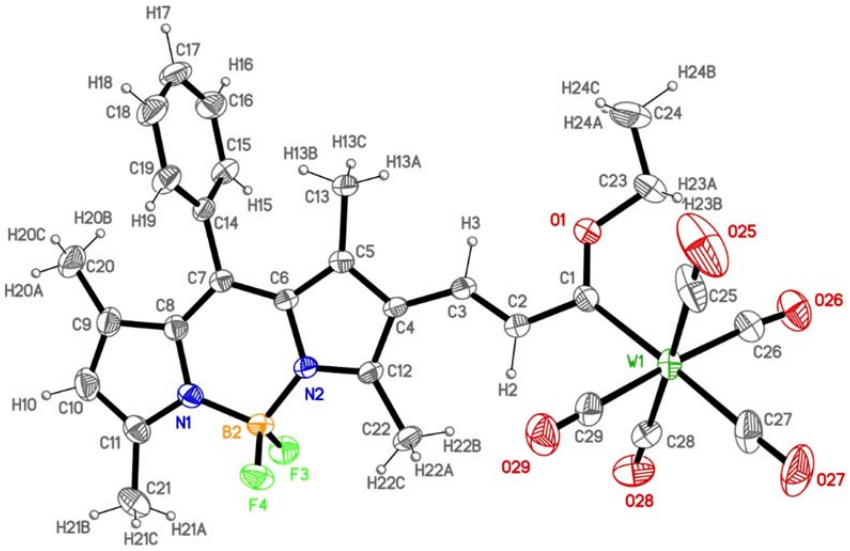

Figure 1. ORTEP of compound **3ba**. Ellipsoids are set at 30% probability.

Another important geometrical feature revealed by this experimental–computational study is the high planarity exhibited by alkoxycarbenes **3** (computed Cr-C-C-C dihedral angle of 0.0° and 0.4° in **3aa** and **3ac**, respectively)[17] which reflects well the extent of π-conjugation between the BODIPY and metal–carbene fragments through the ethylene bridge. Differently, these fragments are not coplanar in aminocarbenes **4** (computed Cr-C-C-C dihedral angle of 55.8° in **4aa**), thus indicating the lack of π-conjugation between them (Figure 2). This marked difference in the structures of complexes **3** and **4** can be ascribed to the stronger π-donating ability of the nitrogen atom to the to the p_z atomic orbital of the carbene carbon atom compared to the more electronegative oxygen atom. As a consequence, the π-acceptor nature of the pentacarbonylmetal–carbene fragment is clearly diminished in aminocarbenes **4**, which cannot accept additional electronic density from the BODIPY fragment, which in turn behaves as a π-donor group in alkoxycarbene complexes **3** (see below). An important conclusion can be drawn from this simple structural analysis: the ethylene-BODIPY fragment is mainly isolated in aminocarbene complexes **4**, whereas it is fully conjugated in

alkoxycarbene complexes **3**. Therefore, it should be expected that the ethylene-BODIPY moiety in complexes **4** would behave similarly (in terms of photophysical properties) to BODIPY units possessing an ethylene group in position **2**, while markedly different properties should be expected for alkoxy substituted complexes **3** (see below).

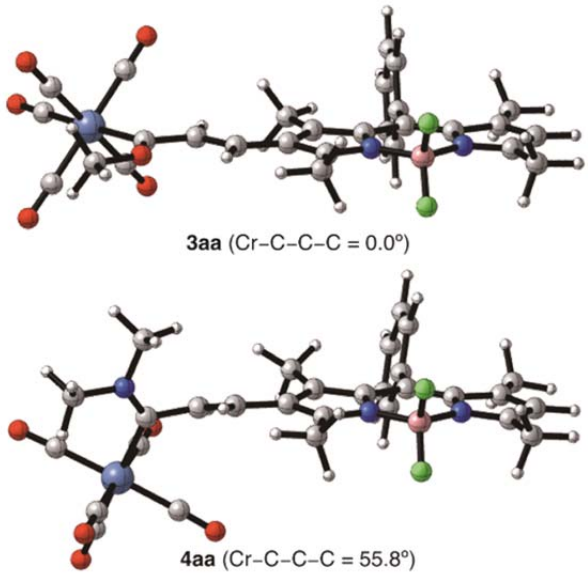

Figure 2. Optimised geometries (B3LYP/def2-SVP level) of complexes **3aa** and **4aa**.

The enhanced π-conjugation in complexes **3** should be in addition reflected in measurable changes in the equilibrium geometry of these species. As a consequence of the strong π-acceptor ability of the {$(CO)_5M$=C(OR)} fragment, the contribution of the resonance structure II depicted in Scheme 3 becomes more important in the description of the equilibrium geometry of complexes **3**. In contrast, resonance form III describes better the equilibrium geometry of complexes **4**. The population of form II thus involves the central C2=C3 double bond becoming weaker whereas the C1-C2 bond becomes stronger. This becomes clear when comparing the corresponding Wiberg Bond Indices (WBIs) computed for **3aa** and **4aa**: WBI(C1-C2): 1.21 versus 1.12 and WBI(C2=C3): 1.61 versus 1.71, respectively. Moreover, the strong π-donor ability of the NMe_2 compared to the OEt group is clearly reflected in the Cr-$C_{carbene}$ bond strength, which is significantly weaker in **4aa** (WBI = 0.74) than in **3aa** (WBI = 0.88).

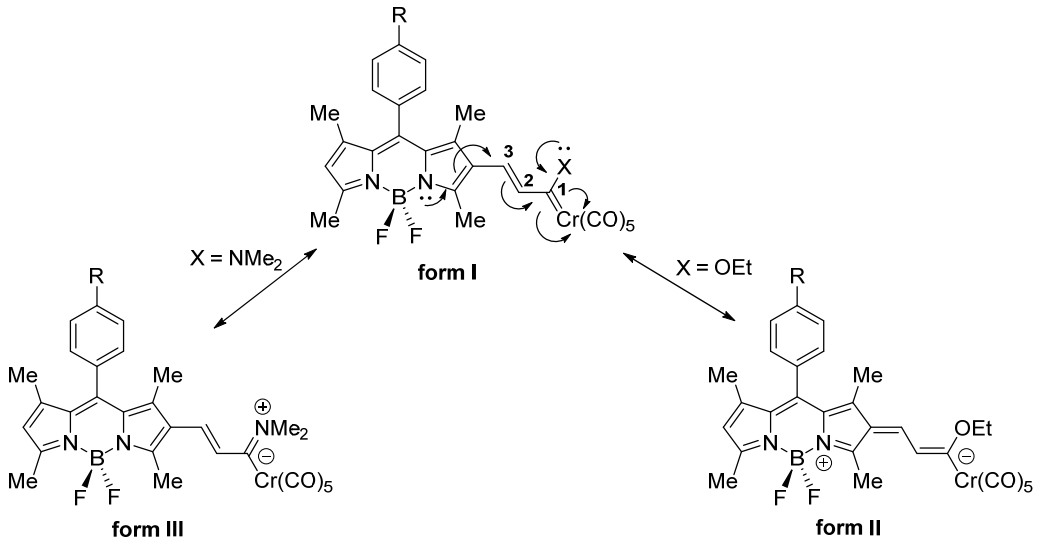

Scheme 3. Resonance formes for complexes **3** (X = OEt) and **4** (X = NMe_2).

Absorption and emission properties: Figure 3 a, b shows the UV/Vis spectra of all of the dyads **3** and **4**, respectively, recorded at 298 K in hexane with a concentration of 10^{-5} mol·L^{-1} (see also Table 1). The spectra of alkoxycarbene complexes **3** exhibit two main absorption bands at the visible region (Figure 3a). The less intense peak at about 425 nm can be tentatively assigned to a ligand-field (LF) transition involving the carbene ligand. Additionally, the intense and broad band at around 570 nm can be assigned to a metal-to-ligand charge transfer (MLCT) absorption band. Moreover, a shoulder is found at about 520 nm in the MLCT band, which is more noticeable in **3aa** and **3ab** complexes, that can be reasonably assigned to a transition involving the BODIPY fragment by comparison with the spectra of the parent formyl-BODIPY species **2** (see inset in Figure 3a). This assignment is in good agreement with the corresponding maxima ($\lambda_{max} \approx 527$ nm) of the excitation spectra of alkoxycarbene complexes **3** (see Table 1 and the Supporting Information). Different results are obtained in aminocarbene complexes **4** (Figure 3b), which exhibit more intense MLCT absorption bands at about 530 nm. Noticeably, no significant differences have been observed in the UV/Vis spectra of the tungsten(0) carbene complexes **3ba** and **4ba**.

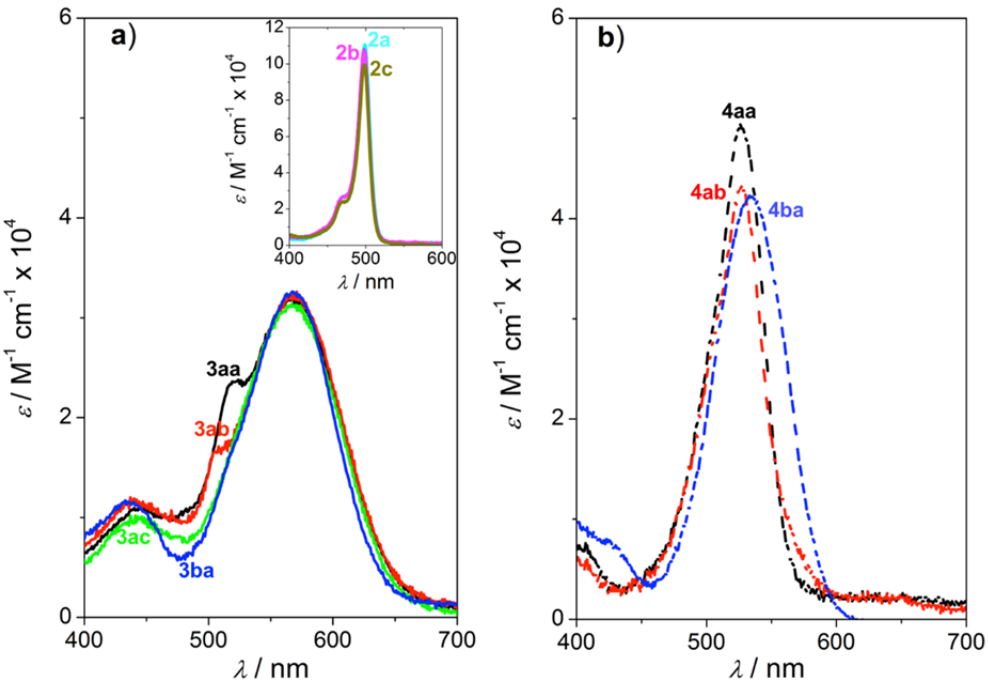

Figure 3. a) UV/Vis spectra of the alkoxycarbene complexes **3aa**, **3ab**, **3ac**, and **3ba**. The inset shows the UV/Vis spectra of the parent formyl-BODIPY's **2a**, **2b** and **2c**. b) UV/Vis spectra of the aminocarbene complexes **4aa**, **4ab**, and **4ba**. All of the measurements were carried out in a diluted solution in hexane (concentration 10^{-5} mol·L^{-1}, optical density < 0.1) at 298 K.

Table 1. Photophysical properties of complexes **3-5** and their parent formyl-BODIPY compounds **2a**.[a]

Compound	λ_{abs} [nm][b]	ε_{abs}[d]	λ_{em} [nm][f]	λ_{max} [nm][g]
2a	499	14.3	506	498
2b	498	10.8	506	498
2c	498	10.0	506	498
3aa	568 (549)[c]	3.2 (0.64)[e]	537	527
3ab	568	3.3	540	527
3ac	567 (545)[c]	3.1 (0.67)[e]	542	528
3ba	568	3.2	541	527
4aa	524	4.9	542	527
4ab	527	4.3	550	527
4ba	535	4.2	534	527
5ca	532	4.9	545	528

[a] All of the samples were recorded at 298 K in hexane (concentration of 10^{-6} mol·L^{-1}, optical density < 0.1). [b] Maximum of the UV/Vis spectrum. [c] Calculated TD-DFT excitation energy (in nm). [d] Molar extinction coefficient ε (L·mol^{-1}·cm^{-1} x 10^4). [e] Calculated TD-DFT oscillator strength. [f] Maximum of the emission spectrum using λ_{exc} = 460 nm. [g] Maximum of the excitation spectrum using λ_{obs} = 600 nm.

Compared to related styryl ethoxycarbene complexes,[14] the presence of the BODIPY substituent in complexes **3** induces a significant bathochromic shift on the MLCT absorption band (from ca. 475 nm in styryl ethoxycarbene complexes to ca. 570 nm in complexes **3**). This is a quite remarkable result as it was demonstrated that the position of the MLCT band in this type of complexes remains mostly unaltered regardless the electronic nature of the substituent attached to the styryl group linked to the metal–carbene fragment.[14] A comparable red-shift has only been observed in biscarbene complexes, where the cooperative effect of both {$(CO)_5M=C(OR)$} fragments greatly enhances the π-conjugation between the tether and the metal–carbene moieties.[18] Therefore, dyads **3** can be considered as new push–pull systems with extended π-conjugation, where the BODIPY fragment behaves as a π-donor substituent forced by the strong electron-withdrawing effect of the pentacarbonylmetal–carbene unit through the ethylenic spacer.[19]

Differently, the bathochromic shift induced in the MLCT absorption band of aminocarbene complexes **4** is not that significant ($\lambda_{abs} \approx 530$ nm), reflecting the lower extension of the π conjugation between the BODIPY and the metal–carbene fragments in these complexes. Moreover, and as expected from the lack of coplanarity between the indacene and the C8-aryl fragment owing to the steric hindrance of the indacene methyl groups (Figures 1 and 2), no dependence of the position of the MLCT band with the substitution in the C8-aryl fragment was observed in complexes **3** or **4**.

Time-dependent DFT (TD-DFT) calculations were carried out on complexes **3aa** and **3ac** to determine the nature of the vertical transitions associated with the observed UV/Vis absorptions. A very good agreement between the vertical excitation energies (computed in hexane as solvent) and the wavelengths of the absorption maxima in the experimental UV/Vis spectra was found, which allows the accurate assignment of the experimentally observed bands. Thus, our calculations indicate that the band at about 570 nm is the result of the one-electron promotion from the HOMO to the LUMO. As shown in Figure 4, the HOMO is a π-molecular orbital that is mainly located at the metal fragment with a

small contribution at the BODIPY moiety. In contrast, the LUMO is a π-molecular orbital that is fully delocalized within the indacene moiety. Therefore, the observed band can indeed be considered as a MLCT band with a remarkable π-π* character. As expected, no contribution of the aryl fragment attached to the C8 position of the indacene into the HOMO or the LUMO is observed, thus confirming the spectator role of this substituent on the electronic properties of these BODIPY–metal carbene dyads.

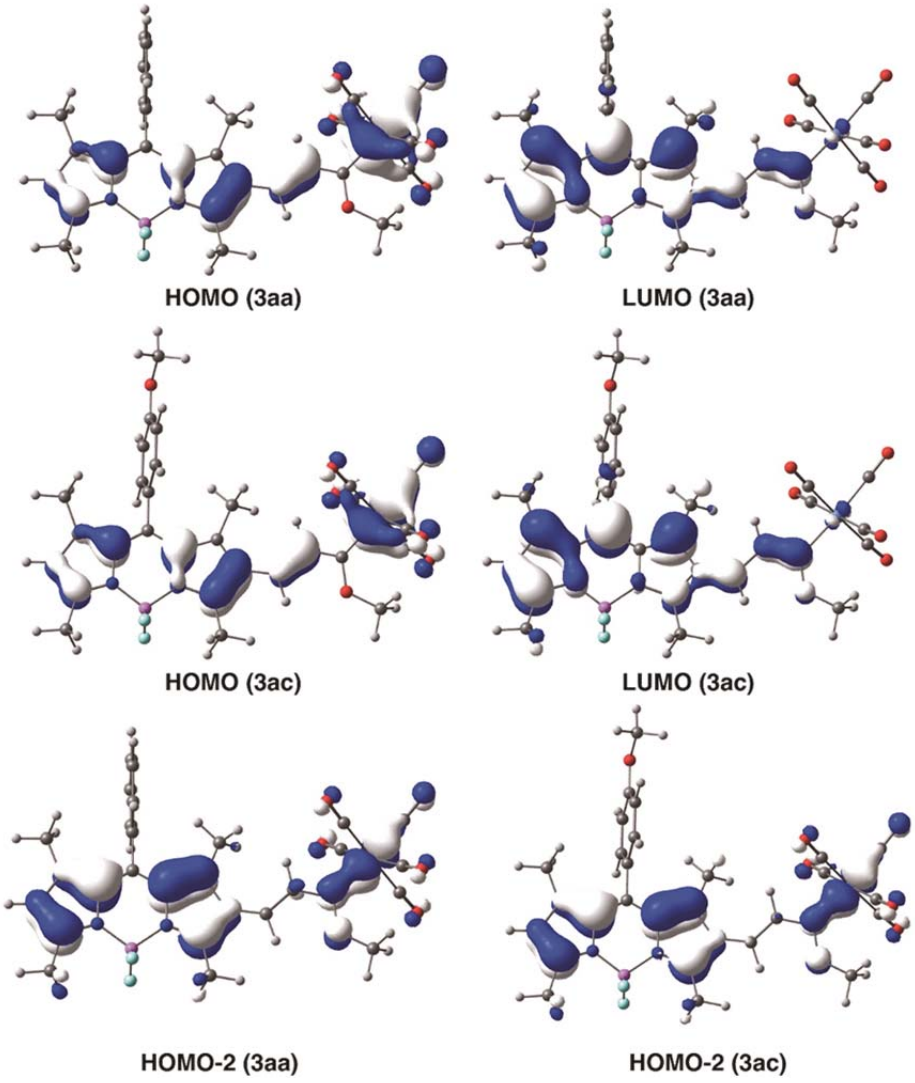

Figure 4. Computed molecular orbitals of complexes **3aa** and **3ac** (isosurface value of 0.035 au).

According to our TD-DFT calculations, the band appearing at about 425 nm is mainly the result of the promotion of one electron from the HOMO-2 to the LUMO. As shown in Figure 4, the HOMO-2 is again a π-molecular orbital that is

mainly localized in the indacene fragment with only a small contribution coming from the metal fragment. In agreement with our initial tentative assignment, this band can be considered as a π-π* LF transition involving the BODIPY moiety.

To compare the energy transfer process after excitation of the energy-push component in dyads **3** and **4**, we have to consider that no selective excitation on the BODIPY absorption band is possible owing to the full overlap with the MLCT absorption band. However, the spectra of complexes **3** and **4** show isoabsorptive points at about 460 nm with the parent formyl-BODIPY compounds **2**, in which the BODIPY moiety is expected to absorb a similar fraction of the incident light, thus allowing a qualitative understanding of the emissive properties.

Figure 5 shows the emission spectra of complexes **3** and **4**. Both type of dyads display broad emission bands centred at about 545 nm, which are considerably red-shifted (ca. 40 nm) relative to the parent formyl-BODIPY compounds **2**, owing to the presence of conjugated systems in position **2** of the fluorophore that lowers its LUMO level and consequently, the energy of the emission transition.[2b] The emission redshifts are in good agreement with those observed at the excitation spectra (see Table 1 and the Supporting Information), keeping the Stokes shift of dyads **3** and **4** approximately constant with respect to the parent formyl-BODIPY species **2**. From Figure 5, it is noteworthy that the alkoxycarbene complexes **3** show very low emission intensities. The practically total suppression of the BODIPY-based emission can be attributed to a very efficient energy transfer occurring from the higher-lying BODIPY excited state to the lower-lying carbene state owing to π-conjugation with the metal–carbene fragment (see above). In contrast, aminocarbene complexes **4** show a small quenching of the fluorescence (about three times lower) when compared with the emission of parent formyl-BODIPY species **2** (see Figure 5). This result reveals that the π-conjugation between the ethylene-BODIPY and the metal–carbene fragments is strongly hindered by the introduction of the NMe_2 group. Taking into account the similar distances between the BODIPY and metal–carbene moieties within dyads **3** and **4** (B···C carbene distance of 7.5Å), a Dexter-type energy

transfer through-bond mechanism seems to be operative in the observed suppression of the emission properties of carbene complexes **3**. Therefore, our results indicate that the emission of BODIPY can be easily switched on/off by controlling the extent of conjugation with the pentacarbonylmetal–carbene moiety.

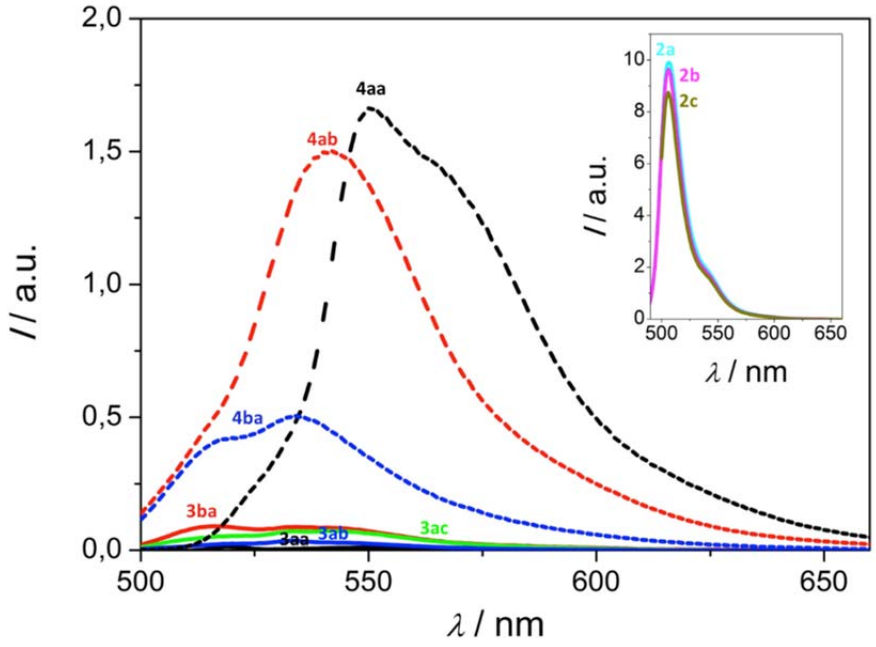

Figure 5. Emission spectra of the alkoxycarbene complexes (——) **3aa**, **3ab**, **3ac**, and **3ba**, and emission spectra of the aminocarbene complexes (-----) **4aa**, **4ab**, and **4ba**. Inset: emission spectra of the parent formyl-BODIPY compounds **2a**, **2b**, and **2c**. All of the measurements were carried out in a diluted solution in hexane (concentration ca. 10^{-6} mol·L^{-1}, optical density < 0.1) at 298 K (λ_{exc} = 460 nm).

To further confirm the effect of the π-conjugation on the properties of these dyads, we finally synthesized complex **5ca**, which possesses a sulfur atom directly attached to the carbene carbon atom. The synthesis of this complex was conducted similarly to complexes **3**. Thus, from thiocarbene complex **1c** and formyl-BODIPY derivate **2a** in the presence of Et_3N and TMSCl, dyad **5ca** was obtained in 30 % reaction yield (Scheme 4).

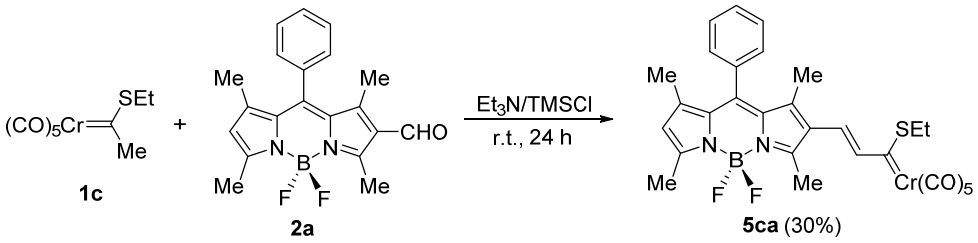

Scheme 4. Synthesis of complex **5ca**.

As the π-donor ability of the SEt group is lower than that of NMe_2 and the electronegativity of the sulfur atom is lower than the electronegativity of oxygen, an intermediate equilibrium geometry for thiocarbene **5ca** should be expected between the extreme situations represented by the ethoxycarbene **3aa** and the aminocarbene **4aa**. Indeed, the optimized geometry of **5ca** at the B3LYP/def2-SVP level (Figure 6) shows a computed Cr-C1-C2-C3 dihedral angle of 31.0° (which is intermediate between 0.0° and 55.8° computed for **3aa** and **4aa**, respectively). Furthermore, the corresponding WBIs of 1.62 and 0.84 for the C2-C3 and Cr-C1 bonds, respectively, confirms well that the extent of π-conjugation in thiocarbene is also intermediate between that in alkoxy- and aminocarbene complexes. As a consequence, the corresponding MLCT band maximum appears at about 532 nm (intermediate between amino- and alkoxycarbenes; see Table 1) and again, corresponds to the HOMO → LUMO vertical excitation according to TD-DFT calculations. Not surprisingly, the fluorescence of BODIPY in thiocarbene **5ca** is only partially quenched (Figure 7). Thus, an emission band at 545 nm appears in the corresponding emission spectrum, although its relative intensity respect to the parent formyl-BODIPY compounds **2** is clearly much lower (about six times lower). Although the emission of this complex is therefore lower than that observed for its aminocarbene analogue **4aa**, it is not suppressed as it occurs in alkoxycarbenes. This result supports well the idea that the photophysical properties of the BODIPY fragment can be tuned by subtle modifications of the electronic nature of the metal–carbene fragment, which controls the extent of π-conjugation of the dyad.

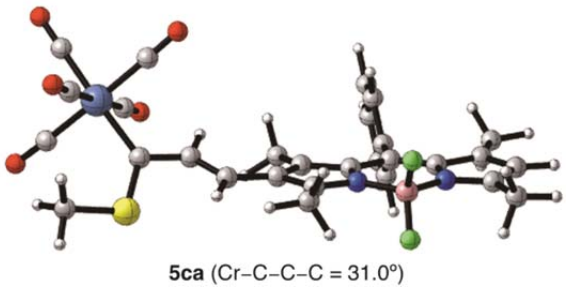

Figure 6. Optimised geometry (B3LYP/def2-SVP level) of complex **5ca**.

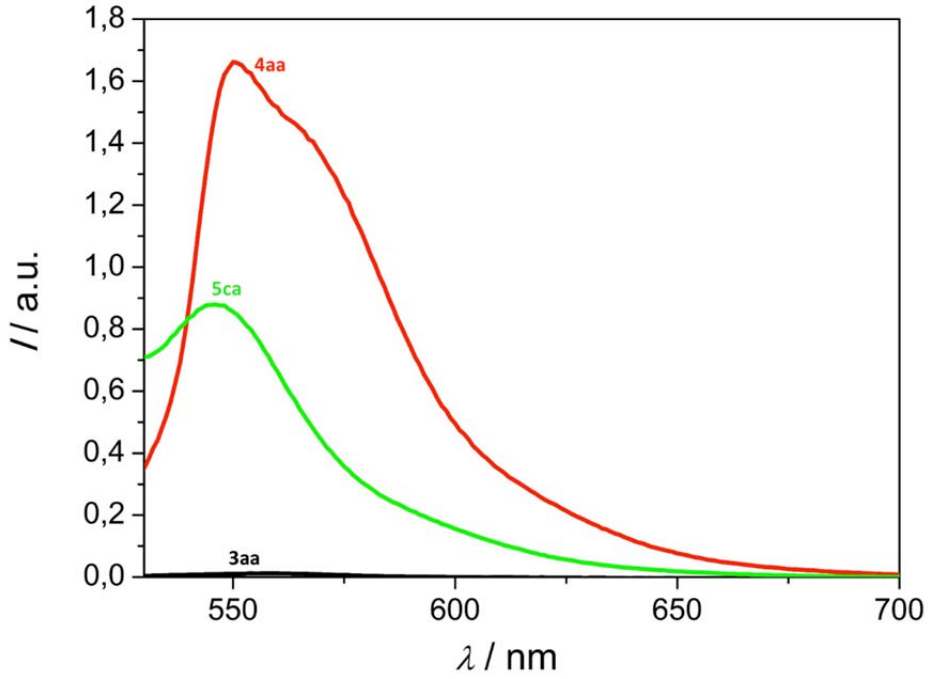

Figure 7. Comparison between emission spectra of the dyads **3aa**, **4aa**, and **5ca** (λ_{exc} = 460 nm). All of the measurements were carried out in a diluted solution in hexane (concentration 10^{-6} mol·L^{-1}, optical density < 0.1) at 298 K.

IV.4. Conclusions

From the joint experimental–computational study reported herein, it becomes obvious that the photophysical properties of the BODIPY chromophore can be modified, in principle at will, by means of direct π-conjugation with Fischer carbene complexes. The extent of π-conjugation is decisive in altering the equilibrium geometry, and consequently, the photophysical properties of the BODIPY chromophore. Thus, when an alkoxycarbene complex is present in the

BODIPY–metal carbene dyad, the π-conjugation is maximized. This is reflected in a significant bathochromic shift of the corresponding MLCT band, which is the result of the π-donor behavior of the BODIPY moiety. In contrast, π-conjugation is strongly diminished when an aminocarbene complex is present in the dyad. As a consequence, the BODIPY moiety is now mainly isolated in these compounds which exhibit a similar fluorescence than formyl-BODIPY derivatives. In contrast, as the electronic structure of the BODIPY fragment is strongly altered by π-conjugation with the alkoxycarbene moiety, complexes **3** exhibit a complete suppression of the fluorescence associated with the BODIPY chromophore. An intermediate situation is found in BODIPY– thiocarbene complex dyads owing to lower electronegativity (compared to oxygen) and π-donor ability (compared to nitrogen) of the sulfur atom, which confirms the importance of π conjugation in controlling the properties of the BODIPY units.

It is hoped that the present study will be of future use in materials chemistry owing to the ease of tuning the photophysical properties of BODIPY units by subtle modifications on the metal–carbene moiety.

IV.5. Computational Details

Geometry optimizations without symmetry constraints were carried out using the Gaussian 09 suite of programs[20] using the B3LYP[21] functional in combination with the double-ζ plus polarisation def2-SVP basis sets[22] for all atoms. This level is denoted B3LYP/def2-SVP. Stationary points were characterized as minima by calculating the Hessian matrix analytically at this level. Calculations of absorption spectra were accomplished by using the time-dependent density functional theory (TD-DFT)[23] method at the same level. TD-DFT calculations were performed in *n*-hexane as solvent using the polarizable continuum model (PCM) method.[24] The assignment of the excitation energies to the experimental bands was performed on the basis of the energy values and oscillator strengths. The B3LYP Hamiltonian was chosen because it was shown to provide reasonable UV/Vis spectra for a variety of chromophores,[25] including Fischer carbene complexes[14,18] and other organometallic species.[26] Wiberg bond indices were computed by using the natural bond orbital (NBO) method.[27]

IV.6. Experimental Section

General Procedures. All reactions were carried out under an argon atmosphere. All solvents used in this work were purified by distillation and were freshly distilled immediately before use. Triethylamine (Et_3N) was distilled from calcium hydride, whereas tetrahydrofuran (THF) and diethylether (Et_2O) were distilled from sodium/benzophenone. Flame-dried glassware was used for moisture-sensitive reactions. Silica gel (Merck: 230-400 mesh) were used as stationary phases for purification of crude reaction mixtures by flash column chromatography. Identification of products was made by thin-layer chromatography (Kieselgel 60F-254). UV light (λ 254nm) and 5% phosphomolybdic acid solution in 95% EtOH were used to develop the plates. NMR spectra were recorded at 25 °C in $CDCl_3$, on Bruker Avance 300 (300 MHz for ^1H and 75 MHz for ^{13}C). Chemical shifts are given in ppm relative to $CDCl_3$ (^1H, 7.27 ppm and ^{13}C, 77.0 ppm). IR spectra were taken on a MIR (8000−400 cm^{-1}) spectrometer as solid films by slow evaporation of the solvent using the ATR (attenuated total reflectance) technique. MS spectra (HRMS) were acquired on a QTOF 6520: HP-1200 (Agilent Technologies) mass spectrometer or a FTMS Bruker APEX Q IV.

Absorption and Fluorescence Spectroscopies. All experiments were carried out at 298 K, in hexane (concentration of ca. $1 \cdot 10^{-6}$ $mol \cdot L^{-1}$, optical density < 0.1), using quartz cuvettes with optical paths of 1 cm. UV absorption spectra were registered using a UVICON XL spectrophotometer (Bio-Tex Instruments). Steady-state fluorescence spectra were recorded using an AMINCO Bowman Series 2 spectrofluorometer, with 1.0 nm bandwidth for emission and excitation. The excitation wavelengths were fixed at 460 nm and 490 nm in the measurement of the emission spectra. The emission wavelength was fixed at 600 nm for the determination of all the excitation spectra.

All commercially available products were used without further purification. The following BODIPYs were prepared according to literature: **2a**,[28] **2b**,[29] **2c**[28]. The

following metal-carbenes were prepared according to previously described methods: Pentacarbonyl [(ethoxy) (methyl)carbene]chromium(0),[30] pentacarbonyl[(ethoxy)(methyl)carbene]tungsten(0),[31] pentacarbonyl[1-(ethyl-thio)(methyl)carbene]chromium(0).[32]

General procedure of Aumann's reaction. To a solution of the corresponding aldehyde (1 mmol) in anhydrous Et_2O (5 mL) were added Et_3N (4 mmol) and TMSCl (3 mmol). Immediately a solution of the corresponding Fischer carbene complex (1.5 mmol) in anhydrous Et_2O (1 mL) were added to the solution mixture at room temperature. The mixture was stirred until total disappearance of the starting material (checked by TLC). The solvent was removed under reduced pressure and the product purified by flash chromatography on silica gel under argon pressure.

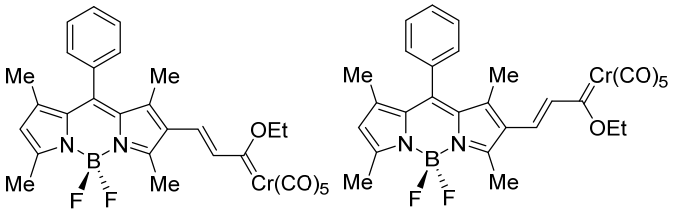

Complex 3aa: To a solution of **2a** (200 mg, 0.57 mmol), Et_3N (0.7 mL, 5.02 mmol) and TMSCl (220 μL, 1.71 mmol) in 3.0 mL of dry Et_2O was added the carbene complex **1a** (227 mg, 0.86 mmol) in 0.6 mL of dry Et_2O. The reaction mixture was stirred at room temperature for 24h. The solvent was removed under reduced pressure and purified by flash chromatography to yield compound **3aa** as a purple solid (271 mg, 78%). ^{1}H NMR (300 MHz, ppm): δ 7.60-7.5 (m, 8H), 7.37 (m, 4H), 7.20 (d, *J* = 15.4Hz, 1H), 7.13 (d, *J* = 15.4Hz, 1H), 6.12 (s, 1H), 6.11 (s, 1H), 5.06-4.96 (m, 4H), 2.75 (s, 6H), 2.61 (s, 6H), 1.65 (t, *J* = 7.1 Hz, 6H), 1.54 (s, 3H), 1.53 (s, 3H), 1.42 (s, 6H). ^{13}C NMR (75 MHz, ppm) δ 326.4, 325.4, 224.5, 224.4, 217.3, 217.2, 159.8, 159.7, 155.9, 155.8, 146.2, 146.1, 145.4, 142.4, 142.2, 140.8, 140.1, 138.9, 138.2, 134.8, 134.4, 133.2, 131.0, 130.9, 129.5, 129.4, 129.3, 129.3, 128.1, 127.9, 127.8, 126.1, 125.1, 124.6, 124.3, 123.4, 75.2, 75.1, 15.4, 15.3, 15.1, 14.9, 14.8, 14.7, 14.4, 14.3, 13.1, 13.0. IR (CH_2Cl_2): ν 2052, 1921, 1539, 1511, 1192, 664 cm^{-1}. HRMS (ESI): *m/z* calcd for $C_{29}H_{26}BCrF_2N_2O_6$ [M + H] 599.1258, found 599.1252.

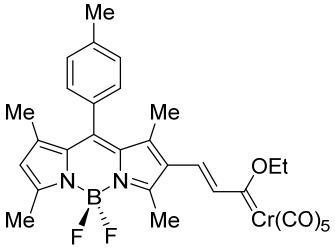

Complex 3ab: To a solution of **2b** (465 mg, 1.27 mmol), Et_3N (1.5 mL, 10.75 mmol) and TMSCl (500 μL, 3.93 mmol) in 6.8 mL of dry Et_2O was added the carbene complex **1a** (503 mg, 1.90 mmol) in 1.3 mL of dry Et_2O. The reaction mixture was stirred at room temperature for 24h. The solvent was removed under reduced pressure and purified by flash chromatography to yield compound **3ab** as a purple solid (298 mg, 38%). ^{1}H NMR (300 MHz, ppm): δ 7.57 (d, *J* = 15.3 Hz, 1H), 7.37 (d, *J* = 7.7 Hz, 2H), 7.17 (d, *J* = 7.7 Hz, 2H), 7.16 (d, *J* = 15.3 Hz, 1H), 6.11 (s, 1H), 5.02 (q, *J* = 7.1 Hz, 2H), 2.74 (s, 3H), 2.61 (s, 3H), 2.48 (s, 3H), 1.65 (t, *J* = 7.1 Hz, 3H), 1.56 (s, 3H), 1.45 (s, 3H). ^{13}C NMR (75 MHz, ppm): δ 326.2, 224.4, 217.2, 159.6, 155.8, 146.3, 142.9, 140.8, 139.5, 138.8, 133.5, 131.4, 131.2, 130.0, 127.7, 125.5, 124.4, 123.2, 75.2, 21.4, 15.1, 14.9, 13.9, 13.8, 13.2. IR (CH_2Cl_2): ν 2053, 1929, 1540, 1516, 1190, 665 cm^{-1}. HRMS (ESI): *m/z* calcd for $C_{30}H_{28}BCrF_2N_2O_6$ [M + H] 613.1415, found 613.1431.

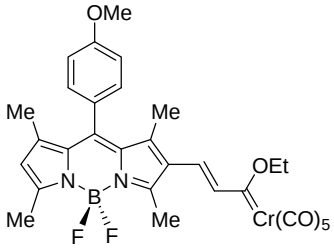

Complex 3ac: To a solution of **2c** (126 mg, 0.33 mmol), Et_3N (0.4 mL, 1.32 mmol) and TMSCl (120 μL, 0.99 mmol) in 1.8 mL of dry Et_2O was added the carbene complex **1a** (131 mg, 0.50 mmol) in 0.3 mL of dry Et_2O. The reaction mixture was stirred at room temperature for 24h. The solvent was removed under reduced pressure and purified by flash chromatography to yield compound **3ac** as a purple solid (90 mg, 43%). ^{1}H NMR (300 MHz, ppm): δ 7.57 (d, *J* = 15.4 Hz, 1H), 7.21-7.05 (m, 5H), 6.12 (s, 1H), 5.02 (q, *J* = 7.1 Hz, 2H), 3.91 (s, 3H), 2.74 (s, 3H), 2.61 (s, 3H), 1.65 (t, *J* = 7.1 Hz, 3H), 1.59 (s, 3H), 1.48 (s, 3H). ^{13}C NMR (75 MHz, ppm): δ 326.2, 224.4, 217.2, 160.5, 159.6, 155.8, 146.2, 142.5, 140.8, 138.8, 133.7, 131.4, 129.2, 126.4, 125.2, 124.5, 123.2, 114.8, 75.2, 55.3, 15.1, 15.0, 14.9, 13.9, 13.3. IR (CH_2Cl_2): ν 2052, 1922, 1538, 1514, 1192, 664 cm^{-1}. HRMS (ESI): *m/z* calcd for $C_{30}H_{28}BCrF_2N_2O_7$ [M + H] 629.1364, found 629.1361.

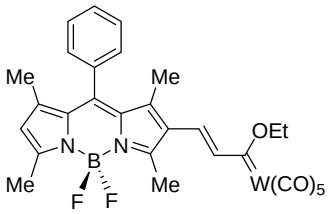

Complex 3ba: To a solution of **2a** (170 mg, 0.46 mmol), Et_3N (0.6 mL, 4.30 mmol) and TMSCl (200 μL, 1.56 mmol) in 2.5 mL of dry Et_2O was added the carbene complex **1b** (285 mg, 1.01 mmol) in 0.6 mL of dry Et_2O. The reaction mixture was stirred at room temperature for 24h. The solvent was removed under reduced pressure and purified by flash chromatography to yield compound **3ba** as a purple solid (138 mg, 40%). ^{1}H NMR (300 MHz, ppm): δ 7.56-7.49 (m, 4H), 7.38 (d, *J* = 15.5 Hz, 1H), 7.32-7.29 (m, 2H), 6.13 (s, 1H), 4.88 (q, *J* = 7.2 Hz, 2H), 2.75 (s, 3H), 2.61 (s, 3H), 1.63 (t, *J* = 7.2 Hz, 3H), 1.52 (s, 3H), 1.42 (s, 3H). ^{13}C NMR (75 MHz, ppm): δ 300.9, 203.8, 197.9, 159.9, 155.7, 146.3, 142.7, 142.4, 140.7, 134.4, 133.3, 131.1, 129.6, 129.4, 129.3, 127.8, 124.8, 123.4, 78.0, 14.9, 14.7, 14.0, 13.9, 13.0. IR (CH_2Cl_2): ν 2061, 1913, 1538, 1510, 1191, 724 cm^{-1}. HRMS (ESI): *m/z* calcd for $C_{29}H_{26}BF_2N_2O_6W$ [M + H] 731.1365, found 731.1345.

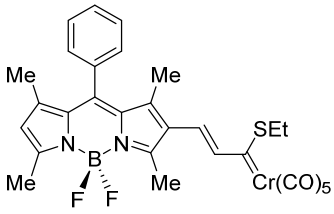

Complex 5ca: To a solution of **2a** (110 mg, 0.31 mmol), Et_3N (0.4 mL, 2.90 mmol) and TMSCl (120 μL, 0.93 mmol) in 1.7 mL of dry Et_2O was added the carbene complex **1c** (132 mg, 0.47 mmol) in 0.5 mL of dry Et_2O. The reaction mixture was stirred at room temperature for 24h. The solvent was removed under reduced pressure and purified by flash chromatography to yield compound **5ca** as a purple solid (57 mg, 30%). ^{1}H NMR (300 MHz, ppm): δ 7.84 (d, *J* = 15.0 Hz, 1H), 7.77 (d, *J* = 15.0 Hz, 1H), 7.57-7.53 (m, 3H), 7.34-7.31 (m, 2H), 6.17 (s, 1H), 3.15 (q, *J* = 7.6 Hz, 2H), 2.83 (s, 3H), 2.64 (s, 3H), 1.59 (s, 3H), 1.44 (s, 3H), 1.36 (t, *J* = 7.6 Hz, 3H). ^{13}C NMR (75 MHz, ppm): δ 322.3, 227.1, 217.7, 161.2, 155.6, 147.1, 144.6, 142.5, 140.6, 136.1, 134.2, 133.8, 131.1, 129.6, 129.5, 127.9, 126.1, 124.0, 35.5, 15.1, 14.9, 14.5, 12.9, 12.2. IR (CH_2Cl_2): ν 2047, 1919, 1538, 1506, 1162, 655 cm^{-1}. HRMS (ESI): *m/z* calcd for $C_{29}H_{26}BCrF_2N_2O_5S$ [M + H] 615.1030, found 615.1006.

General Procedure for the Preparation of Amino-Carbene Complexes. A solution of dimethylamine (2 equiv, 2.0 M in THF) was added dropwise to a solution of the corresponding ethoxy-carbene complex (1 equiv) in dry THF at -100 °C. The reaction mixture was stirred under argon at this temperature until total consumption of the starting material. The solvent was then evaporated *in vacuo* and the resulting crude reactions purified by flash column chromatography under argon pressure.

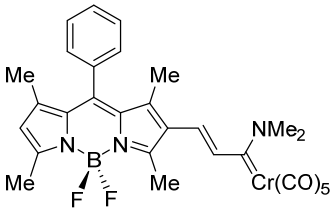

Complex 4aa: To a solution of **3aa** (50 mg, 0.08 mmol) in dry THF (0.7 mL) was added a solution of dimethylamine in THF (80 μL, 0.16 mmol) at -100 °C. The reaction mixture was stirred at room temperature for 10 min. The solvent was removed under reduced pressure and purified by flash chromatography to yield compound **4aa** as a pink dark solid (40 mg, 80%). ^{1}H NMR (300 MHz, ppm): δ 7.52-7.49 (m,3H), 7.31-7.28 (m, 2H), 6.70 (d, *J* = 17.0 Hz, 1H), 6.03 (s, 1H), 5.74 (d, *J* = 17.0 Hz, 1H), 3.90 (s, 3H), 3.44 (s, 3H), 2.67 (s, 3H), 2.58 (s, 3H), 1.45 (s, 3H), 1.38 (s, 3H). ^{13}C NMR (75 MHz, ppm): δ 270.8, 223.3, 217.5, 156.8, 153.8, 144.1, 141.8, 139.7, 138.5, 135.9, 134.9, 129.2, 129.1, 128.0, 122.3, 121.9, 114.3, 51.2, 45.6, 14.7, 14.5, 14.1, 12.6. IR (CH_2Cl_2): ν 2051, 1919, 1539, 1514, 1192, 724 cm^{-1}. HRMS (ESI): *m/z* calcd for $C_{29}H_{27}BCrF_2N_3O_5$ [M + H] 598.1418, found 598.1429.

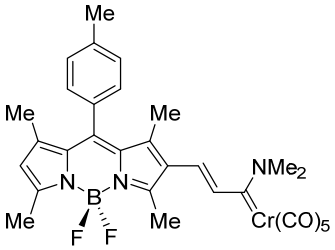

Complex 4ab: To a solution of **3ab** (250 mg, 0.41 mmol) in dry THF (3.2 mL) was added a solution of dimethylamine in THF (410 μL, 0.84 mmol) at -100 °C. The reaction mixture was stirred at room temperature for 10 min. The solvent was removed under reduced pressure and purified by flash chromatography to yield compound **4ab** as a pink dark solid (206 mg, 83%). ^{1}H NMR (300 MHz, ppm): δ 7.31 (d, *J* = 7.8 Hz, 2H), 7.16 (d, *J* = 7.8 Hz, 2H), 6.70 (d, *J* = 16.9 Hz, 1H), 6.02 (s, 1H), 5.74 (d, *J* = 16.9 Hz, 1H), 3.90 (s, 3H), 3.44 (s, 3H), 2.67 (s, 3H), 2.57 (s, 3H), 2.45 (s, 3H), 1.47 (s, 3H), 1.41 (s, 3H). ^{13}C NMR (75 MHz, ppm): δ 270.5, 223.3, 217.5, 157.4, 156.6, 144.2, 142.2, 139.6, 139.0, 138.5, 135.8, 132.2, 131.8, 129.9, 127.8, 126.2, 121.8, 114.4, 51.2, 45.6, 21.4, 14.6, 14.1, 13.7, 12.7. IR (CH_2Cl_2): ν 2051, 1917, 1539, 1517, 1196, 668 cm^{-1}. HRMS (ESI): *m/z* calcd for $C_{30}H_{27}BCrF_2N_3O_5$ [M - H] 610.1429, found 610.1425.

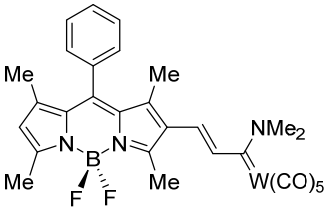

Complex 4ba: To a solution of **3ba** (138 mg, 0.19 mmol) in dry THF (1.6 mL) was added a solution of dimethylamine in THF (190 μL, 0.38 mmol) at -100 °C. The reaction mixture was stirred at room temperature for 10 min. The solvent was removed under reduced pressure and purified by flash chromatography to yield compound **4ba** as a pink dark solid (120 mg, 87%). ^{1}H NMR (300 MHz, ppm): δ 7.52-7.50 (m, 3H), 7.31-7.29 (m, 2H), 6.62 (d, *J* = 16.7 Hz, 1H), 6.04 (s, 1H), 6.03 (d, *J* = 16.7 Hz, 1H), 3.84 (s, 3H), 3.41 (s, 3H), 2.69 (s, 3H), 2.58 (s, 3H), 1.47 (s, 3H),

1.39 (s, 3H). ^{13}C NMR (75 MHz, ppm): δ 251.9, 203.4, 198.6, 157.0, 153.7, 144.3, 141.9, 140.1, 138.6, 134.7, 132.0, 130.7, 129.2, 129.1, 127.9, 126.2, 122.0, 119.0, 53.8, 44.0, 14.7, 14.5, 13.8, 12.6. IR (CH_2Cl_2): ν 2059, 1900, 1539, 1515, 1198, 724 cm^{-1}. HRMS (ESI): *m/z* calcd for $C_{29}H_{26}BF_2N_3O_5W$ [M + H] 730.1525, found 730.1526.

IV.7. References

(1) Treibs, A.; Kreuzer, F.-H. *Justus Liebigs Ann. Chem.* **1968**, *718*, 208.

(2) Recent reviews on the synthesis and properties of BODIPY's: (a) Loudet, A.; Burgess, K. *Chem. Rev.* **2007**, *107*, 4891. (b) Ulrich, G.; Ziessel, R.; Harriman, A. *Angew. Chem.* **2008**, *120*, 1202; *Angew. Chem., Int. Ed.* **2008**, *47*, 1184. (c) Ziessel, R.; Ulrich, G.; Harriman, A. *New J. Chem.* **2007**, *31*, 496. (d) Boens, N.; Leen, V.; Dehaen, W. *Chem. Soc. Rev.* **2012**, *41*, 1130. (e) Kamkaew, A.; Lim, S. H.; Lee, H. B.; Kiew, L. V.; Chung, L. Y.; Burgess, K. *Chem. Soc. Rev.* **2013**, *42*, 77.

(3) Representative examples: (a) Gareis, T.; Huber, C.; Wolfbeis, O. S.; Daub, J. *Chem. Commun.* **1997**, 1717. (b) Rurack, K.; Kollmannsberger, M.; Daub, J. *New J. Chem.* **2001**, *25*, 289. (c) Rurack, K.; Kollmannsberger, M.; Daub, J. *Angew. Chem.* **2001**, *113*, 396; *Angew. Chem., Int. Ed.* **2001**, *40*, 385. (d) DiCesare, N.; Lakowicz, J. R. *Tetrahedron Lett.* **2001**, *42*, 9105. (e) Baki, C. N.; Akkaya, E. U. *J. Org. Chem.* **2001**, *66*, 1512. (f) Turfan, B.; Akkaya, E. U. *Org. Lett.* **2002**, *4*, 2857. (g) Moon, Y. S.; Cha, N. R.; Kim, Y. H.; Chang, S. K. *J. Org. Chem.* **2004**, *69*, 181. (h) Atilgan, S.; Ekmekci, Z.; Lale Dogan, A.; Guc, D.; Akkaya, E. U. *Chem. Commun.* **2006**, 4398. (i) Harriman, A.; Izzet, G.; Ziessel, R. *J. Am. Chem. Soc.* **2006**, *128*, 10868. (j) Carlson, J. C. T.; Meimetis, L. G.; Hilderbrand, S. A.; Weissleder, R. *Angew. Chem.* **2013**, *125*, 7055; *Angew. Chem., Int. Ed.* **2013**, *52*, 6917.

(4) Galletta, M.; Campagna, S.; Quesada, M.; Ulrich, G.; Ziessel, R. *Chem. Commun.* **2005**, 4222.

(5) Rachford, A. A.; Ziessel, R.; Bura, T.; Retailleau, P.; Castellano, F. N. *Inorg. Chem.* **2010**, *49*, 3730.

(6) Nastasi, F.; Puntoriero, F.; Campagna, S.; Diring, S.; Ziessel, R. *Phys. Chem. Chem. Phys.* **2008**, *10*, 3982.

(7) Sun, J.; Zhong, F.; Yi, X.; Zhao, J. *Inorg. Chem.* **2013**, *52*, 6299.

(8) Wu, W.; Zhao, J.; Guo, H.; Sun, J.; Ji, S.; Wang, Z. *Chem. Eur. J.* **2012**, *18*, 1961.

(9) For selected recent reviews on the chemistry and applications of Fischer carbenes, see: (a) Wu, Y.-T.; Kurahashi, T.; de Meijere, A. *J. Organomet. Chem.* **2005**, *690*, 5900. (b) Gómez-Gallego, M.; Mancheño, M. J.; Sierra, M. A. *Acc. Chem. Res.* **2005**, *38*, 44. (c) Sierra, M. A.; Gómez-Gallego, M.; Martínez-Álvarez, R. *Chem. Eur. J.* **2007**, *13*, 736. (d) Sierra, M. A.; Fernández, I.; Cossío, F. P. *Chem. Commun.* **2008**, 4671. (e) Dötz, K. H.; Stendel, J. *Chem. Rev.* **2009**, *109*, 3227. (f) Herndon, J. W. *Coord. Chem. Rev.* **2010**, *254*, 103. (g) Fernández-Rodríguez, M. A.; García-García, P.; Aguilar, E. *Chem. Commun.* **2010**, *46*, 7670. (h) Fernández, I.; Cossío, F. P.; Sierra, M. A. *Acc. Chem. Res.* **2011**, *44*, 479. (i) Fernández, I.; Sierra, M. A. *Top. Heterocycl. Chem.* **2013**, *30*, 65.

(10) (a) Fernández, I.; Sierra, M. A.; Cossío, F. P. *J. Org. Chem.* **2008**, *73*, 2083. (b) Fernández, I.; Sierra, M. A.; Cossío, F. P. *J. Org. Chem.* **2006**, *71*, 6178. (c) Andrada, D. M.; Granados, A. M.; Solà, M.; Fernández, I. *Organometallics* **2011**, *30*, 466.

(11) (a) Leroux, F.; Stumpt, R.; Fischer, H. *Eur. J. Inorg. Chem.* **1998**, 1225. (b) Licandro, E.; Maiorana, S.; Papagani, A.; Hellier, P.; Capella, L.; Persoons, A.; Houbrechts, S. *J. Organomet. Chem.* **1999**, *583*, 111. (c) Robin-Le Guen, F.; Le Poul, P.; Caro, B.; Pichon, R.; Kervarec, N. *J. Organomet. Chem.* **2001**, *626*, 37. (d) Faux, N.; Caro, B.; Robin-Le Guen, F.; Le Poul, P.; Nakatani, K.; Ishow, E. *J. Organomet. Chem.* **2005**, *690*, 4982.

(12) Aumann, R.; Heinen, H. *Chem. Ber.* **1987**, *120*, 537.

(13) Péron, V.; Porhiel, E.; Ferrand, V.; Le Bozec, H. *J. Organomet. Chem.* **1997**, *539*, 201.

(14) Lage, M. L.; Fernández, I.; Mancheño, M. J.; Sierra, M. A. *Inorg. Chem.* **2008**, *47*, 5253.

(15) CCDC 946941 contains the supplementary crystallographic data for this paper. These data can be obtained free of charge from The Cambridge Crystallographic Data Centre via www.ccdc.cam.ac.uk/data_request/cif.

(16) (a) Fernández, I.; Cossío, F. P.; Arrieta, A.; Lecea, B.; Mancheño, M. J.; Sierra, M. A. *Organometallics* **2004**, *23*, 1065. (b) Andrada, D. M.; Zoloff Michoff, M. E.; Fernández, I.; Granados, M. A.; Sierra, M. A. *Organometallics* **2007**, *26*, 5854. (c) Valyaev, D. A.; Brousses, R.; Lugan, N.; Fernández, I.; Sierra, M. A. *Chem. Eur. J.* **2011**, *17*, 6602. (d) Lugan, N.; Fernández, I.; Brousses, R.; Valyaev, D. A.; Lavigne, G.; Ustynyuk, N. A. *Dalton Trans.* **2013**, *42*, 898.

(17) In the solid state, **3ba** exhibits a higher Cr-C-C-C dihedral angle of 12.8°, which may be attributable to packing forces.

(18) Chu, G. M.; Fernández, I.; Sierra, M. A. *Chem. Eur. J.* **2013**, *19*, 5899.

(19) Usually the BODIPY fragment behaves as an electron-acceptor group; see, for example: Liu, S.-R.; Wu, S.-P. *Org. Lett.* **2013**, *15*, 878.

(20) Gaussian 09, Revision B.01, Frisch, M. J.; Trucks, G. W.; Schlegel, H. B.; Scuseria, G. E.; Robb, M. A.; Cheeseman, J. R.; Scalmani, G.; Barone, V.; Mennucci, B.; Petersson, G. A.; Nakatsuji, H.; Caricato, M.; Li, X.; Hratchian, H. P.; Izmaylov, A. F.; Bloino, J.; Zheng, G.; Sonnenberg, J. L.; Hada, M.; Ehara, M.; Toyota, K.; Fukuda, R.; Hasegawa, J.; Ishida, M.; Nakajima, T.; Honda, Y.; Kitao, O.; Nakai, H.; Vreven, T.; Montgomery, J. A., Jr.; Peralta, J. E.; Ogliaro, F.; Bearpark, M.; Heyd, J. J.; Brothers, E.; Kudin, K. N.; Staroverov, V. N.; Kobayashi, R.; Normand, J.; Raghavachari, K.; Rendell, A.; Burant, J. C.; Iyengar, S. S.; Tomasi, J.; Cossi, M.; Rega, N.; Millam, J. M.; Klene, M.; Knox, J. E.; Cross, J. B.; Bakken, V.; Adamo, C.; Jaramillo, J.; Gomperts, R.; Stratmann, R. E.; Yazyev, O.; Austin, A. J.; Cammi, R.; Pomelli, C.; Ochterski, J. W.; Martin, R. L.; Morokuma, K.; Zakrzewski, V. G.; Voth, G. A.; Salvador, P.; Dannenberg, J. J.; Dapprich, S.; Daniels, A. D.; Farkas, Ö.; Foresman, J. B.; Ortiz, J. V.; Cioslowski, J.; Fox, D. J. Gaussian, Inc., Wallingford CT, **2009**.

(21) (a) Becke, A. D. *J. Chem. Phys.* **1993**, *98*, 5648. (b) Lee, C.; Yang, W.; Parr, R. G. *Phys. Rev. B* **1988**, *37*, 785.

(22) Weigend, F.; Alhrichs, R. *Phys. Chem. Chem. Phys.* **2005**, *7*, 3297.

(23) (a) Casida, M. E. *Recent Developments and Applications of Modern Density Functional Theory, Vol. 4*, Elsevier, Amsterdam, **1996**. (b) Casida, M. E.; Chong, D. P. *Recent Advances in Density Functional Methods, Vol. 1*, World Scientific, Singapore, **1995**, p. 155.

(24) (a) Miertuš, S.; Scrocco, E.; Tomasi, J. *Chem. Phys.* **1981**, *55*, 117. (b) Pascual-Ahuir, J. L.; Silla, E.; Tuñón, I. *J. Comput. Chem.* **1994**, *15*, 1127. (c) Barone, V.; Cossi, M. *J. Phys. Chem. A* **1998**, *102*, 1995.

(25) For a review, see: Dreuw, A.; Head-Gordon, M. *Chem. Rev.* **2005**, *105*, 4009.

(26) Some recent examples: (a) Nemykin, V. N.; Makarova, E. A.; Grosland, J. O.; Hadt, R. G.; Koposov, A. I. *Inorg. Chem.* **2007**, *46*, 9591. (b) Braunschweig, H.; Herbst, T.; Rais, D.; Ghosh, S.; Kupfer, T.; Radacki, K.; Crawford, A. G.; Ward, R. W.; Marder, T. B.; Fernández, I.; Frenking, G. *J. Am. Chem. Soc*. **2009**, *131*, 8989. (c) López-Alberca, M. P.; Mancheño, M. J.; Fernández, I.; Gómez-Gallego, M.; Sierra, M. A.; Torres, R. *Chem. Eur. J.* **2009**, *15*, 3595.

(27) (a) Foster, J. P.; Weinhold, F. *J. Am. Chem. Soc.* **1980**, *102*, 7211. (b) Reed, A. E.; Weinhold, F. *J. Chem. Phys.* **1985**, *83*, 1736. (c) Reed, A. E.; Weinstock, R. B.; Weinhold, F. *J. Chem. Phys.* **1985**, *83*, 735. (d) Reed, A. E.; Curtiss, L. A.; Weinhold, F. *Chem. Rev.* **1988**, *88*, 899.

(28) Jiao, L.; Yu, C.; Li, J.; Wang, Z.; Wu, M.; Hao, E. *J. Org. Chem.* **2009**, *74*, 7525.

(29) Ye, J.; Ye, W.; Xiao, C.; Chen, Y.; Wang, G.; Zhang, W. *Youji Huaxue* **2012**, *32*, 1503.

(30) Hegedus, L. S.; McGuire, M. A.; Schultze, L. M. *Org. Synth.* **1987**, *65*, 140.

(31) Fischer, E. O.; Massböl, A. *Chem. Ber.* **1967**, *100*, 2445.

(32) Fischer, E. O.; Leupold, M.; Kreiter, C. G.; Mueller, J. *Chem. Ber.* **1972**, *105*, 150.

IV.8. Supporting Information

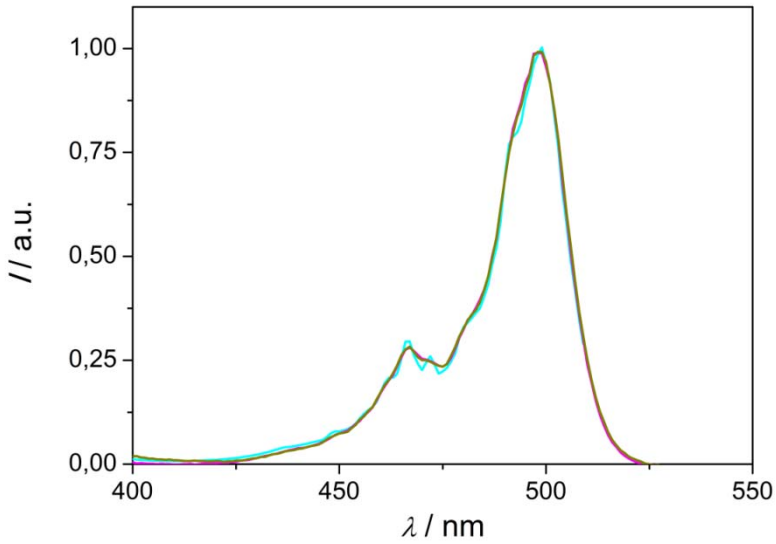

Figure S1. Normalized excitation spectra (λ_{obs} = 600 nm) of the parent formyl-BODIPY's **2a** (cyan), **2b** (magenta) and **2c** (brown).

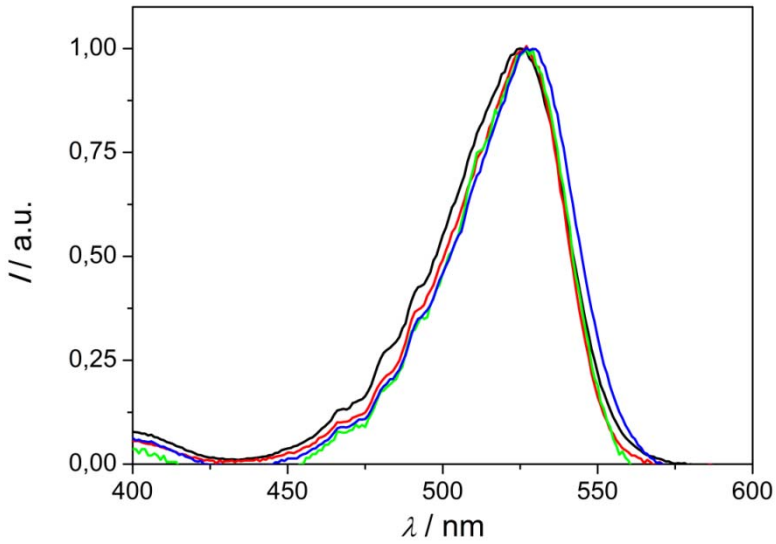

Figure S2. Normalized excitation spectra (λ_{obs} = 600 nm) of the alkoxycarbene complexes **3aa** (black), **3ab** (red), **3ac** (green) and **3ba** (blue).

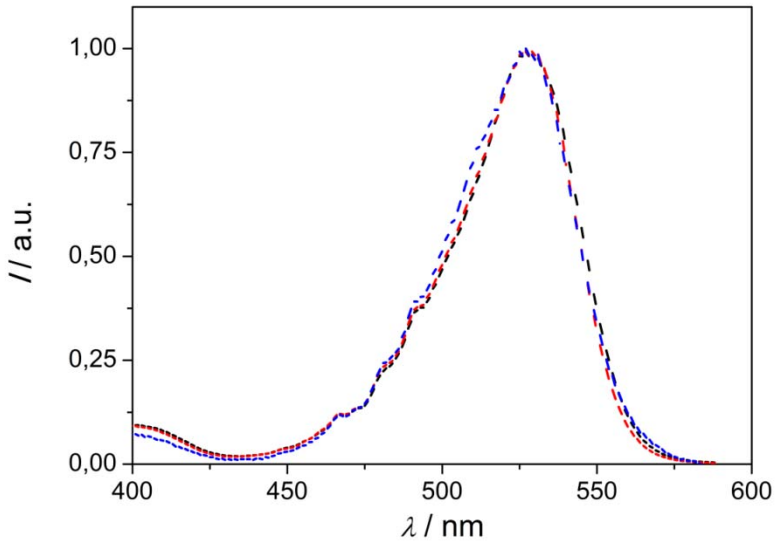

Figure S3. Normalized excitation spectra of the aminocarbene complexes **4aa** (black), **4ab** (red) and **4ba** (blue).

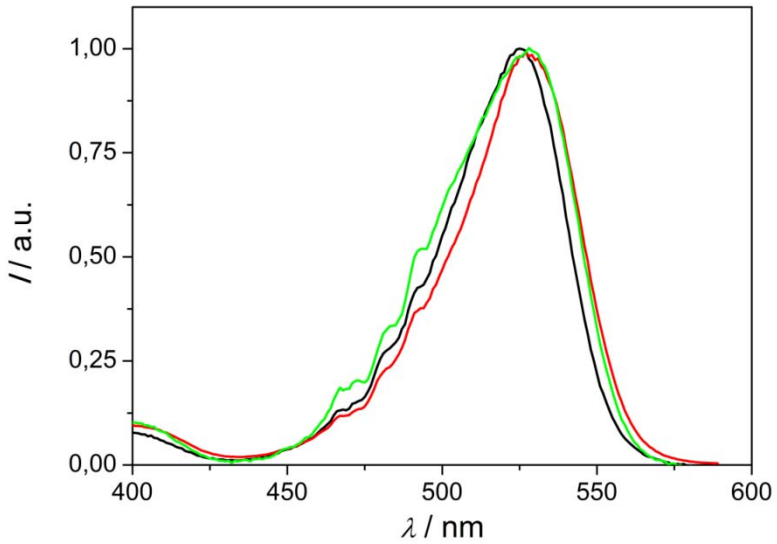

Figure S4. Normalized excitation spectra (λ_{obs} = 600 nm) of the dyads **3aa** (black), **4aa** (red) and **5ca** (green).

V. *CAPÍTULO 3*

V.1. *Remote Control by π-Conjugation of the Emissive Properties of Novel Fischer Carbene-BODIPY Dyads*

Abstract: The synthesis, structure and complete characterization of novel mono- and bimetallic dyads joining Fischer carbene complexes and BODIPY chromophores are reported. In these organometallic species, the Fischer carbene complex is attached to the BODIPY moiety through a p-aminophenyl group linked at the C8 carbon atom of the BODIPY core. The photophysical properties, namely the corresponding UV/Vis absorption and emission spectra of these new metal-carbene complexes, are analysed and discussed. It is found that whereas the absorption of the considered dyads strongly resembles that of the parent 4-anilinyl-substituted BODIPY, the fluorescence emission is significantly reduced in these species very likely as a result of a Dexter-type energy transfer mechanism. At variance, the replacement of the pentacarbonyl-metal(0) fragment by a carbonyl group leads to high fluorescence emission intensity. This suggests that the emission properties of the BODIPY core can be controlled by remote groups by means of π-conjugation as supported by Density Functional Theory calculations.

Submitted to: *Inorg. Chem.*

V.2. Introduction

The chemistry of boradiazaindacenes, known as BODIPY's, has experienced a tremendous development in recent years.[1] This is mainly due to the fascinating optical properties associated with these species which make them highly useful in different fields such as material science or medicinal chemistry. For instance, these compounds usually exhibit excellent thermal and photochemical stabilities, high fluorescence quantum yields, negligible triplet-state formation and intense absorption profiles.[1]

Interestingly, a good number of different synthetic methodologies have been reported allowing the access to novel BODIPY derivatives having tailored properties.[2] In this sense, the attachment of transition metal complexes to the BODIPY moiety, either directly to the BODIPY core or to its periphery, is attracting considerable attention nowadays.[3] This is mainly due to the number of modifications that can be effected in the dyad just by simply modifying the nature of the transition metal and/or the ligands in its coordination sphere. In this regard, we recently described a series of BODIPY derivatives having a Fischer-type carbene complex directly attached to the BODIPY core (Figure 1).[4] In these species, the emission properties can be efficiently switched on/off just by changing the substituent attached to the carbene carbon atom. Thus, whereas alkoxy-Fischer carbene dyads **1** are non-emissive, the aminocarbene **2** analogues are highly emissive. This differential behaviour was ascribed to the extent of the π-conjugation between the carbene complex and the BODIPY core, which is reflected into significant changes in the geometry of the dyads. Indeed, whereas the π-conjugation between both chromophores is hampered in the non-planar aminocarbene dyads, the conjugation is maximized in the planar alkoxy-carbene counterparts, which provokes the complete suppression of its fluorescence (Figure 1).

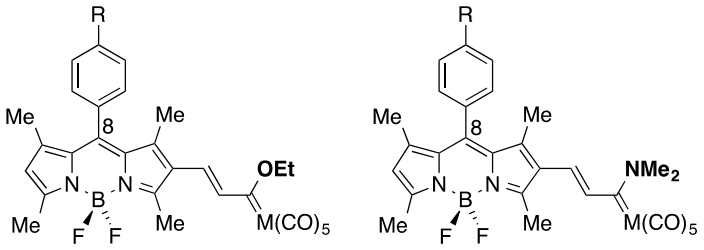

1 *(planar, NON-EMISSIVE)* **2** *(non-planar, EMISSIVE)*

Figure 1. Fischer carbene-BODIPY (see reference 4).

Not surprisingly, we also found that substituents directly attached to the *para*-position of the aryl group placed at position 8 of the BODIPY core have almost a negligible influence on the photophysical properties of the prepared dyads. This is due to the hampered π-conjugation between these substituents and the BODIPY moiety due to the steric hindrance of the adjacent methyl groups, which in turn make the rotation of the C8-aryl group difficult.[5] Despite that, we hypothesized that the exceptional π-acceptor ability of the pentacarbonly-metal fragment of the carbene complex[6,7] might influence the electronic properties of BODIPY even when placed remotely at the C8-aryl position, i.e. not directly attached to the BODIPY core. Reported herein is the synthesis and complete characterization of novel organometallic BODIPY dyads whose emissive properties can be efficiently modulated by remote π-conjugation within the transition metal fragment.

V.3. Results and Discussion

Synthesis and structure of the new BODIPY derivatives: Aniline-BODIPY derivative **4**[8] was selected to join the BODIPY core and the Fischer carbene fragment. To this end, α,β-unsaturated organometallic dyads **5a-i** were efficiently prepared by 1,4-addition of aniline-BODIPY **4** to the corresponding alkynylmetal(0) (M = Cr, W) carbene complexes **3a-i** at room temperature and using anhydrous tetrahydrofuran as solvent, according to the standard reported protocol (Scheme 1a).[9,10] Similarly, compounds **5j,k** having two Fischer carbenes in their structure

were also prepared by reacting two equivalents of the parent BODIPY **4** with the appropriate bis-alkynyl Fischer carbene complex **3j,k** (Scheme 1b).

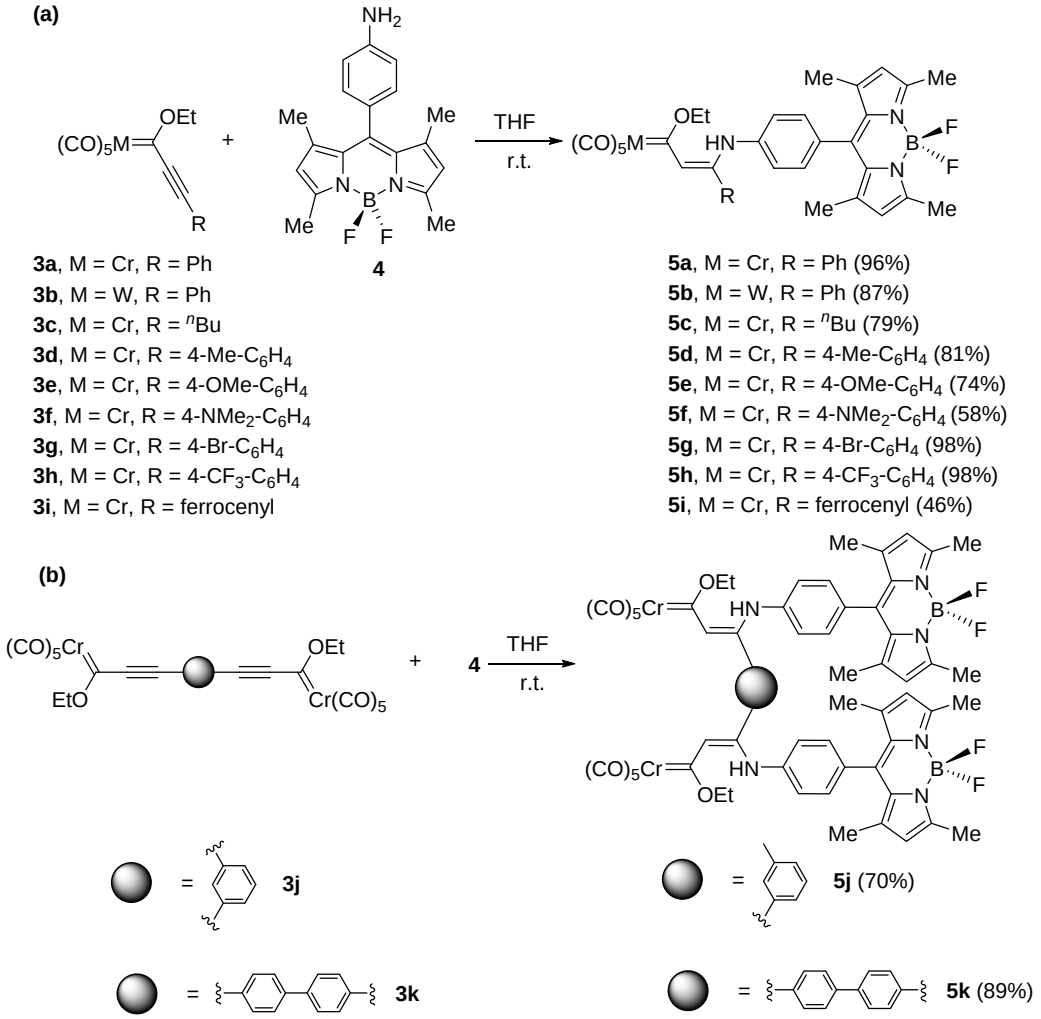

Scheme 1. Synthesis of Fischer carbene-BODIPY dyads **5**.

The structures of the organometallic BODIPY derivatives **5** were established by standard 1D and 2D-NMR experiments and by comparison with the data reported for related chromium(0) and tungsten(0) α,β-unsaturated Fischer carbene complexes.[9,10] Thus, the carbene carbon atom directly attached to chromium(0) in alkoxy-carbenes **5** appears at δ ≈ 300 ppm in the corresponding ^{13}C-NMR spectra, while, as expected, a lower value of δ ≈ 280 ppm was found for the tungsten(0) derivative **5b**. Despite that, two possible stereoisomers for dyads **5** can be envisaged, namely the *E*- and *Z*-isomers derived from the newly formed double bond. Density Functional Theory (DFT) calculations carried out on the possible isomers of the chromium(0)-BODIPY **5a** clearly indicate that isomer **5a-*Z***

is much more stable than the **5a-*E*** (ΔE = 4.5 kcal/mol, Figure 2). This is in part due to the formation of an intramolecular hydrogen bond between the NH of the aniline moiety and the ethoxy-substituent attached to the carbene carbon atom which greatly stabilizes the *Z*-configuration. This intramolecular N-H···OR hydrogen bond has also been found to be responsible for the high stability of the *Z*-configuration in related enaminocarbenes,[9,10] including those found in macrocycles tetrametallic complexes.[11] In addition, this intramolecular interaction also stabilizes the *anti*-conformation exhibited by the ethoxy-substituent (i.e., the CH_2 group directly attached to the oxygen atom is oriented towards the CO wall of the metal fragment), which is the preferred conformation for most of the alkoxy Fischer carbene complexesboth in gas phase[12] and in solid state.[13] Single crystals of BODIPY dyad **5b** suitable for X-ray diffraction analysis were grown in pentane/ethyl acetate solution at –20 °C. The crystal structure of **5b** shows two independent molecules in the asymmetric unit with the expected *Z*-configuration and ethoxy *anti*-conformation with C(5)-O(1)-C(1)-C(2) torsion angles of 163.5(2) and 178.1(2)°, respectively (see Figure 3). In the crystal, an NH···OEt intramolecular hydrogen bond [N(4)-H(4)···O(1)] is present for both independent molecules [N(4)···O(1) 2.646(3) / 2.651(3) Å, H(4)···O(1) 2.05(3) / 1.97(3) Å, N(4)-H(4)···O(1) 127(3) / 136(3)°], as expected from solution data and theoretical studies.

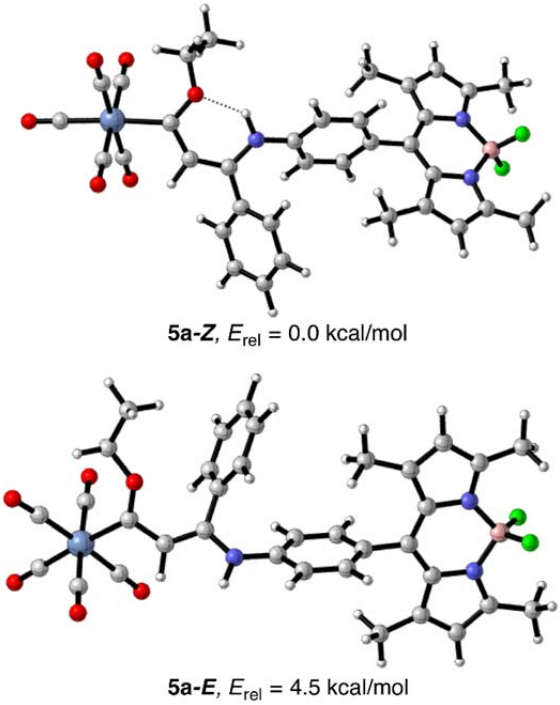

Figure 2. Fully optimized geometries and relative energies of the possible isomers of complex **5a**. All data have been computed at the B3LYP-D3/def2-SVP level.

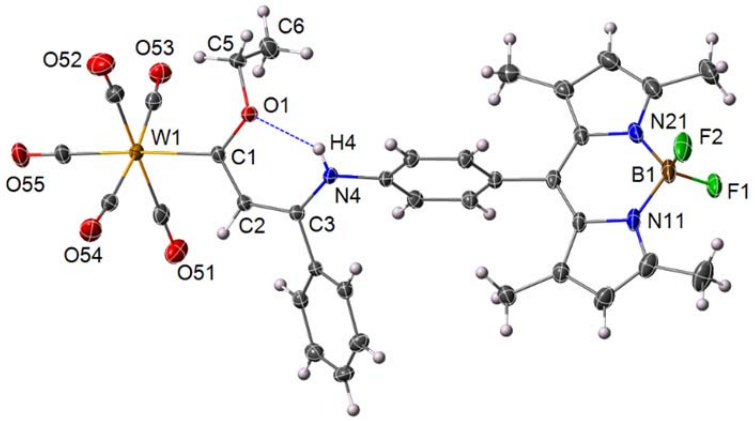

Figure 3. Ellipsoid plot of one of the independent molecules of **5b** (50% probability level) showing the intramolecular N(4)–H(4)···O(1) hydrogen bond.

Another important geometrical feature revealed by this experimental–computational study is that the dihedral angle between the *p*-anilinyl group and the BODIPY core is almost perpendicular (experimental C–C–C–C angle of 95.6° for tungsten(0) complex **5b**), which is a direct consequence of the steric hindrance of the methyl groups of the BODIPY moiety with the aromatic ring. However, this dihedral angle depends upon the substitution on the β-carbon atom of the double

bond. For instance, a value of 90.5° was computed for *n*-butyl-substituted carbene **5c**, whereas a higher value of 102.0° was found for *p*-CF_3-C_6H_4-substituted complex **5h**. This finding suggests that such substituents might lead to noticeable differences in the photophysical properties of these readily prepared organometallic dyads (see below).

Absorption and Emission Properties: The UV/Vis spectra of dyads **5** and the parent *p*-aminophenyl-BODIPY **4** (recorded at 298 K in dichloromethane with a concentration of $1 \cdot 10^{-5} mol \cdot L^{-1}$) are displayed in Figure 4 (see also Table 1). Dyads **5** exhibit three main absorptions in the range of 350-550 nm. The more intense band is located at $\lambda_{max} \approx 500$ nm and can be tentatively assigned to the typical π-π^* transition involving the BODIPY fragment. Indeed, this absorption is practically identical in terms of both wavelength maxima and corresponding extinction coefficient ($\varepsilon \approx 9 \times 10^4 M^{-1}cm^{-1}$) to that observed for the parent BODIPY **4** (λ_{max} = 499 nm, $\varepsilon = 9.7 \times 10^4 M^{-1}cm^{-1}$, see Table 1). In addition, bimetallic dyads **5j** and **5k**, exhibit a similar absorption located a ca. 500 nm which is almost twice as intense as the absorptions for the rest of the monometallic dyads **5**. This is of course due to the presence of two BODIPY moieties in the structures of **5j** and **5k**, which further supports our tentatively assignment for this band. The remaining less intense absorptions located at ca. 475 nm and 350 nm can be reasonably assigned to the metal-to-ligand charge transfer (MLCT) and ligand-field (LF) transition, respectively, involving the pentacarbonylmetal-carbene complex. These assignments can be done by comparison with the UV/Vis spectrum of the parent carbene complex $(CO)_5Cr{=}C(OEt)CH{=}C(Ph)(NHPh)$ whose MLCT and LF bands appear at λ_{max} = 465 nm ($\varepsilon \approx 2.2 \times 10^4 M^{-1}cm^{-1}$) and λ_{max} = 337 nm ($\varepsilon \approx 1.3 \times 10^4 M^{-1}cm^{-1}$), respectively. Therefore, it can be concluded that the attachment of the BODIPY moiety to the carbene fragment does not alter significantly the absorption properties of both chromophores.

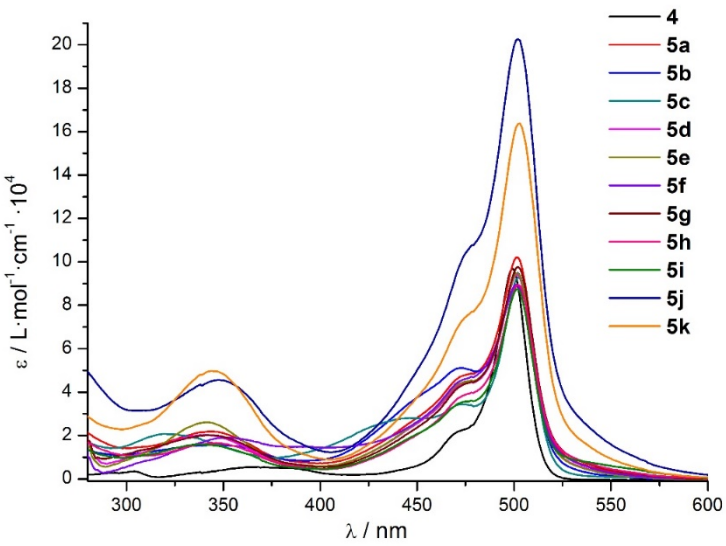

Figure 4. UV/Vis spectra Fischer carbene-BODIPY dyads **5a-k** and parent *p*-aminophenylBODIPY **4**. All measurements were carried out in a diluted solution in dichloromethane (concentration of $1 \cdot 10^{-5}$mol·L^{-1}, optical density < 0.1) at 298K.

Table1. Photophysical properties of complexes **5** and parent *p*-aminophenyl-BODIPY **4**.

Compound	λ_{abs} / nm[a]	ε_{abs}[b]	λ_{em} / nm[c]
4	499	9.7	511
5a	501	10.2	510
5b	502	9.5	511
5c	502	9.3	510
5d	501	9.4	510
5e	502	9.5	510
5f	501	9.0	511
5g	502	9.8	511
5h	502	8.9	511
5i	502	8.7	511
5j	502	20.3	512
5k	503	16.4	512

All the samples were recorded at 298 K in dichloromethane (concentration of $1 \cdot 10^{-5}$mol·L^{-1}, optical density < 0.1).[a] Maximum of the UV/Vis spectrum. [b] Molar extinction coefficient ε ($M^{-1}cm^{-1} \times 10^4$). [c] Maximum of the emission spectrum using λ_{exc} = 460 nm.

In order to gain more insight into the nature of the observed absorptions, time-dependent DFT (TD-DFT) calculations were carried out on complex **5a** to determine the nature of the vertical transitions associated with these absorptions.

Thus, our calculations indicate that the band at ca. 500nm is the result of the one-electron promotion from the HOMO to the LUMO, which, as depicted in Figure 5, can be viewed as π and π*-molecular orbitals fully delocalized within the indacene moiety. Therefore, it is confirmed that this absorption exclusively involves the BODIPY moiety. In addition, the band around 470 nm is assigned to the vertical promotion of one-electron from the HOMO-1 to the LUMO+1. As clearly seen in Figure 5, the latter molecular orbitals are located at the transition metal fragment and at the carbene ligand, respectively, thus confirming the MLCT nature of this absorption.

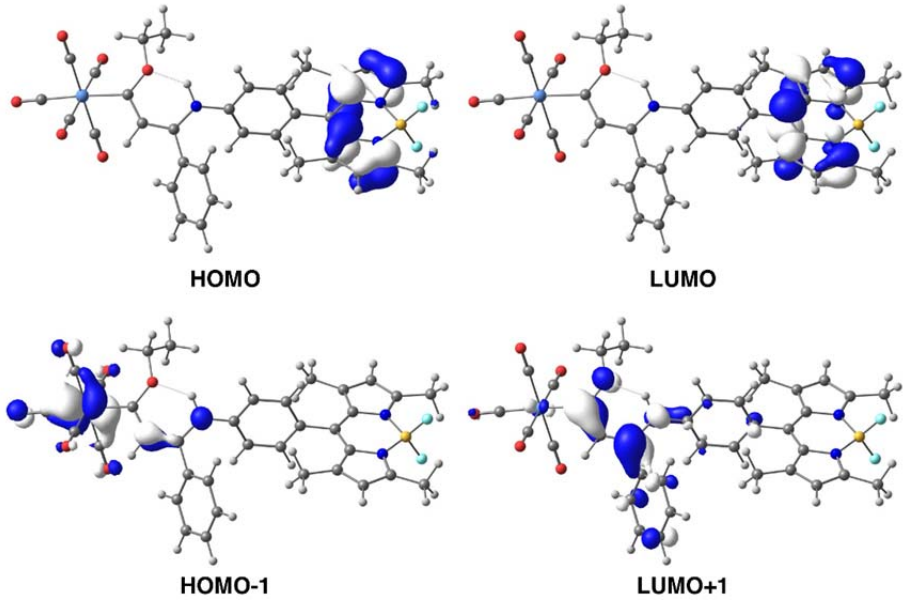

Figure 5. Computed (TD-CAM-B3LYP/def2-SVP level) molecular orbitals of dyad **5a** (isosurface value of 0.05 au).

Figure 6 shows the emission spectra of the parent BODIPY **4**, the metal-carbene complex **5a** and the corresponding ester derivate **6** where the pentacarbonyl-chromium(0) fragment was transformed into a carbonyl group by exposing **5a** to KF in an open air flask for 24h (Scheme 2).[14]

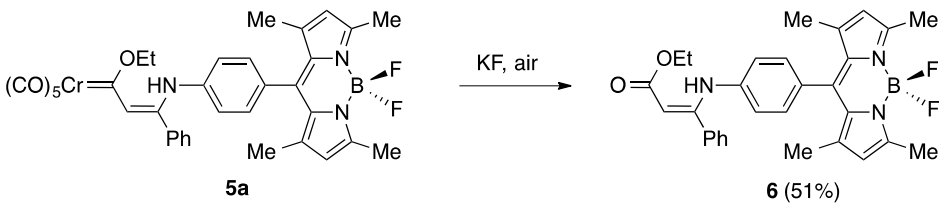

Scheme 2. KF-promoted oxidation of carbene complex **5a** into ester **6**.

As readily seen in Figure 6, the fluorescence intensity of the α,β-unsaturated ester **6** is higher than that measured for the parent BODIPY **4**. This can be ascribed to the π-acceptor ability of the carbonyl group which is able to accept electronic density coming from the lone pair (LP) of the anilinyl-nitrogen atom. Indeed, the Second Order Pertubation Theory (SOPT) of the Natural Bond Orbital (NBO) method clearly indicates that the delocalization of the nitrogen-LP into the adjacent π*-molecular orbital of the aryl fragment, which is directly connected to the BODIPY core, is significantly reduced in **6** as compared to **4** (associated SOPT-energies, $\Delta E^{(2)}$, of –24.6 kcal/mol and –32.5 kcal/mol, for **6** and **4**, respectively). As a result, the emission of **6** resembles that of unsubstituted BODIPYs whereas the emission of the push-pull species **4**, where the BODIPY core behaves as a π-acceptor, is reduced. A similar effect has been observed in BODIPY derivatives where the anilinyl-nitrogen atom was acylated. Thus, as a consequence of the delocalization of the nitrogen-LP into the adjacent carbonyl group instead of into the aryl-BODIPY moiety, a much higher fluorescence quantum yield has been measured for the acylated species as compared to **4**.[8a]

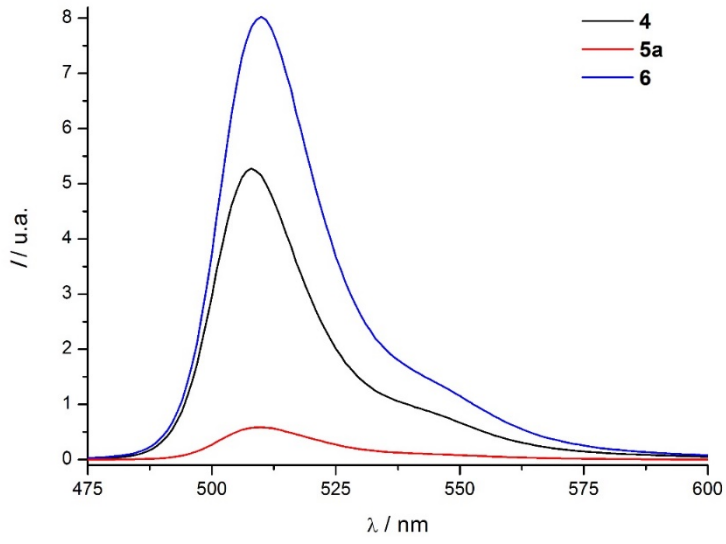

Figure 6. Emission spectra of the alkoxycarbene complex **5a**, its ester counterpart **6**, and the parent BODIPY **4**. All measurements were carried out in a diluted solution in dichloromethane (concentration of ca. $1 \cdot 10^{-6}$ mol·L^{-1}, optical density < 0.1) at 298K.

According to this explanation based on this π-conjugation competence, one should expect even a higher emission intensity for the carbene complex **5a** due to the much higher π-acceptor ability of the pentacarbonyl-chromium(0) fragment compared to the ester moiety of compound **6**.[6] Indeed, the computed delocalization of the nitrogen-LP into the aryl-BODIPY substituent is, as expected, lower than in ester **6** ($\Delta E_{(2)}$ = –22.1 kcal/mol). However, as shown in Figure 6, the fluorescence in complex **5a** is almost suppressed. Considering that there exists a clear overlap between of emission spectra of the BODIPY donor fragment and the Fischer carbene acceptor moiety (see Figure 7a), and the distance between both chromophores (experimental W(carbene)–C8(BODIPY) distance of 10.8 Å in **5b**, computed Cr(carbene)-C8(BODIPY) distance of 10.6 Å for **5a**), a Dexter-type energy transfer mechanism, which typically occurs within 10Å, seems to be responsible for the observed significant reduction of the fluorescence intensity. Moreover, the computed frontier molecular orbitals (FMO) for both isolated chromophores agree reasonably well with this explanation. As depicted in Figure 7b, both the HOMO and LUMO of the carbene complex are lower in energy than the corresponding FMO of the fluorophore BODIPY. As a consequence, when the BODIPY moiety is photoexcited, an intramolecular electron transfer from the BODIPY fragment to the carbene complex may occur therefore leading to observed reduced emission. In sharp contrast, the LUMO of the ester chromophore is higher in energy than the BODIPY-LUMO which precludes a similar electron transfer mechanism. As a consequence, the fluorescence in the ester derivative **6** is not quenched as experimentally observed.

(a)

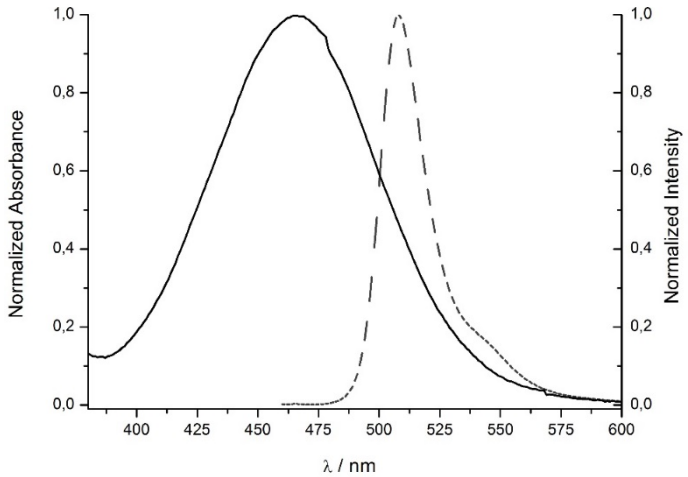

(b)

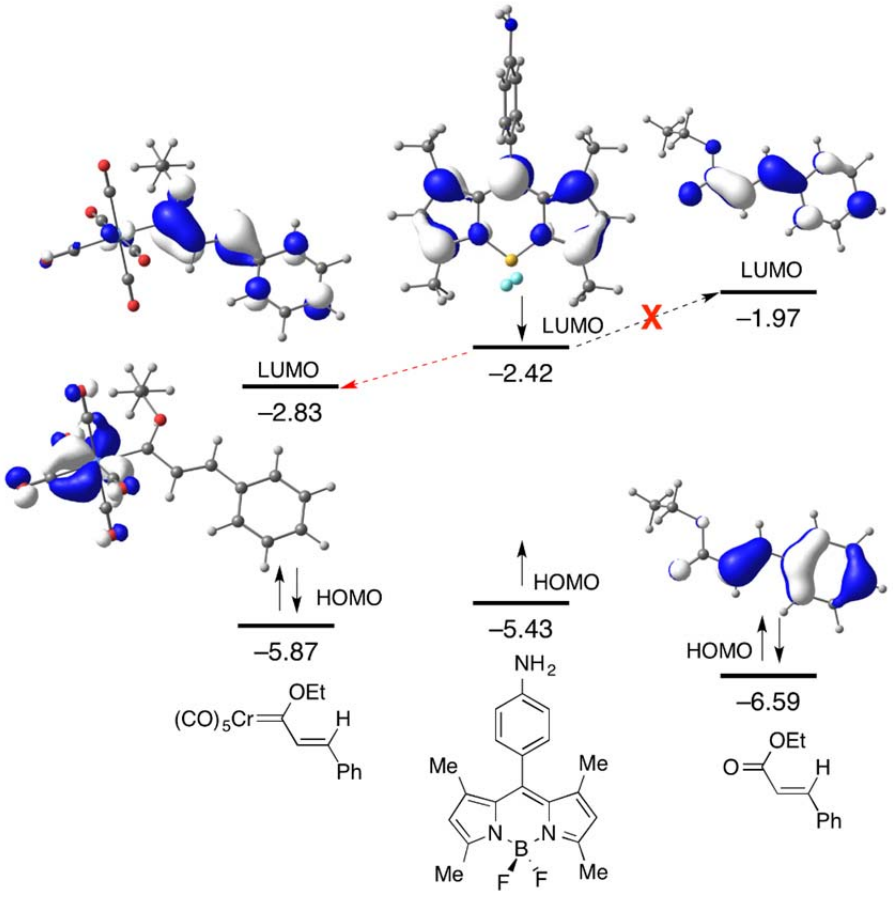

Figure 7. (a) Overlap between the emission spectrum of the donor **4** (dotted lines) and the absorption spectrum (solid lines) of the acceptor Fischer carbene complex, $(CO)_5Cr=C(OEt)CH=C(Ph)NHPh$. (b) Computed frontier molecular orbitals (isosurface value of 0.05 au) of the isolated chromophores present in **5a** and **6**.

Despite the remarkable reduction of the fluorescence intensity, a noticeable substituent effect on the emission of the strongly related aryl-substituted dyads **5a-i** is observed. As shown in Figure 8, apart from derivative **5i** where the fluorescence is completely suppressed by a well-known photoelectron transfer mechanism induced by the ferrocenyl group,[15] π-donor groups such as methoxy- or dimethylamino substituents at the 4-position of the aryl group attached to the β-carbon atom leads to higher emission intensities (**5e** and **5f**) than π-acceptor groups (like Br or CF_3 groups in **5g** and **5h**, respectively).

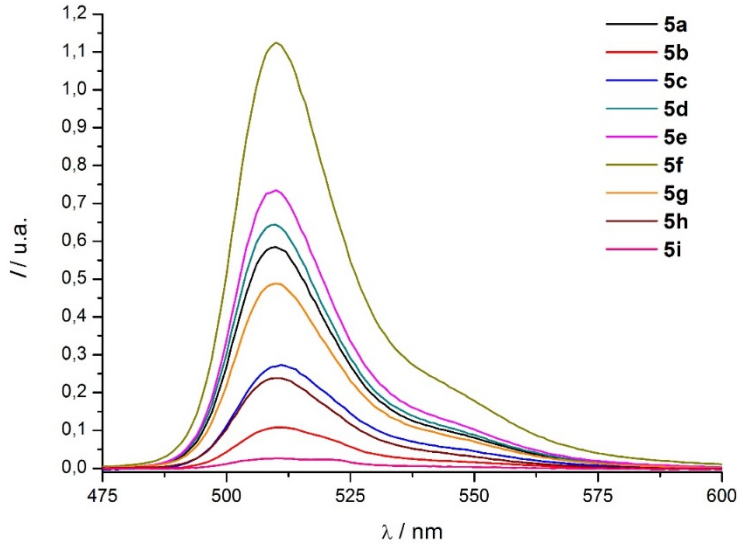

Figure 8. Comparison between emission spectra of the aryl-substituted dyads **5**. All measurements were carried out in a diluted solution in dichloromethane (concentration of $1 \cdot 10^{-6}$ mol·L^{-1}, optical density < 0.1) at 298K.

Indeed, good linear relationships (correlation coefficient of 0.98) have been found when plotting the measured fluorescence intensity either versus the corresponding σ_p^+-Hammett substituent constants[16] or the ^{13}C-NMR chemical shift of the carbene carbon atom (see Figures 9a and 9b). Both parameters have been used as an indirect measure of the conjugative strength in rather different π-conjugated systems.[17,18] Both linear correlations provide further support to a Dexter-type mechanism as responsible for the observed significant suppression of the fluorescence in dyads **5**.

(a)

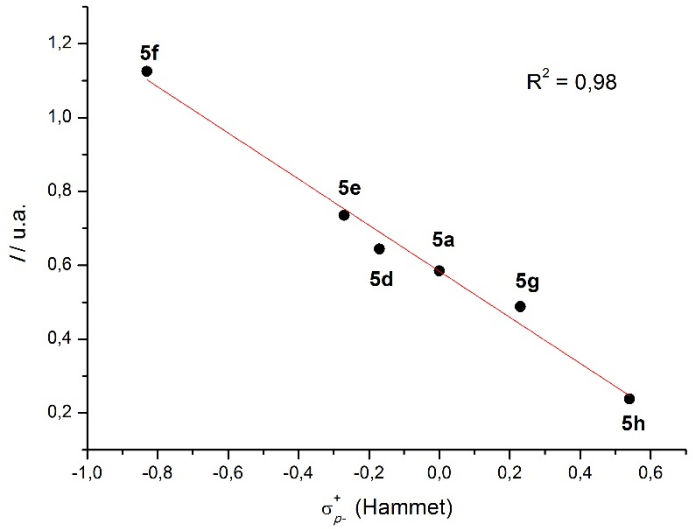

(b)

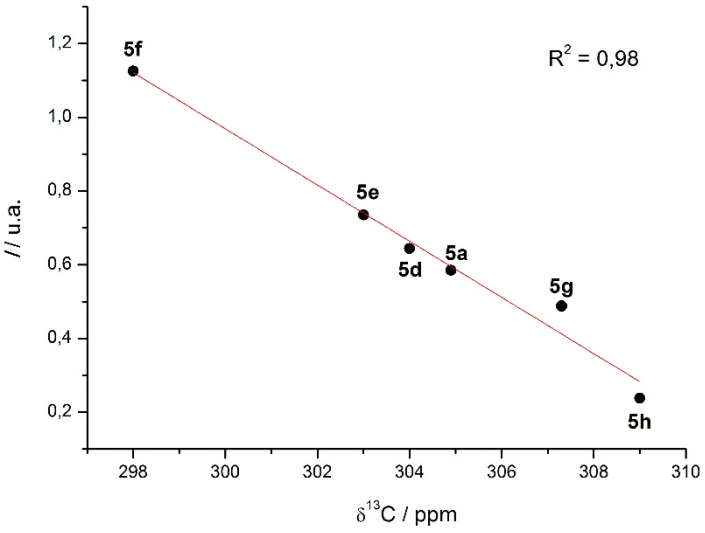

Figure 9. Plot of the fluorescence intensity of aryl-substituted dyads **5** versus the σ_p^+-Hammett substituent constants (a) and the ^{13}C-NMR chemical shift of the carbene carbon atom (b).

Therefore, the observed substituent effect can be explained by the extent of the delocalization by means of π-conjugation of the *p*-aminophenyl-nitrogen LP into the adjacent aryl-BODIY fragment. Similar to the behaviour in related α,β-unsaturated Fischer carbenes,[19] the π-donor group of the Cβ-aryl fragment may

delocalize into the transition metal-carbene fragment, which leads to the resonance form **5f-I** (Figure 10). In turn, the key nitrogen-LP may also delocalize into the so-formed quinoid resonance structure **5f-I** to produce the additional stabilizing resonance structure **5f-II**. This delocalization into the carbene ligand therefore involves a reduction of the delocalization into the BODIPY-fragment, and as a result, the fluorescence emission of the donor-substituted dyads **5e,f** is higher than hydrogen-substituted **5a** or π-acceptor substituted **5g,h**. Further support to this hypothesis is provided by dyad **5c**, where the β-aryl fragment is replaced by a *n*-butyl group. In this species, the delocalization of the nitrogen-LP is severely hampered, as only weak hyperconjugation is possible. As a consequence, the measured fluorescence intensity for this dyad is low, and comparable to CF_3-substituted dyad **5h**. In addition, our DFT calculations also agree with this remote control of the emission by π-conjugation. According to this control, one should expect a lower value of the delocalization of the nitrogen-LP into the aryl-BODIPY for -NMe_2 and -OMe substituted dyads **5e,f** than for the parent species **5a** (R = Ph) or the butyl-substituted compound **5c**. Indeed, the computed SOPT-energies nicely follow the predicted trend: $\Delta E^{(2)}$ = -20.5 kcal/mol (**5f**) < -21.0 kcal/mol (**5e**) < -22.1 kcal/mol (**5a**) < -23.4 kcal/mol (**5c**).

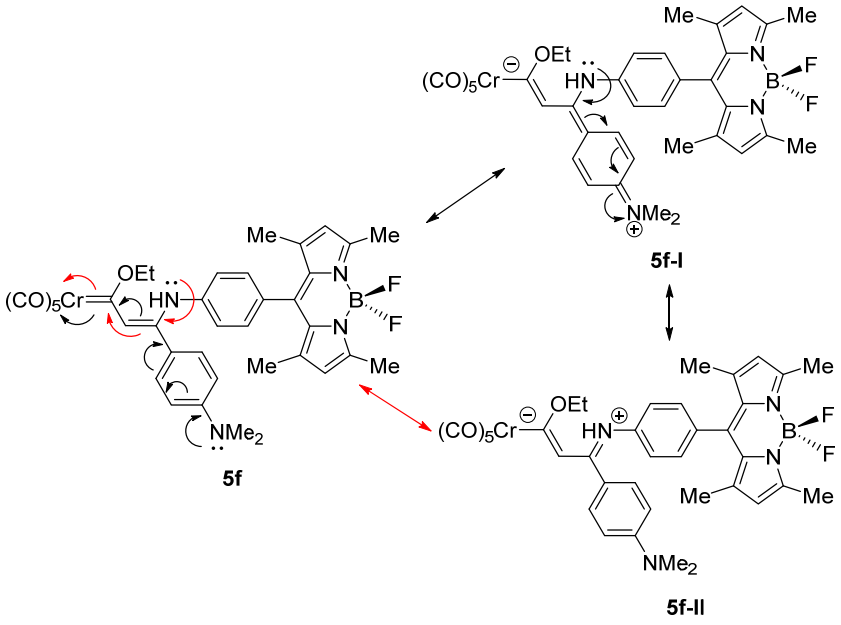

Figure 10. Possible resonance structures of Fischer carbene complex **5f**.

V.4. Conclusions

From the joint experimental-computational study reported herein, the following conclusions can be drawn: (i) the attachment of a Fischer-type carbene complex to a BODIPY moiety through a *p*-aminophenyl group linked at the C8 carbon atom of the BODIPY core does not alter significantly the absorption properties of both chromophores. (ii) In all cases, the UV-Vis spectra of the novel organometallic dyads are characterized by three main absorptions in the range of 350-550 nm, where the more intense band (located at $\lambda_{max} \approx 500$ nm) can be assigned to the typical π-π^* transition involving the BODIPY fragment. (iii) Despite that, it is found that the pentacarbonyl-metal fragment dramatically reduces the corresponding fluorescence emission properties of the BODIPY moiety. (iv) This is very likely the result of a Dexter-type energy transfer mechanism as inferred by the noticeable influence on the emission intensity by substituents placed at the 4-position of the aryl group attached to the β-carbon atom of the carbene complexes **5**. (v) Further support to this finding is provided by DFT-calculations and by the good linear relationships observed when plotting the emission intensity versus the Hammett-parameters and ^{13}C-NMR chemical shifts of the carbene carbon atom. (vi) Therefore, it can be concluded that the emission properties of the BODIPY core can be controlled by means of π-conjugation even by remote substituents placed at the C8 position.

V.5. Computational Details

Geometry optimizations without symmetry constraints were carried out using the Gaussian09 suite of programs[20] using the B3LYP[21] functional in combination with the double-ζ plus polarization def2-SVP basis sets[22] for all atoms. This level is denoted B3LYP/def2-SVP. Stationary points were characterized as minima by calculating the Hessian matrix analytically at this level. Calculations of absorption spectra were accomplished by using the time-dependent density functional theory (TD-DFT)[23] method at the same level. TD-DFT calculations were performed in *n*-hexane as solvent using the polarizable continuum model (PCM) method.[24] The assignment of the excitation energies to the experimental bands was performed on the basis of the energy values and oscillator strengths computed at the CAM-B3LYP[25]/def2-SVP level. Second-Order Pertubation Theory calculations were carried out by using the natural bond orbital (NBO) method.[26]

V.6. Experimental Section

General Procedures. All reactions were carried out under argon atmosphere unless otherwise stated. All solvents used in this work were purified by distillation and were freshly distilled immediately before use. Tetrahydrofuran (THF) was purified using a Pure Solv PS-MD-5 system. Flame-dried glassware was used for moisture-sensitive reactions. Silica gel (Merck: 230-400 mesh) was used as stationary phases for purification of crude reaction mixtures by flash column chromatography. Identification of products was made by thin-layer chromatography (Kieselgel 60F-254). UV light (λ 254nm) and 5% phosphomolybdic acid solution in 95% EtOH were used to develop the plates. NMR spectra were recorded at 25 °C in $CDCl_3$, on 300 (300 MHz for ^{1}H and 75 MHz for ^{13}C) spectrometers. Chemical shifts are given in ppm relative to $CDCl_3$ (^{1}H, 7.27 ppm and ^{13}C, 77.0 ppm).

Absorption and Fluorescence Spectroscopies. All experiments were carried out at 298 K, in dichloromethane (concentration of ca. $1\cdot10^{-6}mol\cdot L^{-1}$, optical density < 0.1), using quartz cuvettes with optical paths of 1 cm. UV absorption spectra were registered using a UVICON XL spectrophotometer (BioTex Instruments). Steady-state fluorescence spectra were recorded using an AMINCO Bowman Series 2 spectrofluorometer, with 1.0 nm bandwidth for emission and excitation. The excitation wavelengths were fixed at 450 nm and 500 nm in the measurement of the emission spectra. The emission wavelength was fixed at 550 nm for the determination of all the excitation spectra.

All commercially available products were used without further purification. The following metal-carbenes were prepared according to previously described methods: pentacarbonyl[(ethoxy)(phenylethynyl)carbene]chromium(0) **3a**,[27] pentacarbonyl[(ethoxy)(phenylethynyl)carbene]tungsten(0) **3b**,[28] pentacarbonyl[(ethoxy)(*n*-butylethynyl)carbene]chromium(0) **3c**,[28] pentacarbonyl[(ethoxy)(2-(4-methylphenyl)ethynyl)carbene]chromium(0) **3d**,[29] pentacarbonyl[(ethoxy)(2-(4-methoxyphenyl)ethynyl)carbene]chromium(0) **3e**,[29]

pentacarbonyl[(2-(4-dimethylaminophenyl)ethynyl)(ethoxy)carbene] chromium (0) **3f**,[30] pentacarbonyl[(ethoxy)(2-(4-bromophenyl)ethynyl)carbene]chromium (0) **3g**,[31] pentacarbonyl[(ethoxy)(2-(*p*-trifluoromethylphenyl)ethynyl)cabene]-chromium (0) **3h**,[10b] pentacarbonyl[(ethoxy)(2-ferrocenylethynyl)carbene]-chromium(0) **3i**,[10b] decacarbonyl-[1,3-phenylenediethynyl)bis(ethoxycarbene)]-dichromium(0) **3j**[10a] and decacarbonyl-[1,4-biphenylenediethynyl)bis(ethoxy-carbene)]dichromium(0) **3k**.[32] 4,4-Difluoro-8-(4-aminophenyl)-1,3,5,7-tetramethyl-4-bora-3a,4a-diaza-*s*-indacene **4**, were prepared according to the literature.[8]

General procedure for 1,4-addition of amines to alkynylidene carbene complexes. To a solution of the corresponding alkynylidene carbene complex (1 mmol) and the BODIPY **4** (1 mmol) in anhydrous THF (40 mL) were stirred at room temperature until total disappearance of the starting material (checked by TLC). The solvent was removed under reduced pressure and the product purified by flash chromatography (hexane/EtOAc, 5:1) on silica gel under argon pressure.

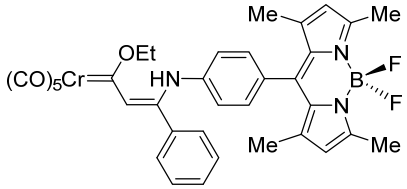

Complex 5a: A solution of **3a** (100 mg, 0.29 mmol) and BODIPY **4** (98 mg, 0.29 mmol) in 11.6 mL of dry THF was stirred for 3 hours. The solvent was removed under reduced pressure and the crude was purified by flash chromatography to yield complex **5a** as a dark red solid (192 mg, 96%). ^{1}H NMR (300 MHz, ppm): δ 10.42 (s, 1H), 7.45-7.29 (m, 5H), 7.07 (d, *J* = 8.3 Hz, 2H), 6.83 (d, *J* = 8.3 Hz, 2H), 6.74 (s, 1H), 5.99 (s, 2H), 5.07 (q, *J* = 7.0 Hz, 2H), 2.55 (s, 6H), 1.74 (t, *J* = 7.0 Hz, 3H), 1.37 (s, 6H). ^{13}C NMR (75 MHz, ppm): δ 304.9, 224.0, 218.0, 155.6, 145.9, 142.6, 140.2, 139.2, 134.6, 131.6, 131.2, 130.4, 129.1, 128.8, 128.7, 123.7, 122.6, 121.3, 74.7, 15.7, 14.6, 14.5. IR (CH_2Cl_2): ν 2050, 1909, 1583, 1541, 1511, 1471, 1409, 1374, 1308, 1195, 1157, 1089, 983, 668 cm^{-1}. HRMS (ESI): *m/z* calcd for $C_{35}H_{31}BCrF_2N_3O_6$ [M + H] 690.1679, found 690.1663.

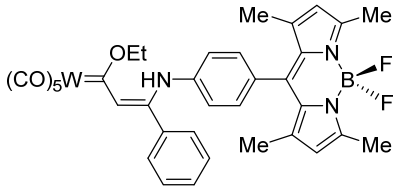

Complex 5b: A solution of **3b** (142 mg, 0.29 mmol) and BODIPY **4** (100 mg, 0.29 mmol) in 11.8 mL of dry THF was stirred for 2 hours. The solvent was removed under reduced pressure and the crude was purified by flash chromatography to yield complex **5b** as a red solid (212 mg, 87%). ^{1}H NMR (300 MHz, ppm): δ 10.54 (s, 1H), 7.46-7.29 (m, 5H), 7.07 (d, *J* = 8.5 Hz, 2H), 6.86 (d, *J* = 8.5 Hz, 2H), 6.78 (s, 1H), 5.99 (s, 2H), 4.91 (q, *J* = 7.0 Hz, 2H), 2.55 (s, 6H), 1.72 (t, *J* = 7.0 Hz, 3H), 1.37 (s, 6H). ^{13}C NMR (75 MHz, ppm): δ 280.6, 203.7, 198.7, 155.6, 149.9, 142.6, 140.2, 139.1, 134.5, 131.8, 131.1, 130.5, 128.9, 128.8, 128.7, 125.4, 123.7, 121.3, 76.6, 15.5, 14.6, 14.5. IR (CH_2Cl_2): ν 2058, 1902, 1583, 1538, 1511, 1472, 1409, 1374, 1308, 1194, 1156, 1089, 982, 598 cm^{-1}. HRMS (ESI): *m/z* calcd for $C_{35}H_{31}BF_2N_3O_6W$ [M + H] 822.1783, found 822.1744.

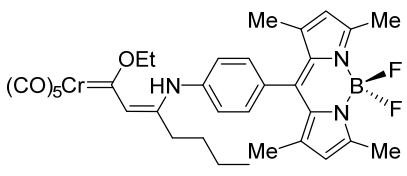

Complex 5c: A solution of **3c** (49 mg, 0.15 mmol) and BODIPY **4** (50 mg, 0.15 mmol) in 6.0 mL of dry THF was stirred for 1 hour. The solvent was

removed under reduced pressure and the crude was purified by flash chromatography to yield complex **5c** as an orange solid (77 mg, 79%). ^{1}H NMR (300 MHz, ppm): δ 10.57 (s, 1H), 7.38 (d, *J* = 8.2 Hz, 2H), 7.28 (d, *J* = 8.2 Hz, 2H), 6.49 (s, 1H), 6.02 (s, 2H), 4.94 (q, *J* = 7.1 Hz, 2H), 2.57 (s, 6H), 2.36-2.31, (m, 2H), 1.62 (t, *J* = 7.1 Hz, 3H), 1.50-1.46 (m, 2H), 1.43 (s, 6H), 1.34-1.24 (m, 2H), 0.85 (t, *J* = 7.3 Hz, 3H). ^{13}C NMR (75 MHz, ppm): δ 297.0, 223.8, 218.4, 156.0, 153.5, 142.5, 139.8, 137.8, 134.1, 131.2, 129.6, 125.7, 121.5, 119.9, 74.1, 32.3, 30.6, 22.4, 15.9, 14.6, 14.5, 13.6.. IR (CH_2Cl_2): ν 2049, 1907, 1544, 1511, 1470, 1411, 1374, 1307, 1195, 1157, 1084, 983, 670 cm^{-1}. HRMS (ESI): *m/z* calcd for $C_{33}H_{35}BCrF_2N_3O_6$ [M + H] 670.1992, found 670.1993.

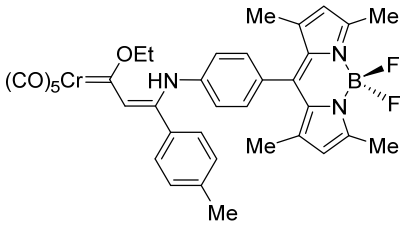

Complex 5d: A solution of **3d** (54 mg, 0.15 mmol) and BODIPY **4** (50 mg, 0.15 mmol) in 5.8 mL of dry THF was stirred for 6 hours. The solvent was removed under reduced pressure and the crude was purified by flash chromatography to yield complex **5d** as a dark red solid (85 mg, 81%). ^{1}H NMR (300 MHz, ppm): δ 10.41 (s, 1H), 7.24 (d, *J* = 8.2 Hz, 2H), 7.11 (d, *J* = 8.6 Hz, 2H), 7.08 (d, *J* = 8.6 Hz, 2H), 6.84 (d, *J* = 8.2 Hz, 2H), 6.72 (s, 1H), 6.00 (s, 2H), 5.04 (q, *J* = 7.0 Hz, 2H), 2.55 (s, 6H), 2.38, (s, 3H), 1.72 (t, *J* = 7.0 Hz, 3H), 1.38 (s, 6H). ^{13}C NMR (75 MHz, ppm): δ 304.0, 224.0, 218.1, 155.7, 146.2, 142.6, 141.0, 140.3, 139.4, 131.6, 131.2, 129.4, 129.1, 128.9, 123.6, 122.6, 121.3, 74.5, 21.4, 15.8, 14.6. IR (CH_2Cl_2): ν 2049, 1907, 1580, 1539, 1510, 1471, 1411, 1373, 1307, 1194, 1156, 1088, 982, 667 cm^{-1}. HRMS (ESI): *m/z* calcd for $C_{36}H_{33}BCrF_2N_3O_6$ [M + H] 704.1836, found 704.1842.

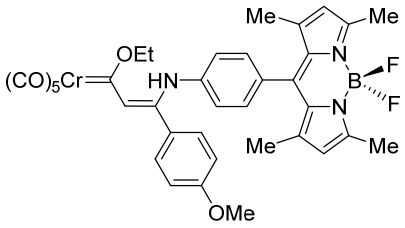

Complex 5e: A solution of **3e** (56 mg, 0.15 mmol) and BODIPY **4** (50 mg, 0.15 mmol) in 5.8 mL of dry THF was stirred for 18 hours. The solvent was removed under reduced pressure and the crude was purified by flash chromatography to yield complex **5e** as a dark red solid (78 mg, 74%). ^{1}H NMR (300 MHz, ppm): δ 10.37 (s, 1H), 7.30 (d, *J* = 8.7 Hz, 2H), 7.10 (d, *J* = 8.3 Hz, 2H), 6.85 (d, *J* = 8.3 Hz, 2H), 6.81 (d, *J* = 8.7 Hz, 2H), 6.71 (s, 1H), 5.99 (s, 2H), 5.02 (q, *J* = 7.0 Hz, 2H), 3.84 (s, 3H), 2.55 (s, 6H), 1.70 (t, *J* = 7.0 Hz, 3H), 1.39 (s, 6H). ^{13}C NMR (75 MHz, ppm): δ 303.0, 224.0, 218.1, 161.4, 155.7, 145.9, 142.6, 140.3, 139.6, 131.6, 131.3, 130.9, 128.9, 126.4, 123.6, 122.5, 121.3, 114.2, 74.5, 55.4, 15.8, 14.6. IR (CH_2Cl_2): ν 2048, 1910, 1582, 1543, 1512, 1471, 1409, 1375, 1305, 1196, 1089, 980, 667 cm^{-1}. HRMS (ESI): *m/z* calcd for $C_{36}H_{33}BCrF_2N_3O_7$ [M + H] 720.1785, found 720.1768.

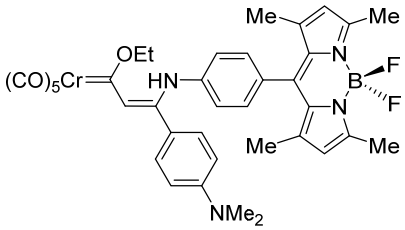

Complex 5f: A solution of **3f** (58 mg, 0.15 mmol) and BODIPY **4** (50 mg, 0.15 mmol) in 5.8 mL of dry THF was stirred for 24 hours. The solvent was removed under reduced pressure and the crude was purified by flash chromatography to yield complex **5f** as a dark red solid (62 mg, 58%). ^{1}H

NMR (300 MHz, ppm): δ 10.35 (s, 1H), 7.24 (d, *J* = 8.7 Hz, 2H), 7.10 (d, *J* = 8.3 Hz, 2H), 6.90 (d, *J* = 8.3 Hz, 2H), 6.72 (s, 1H), 6.54 (d, *J* = 8.7 Hz, 2H), 5.99 (s, 2H), 4.96 (q, *J* = 7.0 Hz, 2H), 3.02 (s, 6H), 2.55 (s, 6H), 1.66 (t, *J* = 7.0 Hz, 3H), 1.4. (s, 6H). ^{13}C NMR (75 MHz, ppm): δ 298.0, 224.1, 218.4, 155.6, 151.8, 147.2, 142.6, 140.6, 140.3, 131.3, 131.1, 131.0, 128.8, 123.4, 122.1, 121.3, 120.2, 111.3, 74.0, 40.0, 15.8, 14.7, 14.6. IR (CH_2Cl_2): ν 2048, 1911, 1579, 1543, 1521, 1473, 1408, 1371, 1308, 1198, 1157, 1089, 983, 669 cm^{-1}. HRMS (ESI): *m/z* calcd for $C_{37}H_{36}BCrF_2N_4O_6$ [M + H] 733.2101, found 733.2091.

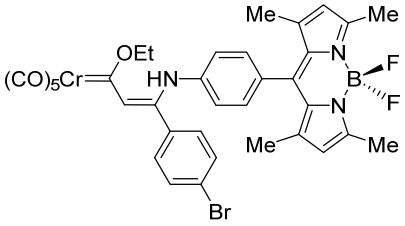

Complex 5g: A solution of **3g** (33 mg, 0.08 mmol) and BODIPY **4** (26 mg, 0.08 mmol) in 3.1 mL of dry THF was stirred for 4 hours. The solvent was removed under reduced pressure and the crude was purified by flash chromatography to yield complex **5g** as a dark red solid (61 mg, 98%). ^{1}H NMR (300 MHz, ppm): δ 10.29 (s, 1H), 7.44 (d, *J* = 8.6 Hz, 2H), 7.22 (d, *J* = 8.6 Hz, 2H), 7.11 (d, *J* = 8.2 Hz, 2H), 6.84 (d, *J* = 8.2 Hz, 2H), 6.69 (s, 1H), 6.00 (s, 2H), 5.06 (q, *J* = 7.0 Hz, 2H), 2.55 (s, 6H), 1.73 (t, *J* = 7.0 Hz, 3H), 1.36 (s, 6H). ^{13}C NMR (75 MHz, ppm): δ 307.3, 223.9, 217.9, 155.8, 144.1, 142.5, 140.0, 139.1, 133.7, 132.1, 132.0, 131.2, 130.6, 129.1, 124.9, 123.8, 122.5, 121.4, 74.8, 15.8, 14.6. IR (CH_2Cl_2): ν 2049, 1911, 1537, 1468, 1409, 1374, 1305, 1193, 1083, 980, 664 cm^{-1}. HRMS (ESI): *m/z* calcd for $C_{35}H_{30}BBrCrF_2N_3O_6$ [M + H] 768.0784, found 768.0705.

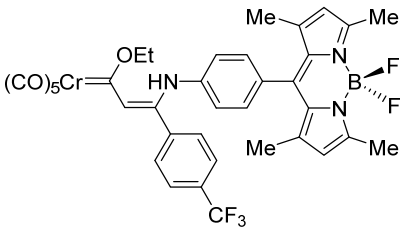

Complex 5h: A solution of **3h** (62 mg, 0.15 mmol) and BODIPY **4** (50 mg, 0.15 mmol) in 6.0 mL of dry THF was stirred for 4 hours. The solvent was removed under reduced pressure and the crude was purified by flash chromatography to yield complex **5h** as a dark red solid (111 mg, 98%). ^{1}H NMR (300 MHz, ppm): δ 10.28 (s, 1H), 7.58 (d, *J* = 8.2 Hz, 2H), 7.48 (d, *J* = 8.2 Hz, 2H), 7.11 (d, *J* = 8.4 Hz, 2H), 6.84 (d, *J* = 8.4 Hz, 2H), 6.72 (s, 1H), 5.99 (s, 2H), 5.10 (q, *J* = 7.0 Hz, 2H), 2.54 (s, 6H), 1.75 (t, *J* = 7.0 Hz, 3H), 1.32 (s, 6H). ^{13}C NMR (75 MHz, ppm): δ 309.0, 223.8, 217.7, 155.9, 143.5, 142.4, 139.9, 138.9, 138.6, 132.3, 132.2, 131.8, 131.2, 129.5, 129.2, 125.6 (q, *J* = 3.7 Hz), 124.0, 122.6, 121.4, 75.0, 15.8, 14.5, 14.5. IR (CH_2Cl_2): ν 2051, 1909, 1584, 1541, 1513, 1471, 1414, 1375, 1309, 1194, 1157, 1087, 983, 667 cm^{-1}. HRMS (ESI): *m/z* calcd for $C_{36}H_{30}BCrF_5N_3O_6$ [M + H] 758.1553, found 758.1583.

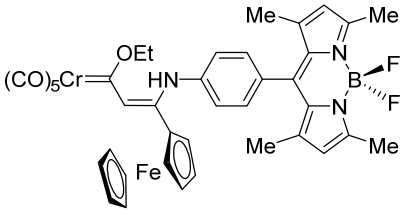

Complex 5i: A solution of **3i** (135 mg, 0.29 mmol) and BODIPY **4** (100 mg, 0.29 mmol) in 11.8 mL of dry THF was stirred for 6 hours. The solvent was removed under reduced pressure and the crude was purified by flash chromatography to yield complex **5i** as a dark red solid (108 mg, 46%). ^{1}H NMR (300 MHz, ppm): δ 10.46 (s, 1H), 7.20 (s, 1H), 7.14 (d, *J* = 8.2 Hz, 2H), 6.93 (d, *J* = 8.2 Hz, 2H), 6.00 (s, 2H), 4.90 (q, *J* = 7.0 Hz, 2H), 4.37-4.32 (m, 4H), 4.28 (s, 5H), 2.55 (s, 6H), 1.61 (t, *J* = 7.0 Hz, 3H), 1.42 (s, 6H). ^{13}C NMR (75 MHz, ppm): δ 293.2,

223.9, 218.7, 155.7, 149.5, 142.6, 140.3, 139.6, 132.0, 131.3, 128.8, 124.1, 123.2, 121.4, 78.4, 73.9, 71.3, 71.2, 70.4, 15.7, 14.7, 14.6. IR (CH_2Cl_2): ν 2046, 1905, 1578, 1542, 1510, 1471, 1411, 1314, 1308, 1197, 1157, 1079, 983, 669 cm^{-1}. HRMS (ESI): *m/z* calcd for $C_{39}H_{35}BCrF_2FeN_3O_6$ [M + H] 798.1342, found 798.1350.

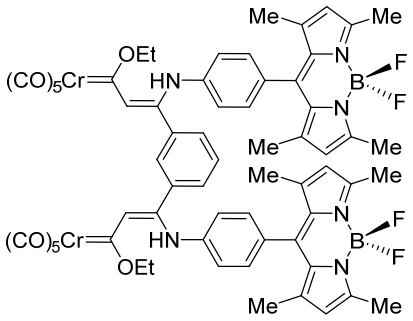

Complex 5j: A solution of **3j** (46 mg, 0.075 mmol) and BODIPY **4** (50 mg, 0.15 mmol) in 6.0 mL of dry THF was stirred for 30 minutes. The solvent was removed under reduced pressure and the crude was purified by flash chromatography to yield complex **5j** as a dark red solid (68 mg, 70%). ^{1}H NMR (300 MHz, ppm): δ 10.24 (s, 2H), 7.46-7.43 (m, 3H), 7.31 (d, *J* = 7.4 Hz, 1H), 7.09 (d, *J* = 8.3 Hz, 4H), 6.75 (d, *J* = 8.3 Hz, 4H), 6.71 (s, 2H), 5.91 (s, 4H), 5.10 (q, *J* = 6.9 Hz, 4H), 2.52 (s, 12H), 1.75 (t, *J* = 6. Hz, 6H), 1.28 (s, 12H). ^{13}C NMR (75 MHz, ppm): δ 309.3, 223.8, 217.7, 155.9, 142.3, 142.2, 149.7, 139.0, 135.5, 131.8, 131.1, 131.0, 129.8, 129.4, 129.1, 123.0, 122.9, 121.4, 75.0, 15.8, 14.6, 14.4. IR (CH_2Cl_2): ν 2051, 1913, 1586, 1542, 1512, 1467, 1410, 1374, 1308, 1194, 1157, 1089, 982, 667 cm^{-1}. HRMS (ESI): *m/z* calcd for $C_{64}H_{54}B_2Cr_2F_4N_6NaO_{12}$ [M + Na] 1323.2630, found 1323.2669.

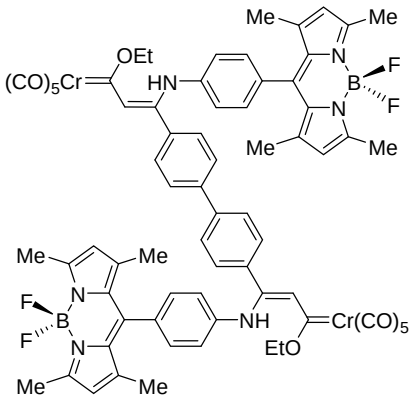

Complex 5k: A solution of **3k** (52 mg, 0.075 mmol) and BODIPY **4** (50 mg, 0.15 mmol) in 6.0 mL of dry THF was stirred for 3 hours. The solvent was removed under reduced pressure and the crude was purified by flash chromatography to yield complex **5k** as a dark red solid (90 mg, 89%). ^{1}H NMR (300 MHz, ppm): δ 10.37 (s, 2H), 7.49 (d, *J* = 8.5 Hz, 4H), 7.44 (d, *J* = 8.5 Hz, 4H), 7.10 (d, *J* = 8.4 Hz, 4H), 6.86 (d, *J* = 8.4 Hz, 4H), 6.77 (s, 2H), 5.95 (s, 4H), 5.07 (q, *J* = 7.0 Hz, 4H), 2.53 (s, 12H), 1.74 (t, *J* = 7.0 Hz, 6H), 1.37 (s, 12H). ^{13}C NMR (75 MHz, ppm): δ 306.3, 223.9, 218.0, 155.9, 144.6, 142.4, 141.6, 140.1, 139.3, 134.4, 131.8, 131.2, 129.9, 129.0, 127.2, 123.6, 122.7, 121.4, 74.8, 15.8, 14.6, 14.5. IR (CH_2Cl_2): ν 2049, 1906, 1579, 1540, 1521, 1470, 1409, 1374, 1308, 1193, 1156, 1089, 982, 667 cm^{-1}. HRMS (ESI): *m/z* calcd for $C_{70}H_{58}B_2Cr_2F_4N_6NaO_{12}$ [M + Na] 1399.2943, found 1399.2964.

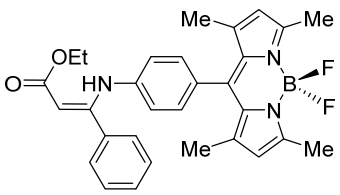

Oxidation of complex 5a into 6. In an open-air flask, KF (7 mg, 0.11 mmol) was added to a solution of complex **5a** (50 mg, 0.075 mmol) in 2.3 mL of DME. The reaction was carried out at room temperature for 24 hours (checked by TLC). Silica gel was added, the solvent was removed under reduced pressure and the crude was purified by flash chromatography to yield BODIPY **4** as an orange solid (20 mg, 52%). ^{1}H NMR (300 MHz, ppm): δ 10.36 (s, 1H), 7.35-7.26 (m, 5H), 6.99 (d, *J* = 8.4 Hz, 2H), 6.79 (d, *J* = 8.4 Hz, 2H), 5.96 (s, 2H), 5.10 (s, 1H), 4.24 (q, *J* = 7.1 Hz,

2H), 2.53 (s, 6H), 1.36 (s, 6H), 1.35 (t, *J* = 7.1 Hz, 3H). ^{13}C NMR (75 MHz, ppm): δ 170.2, 158.7, 155.3, 142.9, 141.3, 141.2, 135.5, 131.5, 129.6, 129.5, 128.4, 128.3, 128.3, 123.4, 121.1, 91.9, 59.5, 14.6, 14.6, 14.5. IR (CH_2Cl_2): ν 1659, 1605, 1546, 1512, 1471, 1409, 1368, 1285, 1188, 1082, 980, 705.6 cm^{-1}. HRMS (ESI): *m/z* calcd for $C_{30}H_{31}BF_2N_3O_2$ [M + H] 514.2477, found 514.2492.

Crystal data for compound 5b: $C_{35}H_{30}BF_2N_3O_6W$, *M* = 821.28, triclinic, *a* = 9.6685(19), *b* = 16.122(3), *c* = 22.139(4) Å, α = 78.12(3), β = 82.89(3), γ = 89.30(3)°, *V* = 3350.8(12) Å^3, space group $P\bar{1}$, *Z* = 4, *T* = 120(2) K, λ = 0.71073 Å, D_{calcd} = 1.628 g·cm^{-3}, μ = 3.508 cm^{-1}, 38333 reflections measured, 19606 unique (R_{int} = 0.0183), crystal structure was solved by direct methods and all non hydrogen atoms refined anisotropically on F^2 using the programs SHELXT and SHELXL-2014,[33] N-H hydrogen atoms were found in a Fourier difference map and refined with a restrained N-H distance, methyl groups hydrogen atoms were included using a rigid model and other hydrogen atoms as *riding*, *R* (F_o, I > 2σ(I)) = 0.0213, R_w (F_o^2, all data) = 0.0728.

V.7. References

(1) Recent reviews on the synthesis and properties of BODIPY's: (a) Loudet, A.; Burgess, K. *Chem. Rev.* **2007**, *107*, 4891. (b) Ulrich, G.; Ziessel, R.; Harriman, A. *Angew. Chem., Int. Ed.* **2008**, *47*, 1184. (c) Ziessel, R.; Ulrich, G.; Harriman, A. *New J. Chem.* **2007**, *31*, 496. (d) Boens, N.; Leen, V.; Dehaen, W. *Chem. Soc. Rev.* **2012**, *41*, 1130. (e) Kamkaew, A.; Lim, S. H.; Lee, H. B.; Kiew, L. V.; Chung, L. Y.; Burgess, K. *Chem. Soc. Rev.* **2013**, *42*, 77.

(2) Representative examples: (a) Gareis, T.; Huber, C.; Wolfbeis, O. S.; Daub, *J. Chem. Commun.* **1997**, 1717. (b) Rurack, K.; Kollmannsberger, M.; Daub, J. *New J. Chem.* **2001**, *25*, 289. (c) DiCesare, N.; Lakowicz, J. R. *Tetrahedron Lett.* **2001**, *42*, 9105. (d) Baki, C. N.; Akkaya, E. U. *J. Org. Chem.* **2001**, *66*, 1512. (e) Turfan, B.; Akkaya, E. U. *Org. Lett.* **2002**, *4*, 2857. (f) Moon, Y. S.; Cha, N. R.; Kim, Y. H.; Chang, S. K. *J. Org. Chem.* **2004**, *69*, 181. (g) Atilgan, S.; Ekmekci, Z.; Lale Dogan, A.; Guc, D.; Akkaya, E. U. *Chem. Commun.* **2006**, 4398. (h) Harriman, A.; Izzet, G.; Ziessel, R. *J. Am. Chem. Soc.* **2006**, *128*, 10868. (i) Carlson, J. C. T.; Meimetis, L. G.; Hilderbrand, S. A.; Weissleder, R. *Angew. Chem., Int. Ed.* **2013**, *52*, 6917.

(3) Recent examples: (a) Rosenthal, J.; Lippard, S. J. *J. Am. Chem. Soc.* **2010**, *132*, 5536. (b) Whited, M. T.; Djurovich, P. I.; Roberts, S. T.; Durrell, A. C.; Schlenker, C. W.; Bradforth, S. E.; Thompson, M. E. *J. Am. Chem. Soc.* **2011**, *133*, 88. (c) Sozmen, F.; Oksal, B. S.; Bozdemir, O. A.; Buyukcakir, O.; Akkaya, E. U. *Org. Lett.* **2012**, *14*, 5286. (d) Shi, W.-J.; Menting, R.; Ermilov, E. A.; Lo, P.-C.; Röder, B.; Ng, D. K. P. *Chem. Commun*, **2013**, *49*, 5277. (e) Sun, J. F.; Zhong, F. F.; Yi, X. Y.; Zhao, J. Z. *Inorg. Chem.* **2013**, *52*, 6299. (f) Bartelmess, J.; Weare, W. W.; Sommer, R. D. *Dalton Trans.* **2013**, *42*, 14883. (g) Bartelmess, J.; Francis, A. J.; Roz, K. A. E.; Castellano, F. N.; Weare, W. W.; Sommer, R. D. *Inorg. Chem.* **2014**, *53*, 4527. (h) Li, M.; Yao, Y.; Ding, J.; Liu, L.; Qin, J.; Zhao, Y.; Hou, H.; Fan, Y. *Inorg. Chem.* **2015**, *54*, 1346.

(4) Chu, G. M.; Guerrero-Martínez, A.; Fernández, I.; Sierra, M. A. *Chem. Eur. J.* **2014**, *20*, 1367.

(5) (a) Kee, H. L.; Kirmaier, C.; Yu, L.; Thamyongkit, P.; Youngblood, W. J.; Calder, M. E.; Ramos, L.; Noll, B. C.; Bocian, D. F.; Scheidt, W. R.; Birge, R. R.; Lindsey, J. S.; Holten, D. *J. Phys. Chem. B* **2005**, *109*, 20433. (b) Hedley, G. J.; Ruseckas, A.; Harriman, A.; Samuel, I. D. W. *Angew. Chem., Int. Ed.* **2011**, *50*, 6634.

(6) (a) Fernández, I.; Sierra, M. A.; Cossío, F. P. *J. Org. Chem.* **2008**, *73*, 2083. (b) Fernández, I.; Sierra, M. A.; Cossío, F. P. *J. Org. Chem.* **2006**, *71*, 6178. (c) Andrada, D. M.; Granados, A. M.; Solà, M.; Fernández, I. *Organometallics* **2011**, *30*, 46610.

(7) For selected recent reviews on the chemistry and applications of Fischer carbenes, see: (a) Wu, Y.-T.; Kurahashi, T.; de Meijere, A. *J. Organomet. Chem.* **2005**, *690*, 5900. (b) Gómez-Gallego, M.; Mancheño, M. J.; Sierra, M. A. *Acc. Chem. Res.* **2005**, *38*, 44. (c) Sierra, M. A.; Gómez-Gallego, M.; Martínez-Álvarez, R. *Chem. Eur. J.* **2007**, *13*, 736. (d) Sierra, M. A.; Fernández, I.; Cossío, F. P. *Chem. Commun.* **2008**, 4671. (e) Dötz, K. H.; Stendel, J. *Chem. Rev.* **2009**, *109*,

3227. (f) Herndon, J. W. *Coord. Chem. Rev.* **2010**, *254*, 103. (g) Fernández-Rodríguez, M. A.; García-García, P.; Aguilar, E. *Chem. Commun.* **2010**, *46*, 7670. (h) Fernández, I.; Cossío, F. P.; Sierra, M. A. *Acc. Chem. Res.* **2011**, *44*, 479. (i) Fernández, I.; Sierra, M. A. *Top. Heterocycl. Chem.* **2013**, *30*, 65.

(8) (a) Cui, A.; Peng, X.; Fan, J.; Chen, X.; Wu, Y.; Guo, B. *J. Photochem. Photobiol. A* **2007**, *186*, 8. See also: (b) Yu, M.; Wong, J. K.-H.; Tang, C.; Turner, P.; Todd, M. H.; Rutledge, P. J. *Beilstein J. Org. Chem.* **2015**, *11*, 37.

(9) For a review on the chemistry of α,β-unsaturated Fischer carbene complexes, see: de Meijere, A.; Schirmer, H.; Duetsch, M. *Angew. Chem. Int. Ed.* **2000**, *39*, 3964.

(10) Selected examples from our laboratories: (a) Fernández, I.; Sierra, M. A.; Mancheño, M. J.; Gómez-Gallego, M.; Ricart, S. *Organometallics* **2001**, *20*, 4304. (b) Sierra, M. A.; Mancheño, M. J.; del Amo, J. C.; Fernández, I.; Gómez-Gallego, M. *Chem. Eur. J.* **2003**, *9*, 4943. (c) López-Alberca, M. P.; Mancheño, M. J.; Fernández, I.; Gómez-Gallego, M.; Sierra, M. A.; Torres, R. *Org. Lett.* **2007**, *8*, 1757. (d) López-Alberca, M. P.; Mancheño, M. J.; Fernández, I.; Gómez-Gallego, M.; Sierra, M. A.; Torres, R. *Chem. Eur. J.* **2009**, *15*, 3595. (e) Rivero, A. R.; Fernández, I.; Sierra, M. A. *J. Org. Chem.* **2012**, *77*, 6648.

(11) (a) Fernández, I.; Mancheño, M. J.; Gómez-Gallego, M.; Sierra, M. A. *Org. Lett.* **2003**, *5*, 1237. (b) López-Alberca, M. P.; Mancheño, M. J.; Fernández, I.; Gómez-Gallego, M.; Sierra, M. A.; Hemmert, C.; Gornitzka, H. *Eur. J. Inorg. Chem.* **2011**, 842.

(12) (a) Fernández, I.; Cossío, F. P.; Arrieta, A.; Lecea, B.; Mancheño, M. J.; Sierra, M. A. *Organometallics* **2004**, *23*, 1065. (b) Andrada, D. M.; Zoloff Michoff, M. E.; Fernández, I.; Granados, A.; Sierra, M. A. *Organometallics* **2007**, *26*, 5854.

(13) (a) Valyaev, D. A.; Brousses, R.; Lugan, N.; Fernández, I.; Sierra, M. A. *Chem. Eur. J.* **2011**, *17*, 6602. (b) Lugan, N.; Fernández, I.; Brousses, R.; Valyaev, D. A.; Lavigne, G.; Ustynyuk, N. A. *Dalton Trans.* **2013**, *42*, 898.

(14) Barluenga, J.; Andina, F.; Fernández-Rodríguez, M. A.; García-García, P.; Merino, I.; Aguilar, E. *J. Org. Chem.* **2004**, *69*, 7352.

(15) See, for instance: (a) Rao, M. R.; Kumar, K. V. P.; Ravikanth, M. *J. Organomet. Chem.* **2010**, *695*, 863. (b) Liu, J.-Y.; El-Khouly, M. E.; Fukuzumi, S.; Ng, D. K. P. *ChemPhysChem* **2012**, *13*, 2030.

(16) (a) Hammett, L. P. *Chem. Rev.* **1935**, *17*, 125. (b) Hammett, L. P. *Physical Organic Chemistry*, 2nd ed.; McGraw-Hill: New York, **1970**.

(17) Fernández, I.; Frenking, G. *J. Org. Chem.* **2006**, *71*, 2251.

(18) (a) Moonen, N. N. P.; Pomerantz, W. C.; Gist, R.; Boudon, C.; Gisselbrecht, J.-P.; Kawai, T.; Kishioka, A.; Gross, M.; Irie, M.; Diederich, F. *Chem. Eur. J.* **2005**, *11*, 3325. (b) Fernández, I.; Frenking, G. *Chem. Commun.* **2006**, 5030.

(19) Lage, M. L.; Fernández, I.; Mancheño, M. J.; Sierra, M. A. *Inorg. Chem.* **2008**, *47*, 5253.

(20) Gaussian 09, Revision D.01, Frisch, M. J.; Trucks, G. W.; Schlegel, H. B.; Scuseria, G. E.; Robb, M. A.; Cheeseman, J. R.; Scalmani, G.; Barone, V.; Mennucci, B.; Petersson, G. A.; Nakatsuji, H.; Caricato, M.; Li, X.; Hratchian, H. P.; Izmaylov, A. F.; Bloino, J.; Zheng, G.; Sonnenberg, J. L.; Hada, M.; Ehara, M.; Toyota, K.; Fukuda, R.; Hasegawa, J.; Ishida, M.; Nakajima, T.; Honda, Y.; Kitao, O.; Nakai, H.; Vreven, T.; Montgomery, J. A., Jr.; Peralta, J. E.; Ogliaro, F.; Bearpark, M.; Heyd, J. J.; Brothers, E.; Kudin, K. N.; Staroverov, V. N.; Kobayashi, R.; Normand, J.; Raghavachari, K.; Rendell, A.; Burant, J. C.; Iyengar, S. S.; Tomasi, J.; Cossi, M.; Rega, N.; Millam, J. M.; Klene, M.; Knox, J. E.; Cross, J. B.; Bakken, V.; Adamo, C.; Jaramillo, J.; Gomperts, R.; Stratmann, R. E.; Yazyev, O.; Austin, A. J.; Cammi, R.; Pomelli, C.; Ochterski, J. W.; Martin, R. L.; Morokuma, K.; Zakrzewski, V. G.; Voth, G. A.; Salvador, P.; Dannenberg, J. J.; Dapprich, S.; Daniels, A. D.; Farkas, Ö.; Foresman, J. B.; Ortiz, J. V.; Cioslowski, J.; Fox, D. J. Gaussian, Inc., Wallingford CT, **2009**.

(21) (a) Becke, A. D. *J. Chem. Phys.* **1993**, *98*, 5648. (b) Lee, C.; Yang, W.; Parr, R. G. *Phys. Rev. B* **1988**, *37*, 785.

(22) Weigend, F.; Alhrichs, R. *Phys. Chem. Chem. Phys.* **2005**, *7*, 3297.

(23) (a) Casida, M. E. *Recent Developments and Applications of Modern Density Functional Theory*, Vol. 4, Elsevier, Amsterdam, **1996**. (b) Casida, M. E.; Chong, D. P. *Recent Advances in Density Functional Methods*, Vol. 1, World Scientific, Singapore, **1995**, p. 155.

(24) (a) Miertuš, S.; Scrocco, E.; Tomasi, *J. Chem. Phys.* **1981**, *55*, 117. (b) Pascual-Ahuir, J. L.; Silla, E.; Tuñón, I. *J. Comp. Chem.* **1994**, *15*, 1127. (c) Barone, V.; Cossi, M. *J. Phys. Chem. A* **1998**, *102*, 1995.

(25) Yanai, T.; Tew, D.; Handy, N. *Chem. Phys. Lett.* **2004**, *393*, 51.

(26) (a) Foster, J. P.; Weinhold, F. *J. Am. Chem. Soc.* **1980**, *102*, 7211. (b) Reed, A. E.; Weinhold, F. *J. Chem. Phys.* **1985**, *83*, 1736. (c) Reed, A. E.; Weinstock, R. B.; Weinhold, F. *J. Chem. Phys.* **1985**, *83*, 735. (d) Reed, A. E.; Curtiss, L. A.; Weinhold, F. *Chem. Rev.* **1988**, *88*, 899.

(27) Aumann, R.; Hinterding, P. *Chem. Ber.* **1993**, *126*, 421.

(28) Fischer, E. O.; Kreissl, F. R. *J. Organomet. Chem.* **1972**, *35*, C47.

(29) Vázquez, M. A.; Reyes, L.; Miranda, R.; García, J. J.; Jiménez-Vázquez, H. A.; Tamariz, J.; Delgado, F. *Organometallics* **2005**, *24*, 3413.

(30) Kessler, F.; Szesni, N.; Maass, C.; Hohberger, C.; Weibert, B.; Fischer, H. *J. Organomet. Chem.* **2007**, *692*, 3005.

(31) Giner, E. A.; Santiago, A.; Gómez-Gallego, M.; Ramírez de Arellano, C.; Poulten, R. C.; Whittlesey, M. K.; Sierra, M. A. *Inorg. Chem.* **2015**, *54*, 5450.

(32) López-Alberca, M. P.; Mancheño, M. J.; Fernández, I.; Gómez-Gallego, M.; Sierra, M. A. *Org. Lett.* **2008**, *10*, 365.

(33) Sheldrick, G. M. *Acta Cryst.* **2008**, *A64*, 112.

VI. *CAPÍTULO 4*

VI.1. *Fluorescence Quenching in BODIPYs Having Ir- and Rh-Tethered Complexes*

Abstract: The effect of Rh- and Ir-centers on the optical properties of the BODIPY core is studied. To this end, novel metal complexes tethered to BODIPY have been prepared through an easy and versatile procedure using N-directed C–H activation reactions. The organometallic moiety has a tremendous influence on the emissive properties of the BODIPY fragment. A Photoinduced Electron Transfer (PET) mechanism is suggested as the main mechanism responsible for the suppression of the BODIPY fluorescence emission in the newly formed dyads. The efficiency of the PET depends on both the distance between the chromophores in the dyad and the nature of the transition metal (Rh vs Ir).

In press: *Eur. J. Inorg. Chem.,* doi: 10.1002/ejic.201501283

VI.2. Introduction

The 4,4-difluoro-4-bora-3a,4a-diaza-*s*-indacene (BODIPY)[1] core is arguably one of the most versatile organic luminophore having useful applications in different fields ranging from sensors to medicinal chemistry. The chemistry of BODIPY derivatives and their applications have been profusely reviewed.[2] The importance of BODIPYs is due to their photophysical properties that include intense visible absorption, relatively sharp fluorescence combined with high quantum yield and good thermal and photochemical stabilities (including reasonable stability to physiological conditions). As a consequence, a significant number of synthetic methodologies have been developed allowing the access to BODIPY derivatives with tunable properties.[2c]

One additional feature of the BODIPY motif is its susceptibility to experience drastic changes in its emission properties derived from subtle changes in its structure. Therefore, attaching a transition metal complex to a BODIPY core is particularly attractive, in terms of manipulation of the photophysical properties of this system. In fact, the properties of transition metal complex–BODIPY dyads can be drastically changed by modifying either the nature of the transition metal or the surrounding ligands. Obviously, the distance between the metal center and the BODIPY is an additional variable to play with. Therefore, it is not strange that several metal–BODIPY systems have been prepared,[3] spanning from discrete organometallic structures to complex metal-organic frameworks (MOFs). Nevertheless, the versatile and efficient C–H activation/cyclometallation[4] sequence has not been reported to prepare transition metal complex–BODIPY dyads so far.

Work from our laboratories has shown that the attachment of a group 6 metal (Fischer) carbene complex to the pyrrole unit of the BODIPY core is able to modulate the emission of the fluorophore by controlling the planarity and π-conjugation of the system.[3b] Thus, whereas alkoxy-carbene complexes **1** containing a planar dyad are non-emissive, non-planar complexes **2** are emissive. Interestingly, the related thio-carbene complexes **3** show an intermediate

emission behavior, in concordance with the intermediate angle between the BODIPY and the metal-carbene center compared to **1** and **2** (Figure 1).

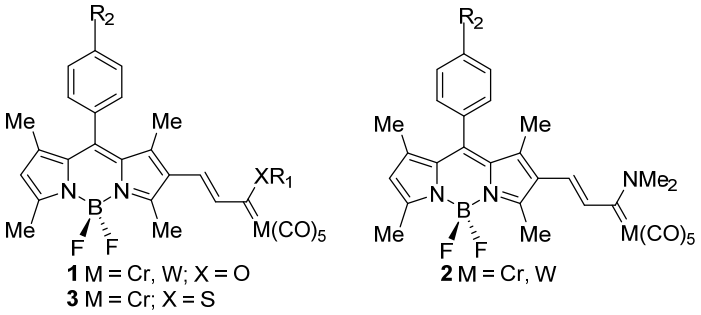

Figure 1. BODIPY-metal (Fischer) carbene complexes previously studied.

Following these results we devised the possibility of tethering a metal center to the BODIPY core by using a preformed all-organic fluorophore and placing the metal moiety using a C–H activation/cyclometallation sequence in an adequate tether.[5] In this way, by modifying the distance between the two components of the dyad, the influence of the transition metal fragment on the emission properties of the dyad will be studied. Different to the usual work in which the proximity of the metal to the BODIPY is used to quench the fluorescence of the emissive system (probe-off state),[3h] in this approach the existence of fluorescence will be used as a probe for studying the effect of the metal on the luminescence of the boron fluorophore.

VI.3. Results and Discussion

Compounds **7**-**9** (Scheme 1) were chosen for these studies. These compounds share two common features, namely an easy, straightforward synthetic route toward the carbon-boron framework and the structure required for incorporating the transition metal fragment by *N*-directed C–H activation/cyclometallation. Additionally, they are versatile in terms of being suitable to place different tethers separating the boron fluorophore from the transition metal moiety. In this regard, aldehydes **4** were reacted with pyrroles **5** to form dipyrromethanes **6**, which upon treatment with DDQ and subsequent reaction with Et_3N and $Et_2O{\cdot}BF_3$ formed BODIPYs **7**. Then, exposure of one

equivalent of BODIPY derivatives **7** to 0.5 equivalents of $[MCp^*Cl_2]_2$ (M = Ir and Rh) in the presence of NaOAc in CH_2Cl_2 as solvent at room temperature affords the organometallic dyads **8** and **9** in good to excellent yields (55 to 97%, Scheme 1).

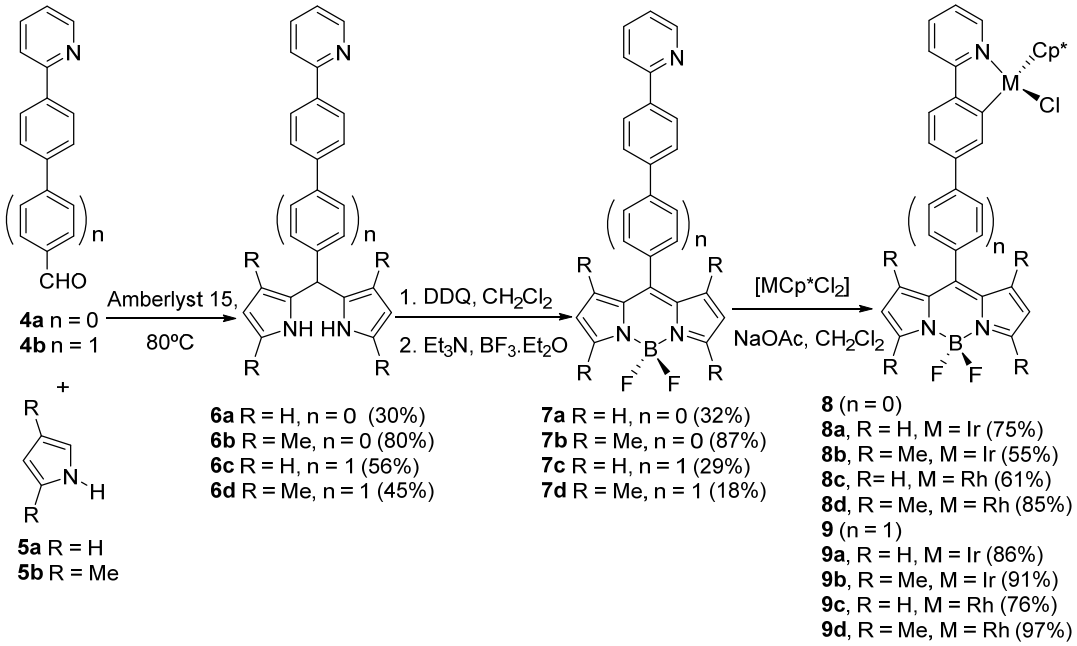

Scheme 1. The synthesis of the compounds used in this work.

Standard 1D- and 2D-NMR techniques were used to characterize the novel BODIPY derivatives. The spectroscopical data are compatible with the formation of the five-membered irida- and rhodacycles. For instance, the ^{13}C-NMR spectra of metallated derivatives **8** and **9** clearly confirm the presence of the aromatic carbon atom directly attached to the metal ($\delta \approx 167$ and 180 ppm, for Ir and Rh, respectively). In addition, single crystals of compounds **8b** and **9d** suitable for X-ray diffraction analysis were grown. The resulting X-ray structures (Figure 2) fully confirm that the novel dyads result from the *N*-directed C–H bond activation/cyclometallation reaction in the 2-pyridylaryl moiety.[6]

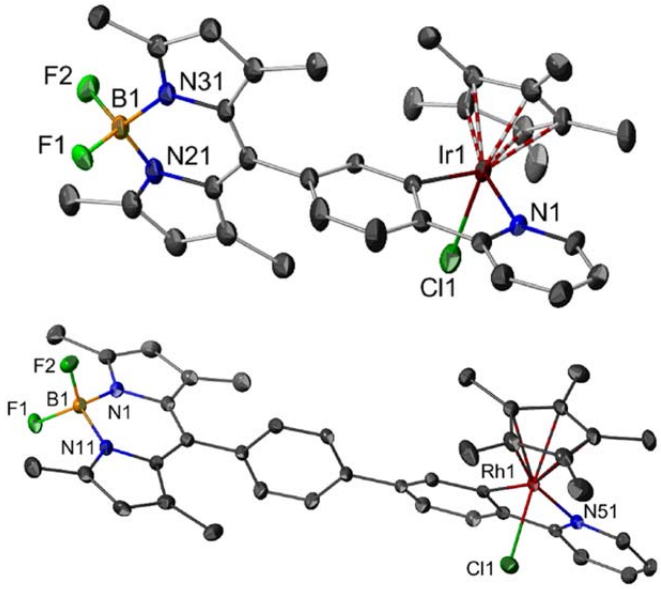

Figure 2. Ellipsoid plot (50% probability level) for compounds **8b** (up) and **9d** (bottom). Selected bond lengths (Å) and angles (°): **8b**. Ir(1)-C(12) 2.027(2), Ir(1)-N(1) 2.089(2), Ir(1)-Cl(1) 2.4170(7), C(12)-Ir(1)-N(1) 78.27(9), C(12)-Ir(1)-Cl(1) 85.27(7), N(1)-Ir(1)-Cl(1) 87.89(6), N(21)-B(1)-N(31) 106.6(2); **9d**. Rh(1)-C(43) 2.0340(17), Rh(1)-N(51) 2.0869(15), Rh(1)-Cl(1) 2.4025(5), C(43)-Rh(1)-N(51) 78.82(6), C(43)-Rh(1)-Cl(1) 90.17(5), N(51)-Rh(1)-Cl(1) 87.50(4), N(1)-B(1)-N(11) 106.66(15).

The structure of the novel BODIPY derivatives **8** and **9** deserves further discussion. As clearly seen in Figure 2, the organometallic fragment is nearly orthogonal to the BODIPY core (C–C–C–C dihedral angle of 99.3° and 90.6° for **8b** and **9d**, respectively). The lack of coplanarity between both moieties of the dyad is mainly due to the steric hindrance of the indacene methyl groups as reported for related non-organometallic BODIPY derivatives.[7,8] Density Functional Theory (DFT) calculations[9] on **8a**, lacking the indacene methyl groups, indicate that both fragments are more planar in the gas-phase equilibrium geometry (dihedral angle of –52.5°). This subtle structural difference makes **8a** and the rest of hydrogen substituted BODIPY's non-emissive (see below) due to the unrestricted C8-aryl rotation.[8]

The influence of the structure of compounds **8** and **9** on their photophysical properties was studied next using a combination of experimental and computational tools. Figure 3 shows the UV/Vis spectra of compounds **8a-d**

together with non-metallated BODIPY's **7a**, and **7b** recorded at 298 K in CH_2Cl_2 with a concentration of $1 \cdot 10^{-6} mol \cdot L^{-1}$. Figure 4 shows the analogous spectra of compounds **9a-d** and the non-metallated BODIPY's **7c** and **7d**. Table 1 compiles the data in Figures 3 and 4. Clearly, the intense absorption of the parent BODIPYs **7a-d** at $\lambda_{max} \approx 500$ nm remains unaltered by the presence of the metallacycle (compounds **8a-d** and **9a-d**). Interestingly, the additional aryl ring in compounds **9** has no effect on the position of the wavelength of absorption maxima. These results suggest that the π-conjugation between the metallacycle and the BODIPY moieties is not significant which allows us to tentatively assign this band to the typical π-π^* absorption involving exclusively the BODIPY core.

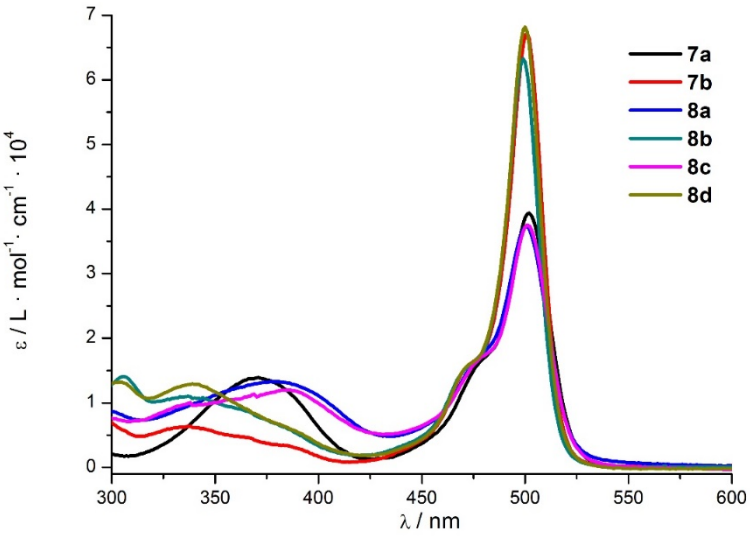

Figure 3. UV/Vis spectra of compounds **7a**, **7b** and **8a-d**, recorded at 298 K in CH_2Cl_2 with a concentration of $1 \cdot 10^{-6} mol \cdot L^{-1}$.

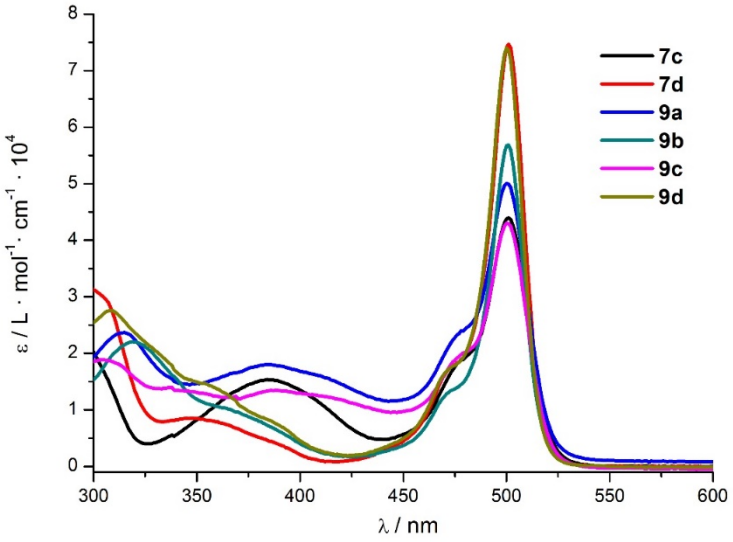

Figure 4. UV/Vis spectra of compounds **7c**, **7d** and **9a-d**, recorded at 298 K in CH_2Cl_2 with a concentration of $1 \cdot 10^{-6}$mol·L^{-1}.

Table 1. Spectral parameters of compounds **7-9**.[a]

Compound	λ_{abs} / nm[b]	ε[c]	λ_{em} / nm[e]	Φ_f[e]
7a	502	3.94	517	0.002
7b	501	6.72 (0.61)[d]	511	0.452
7c	501	4.40	518	0.009
7d	501	7.47	510	0.557
8a	501	3.72	509	0.001
8c	501	3.75	514	0.001
8b	499	6.32 (0.54)[d]	510	0.001
8d	500	6.82	510	0.014
9a	500	5.01	511	0.003
9c	500	4.30	515	0.002
9b	501	5.65 (0.59)[d]	510	0.062
9d	500	7.40	510	0.125

[a] All of the samples were recorded at 298 K in CH_2Cl_2 (concentration of 10^{-6}mol·L^{-1}, optical density < 0.1). [b] Maximum of the UV/Vis spectrum. [c] Molar extinction coefficient ε (L·mol^{-1} ·cm^{-1} ×10^4). [d] Calculated TD-DFT oscillator strength. [e] Maximum of the emission spectrum using λ_{exc} = 450 nm.

Time-dependent DFT (TD-DFT) calculations[9] were carried out on complexes **8b** and **9b** and BODIPY **7b** to determine the nature of the vertical transitions associated with the observed UV/Vis absorptions. Our (TD)-DFT calculations nicely agree with the above tentative assignment. Thus, the band at ca. 500 nm in compounds **8** and **9** is the result of the one-electron promotion from the HOMO-1

to the LUMO, which can be viewed as π and π*-molecular orbitals fully delocalized within the indacene moiety (see Figure 5). Similar molecular orbitals are involved in the HOMO → LUMO vertical transition in the parent BODIPY **7b**, which further supports the exclusive involvement of the indacene moiety in the observed absorption. Moreover no orbital contribution coming from the aryl fragment attached to the C8 position of the indacene into these molecular orbitals is observed, thus confirming the spectator role of the metallacycle on the UV/Vis properties of these BODIPY-derivatives. Again, data above fully support that the π-conjugation between the Ir or Rh-centres and the BODIPY fragment is almost negligible.

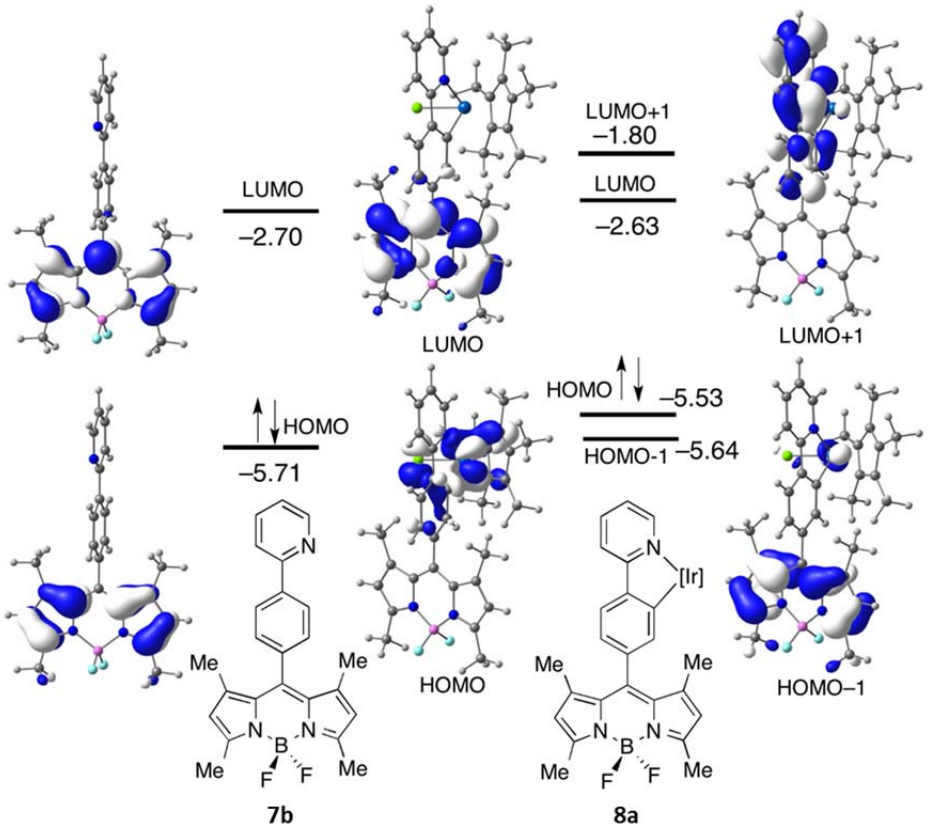

Figure 5. Computed (B3LYP/def2-SVP level) molecular orbitals of **7b** and **8a**.

The emissive properties of these species were studied next. The emission of the parent compounds **7b-d** (Figure 6) shows the expected strong fluorescence of the BODIPY core (around 515 nm, quantum yields of 0.452 and 0.557, respectively). As commented above, hydrogen substituted BODIPY's **7a** and **7c** are

non-emissive species due to the well-known effect of the unrestricted aryl rotation attached to the C8-carbon atom.[8]

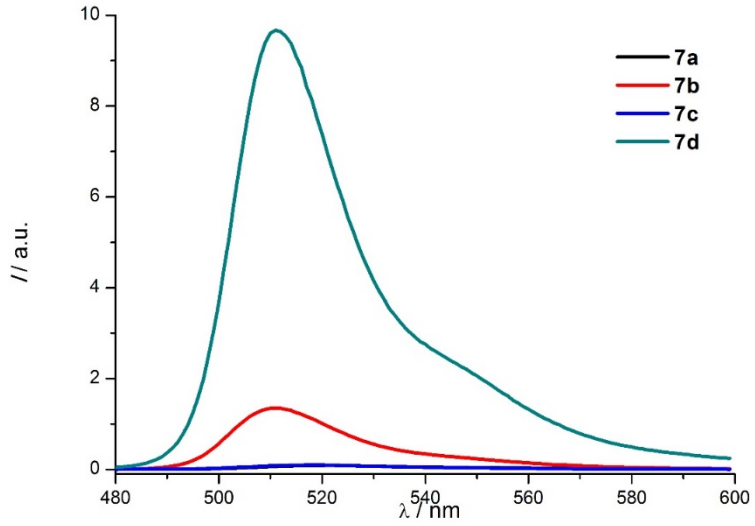

Figure 6. Emission spectra of compounds **7**. All of the measurements were recorded at 298 K in CH_2Cl_2 with a concentration of $1 \cdot 10^{-6} mol \cdot L^{-1}$ (λ_{exc} = 450 nm; optical density < 0.1).

The emission of complexes **8b**, **8d**, **9b** and **9d** is shown in Figure 7. It becomes evident that the intense fluorescence emission of the BODIPY core in **7b** and **7d** is completely quenched in compound **8b** (M = Ir) and almost completely in **8d** (M = Rh). Albeit in lesser extent, the fluorescence quenching is also strong in complexes **9b** (M = Ir) and **9d** (M = Rh) having an additional aryl fragment (quantum yields of 0.062 and 0.125, respectively). Again the Rh-complex was less efficient than the Ir-complex in quenching the BODIPY fluorescence. Obviously, the introduction of a metal-fragment in non-emissive BODIPYs **7a** and **7c** provokes no-changes in the emission of these species.

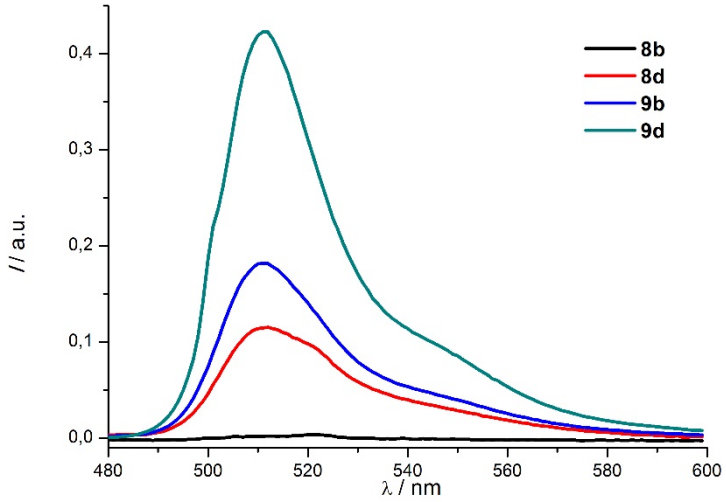

Figure 7. Emission spectra of compounds **8b**, **8d**, **9b** and **9d**. All of the measurements were recorded at 298 K in CH_2Cl_2 with a concentration of $1 \cdot 10^{-6} mol \cdot L^{-1}$ (λ_{exc} = 450 nm; optical density < 0.1).

In order to understand the origin of the quenching (namely, the origin of the energy-transfer mechanism), the emission spectrum of the isolated donor (BODIPY) and the absorption spectra of the acceptor (the transition metal complex) was measured for the parent phenyl-substituted BODIPY **11** and phenylpyridine iridium complex **12**.[10] Figure 8 shows the superimposition of both spectra where there overlap between the emission of the donor **11** and the absorption of the acceptor **12** is almost negligible, which makes the energy-transfer by either a Förster (through space) or a Dexter (through skeleton) mechanism unlikely for the observed fluorescence quenching in complexes **8b**, **8d**, **9b** and **9d**.[11]

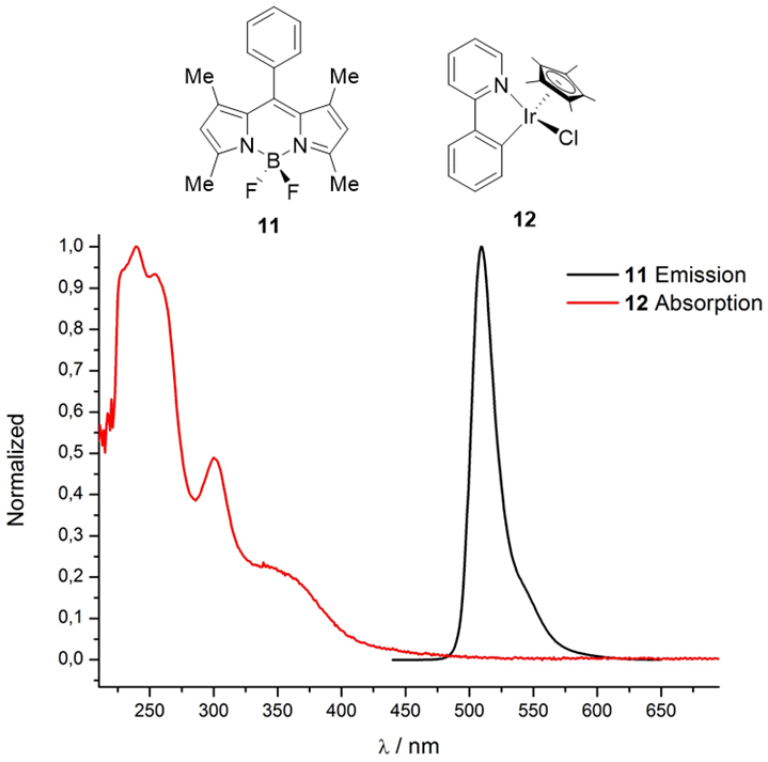

Figure 8. The emission spectra of the donor **11** and the absorption spectra of the acceptor **12**.

Once the mechanisms for the quenching of the fluorescence were ruled out, a photoinduced electron transfer (PET) quenching mechanism seems to be a reasonable alternative to explain the experimental findings. DFT calculations were carried out to investigate the mechanism responsible for the observed fluorescence quenching in the newly prepared organometallic-dyads. In principle, upon photoexcitation the BODIPY fragment can act as both electron donor and electron acceptor. This can be roughly estimated by comparing the relative energies of the frontier molecular orbitals (FMO) of the fragments present in the dyads.[12] As depicted in Figure 9, the HOMO of the metallacycle is slightly higher in energy than that of the fluorophore BODIPY. Similarly, the LUMO of the transition-metal fragment is also higher in energy than that of the BODIPY core. As a consequence, when the BODIPY moiety is photoexcited, the intramolecular electron transfer from the metallacyclic moiety to the BODIPY fragment is energetically favorable (ΔE = 0.46 eV). Therefore, the BODIPY fragment behaves, upon photoexcitation, as an electron acceptor. As a result, the fluorescence of the

BODIPY moiety in dyads **8** is quenched through the so-called acceptor-excited PET (a-PET) process (Φ_f < 0.01).[13] According to the relative FMO energies shown in Figure 9, a similar a-PET mechanism should occur in dyads **9** which possess an additional aryl fragment connecting both chromophores. However, the corresponding fluorescence quantum yields are not negligible (see Table 1) which suggests that the efficiency of the PET-quenching depends on both the relative distance between the chromophores in the dyad and the nature of the transition metal. Thus, the extent of the PET mechanism decreases when lengthening the distance between the transition metal fragment and the BODIPY core and when going up in the group 9 (Ir < Rh).[14]

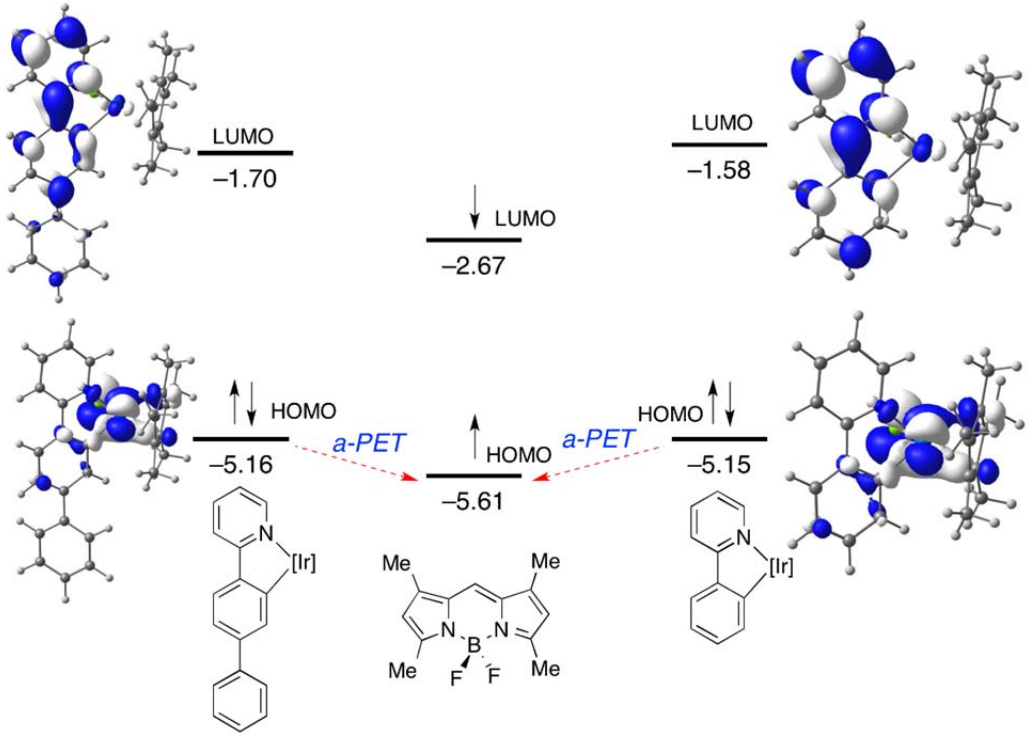

Figure 9. Proposed photoinduced electron transfer mechanism between BODIPY and metallacycles present in dyads **8** and **9**.

Further experimental support to the above computed molecular orbital levels is given by the electrochemical data recorded for compounds **7b**, **8b** and **12**. As readily seen in Figure 10, the oxidation potential of these species follow the order 0.94 V (**12**) < 1.01 V (**7b**) < 1.36 V (**8b**). The observed electrochemical trend nicely correlates with the computed energy of the corresponding HOMO: -5.15 eV

(**12**) < -5.53 eV (**7b**) < -5.71 eV (**8b**) which indicates that a less stabilized (i.e., less negative) HOMO is translated into a lower oxidation potential.

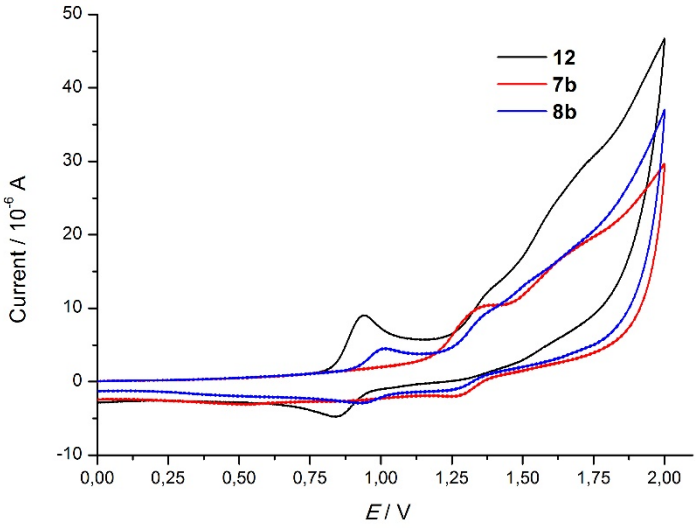

Figure 10. CVs of solutions of compounds **12**, **7b** and **8b** in CH_2Cl_2/0.1 M $[N(nBu)_4][ClO_4]$ on a glassy carbon-working electrode.

VI.4. Conclusions

We have developed an efficient synthetic methodology based on *N*-directed C-H bond activation/cyclometallation reaction which allows the efficient access to novel BODIPY dyads containing irida- and rhodacycles in their structures. This simple synthetic procedure makes it possible to produce organometallic BODIPYs differing in the nature of the transition metal fragment, the distance between the fluorophore and the metal, as well as the substitution of the pyrrole framework. It is found that the organometallic moiety has little influence on the position and extinction coefficient of the wavelength of the BODIPY absorption maxima. On the contrary, the distance between the metal and the BODIPY influences the emissive properties of irida- and rhoda-BODIPYs. Thus, dyads having the metal-center and the BODIPY separated by a phenyl ring are non-emissive, while a noticeable emission is observed when the metal and the BODIPY are separated by two phenyl groups.

Since the overlap between the emission of the donor fragment and the absorption of the acceptor moiety is negligible, either an energy-transfer by traditional Förster or Dexter mechanisms can be ruled out as responsible for the observed fluorescence quenching. According to DFT calculations, the observed complete suppression of the intense BODIPY fluorescence is due to an acceptor-excited PET-quenching mechanism as a result of the donation of electron density from the transition metal fragment to the photoexcited acceptor BODIPY moiety. Our results also indicate that the efficiency of the PET depends on both the distance between both chromophores in the dyad and the nature of the transition metal fragment, which opens doors to the preparation of new BODIPY derivatives having tailored photophysical properties.

VI.5. Experimental Section

All reactions were carried out under an argon atmosphere. All solvents used in this work were purified by distillation and were freshly distilled immediately before use. Triethylamine (Et_3N), *N*,*N*-diisopropylethylamine (DIPEA) and pyrrole were distilled from calcium hydride, whereas dichloromethane (CH_2Cl_2) was purified using a Pure Solv PS-MD-5 system. Boron trifluoride diethyl etherate ($Et_2O{\cdot}BF_3$) was distilled prior to use. Flame-dried glassware was used for moisture-sensitive reactions. Silica gel (Merck: 230-400 mesh) were used as stationary phases for purification of crude reaction mixtures by flash column chromatography. Identification of products was made by thin-layer chromatography (Kieselgel 60F-254). NMR spectra were recorded at 25 °C in $CDCl_3$, on Bruker Avance 300 (300 MHz for ^1H and 75 MHz for ^{13}C). Chemical shifts are given in ppm relative to $CDCl_3$ (^1H, 7.27 ppm and ^{13}C, 77.0 ppm). IR spectra were taken on a MIR (8000−400 cm^{-1}) spectrometer as solid films by slow evaporation of the solvent using the ATR (attenuated total reflectance) technique. MS spectra (HRMS) were acquired on a QTOF 6520: HP-1200 (Agilent Technologies) mass spectrometer.

All commercially available products were used without further purification. 2-(4-bromophenyl)pyridine[15] and 4-(2-pyridyl)benzaldehyde[16] were prepared according to literature.

Absorption and fluorescence spectroscopy. Experiments were carried out at 298 K, in CH_2Cl_2 (concentration of ca. 10^{-6} mol·L^{-1}, optical density < 0.1), using quartz cuvettes with optical paths of 1 cm. UV absorption spectra were registered using a UVICON XL spectrophotometer (Bio-Tex Instruments). Steadystate fluorescence spectra were recorded using an AMINCO Bowman Series 2 spectrofluorometer, with 1.0 nm bandwidth for emission and excitation. The excitation wavelengths were fixed at 450 nm and 500 nm in the measurement of the emission spectra. The emission wavelength was fixed at 550 nm for the determination of all the excitation spectra. The fluorescence quantum yields (Φ_x) were determined using the following equation:[17]

$$\Phi_x = \Phi_R \cdot \frac{I_x}{I_R} \cdot \frac{A_R}{A_x} \cdot \frac{n_x^2}{n_R^2}$$

where Φ_x is the quantum yield, *I* is the area from the integrated emission spectra, *A* is the absorbance at the excitation wavelength (λ = 496 nm) and *n* is the refractive index. The subscript *R* represents the reference fluorophore and *x* stands for the sample. The reference used was fluorescein in NaOH 0.1 M (Φ_R= 0.95).[18] The refractive indexes are n_x = 1.42 for CH_2Cl_2 and n_R = 1.33 for the basic solution. Quantum yields were calculated with an error of ± 0.005.

General synthesis of dipyrromethane derivatives:[19] A mixture of the corresponding pyrrole (3 mmol), the corresponding aldehyde (1 mmol) and Amberlyst 15 (20 mg) was stirred at 80 °C. The mixture was stirred until total disappearance of the starting material (checked by TLC). The reaction crude was

cooled to room temperature, diluted with CH_2Cl_2 and filtered. The solvent was removed under reduced pressure and purified by flash chromatography on silica gel (hexane/EtOAc).

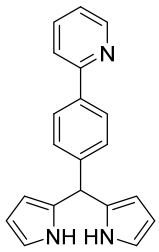

Dipyrromethane **6a**: Pyrrole (988 mg, 14.7 mmol), 4-(2-pyridin)benzaldehyde (900 mg, 4.9 mmol) and Amberlyst 15 (105 mg) was stirred at 80 ^{o}C for 1 hour. After completion of the reaction, the mixture was cooled to room temperature, diluted with CH_2Cl_2 and filtered. The solvent was removed under reduced pressure and purified by flash chromatography on silica gel to yield compound **6a** as a dark brown solid (435 mg, 30%). ^{1}H NMR (300 MHz, ppm): δ 8.62 (d, *J* = 4.9 Hz, 1H), 8.39 (bs, *J* = Hz, 2H), 7.93 (d, *J* = 8.0 Hz, 2H), 7.77-7.68 (m, 2H), 7.30 (d, *J* = 8.0 Hz, 2H), 7.22 (t, *J* = 5.8 Hz 1H), 6.66 (s, 2H), 6.22 (d, *J* = 2.9 Hz, 2H), 5.98 (s, 2H), 5.46 (s, 1H). ^{13}C NMR (75 MHz, ppm): δ 156.8, 149.2, 143.0, 137.5, 136.7, 132.2, 128.6, 126.9, 121.9, 120.4, 117.2, 107.9, 107.0, 43.4. IR (CH_2Cl_2): ν 3348, 3100, 2922, 2850, 1703, 1590, 1566, 1468, 1433, 1403, 1265, 1119, 1094, 761, 725 cm^{-1}. HRMS (ESI): *m/z* calcd for $C_{20}H_{18}N_3$ [M + H] 300.1501, found 300.1502.

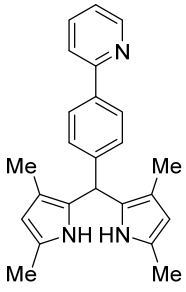

Dipyrromethane **6b**: 2,4-dimethylpyrrole (1.1 g, 11.5 mmol), 4-(2-pyridin)benzaldehyde (700 mg, 3.8 mmol) and Amberlyst 15 (82 mg) was stirred at 80 ^{o}C for 1 hour. After completion of the reaction, the mixture was cooled to room temperature, diluted with CH_2Cl_2 and filtered. The solvent was removed under reduced pressure and purified by flash chromatography on silica gel to yield compound **6b** as a dark red solid (754 mg, 56%). ^{1}H NMR (300 MHz, ppm): δ 8.69 (ddd, *J* = 4.8 Hz, *J* = 1.9 Hz, *J* = 1.6 Hz, 1H), 7.93 (AA'XX' system, *J* = 8.3 Hz, 2H), 7.80-7.70 (m, 2H), 7.31-7.21 (m, 5H), 5.74 (s, 1H), 5.73 (s, 1H), 5.51 (s, 1H), 2.17 (s, 6H), 1.86 (s, 6H). ^{13}C NMR (75 MHz, ppm): δ 149.6, 143.2, 137.8, 136.8, 130.2, 128.7, 127.3, 125.8, 125.6, 122.0, 120.6, 115.0, 108.5, 40.3, 13.0, 11.0. IR (CH_2Cl_2): ν 3322, 3055, 2921, 2861, 1696, 1587, 1513, 1466, 1435, 1399, 1286, 1215, 1152, 779, 742 cm^{-1}. HRMS (ESI): *m/z* calcd for $C_{24}H_{26}N_3$ [M + H] 356.2127, found 356.2096.

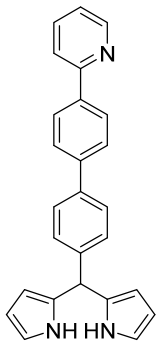

Dipyrromethane **6c**: Pyrrole (543 mg, 8.1 mmol), 4-[4-phenyl-(2-pyridin)]benzaldehyde **7** (700 mg, 2.7 mmol) and Amberlyst 15 (58 mg) was stirred at 80 ^{o}C for 1 hour. After completion of the reaction, the mixture was cooled to room temperature, diluted with CH_2Cl_2 and filtered. The solvent was removed under reduced pressure and purified by flash chromatography on silica gel to yield compound **6c** as a brown solid (458 mg, 45%). ^{1}H NMR (300 MHz, ppm): δ 8.72 (ddd, *J* = 4.8 Hz, *J* = 1.8 Hz, *J* = 1.3 Hz, 1H), 8.08 (d, *J* = 8.5 Hz, 2H), 8.04 (bs, 2H), 7.90-7.86 (m, 2H), 7.71 (d, *J* = 8.5 Hz, 2H), 7.62 (d, *J* = 8.3 Hz, 2H), 7.32 (d, *J* = 8.3 Hz, 2H), 7.28-7.23 (m, 2H), 6.74 (dd, *J* = 3.6 Hz, *J* = 2.6 Hz, 2H), 6.20 (dd, *J* = 6.6 Hz, *J* = 2.6 Hz, 2H), 5.99 (bs, 2H), 5.55 (s, 1H). ^{13}C NMR (75 MHz, ppm): δ 156.9, 149.6, 141.5, 141.2, 139.1, 138.1, 136.9, 132.3, 128.8, 127.4, 127.3, 127.2, 122.1, 120.5, 117.3, 108.4, 107.2, 43.7. IR (CH_2Cl_2): ν 3375, 3098,

3052, 2851, 1695, 1587, 1566, 1467, 1434, 1397, 1262, 1117, 1091, 1027, 838, 771, 722 cm^{-1}. HRMS (ESI): *m/z* calcd for $C_{26}H_{22}N_3$ [M + H] 376.1814, found 376.1798.

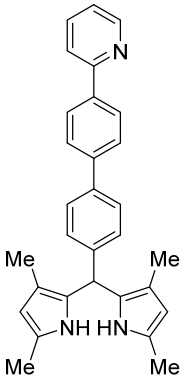

Dipyrromethane **6d**: 2,4-dimethylpyrrole (771 mg, 8.1 mmol), 4-[4-phenyl-(2-pyridin)]benzaldehyde **7** (700 mg, 2.7 mmol) and Amberlyst 15 (58 mg) was stirred at 80 ^{o}C for 1 hour. After completion of the reaction, the mixture was cooled to room temperature, diluted with CH_2Cl_2 and filtered. The solvent was removed under reduced pressure and purified by flash chromatography on silica gel to yield compound **6d** as a dark red solid (960 mg, 82%). ^{1}H NMR (300 MHz, ppm): δ 8.71 (d, *J* = 4.8 Hz, 1H), 8.10 (d, *J* = 8.3 Hz, 2H), 7.81-7.77 (m, 2H), 7.74 (d, *J* = 8.3 Hz, 2H), 7.63 (d, *J* = 8.1 Hz, 2H), 7.40 (bs, 2H), 7.29-7.23 (m, 3H), 5.77 (s, 1H), 5.76 (s, 1H), 5.54 (s, 1H), 2.20 (s, 6H), 1.91 (s, 6H). ^{13}C NMR (75 MHz, ppm): δ 156.1, 148.9, 141.6, 140.6, 137.7, 137.3, 136.4, 128.4, 126.8, 126.7, 126.6, 125.6, 125.0, 121.7, 120.0, 114.4, 108.1, 39.6, 12.4, 10.7. IR (CH_2Cl_2): ν 3279, 3053, 2976, 2922, 2864, 1688, 1587, 1504, 1465, 1435, 1376, 1290, 1151, 1120, 828, 780, 735, 700 cm^{-1}. HRMS (ESI): *m/z* calcd for $C_{30}H_{28}N_3$ [M + H] 430.2283, found 430.2275.[20]

Synthesis of BODIPY derivatives, 7:

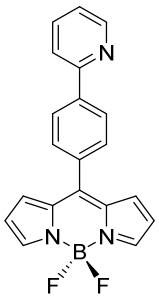

Compound **7a***:* A solution of dipyrromethane **6a** (430 mg, 1.44 mmol) in CH_2Cl_2 (169 mL) was oxidized with DDQ (393 mg, 1.7 mmol) for 30 min. Triethylamine (8.0 mL, 57.6 mmol) and $Et_2O{\cdot}BF_3$ (8.9 mL, 72 mmol), was added to the mixture reaction and stirred at room temperature for 1 h. The solvent was removed under reduced pressure and purified by flash chromatography on silica gel to yield compound **7a** as an orange solid (160 mg, 32%). ^{1}H NMR (300 MHz, ppm): δ 8.76 (ddd, *J* = 4.7 Hz, *J* = 1.8 Hz, *J* = 1.3 Hz, 1H), 8.17 (AA'XX' system, *J* = 8.5 Hz, 2H), 7.97 (bs, 2H), 7.83 (m, 2H), 7.69 (AA'XX' system, *J* = 8.5 Hz, 2H), 7.33 (m, 1H), 7.00 (d, *J* = 4.1 Hz, 2H), 6.57 (dd, *J* = 4.1 Hz, *J* = 1.3 Hz, 2H). ^{13}C NMR (75 MHz, ppm): δ 156.0, 150.0, 146.9, 144.1, 141.8, 137.0, 134.8, 134.2, 131.5, 131.0, 126.9, 122.9, 120.8, 118.6. IR (CH_2Cl_2): ν 1606, 1560, 1538, 1475, 1411, 1385, 1355, 1258, 1224, 1155, 1111, 1075, 1049, 980, 912, 787, 758, 741, 713 cm^{-1}. HRMS (ESI): *m/z* calcd for $C_{20}H_{15}BF_2N_3$ [M + H] 346.1327, found 346.1324.

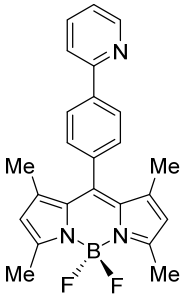

Compound **7b**: A solution of dipyrromethane **6b** (800 mg, 2.25 mmol) in CH_2Cl_2 (265 mL) was oxidized with DDQ (613 mg, 2.7 mmol) at room temperature for 30 min. Triethylamine (12.6 mL, 90 mmol) and immediately $Et_2O{\cdot}BF_3$ (13.9 mL, 113 mmol), was added to the mixture reaction and stirred at room temperature for 1 h. The solvent was removed under reduced pressure and purified by flash chromatography on silica gel to yield compound **7b** as an orange solid (790 mg, 87%). ^{1}H NMR (300 MHz, ppm): δ 8.69 (ddd, *J* = 4.8 Hz, *J* = 1.7 Hz, *J* = 1.2 Hz, 1H), 8.17 (AA'XX' system, *J* = 8.4 Hz, 2H),

7.85-7.78 (m, 2H), 7.42 (AA'XX' system, *J* = 8.4 Hz, 2H), 7.33-7.27 (m, 1H), 6.00 (s, 2H), 2.58 (s, 6H), 1.46 (s, 6H). ^{13}C NMR (75 MHz, ppm): δ 156.2, 155.5, 149.8, 143.1, 141.2, 139.9, 136.9, 135.6, 131.3, 128.5, 127.5, 122.6, 121.2, 120.6, 14.6. IR (CH_2Cl_2): ν 1543, 1510, 1467, 1408, 1308, 1195, 1157, 1084, 982, 759 cm^{-1}. HRMS (ESI): *m/z* calcd for $C_{24}H_{23}BF_2N_3$ [M + H] 402.1953, found 402.1947.

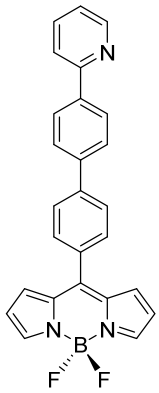

Compound **7c:** A solution of dipyrromethane **6c** (300 mg, 0.80 mmol) in CH_2Cl_2 (31 mL) was oxidized with DDQ (363 mg, 1.6 mmol) for 30 min. DIPEA (0.79 mL, 4.6 mmol) and $Et_2O{\cdot}BF_3$ (0.79 mL, 6.4 mmol), was added to the mixture reaction and stirred at for 1 h. The solvent was removed under reduced pressure and purified by flash chromatography on silica gel to yield compound **7c** as an orange solid (91 mg, 29%). ^{1}H NMR (300 MHz, ppm): δ 8.76 (d, *J* = 4.7 Hz, 1H), 8.16 (d, *J* = 8.4 Hz, 2H), 7.98 (bs, 2H), 7.85-7.80 (m, 6H), 7.70 (d, *J* = 8.4 Hz, 2H), 7.35-7.28 (m, 1H), 7.04 (d, *J* = 4.1 Hz, 2H), 6.59 (dd, *J* = 4.1 Hz, *J* = 1.3 Hz, 2H). ^{13}C NMR (75 MHz, ppm): δ 156.6, 149.6, 144.1, 143.1, 140.2, 138.9, 137.1, 134.9, 133.0, 131.5, 131.2, 127.6, 127.5, 127.1, 122.5, 120.7, 118.6, 118.5. IR (CH_2Cl_2): ν 1605, 1557, 1538, 1467, 1413, 1388, 1260, 1225, 1156, 1114, 1077, 1050, 981, 913, 783, 762, 745 cm^{-1}. HRMS (ESI): *m/z* calcd for $C_{26}H_{19}BF_2N_3$ [M + H] 422.1640, found 422.1660.

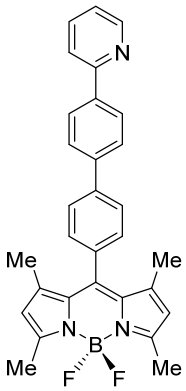

Compound **7d:** A solution of dipyrromethane **6d** (230 mg, 0.53 mmol) in CH_2Cl_2 (21 mL) was oxidized with DDQ (241 mg, 1.06 mmol) for 30 min. DIPEA (0.53 mL, 3.0 mmol) and $Et_2O{\cdot}BF_3$ (0.52 mL, 4.2 mmol), was added to the mixture reaction and stirred at room temperature for 1 h. The solvent was removed under reduced pressure and purified by flash chromatography on silica gel to yield compound **7d** as an orange solid (45 mg, 18%). ^{1}H NMR (300 MHz, ppm): δ 8.75 (ddd, *J* = 4.8 Hz, *J* = 1.8 Hz, *J* = 1.2 Hz, 1H), 8.15 (AA'XX' system, *J* = 8.3 Hz, 2H), 7.84-7.79 (m, 6H), 7.39 (AA'XX' system, *J* = 8.3 Hz, 2H), 7.30-7.25 (m, 1H), 6.01 (s, 2H), 2.58 (s, 6H), 1.48 (s, 6H). ^{13}C NMR (75 MHz, ppm): δ 156.8, 155.5, 149.8, 143.1, 141.4, 141.0, 140.4, 138.8, 136.9, 134.2, 128.6, 127.6, 127.4, 127.3, 122.3, 121.3, 121.2, 120.5, 14.6. IR (CH_2Cl_2): ν 1541, 1509, 1464, 1436, 1408, 1304, 1192, 1157, 1084, 1071, 1048, 981, 825, 765 cm^{-1}. HRMS (ESI): *m/z* calcd for $C_{30}H_{27}BF_2N_3$ [M + H] 478.2266, found 478.2269.

General procedure for the synthesis of cyclometallated complexes, 8 and 9: A mixture of $[MCp^*Cl_2]_2$ (M = Ir, Rh) (1 μmol), NaOAc (4.7 μmol) and the corresponding BODIPY (2 μmol) in 0.1 mL of CH_2Cl_2 was stirred at room temperature until total disappearance of the starting material (checked by TLC). The crude mixture was filtered through a short pad of Celite and evaporated to dryness obtaining the pure complex.

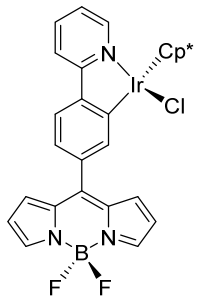

Complex **8a:** BODIPY **7a** (43 mg, 126 μmol) was added to a solution of $[IrCp^*Cl_2]_2$ (50 mg, 63 μmol) and NaOAc (25 mg, 300 μmol) in 6.3 mL of CH_2Cl_2. The reaction mixture was stirred for 16 h. The reaction mixture was filtered through a short pad of Celite and the solvent was removed under reduced pressure to yield complex **8a** as an orange solid (67mg 75%). ^{1}H NMR (300 MHz, ppm): δ 8.78 (d, *J* = 5.8 Hz, 1H), 7.98-7.91 (m, 4H), 7.80 (d, *J* = 8.0 Hz, 1H), 7.76 (ddd, *J* = 8.6 Hz, *J* = 7.8 Hz, *J* = 1.5 Hz, 1H), 7.27 (dd, *J* = 8.0 Hz, *J* = 1.8 Hz, 1H), 7.20 (ddd, *J* = 7.5 Hz, *J* = 5.6 Hz, *J* = 1.3 Hz, 1H), 7.13 (d, *J* = 4.1 Hz, 2H), 6.55 (dd, *J* = 4.1 Hz, *J* = 1.7 Hz, 2H), 1.69 (s, 15H). ^{13}C NMR (75 MHz, ppm): δ 166.0, 163.0, 151.5, 148.6, 147.1, 137.6, 137.3, 135.6, 135.1, 135.0, 125.0, 123.3, 123.2,121.9, 119.7, 118.2, 88.9, 8.9. IR (CH_2Cl_2): ν 2921, 2852, 1605, 1555, 1473, 1411, 1391, 1261, 1221, 1156, 1116, 1076, 1046, 986, 925, 785, 759, 740 cm^{-1}. HRMS (ESI): *m/z* calcd for $C_{30}H_{28}BF_2IrN_3$ [M - Cl] 672.1974, found 672.1971.

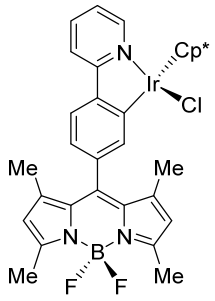

Complex **8b:** BODIPY **7b** (51 mg, 126 μmol) was added to a solution of $[IrCp^*Cl_2]_2$ (50 mg, 63 μmol) and NaOAc (25 mg, 300 μmol) in 6.3 mL of CH_2Cl_2. The reaction mixture was stirred at room temperature for 16 h. The reaction mixture was filtered through a short pad of Celite and the solvent was removed under reduced pressure to yield complex **8b** as an orange solid (53 mg, 55%). ^{1}H NMR (300 MHz, ppm): δ 8.75 (d, *J* = 5.6 Hz, 1H), 7.90 (d, *J* = 8.2 Hz, 1H), 7.79 (d, *J* = 8.0 Hz, 1H), 7.73 (m, 1H), 7.68 (d, *J* = 1.4 Hz, 1H), 7.15 (m, 1H), 6.97 (dd, *J* = 8.0 Hz, *J* = 1.5 Hz, 1H), 6.00 (s, 1H), 5.96 (s, 1H), 2.59 (s, 3H), 2.57 (s, 3H), 1.68 (s, 15H), 1.65 (s, 3H), 1.54 (s, 3H). ^{13}C NMR (75 MHz, ppm): δ 166.4, 163.6, 155.8, 153.7, 151.3, 145.4, 144.9, 143.0, 141.8, 141.8, 137.2, 136.8, 134.3, 131.9, 130.9, 124.0, 122.8, 121.4 120.4, 119.3, 88.7, 15.1, 14.6, 14.5, 14.3, 8.9. IR (CH_2Cl_2): ν 2963, 2921, 1605, 1542, 1509, 1472, 1408, 1307, 1195, 1156, 1086, 982, 759 cm^{-1}. HRMS (ESI): *m/z* calcd for $C_{34}H_{36}BF_2IrN_3$ [M - Cl] 728.2600, found 728.2610.

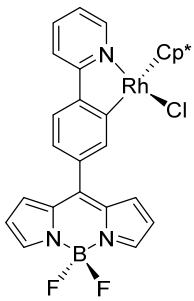

Complex **8c:** BODIPY **7a** (56 mg, 162 μmol) was added to a solution of $[RhCp^*Cl_2]_2$ (50 mg, 81 μmol) and NaOAc (31 mg, 381 μmol) in 8.1 mL of CH_2Cl_2. The reaction mixture was stirred at room temperature for 16 h. The reaction mixture was filtered through a short pad of Celite and the solvent was removed under reduced pressure to yield complex **8c** as an orange solid (61 mg, 61%). ^{1}H NMR (300 MHz, ppm): δ 8.82 (d, *J* = 5.5 Hz, 1H), 7.97-7.88 (m, 4H), 7.81 (ddd, *J* = 8.5 Hz, *J* = 7.5 Hz, *J* = 1.4 Hz, 1H), 7.75 (d, *J* = 8.0 Hz, 1H), 7.30 (dd, *J* = 7.9 Hz, *J* = 1.6 Hz, 1H), 7.26 (ddd, *J* = 7.7 Hz, *J* = 5.5 Hz, *J* = 1.3 Hz, 1H), 7.15 (d, *J* = 4.0 Hz, 2H), 6.56 (dd, *J* = 4.0 Hz, *J* = 1.5 Hz, 2H), 1.64 (s, 15H). ^{13}C NMR (75 MHz, ppm): δ 178.2 (d, *J* = 32.9 Hz), 164.1, 151.4, 148.4, 146.4, 138.5, 137.4, 135.0, 131.0, 126.9, 125.7, 123.0, 122.7, 120.8, 119.8, 118.3, 96.2 (d, *J* = 6.6 Hz), 9.1. IR (CH_2Cl_2): ν 2922, 2855, 1602, 1555, 1533, 1473, 1411, 1391, 1260, 1221, 1156, 1115, 1077, 1047, 985, 923, 786, 759, 740 cm^{-1}. HRMS (ESI): *m/z* calcd for $C_{30}H_{28}BF_2N_3Rh$ [M - Cl] 582.1399, found 582.1403.

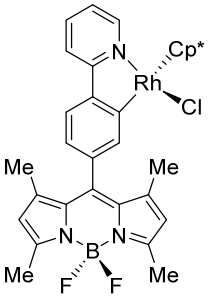

Complex **8d** BODIPY **7b** (65 mg, 162 μmol) was added to a solution of $[RhCp^*Cl_2]_2$ (50 mg, 81 μmol) and NaOAc (31 mg, 381 μmol) in 8.1 mL of CH_2Cl_2. The reaction mixture was stirred at room temperature for 17 h. The reaction mixture was filtered through a short pad of Celite and the solvent was removed under reduced pressure to yield complex **8d** as an orange solid (93 mg, 85%). ^{1}H NMR (300 MHz, ppm): δ 8.78 (d, *J* = 5.5 Hz, 1H), 7.85 (d, *J* = 7.6 Hz, 1H), 7.81-7.69 (m, 3H), 7.21 (ddd, *J* = 7.6 Hz, *J* = 5.5 Hz, *J* = 1.4 Hz, 1H), 7.02 (dd, *J* = 7.8 Hz, *J* = 1.6 Hz, 1H), 6.01 (s, 1H), 5.95 (s, 1H), 2.59 (s, 3H), 2.57 (s, 3H), 1.66 (s, 3H), 1.64 (s, 15H), 1.54 (s, 3H). ^{13}C NMR (75 MHz, ppm): δ 178.7 (d, *J* = 32.9 Hz), 164.6, 156.1, 153.8, 151.2, 145.7, 144.4, 142.9, 141.6, 137.3, 136.2, 135.6, 131.9, 130.9, 123.5, 122.5, 122.3, 121.5, 120.4, 119.5, 96.1 (d, *J* = 6.5 Hz), 15.3, 14.6, 14.5, 14.4, 9.2. IR (CH_2Cl_2): ν 2961, 2921, 2856, 1601, 1541, 1508, 1471, 1407, 1371, 1307, 1255, 1193, 1156, 1085, 1056, 1026, 981, 806, 758, 740 cm^{-1}. HRMS (ESI): *m/z* calcd for $C_{34}H_{36}BF_2N_3Rh$ [M - Cl] 638.2025, found 638.2043.

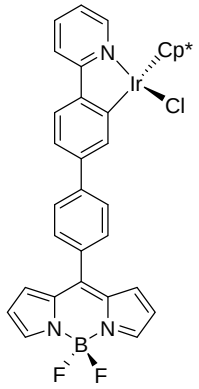

Complex **9a:** BODIPY **7c** (40 mg, 95 μmol) was added to a solution of $[IrCp^*Cl_2]_2$ (37.8 mg, 48 μmol) and NaOAc (18 mg, 220 μmol) in 4.8 mL of CH_2Cl_2. The reaction mixture was stirred at room temperature for 16 h. The reaction mixture was filtered through a short pad of Celite and the solvent was removed under reduced pressure to yield complex **9a** as an orange solid (64mg, 86%). ^{1}H NMR (300 MHz, ppm): δ 8.75 (d, *J* = 5.8 Hz, 1H), 8.14 (d, *J* = 1.7 Hz, 1H), 7.97 (bs, 2H), 7.90-7.85 (m, 3H), 7.80 (d, *J* = 8.1 Hz, 1H), 7.74-7.66 (m, 3H), 7.37 (dd, *J* = 8.1 Hz, *J* = 1.8 Hz, 1H), 7.14 (ddd, *J* = 7.5 Hz, *J* = 5.8 Hz, *J* = 1.3 Hz, 1H), 7.06 (d, *J* = 4.1 Hz, 2H), 6.59 (dd, *J* = 4.1 Hz, *J* = 1.7 Hz, 2H), 1.75 (s, 15H). ^{13}C NMR (75 MHz, ppm): δ 166.7, 151.5, 144.6, 144.5, 143.8, 141.3, 137.1, 134.9, 134.4, 132.5, 131.9, 131.6, 131.0, 127.3, 124.2, 122.6, 121.4, 119.2, 118.5, 118.4, 88.7, 9.0. IR (CH_2Cl_2): ν 2920, 1604, 1560, 1473, 1412, 1387, 1261, 1223, 1157, 1114, 1077, 1048, 982, 913, 781, 761, 745, 716 cm^{-1}. HRMS (ESI): *m/z* calcd for $C_{36}H_{32}BF_2IrN_3$ [M - Cl] 748.2287, found 748.2295.

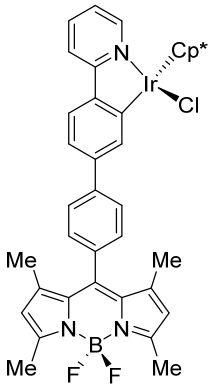

Complex **9b:** BODIPY **7d** (10 mg, 21 μmol) was added to a solution of $[IrCp^*Cl_2]_2$ (8.4 mg, 10.5 μmol) and NaOAc (4 mg, 49 μmol) in 1.1 mL of CH_2Cl_2. The reaction mixture was stirred at room temperature for 16 h. The reaction mixture was filtered through a short pad of Celite and the solvent was removed under reduced pressure to yield complex **9b** as an orange solid (16 mg, 91%). ^{1}H NMR (300 MHz, ppm): δ 8.73 (d, *J* = 5.8 Hz, 1H), 8.17 (d, *J* = 1.7 Hz, 1H), 7.90-7.83 (m, 3H), 7.78 (d, *J* = 8.2 Hz, 1H), 7.71 (ddd, *J* = 8.2 Hz, *J* = 7.7 Hz, *J* = 1.3 Hz, 1H), 7.40-7.34 (m, 3H), 7.13 (ddd, *J* = 7.6 Hz, *J* = 5.6 Hz, *J* = 1.3 Hz, 1H), 6.01 (s, 2H), 2.59 (s, 6H), 1.75 (s, 15H), 1.50 (s, 6H). ^{13}C NMR (75 MHz, ppm): δ 166.8, 163.7, 155.4, 151.5, 144.1, 143.3, 142.4, 141.8, 141.6, 137.1, 134.1, 133.6, 131.5, 128.3, 127.8, 124.1, 122.4, 121.2, 121.2, 119.1, 88.7, 14.7, 14.6, 9.1. IR (CH_2Cl_2): ν 2961, 2921, 2854, 1605, 1543, 1510, 1472, 1409, 1372, 1261, 1195,

1157, 1084, 1053, 1029, 982, 817, 766, 749, 712 cm^{-1}. HRMS (ESI): *m/z* calcd for $C_{40}H_{40}BF_2IrN_3$ [M - Cl] 804.2913, found 804.2943.

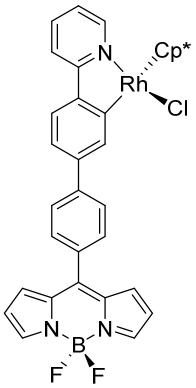

Complex **9c:** BODIPY **7c** (40 mg, 95 μmol) was added to a solution of $[RhCp^*Cl_2]_2$ (29.4 mg, 48 μmol) and NaOAc (18 mg, 220 μmol) in 4.8 mL of CH_2Cl_2. The reaction mixture was stirred at room temperature for 16 h. The reaction mixture was filtered through a short pad of Celite and the solvent was removed under reduced pressure to yield complex **9c** as an orange solid (50 mg, 76%). ^{1}H NMR (300 MHz, ppm): δ 8.78 (d, *J* = 5.5 Hz, 1H), 8.13 (d, *J* = 1.4 Hz, 1H), 7.97 (bs, 2H), 7.89-7.81 (m, 3H), 7.79-7.66 (m, 4H), 7.38 (dd, *J* = 8.1 Hz, *J* = 1.4 Hz, 1H), 7.19 (ddd, *J* = 7.3 Hz, *J* = 5.6 Hz, *J* = 1.1 Hz, 1H), 7.07 (d, *J* = 4.1 Hz, 2H), 6.59 (dd, *J* = 4.1 Hz, *J* = 1.4 Hz, 2H), 1.69 (s, 15H). ^{13}C NMR (75 MHz, ppm): δ 179.2 (d, *J* = 32.4 Hz), 164.7, 151.4, 147.3, 144.5, 143.9, 143.8, 140.8, 137.2, 135.4, 134.8, 132.5, 131.6, 131.6, 131.0, 127.2, 123.7, 122.2, 122.1, 119.3, 118.5, 96.0 (d, *J* = 6.3 Hz), 9.3. IR (CH_2Cl_2): ν 2914, 1602, 1561, 1473, 1412, 1387, 1355, 1260, 1223, 1156, 1114, 1077, 1048, 1025, 981, 912, 781, 762, 745, 715 cm^{-1}. HRMS (ESI): *m/z* calcd for $C_{36}H_{32}BF_2N_3Rh$ [M - Cl] 658.1712, found 658.1722.

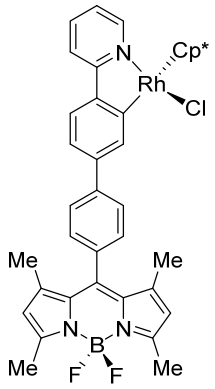

Complex **9d:** BODIPY **7d** (30 mg, 63 μmol) was added to a solution of $[RhCp^*Cl_2]_2$ (19.2 mg, 31 μmol) and NaOAc (12.1 mg, 148 μmol) in 3.1 mL of CH_2Cl_2. The reaction mixture was stirred at room temperature for 16 h. The reaction mixture was filtered through a short pad of Celite and the solvent was removed under reduced pressure to yield complex **9d** as an orange solid (46 mg, 97%). ^{1}H NMR (300 MHz, ppm): δ 8.78 (d, *J* = 5.5 Hz, 1H), 8.16 (d, *J* = 1.6 Hz, 1H), 7.87-7.70 (m, 5H), 7.42-7.35 (m, 3H), 7.13 (ddd, *J* = 7.3 Hz, *J* = 5.4 Hz, *J* = 1.5 Hz, 1H), 6.01 (s, 2H), 2.59 (s, 6H), 1.70 (s, 15H), 1.50 (s, 6H). ^{13}C NMR (75 MHz, ppm): δ 179.0 (d, *J* = 32.9 Hz), 164.9, 155.4, 151.4, 143.6, 143.3, 142.4, 141.7, 141.1, 137.1, 135.1, 133.7, 131.5, 128.3, 127.7, 123.6, 122.1, 122.0, 121.2, 119.3, 96.1 (d, *J* = 6.3 Hz), 14.7, 14.6, 9.3. IR (CH_2Cl_2): ν 2961, 2922, 2856, 1603, 1582, 1544, 1510, 1471, 1437, 1410, 1372, 1306, 1262, 1195, 1157, 1121, 1085, 1053, 1025, 983, 820, 783, 766, 732, 712 cm^{-1}. HRMS (ESI): *m/z* calcd for $C_{40}H_{40}BF_2N_3Rh$ [M - Cl] 714.2338, found 714.2335.

VI.6. References

(1) Treibs, A.; Kreuzer, F.-H. *Justus Liebigs Ann. Chem.* **1968**, *718*, 208.

(2) Selected recent reviews: (a) Boens, N.; Leen, V.; Dehaen, W. *Chem. Soc. Rev.* **2012**, *41*, 1130. (b) Kamkaew, A.; Lim, S. H.; Lee, H. B.; Kiew, L. V.; Chung, L. Y.; Burgess, K. *Chem. Soc. Rev.* **2013**, *42*, 77. (c) Laudet, A.; Burgess, K. *Chem. Rev.* **2007**, *107*, 4891. (d) Shing, S. P.; Gayathri, T. *Eur. J. Org. Chem.* **2014**, 4689. (e) Frath, D.; Massue, J.; Ulrich, G.; Ziessel, R. *Angew. Chem., Int. Ed.* **2014**, *53*, 2290.

(3) Recent Examples: (a) Li, M.; Yao, Y.; Ding, J.; Liu, L.; Qin, J.; Zhao, Y.; Hou, H.; Fan, Y. *Inorg. Chem.* **2015**, *54*, 1346. (b) Chu, G. M.; Guerrero-Martínez, A.; Fernández, I.; Sierra, *Chem.* M. A. *Eur. J.* **2014**, *20*, 1367. (c) Bartelmess, J.; Francis, A. J.; Roz, K. A. E.; Castellano, F. N.; Weare, W. W.; Sommer, R. D. *Inorg. Chem.* **2014**, *53*, 4527. (d) Shi, W.-J.; Menting, R.; Ermilov, E. A.; Lo, P.-C.; Röder, B.; Ng, D. K. P. *Chem. Commun.* **2013**, *49*, 5277. (e) Sun, J.; Zhong, F.; Yi, X.; Zhao, J. *Inorg. Chem.* **2013**, *52*, 6299. (f) Whited, M. T.; Djurovich, P. I.; Roberts, S. T.; Durrell, A. C.; Schlenker, C. W.; Bradforth, S. E.; Thompson, M. E. *J. Am. Chem. Soc.* **2011**, *133*, 88. (g) Sozmen, F.; Oksal, B. S.; Bozdemir, O. A.; Buyukcakir, O.; Akkaya, E. U. *Org. Lett.* **2012**, *14*, 5286. (h) Bartelmess, J.; Weare, W. W.; Sommer, R. D. *Dalton Trans.* **2013**, *42*, 14883. (i) Rosenthal, J.; Lippard, S. J. *J. Am. Chem. Soc.* **2010**, *132*, 5536.

(4) Selected reviews: (a) Albrecht, M. *Chem. Rev.* **2010**, *110*, 576. (b) Lyons, T. W.; Sanford, M. S. *Chem. Rev.* **2010**, *110*, 1147. (c) Ackermann, L.; Vicente, R.; Kapdi, A. R. *Angew. Chem., Int. Ed.* **2009**, *48*, 9792. (d) Chen, X.; Engle, K. M.; Wang, D.-H.; Yu, J.-Q. *Angew. Chem., Int. Ed.* **2009**, *48*, 5094. (e) Daugulis, O.; Do, H.-Q.; Shabashov, D. *Acc. Chem. Res.* **2009**, *42*, 1074. (f) Lewis, J. C.; Bergman, R. G.; Ellman, J. A. *Acc. Chem. Res.* **2008**, *41*, 1013. (g) Alberico, D.; Scott, M. E.; Lautens, M. *Chem. Rev.* **2007**, *107*, 174. See also the special issue on "CH functionalization" in *Acc. Chem. Res.* **2012**, 45 (Eds.: Doyle, M. P. and Goldberg, K. I.).

(5) The C–H activation/cyclometallation sequence occurs with good performance even in challenging substrates. Examples from these laboratories: Nucleosides and nucleotides: (a) Martín-Ortiz, M.; Gómez-Gallego, M.; Ramírez de Arellano, C.; Sierra, M. A. *Chem. Eur. J.* **2012**, *18*, 12603. (b) Valencia, M.; Martín-Ortiz, M.; Gómez-Gallego, M.; Ramírez de Arellano, C.; Sierra, M. A. *Chem. Eur. J.* **2014**, *20*, 3831. β−Lactams: (c) Muntaner, J. G.; Casarrubios, L.; Sierra, M. A. *Org. Biomol. Chem.* **2014**, *11*, 286. (d) Casarrubios, L.; Esteruelas, M. A.; Larramona, C.; Muntaner, J. G.; Oliván, M.; Oñate, E.; Sierra, M. A. *Organometallics* **2014**, *33*, 1820.

(6) CCDC-1045717 and CCDC-1045718 contain the supplementary crystallographic data for compounds **8b** and **9d**, respectively (www.ccdc.cam.ac.uk/data_request/cif).

(7) Kee, H. L.; Kirmaier, C.; Yu, L.; Thamyongkit, P.; Youngblood, W. J.; Calder, M. E.; Ramos, L.; Noll, B. C.; Bocian, D. F.; Scheidt, W. R.; Birge, R. R.; Lindsey, J. S.; Holten, D. *J. Phys. Chem. B* **2005**, *109*, 20433.

(8) Hedley, G. J.; Ruseckas, A.; Harriman, A.; Samuel, I. D. W. *Angew. Chem., Int. Ed.* **2011**, *50*, 6634.

(9) All calculations have been carried out at the B3LYP/def2-SVP level. See Computational Details in the supplementary material.

(10) Ling, L.; Brennessel, W. W.; Jones, W. D. *J. Am. Chem. Soc.* **2008**, *130*, 12414.

(11) Despite that, the slight overlap due to the absorption tail of the iridium complex may also influence the emission properties of the dyads.

(12) Hammes-Schiffer, S. *J. Am. Chem. Soc.* **2015**, *137*, 8860 and the pertinent references therein.

(13) For related PET mechanisms involving BODIPY derivatives, see, for instance: (a) Turfan, B.; Akkaya, E. U. *Org. Lett.* **2002**, *4*, 2857. (b) Chen, Y.; Wang, H.; Wan, L.; Bian, Y.; Jiang, J. *J. Org. Chem.* **2011**, *76*, 3774.

(14) For related intramolecular energy and charge transfer in other BODIPY compounds, see: (a) D'Souza, F.; Smith, P. M.; Zandler, M. E.; McCarty, A. L.; Itou, M.; Araki, Y.; Ito, O. *J. Am. Chem. Soc.* **2004**, *126*, 7898. (b) Lazarides, T.; McCormick, T. M.; Wilson, K. C.; Lee, S.; McCamant, D. W.; Eisenberg, R. *J. Am. Chem. Soc.* **2010**, *133*, 350. (c) Khan, T. K.; Ravikanth, M. *Tetrahedron* **2012**, *68*, 830. (d) Brizet, B.; Eggenspiller, A.; Gros, C. P.; Barbem, J.-M.; Goze, C.; Denat, F.; Harvey, P. D. *J. Org. Chem.* **2012**, *77*, 3646.

(15) Tang, J.-H.; Wu, S.-H.; Shao, J.-Y.; Nie, H.-J.; Zhong, Y.-W. *Organometallics* **2013**, *32*, 4564.

(16) Vandromme, L.; Reißig, H.-U.; Gröper, S.; Rabe, J. P. *Eur. J. Org. Chem.* **2008**, *12*, 2049.

(17) Demas, J. N.; Crosby, G. A. *J. Phys. Chem.* **1971**, *75*, 991.

(18) Brannon, J. H.; Magde, D. *J. Phys. Chem.* **1978**, *82*, 705.

(19) Singh, K.; Sharma, S.; Sharma, A. *J. Mol. Catal. A Chem.* **2011**, *347*, 34.

(20) Compound **6d** easily oxidized in the conditions of HRMS-Spectra measurement with the concomitant loss of 2H.

VII. *CAPÍTULO 5*

VII.1. *Control over the E/Z Selectivity of the Catalytic Dimerization of Group 6 (Fischer) Metal Carbene Complexes*

Abstract: The systematic investigation of the effect of different catalysts and additives in the reaction of self-dimerization of alkoxychromium(0) (Fischer) carbene complexes resulted in the selection of $Pd(P^tBu_3)_2$ *to effect this transformation with good to excellent E selectivities and acceptable to excellent chemical yields. This catalyst will allow the control of the geometry in the synthesis of polyconjugated olefins, one emerging application of these catalytic reactions.*

J. Org. Chem. **2013,** *78,* 865.

VII.2. Introduction

Transmetalation processes from group 6 Fischer metal carbene complexes to late transition metals (Pd, Pt, Cu, Ni, Rh, Au, etc.) lead to new carbene complexes, exhibiting exceedingly different chemical behavior with respect to the starting metal complex.[1] Thus, the new carbene complexes may show an enhanced reactivity compared to the precursor complex[2] or they may undergo different reaction pathways, opening doors to the synthesis of new classes of compounds (Scheme 1). This fascinating process has been profusely exploited since our original report on the self-dimerization of chromium(0) and tungsten(0) carbene complexes promoted by Pd catalysts.[3]

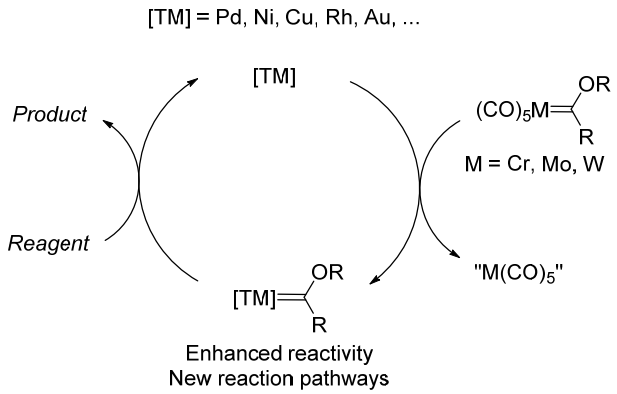

Scheme 1. Effect of transmetalation in the reactivity of group 6 metal carbene complexes.

The reaction mechanism for this transformation, which has been proposed on the basis of experimental and theoretical studies,[3,4] is summarized in Scheme 2. Accordingly, a transmetalation reaction of the carbene ligand from complex **1** to the palladium(0) catalyst leads to a new Pd−carbene complex such as **3**, through a heterobimetallic intermediate **2** that evolves to **3** by extrusion of the $[M(CO)_5]$ (M = Cr, W) fragment, mediated by coordination of the solvent. Subsequent transmetalation from a new molecule of the carbene complex **1** leads to the Pd(0) bis-carbene complex **4**, which produces a mixture of the *E/Z* olefins **5** with concomitant regeneration of the catalyst.

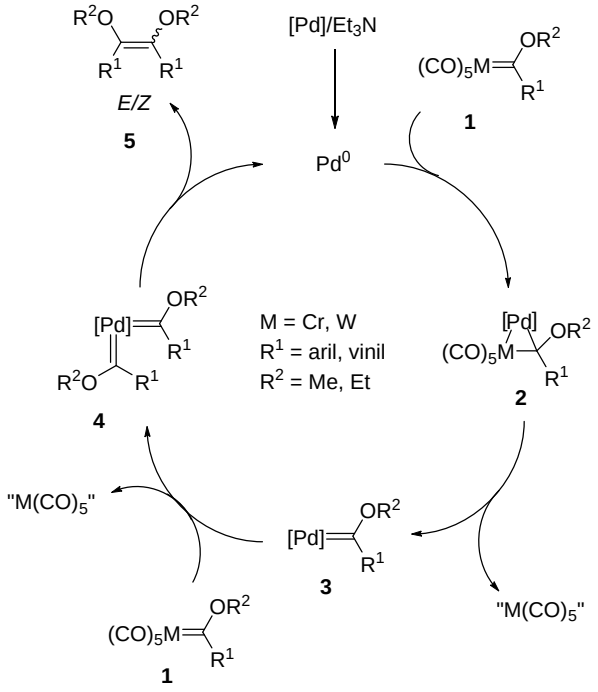

Scheme 2. Catalytic cycle for the self-dimerization of group 6 carbene (Fischer) complexes in the presence of Pd catalysts.

The key intermediates in this catalytic cycle are the monocarbene complexes **3** and bis-carbene complexes **4**. Very recently,[5] Albéniz and Espinet isolated the first Pd alkoxycarbene **7** from the reaction of the W(0) Fischer carbene complex **6** and $[PdCl_2(NCMe)_2]$.[6] In addition, related Cu(I)[7] or Au(I)[8] mono-carbene complexes have been isolated and fully characterized in similar transformations. Moreover, the reaction of β-arylamino-substituted chromium(0) and tungsten(0) carbene complexes **8** with Pd reagents leads to the mononuclear Pd bis-carbene complexes **9**,[9] the putative second key intermediates shown in Scheme 2 (Scheme 3).

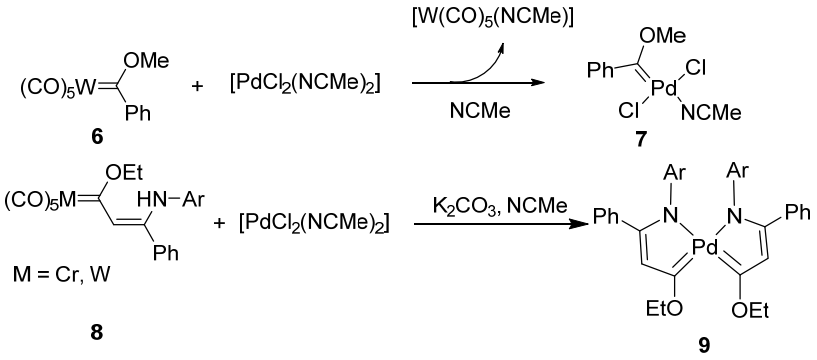

Scheme 3. Examples of isolation of mono- and bis-carbene Pd complexes by transmetalation of group 6 Fischer carbene complexes.

The main shortcoming of the catalytic self-dimerization of group 6 metal carbene complexes is the lack of *E/Z* selectivity. This is highly important due to the emerging applications of this process toward the synthesis of polyconjugated olefins,[10] some of which have been patented as conjugated polymers and devices.[11] Therefore, the control of the *E/Z* selectivity is required for this method to become of full utility in synthesis. Reported herein is a study to accomplish this challenging goal.

VII.3. Results and Discussion

According to the previously reported experimental and computational studies of the transmetalation process (see above) and to the plethora of literature on the influence of ligands in the outcome of Pd-catalyzed reactions,[12] we hypothesized that the ligand directly attached to the catalyst may play a fundamental role in the *E/Z* selectivity of the self-dimerization reactions of group 6 metal (Fischer) carbenes. Thus, series of phosphines differing in their steric volume were initially tested against the self-dimerization of complex **10** (Scheme 4, Table 1) using $PdCl_2(MeCN)_2$ as the catalyst. The *E/Z* ratio of olefins **11** in the absence of an external added phosphine was 1/1.3 in THF and was nearly independent of the reaction solvent (1/1.2 in MeCN, entries 1 and 2 in Table 1). Addition of the bulky P^tBu_3 results in a small decrease of the selectivity (1/1.1, entry 3), while the best selectivities were observed for PPh_3 (1/4.4) and PMe_3 (1/2.4), both showing a moderate selectivity. It is noteworthy that in all cases the reaction was *Z* selective. Other sources of Pd were tested against the addition of P^tBu_3. The use of $Pd(OAc)_2$ proportionates a selectivity of 1/3.5, slightly increased from that obtained without additive (1/2),[3,4] while $[Pd(allyl)Cl]_2$ gave essentially the same selectivity as $PdCl_2(MeCN)_2$.

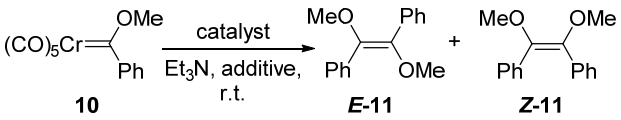

Scheme 4. Self-dimerization of carbene complex **10**.

Table 1. Self-dimerization reactions of complex **10** in the presence of phosphines and phosphites.

Entry	Catalyst[a]	Solvent	Additive[b]	*E/Z*[c]
1	$PdCl_2(MeCN)_2$	THF	none	1/1.3
2	$PdCl_2(MeCN)_2$	MeCN	none	1/1.2
3	$PdCl_2(MeCN)_2$	MeCN	P^tBu_3	1/1.1
4	$PdCl_2(MeCN)_2$	MeCN	PPh_3	1/4.4
5	$PdCl_2(MeCN)_2$	MeCN	PMe_3	1/2.4
6	$Pd(OAc)_2$	MeCN	none	1/2[3b]
7	$Pd(OAc)_2$	MeCN	P^tBu_3	1/3.5
8	$[Pd(allyl)Cl]_2$	MeCN	none	1/1.5
9	$[Pd(allyl)Cl]_2$	MeCN	P^tBu_3	1/1
10	$PdCl_2(MeCN)_2$	MeCN	$P(OMe)_3$	1/1.5
11	$PdCl_2(MeCN)_2$	MeCN	$P(OEt)_3$	1/1.3
12	$Pd(OAc)_2$	MeCN	$P(OMe)_3$	1/3.2

[a] 5% of catalyst was used in all cases. [b] Et_3N (1 mmol/mmol carbene was used in all cases as co-additive). [c] Determined by integration of the ^1H NMR signals corresponding to MeO-groups in the reaction mixtures. 3.61 ppm for *Z* isomer and 3.42 ppm for *E* isomer.[13a]

The use of phosphites follows the same pattern as that observed for phosphines. Thus, while no changes were observed in the selectivity of the reactions using $PdCl_2(MeCN)_2$ (entries 10 and 11), increased *Z* selectivity was observed when $Pd(OAc)_2$was the catalyst (entry 12, Table 1).

N-heterocyclic carbene (NHC) species **12**–**15** (Figure 1) were also tested as additives in the reaction of self-dimerization of carbene complex **10**. However, additives **12**–**14** did not produce changes in the *E/Z* selectivities of the reaction that were equal to those obtained in the absence of additive (*E/Z* = 1/1.3), while NHC **15** proportionates a slight increase in selectivity (*E/Z* = 1/1.5).

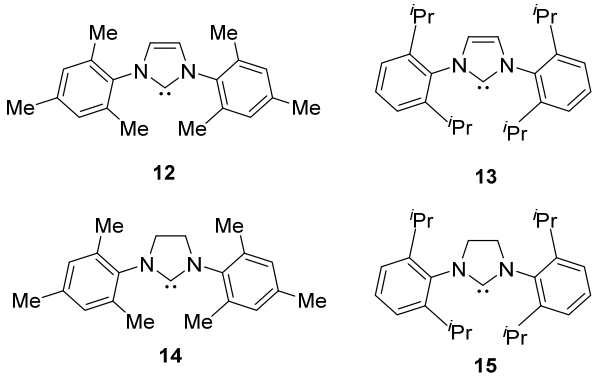

Figure 1. NHC additives used in this work.

The self-dimerization reactions of pentacarbonyl-[ethoxyphenylcarbene] chromium(0) **16** were examined next (Scheme 5) to determine the effect of the substituent at the oxygen atom attached to the carbene carbon atom on the *E/Z* selectivity of the corresponding olefins **17**. The results are collected in Table 2.

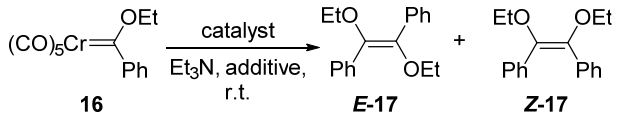

Scheme 5. Self-dimerization of ethoxycarbene complex **16**.

Table 2. Self-dimerization reactions of complex **16** in the presence of phosphines and phosphites.

Entry	Catalyst[a]	Solvent	Additive[b]	*E/Z*[c]
1	$PdCl_2(MeCN)_2$	MeCN	none	1.2/1
2	$PdCl_2(MeCN)_2$	MeCN	P^tBu_3	9.4/1
3	$PdCl_2(MeCN)_2$	MeCN	PMe_3	1/1.4
4	$Pd(OAc)_2$	MeCN	none	1/1.7
5	$Pd(OAc)_2$	MeCN	P^tBu_3	7/1
6	$[Pd(allyl)Cl]_2$	MeCN	none	1/1.3
7	$[Pd(allyl)Cl]_2$	MeCN	P^tBu_3	2.7/1
8	$Pd_2(dba)_3$	MeCN	none	1/2.4
9	$Pd_2(dba)_3$	MeCN	P^tBu_3	1.7/1
10	$Pd(dba)_2$	MeCN	none	1/2.8
11	$Pd(dba)_2$	MeCN	P^tBu_3	1/1.7
12	$Pd(OAc)_2$	MeCN	$P(OMe)_3$	1/1.8
13	$PdCl_2(MeCN)_2$	MeCN	$P(OEt)_3$	1/1.1
14	$PdCl_2(MeCN)_2$	MeCN	$P(OMe)_3$	1/1.3
15	$[Pd(allyl)Cl]_2$	MeCN	PPh_3	1/1.1
16	$[Pd(allyl)Cl]_2$	MeCN	$AsPh_3$	1/1.7
17	$[Pd(allyl)Cl]_2$	MeCN	$BiPh_3$	1/1.1

[a] 5% of catalyst was used in all cases. [b] Et_3N (1 mmol/mmol carbene was used in all cases as co-additive). [c] Determined by integration of the ^1H NMR signals corresponding to CH_2O-groups in the reaction mixtures. 3.80 ppm for *Z*-isomer and 3.57 ppm for *E* isomer.[13b]

The results in Table 2 show a different trend than that obtained for complex **10**. In the absence of additives, the use of $PdCl_2(MeCN)_2$ as the catalyst affords the *E* isomer as the major isomer (although still close to an equimolar ratio). Strikingly, addition of P^tBu_3 resulted in an excellent increase in the *E* selectivity for $Pd(OAc)_2$ and $PdCl_2(MeCN)_2$ catalysts (up to 9.4/1 when the latter catalyst was used). The use

$[Pd(allyl)Cl]_2$ leads to poorer but still noticeable *E* selectivities (*E/Z* = 2.7/1). Other additives (phosphites, PPh_3, $AsPh_3$,$BiPh_3$)[3] give selectivities close to 1/1. In contrast to complex **10**, the use of NHCs carbenes **12**–**15** (Figure 1) in the self-dimerization reaction proportionates low, albeit noticeable, changes in selectivities. Thus, NHC **12** was nearly unselective (*E/Z* = 1/1.1), NHCs **14** and **15** were slightly *Z* selective (*E/Z* = 1/1.4 and 1/1.3, respectively), and NHC **13** was slightly *E* selective (*E/Z* = 1.3/1).

The use of Pd(0) catalysts having monodentate phosphine ($PdCl_2(PPh_3)_2$, $Pd(PPh_3)_4$, and $Pd(P^tBu_3)_2$) and bidentate diphosphine ligands ($Pd(dppe)_2$) was studied next (the combination of $PdCl_2(PPh_3)_2/P^tBu_3$ as the additive was also tested for comparison reasons). The results of these reactions with complexes **10** and **16** are collected in Table 3. For both complexes, the best results were obtained with $Pd(P^tBu_3)_2$ (which affords a remarkable 15.7/1 *E/Z* selectivity for carbene complex **16**). The use of $Pd(PPh_3)_4$ led also to an increased selectivity, but now favoring the *Z* isomer. $Pd(dppe)_2$ catalyst produces good *E* selectivities (5.7/1) with carbene complex **10** while the selectivity decreases and inverts for complex **16** (1/2.2). The use of $PdCl_2(PPh_3)_2$ with added P^tBu_3 reversed the selectivity observed in the absence of the additive (1/1.2 vs 2.4/1), but the *E* selectivity is considerably lower than that obtained with $Pd(P^tBu_3)_2$.

Table 3. Self-dimerization reactions of complex **10** and **16** in the presence of catalysts incorporating phosphine ligands.

Entry	Catalyst[a]	Complex	Additive[b]	*E/Z*[c]
1	$Pd(PPh_3)_4$	**10**	none	1/4.1
2	$PdCl_2(PPh_3)_2$	**10**	none	1/1.8
3	$Pd(P^tBu_3)_2$	**10**	none	9.4/1
4	$Pd(dppe)_2$	**10**	none	5.7/1
5	$Pd(PPh_3)_4$	**16**	none	1/2.6
6	$PdCl_2(PPh_3)_2$	**16**	none	1/1.2
7	$PdCl_2(PPh_3)_2$	**16**	P^tBu_3	2.4/1
8	$Pd(P^tBu_3)_2$	**16**	none	15.7/1
9	$Pd(dppe)_2$	**16**	none	1/2.2

[a] 5% of catalyst was used in all cases. [b] Et_3N (1 mmol/mmol carbene was used in all cases as co-additive, except for Pd (0) catalysts). [c] Determined by integration of the ^1H NMR signals in the reaction mixtures.

Results in Tables 1–3 pointed to P^tBu_3 (as additive or directly as $Pd(P^tBu_3)_2$) and the use of an ethoxy carbene instead of a methoxy carbene complex as the optimum combination for obtaining high *E* selectivities. The influence of the amount of the $Pd(P^tBu_3)_2$ catalyst in the *E/Z* selectivity was tested next in the self-dimerization of complex **16** (Table 4). The selectivity is maintained using higher loads of catalyst (up to 20%), while it steadily decreases with lower catalyst loads (reaching 1/1 ratio for catalyst loads of 1%). Therefore, the optimum balance of catalyst load/selectivity was 5% mol of catalyst/mol of carbene complex.

Table 4. Self-dimerization reactions of complex **16** in the presence of different amounts of $Pd(P^tBu_3)_2$

Entry	Cat. load (%)[a]	*E/Z*[b]
1	20	13.6/1
2	10	14.0/1
3	5	15.7/1
4	2.5	4.6/1
5	1	1.6/1
6	0.5	1/1

[a] Referenced to carbene complex. [b] Determined by integration of the ^{1}H NMR signals in the reaction mixtures.

To test these conclusions, different ethoxychromium(0) complexes **18**–**25** were reacted with $PdCl_2(MeCN)_2$ in the absence of additives or in the presence of 5% of P^tBu_3 (Table 5). From the data in Table 4, it becomes obvious that the trend observed in Tables 2 and 3 also holds in complexes **18**–**22**, with the *E* isomer formation being the main reaction product in the presence of P^tBu_3 (the exception is complex **23**, forming a 1/2.2 *E/Z* mixture). To demonstrate the ability of $Pd(P^tBu_3)_2$ as catalyst for the selective preparation of *E* olefins, the self-dimerization reaction was conducted in a preparative scale using $Pd(P^tBu_3)_2$ as the catalyst (Scheme 6). While yields were usually acceptable (complexes **16**, **19**–**21**, and **23**–**25**) in some cases (complexes **18** and **22**) the corresponding olefins were obtained together with variable amounts of the corresponding esters due to oxidation of the starting materials[14] (probably as a consequence of the instability of the intermediate Pd mono- or bis-carbene complexes having bulky phosphine ligands). Despite that, it is clear in all cases that the use of $Pd(P^tBu_3)_2$ leads to the favored formation of the corresponding *E* olefin.

Table 4. Catalytic self-dimerization reactions of Fischer carbene complexes **18-23**.

Entry	Catalyst[a]	Complex	Additive[b]	*E/Z*[c]
1	$PdCl_2(MeCN)_2$	**18**	none	1/1
2	$PdCl_2(MeCN)_2$	**18**	P^tBu_3	5.8/1
3	$Pd(P^tBu_3)_2$	**18**	none	6.8/1
4	$PdCl_2(MeCN)_2$	**19**	none	1/1.1
5	$PdCl_2(MeCN)_2$	**19**	P^tBu_3	6/1
6	$Pd(P^tBu_3)_2$	**19**	none	8.1/1
7	$PdCl_2(MeCN)_2$	**20**	none	1.5/1
8	$PdCl_2(MeCN)_2$	**20**	P^tBu_3	1.5/1
9	$Pd(P^tBu_3)_2$	**20**	none	11/1
10	$PdCl_2(MeCN)_2$	**21**	none	1/1.5
11	$PdCl_2(MeCN)_2$	**21**	P^tBu_3	7.6/1
12	$Pd(P^tBu_3)_2$	**21**	none	10.8/1
13	$PdCl_2(MeCN)_2$	**22**	none	1/1.4
14	$PdCl_2(MeCN)_2$	**22**	P^tBu_3	1.7/1
15	$Pd(P^tBu_3)_2$	**22**	none	2.2/1
16	$PdCl_2(CH_3CN)_2$	**23**	none	1/2.5
17	$PdCl_2(CH_3CN)_2$	**23**	P^tBu_3	1/2.2
18	$Pd(P^tBu_3)_2$	**23**	none	6/1

[a] 5% of catalyst was used in all cases. [b] Et_3N (1 mmol/mmol carbene was used in all cases as co-additive, except for $Pd(P^tBu_3)_2$ catalyst). [c] Determined by integration of the ^1H NMR signals corresponding to CH_2O-groups in the reaction mixtures.

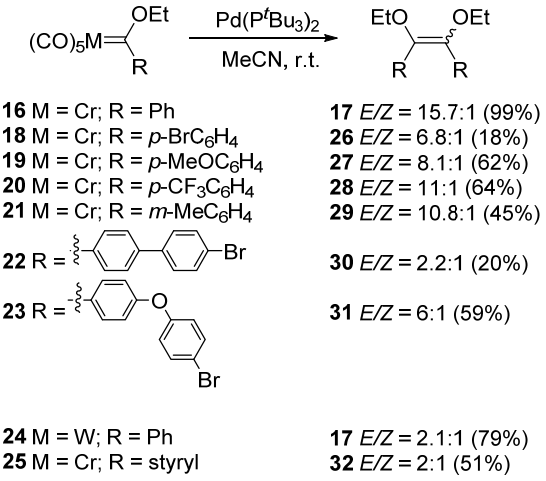

Scheme 6. The self-dimerization of complexes **16**, **18**-**25** catalyzed by $Pd(P^tBu_3)_2$.

Finally, pentacarbonyl[(benzyloxy)(methyl)carbene]-chromium(0) (**33**) was reacted in the presence of $Pd(P^tBu_3)_2$ (5%) under the usual reaction conditions. The self-dimerization product **34** was obtained in a 70% yield as a 1/1.6 *E/Z* mixture (Scheme 7). Although the selectivity of the reaction was low, it is worth noting that

while complex **33** is prone to experience β-elimination processes to yield enol ether **35** in the presence of several Pd(0) catalysts,[3b] $Pd(P^tBu_3)_2$ behaves in this case as $Pd(PPh_3)_4$, which gave **34** as a 1/1.1 *E/Z* mixture in 87% yield.[3b]

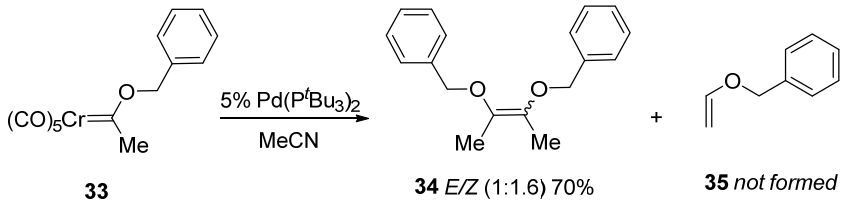

33 **34** *E/Z* (1:1.6) 70% **35** *not formed*

Scheme 7. Self-dimerization of the aliphatic carbene complex **33**.

VII.4. Conclusions

From the systematic investigation of the effects of different catalysts and additives in the reaction of self-dimerization of alkoxychromium(0) (Fischer) carbene complexes, it can be concluded that the *E/Z* selectivity of the process can be indeed controlled with the proper selection of these variables. Thus, the use of $Pd(P^tBu_3)_2$ and chromium(0) ethoxycarbene complexes is recommended in order to obtain good to excellent *E* selectivities and acceptable to excellent chemical yields in most cases. This catalyst will allow the control of the geometry in the synthesis of polyconjugated olefins, one of the main emerging applications of these reactions.

VII.5. Experimental Section

General Procedures. All reactions were carried out under argon atmosphere. All solvents used in this work were purified by distillation and were freshly distilled immediately before use. Acetonitrile (MeCN) and triethylamine (Et_3N) were distilled from calcium hydride, whereas tetrahydrofuran (THF) and diethylether (Et_2O) were purified using a Pure Solv PS-MD-5 system. Flame-dried glassware was used for moisture-sensitive reactions. Silica gel (Merck: 230-400 mesh) was used as stationary phase for purification of crude reaction mixtures by flash column chromatography. Identification of products was made by thin-layer chromatography (Kieselgel 60F-254). UV light (λ 254nm) and 5% phosphomolybdic acid solution in 95% EtOH were used to develop the plates. NMR spectra were recorded at 25 °C in $CDCl_3$, on 300 (300 MHz for ^1H and 75 MHz for ^{13}C) spectrometers. Chemical shifts are given in ppm relative to $CDCl_3$ (^1H, 7.27 ppm and ^{13}C, 77.0 ppm). IR spectra were taken on a MIR (8000−400 cm^{-1}) spectrometer as solid films by slow evaporation of the solvent using the ATR (attenuated total reflectance) technique. MS spectra (HRMS) were acquired on a QTOF: HP-1200 (Agilent Technologies) mass spectrometer.

All commercially available products were used without further purification. The following metal-carbenes were prepared according to previously described methods: pentacarbonyl[(methoxy)(phenyl)carbene]chromium(0),[14] pentacarbonyl[(ethoxy)(phenyl)carbene]chromium(0),[15] pentacarbonyl[(*p*-bromophenyl)(ethoxy)carbene]chromium(0),[16] pentacarbonyl[(*p*-methoxyphenyl)-(ethoxy)carbene]chromium(0),[17] pentacarbonyl[(*m*-tolyl)(ethoxy)carbene]-chromium(0),[18] pentacarbonyl[(ethoxy)(phenyl)carbene]tungsten(0),[19] pentacarbonyl[(2*E*)-1-ethoxy-3-phenyl-2-propen-1-ylidene]chromium(0),[20] pentacarbonyl[(benciloxy)(methyl)carbene]chromium(0).[21]

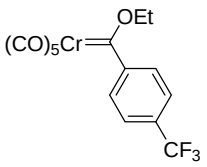

Pentacarbonyl[(*p*-trifluoromethylphenyl)(ethoxy)carbene] chromium (0) (**20**). To a solution of 1-bromo-4-(trifluoromethyl)benzene (0.77 g, 3.42 mmol) in 4 mL of dry Et_2O was added 2.1 mL (3.42 mmol) of *n*-BuLi (1.6 M in hexanes) at -78 °C. After stirring for 30 min, the solution was transferred via cannula at 0 °C to a suspension of $Cr(CO)_6$ (0.75 g, 3.42 mmol) in 8 mL of Et_2O at rt. The mixture was refluxed for 3 h, the solvent was removed under reduced pressure and the residue was dissolved in 6.3 mL of degassed water. Et_3OBF_4 (1.13g, 5.95 mmol) was added slowly to the solution at 0 °C and stirred for 10 min. The mixture was extracted with EtOAc and dried over $MgSO_4$. The solvent was removed in vacuo. The crude product was purified by flash chromatography (hexane) to yield 0.8 g (59%) of a dark red solid; mp 46-48 °C. ^1H NMR (300 MHz, ppm): δ 7.69 (d, *J* = 7.6 Hz, 2H), 7.26 (d, *J* = 7.6 Hz, 2H), 4.98 (br s, 2H), 1.69 (t, *J* = 6.7 Hz, 3H). ^{13}C NMR (75 MHz, ppm): δ 348.4, 223.8, 215.7, 156.3, 131.2, 130.0, 125.4, 122.1, 77.5, 15.1. IR (ATR): ν 2064, 1928 cm^{-1}. HRMS (ESI): *m/z* calcd for $C_{15}H_9CrF_3O_6$ $[M + H]^+$ 394.9840, found 394.9850.

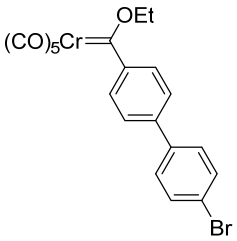

Pentacarbonyl[(*p*-(*p*-bromophenyl)phenyl)(ethoxy)carbene] chromium (0) (22). To a solution of 4,4'-dibromobiphenyl (1.42 g, 4.54 mmol) in 5.4 mL of dry Et_2O was added 2.8 mL (4.54 mmol) of *n*-BuLi (1.6 M in hexanes) at -78 °C. After stirring for 30 min, the solution was transferred via cannula at 0 °C to a suspension of $Cr(CO)_6$ (1 g, 4.54 mmol) in 2.7 mL of Et_2O at rt. The mixture was refluxed for 3 h, the solvent was removed under reduced pressure and the residue was dissolved in 5.4 mL of degassed water. Et_3OBF_4 (1.47g, 7.72 mmol) was added slowly to the solution at 0 °C and stirred for 10 min. The mixture was extracted with EtOAc and dried over $MgSO_4$. The solvent was removed in vacuo. The crude product was purified by flash chromatography (hexane) to yield 570 mg (26%) of a dark red solid; mp 108-110 °C. ^{1}H NMR (300 MHz, ppm): δ 7.68-7.41 (m, 8H), 5.07 (q, *J* = 7.1 Hz, 2H), 1.72 (t, *J* = 7.1 Hz, 3H). ^{13}C NMR (75 MHz, ppm): δ 346.5, 224.0, 216.3, 152.5, 141.9, 138.6, 132.0, 128.6, 126.5, 124.5, 122.4, 77.2, 15.2. IR (ATR): ν 2064, 1928 cm^{-1}. HRMS (ESI): *m/z* calcd for $C_{20}H_{13}BrCrO_6$ $[M + H]^+$ 480.9384, found 480.9386.

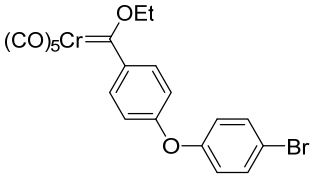

Pentacarbonyl[(*p*-bromophenoxyphenyl)(ethoxy) carbene] chromium(0) (23). To a solution of bis-(4-bromophenyl)-ether (1.49 g, 4.54 mmol) in 5.4 mL of dry Et_2O was added 2.8 mL (4.54 mmol) of *n*-BuLi (1.6 M in hexanes) at -78 °C. After stirring for 30 min, the solution was transferred via cannula at 0 °C to a suspension of $Cr(CO)_6$ (1 g, 4.54 mmol) in 2.7 mL of Et_2O at rt. The mixture was refluxed for 3 h, the solvent was removed under reduced pressure and the residue was dissolved in 5.4 mL of degassed water. Et_3OBF_4 (1.47 g, 7.72 mmol) was added slowly to the solution at 0 °C and stirred for 10 min. The mixture was extracted with EtOAc and dried over $MgSO_4$. The solvent was removed in vacuo. The crude product was purified by flash chromatography (hexane) to yield 1.1 g (47%) of a dark red solid; mp 84-86 °C. ^{1}H NMR (300 MHz, ppm): δ 7.59 (d, *J* = 8.8 Hz, 2H), 7.51 (d, *J* = 8.8 Hz, 2H), 7.00-6.95 (m, 4H) 5.14 (q, *J* = 7.1 Hz, 2H), 1.72 (t, *J* = 7.1 Hz, 3H). ^{13}C NMR (75 MHz, ppm): δ 342.0, 223.8, 216.5, 160.1, 154.8, 148.4, 133.0, 128.0, 121.7, 117.2, 117.0, 77.2, 17.9. IR (ATR): ν 2059, 1926 cm^{-1}. HRMS (ESI): *m/z* calcd for $C_{20}H_{13}BrCrO_7$ $[M + H]^+$ 496.9333, found 496.9335.

General Procedure for Carbene Ligand Dimerization.

Method A. To a solution of the corresponding alkoxycarbene complex (1 mmol) in MeCN (6 mL/mmol carbene complex) were added the $PdCl_2(MeCN)_2$ catalyst (5%) and the corresponding additive (0.1 mmol) and Et_3N (1 mmol/mmol carbene complex). The reaction mixture was stirred at room temperature until total disappearance of the starting material (checked by TLC). The solvent was then removed under reduced pressure. The residue was dissolved in EtOAc, the solution was filtered through a short pad of Celite, and finally the solvent was removed again under reduced pressure. A *E/Z* isomer mixtue was obtained. The crude product was then purified by flash column chromatography (hexane/EtOAc 100/1). This method was used for characterizing both *E* and *Z* isomers.

Method B. To a solution of the corresponding alkoxycarbene complex (1 mmol) in MeCN (6 mL/mmol carbene complex) was added $Pd(P^tBu_3)_2$ (5%). The reaction mixture was stirred at room temperature until total disappearance of the starting material (checked by TLC). The solvent was then removed under reduced pressure. The residue was dissolved in EtOAc, the solution was filtered through a short pad of Celite, and finally the solvent was removed again under reduced pressure. A mixture of *E* and *Z* isomers was obtained, together with variable amounts of the corresponding ester formed either by oxidation of the starting carbene complex or by oxidation of Pd carbene intermediates.[14] The crude product was then purified by flash column chromatography (hexane/EtOAc 100/1).[23]

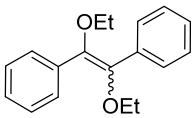

(*Z*)- and (*E*)-α,β-Diethoxystilbene (17).[13b] *Method A*. Carbene complex **16** (200 mg, 0.61 mmol), Pd catalyst (0.031 mmol) and Et_3N (91 μL, 0.61 mmol) were reacted for 3 h, to yield compound **17** as a white solid (70 mg, 82%, *E/Z* = 1.2/1). ***Z* isomer**: ^{1}H-RMN (300 MHz): δ 8.1-7.1 (m, 10H), 3.80 (q, *J* = 7.2 Hz, 4H), 1.15 (t, *J* = 7.2 Hz, 6H). ^{13}C-RMN (75 MHz): δ 144.1, 135.4, 129.8, 127.9, 127.5, 66.4, 15.2. IR (ATR): 1599, 1259 cm^{-1}. ***E* isomer**: .^{1}H-RMN (300 MHz): δ 8.1-7.1 (m, 10H), 3.57 (q, *J* = 7.1 Hz, 4H), 1.15 (t, *J* = 7.1 Hz, 6H). ^{13}C-RMN (75 MHz): δ 142.6, 134.7, 128.3, 127.8, 127.3, 65.9, 15.2. IR (ATR): 1665, 1351 cm^{-1}.

Method B. Carbene complex **16** (200 mg, 0.61 mmol) and $Pd(P^tBu_3)_2$ (16 mg, 0.03 mmol) were reacted for 7 h, to yield compound **17** as a white solid (80 mg, 99%, *E/Z* = 15.7/1).

Method B. Carbene complex **24** (50 mg, 0.11 mmol) and $Pd(P^tBu_3)_2$ (3 mg, 0.006 mmol) were reacted for 28 h, to yield compound **17** as a white solid (12 mg, 79%, *E/Z* = 2.1/1).

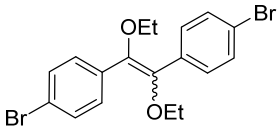

(*Z*)- and (*E*)-1,2-Bis(*p*-bromophenyl)-1,2-diethoxyethylene (26). *Method A*. Carbene complex **18** (200 mg, 0.49 mmol), Pd catalyst (0.025 mmol) and Et_3N (70 μL, 0.49 mmol) were reacted for 6 h, to yield compound **26** as a white solid (100 mg, 96%**,** *E/Z* = 1/1); mp = 77-79 °C. ***Z* isomer**: ^{1}H NMR (300 MHz): δ 7.32 (d, *J* = 8.7 Hz, 4H), 7.05 (d, *J* = 8.7 Hz, 4H), 3.77 (q, *J* = 7.0 Hz, 4H), 1.32 (t, *J* = 7.0 Hz, 6H). ^{13}C NMR (75 MHz): δ 142.1, 134.1, 131.6, 131.1, 121.5, 66.1, 15.5. IR (ATR): 1274, 1107, 1013, 820. ***E* isomer**: ^{1}H NMR (300 MHz): δ 7.65 (d, *J* = 8.7 Hz, 4H), 7.53 (d, *J* = 8.7 Hz, 4H), 3.52 (q, *J* = 7.1 Hz, 4H), 1.13 (t, *J* = 7.1 Hz, 6H). ^{13}C NMR (75 MHz): δ 143.8, 133.5, 131.2, 130.0, 121.5, 66.6, 15.3. IR (ATR): ν 1150, 1105, 1014, 834 cm^{-1}. HRMS (ESI): *m/z* calcd for $C_{18}H_{19}Br_2O_2$ $[M + H]^+$ 425.9780, found 425.9776.

Method B: Carbene complex **18** (200 mg, 0.49 mmol) and $Pd(P^tBu_3)_2$ (13 mg, 0.025 mmol) were reacted for 18 h, to yield compound **26** as a white solid (18 mg, 18%, *E/Z* = 6.8/1).

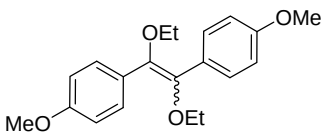

(*Z*)- and (*E*)-1,2-Diethoxy-1,2-bis(*p*-methoxyphenyl) ethylene (27). *Method A*. Carbene complex **19** (50 mg, 0.14 mmol), Pd catalyst (0.007 mmol) and Et_3N (20 μL, 0.14 mmol) were reacted for 4 h, to yield compound **27** as a pale yellow solid (20 mg, 89%, *E/Z* = 1/1.1); mp = 78-80 °C. ***Z* isomer:** ^{1}H NMR (300 MHz):

δ 7.12 (d, *J* = 8.7 Hz, 4H), 6.71 (d, *J* = 8.7 Hz, 4H), 3.77 (s, 6H), 3.76 (q, *J* = 7.0 Hz, 4H), 1.31 (t, *J* = 7.0 Hz, 6H). ***E* isomer**: ^{1}H NMR (300 MHz): δ 7.69 (d, *J* = 8.7 Hz, 4H), 6.93 (d, *J* = 8.7 Hz, 4H), 3.85 (s, 6H), 3.54 (q, *J* = 7.0 Hz, 4H), 1.14 (t, *J* = 7.0 Hz, 6H). ^{13}C NMR (75 MHz): δ 159.0, 143.6, 142.0, 132.0, 131.3, 129.9, 128.3, 113.9, 113.7, 110.0, 66.6, 66.1, 55.6, 55.5, 16.0, 15.7. IR (ATR): ν 1271, 1106, 1073, 815, 759 cm^{-1}. Exact mass data could not be collected for this compound in any of the conditions tested. The reasons for this anomalous result are not known.

Method B. Carbene complex **19** (200 mg, 0.56 mmol) and Pd(P^{t}Bu$_3$)$_2$ (7 mg, 0.014 mmol) were reacted for 18 h, to yield compound **27** as a pale yellow solid (57 mg, 62%, *E/Z* = 8.1/1).

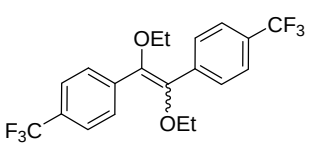

(*Z*)- and (*E*)-1,2-Diethoxy-1,2-bis(*p*-trifluoromethyl phenyl) ethylene (28). *Method A*. Carbene complex **20** (50 mg, 0.17 mmol), Pd catalyst (0.085 mmol) and Et$_3$N (24 μL, 0.17 mmol) were reacted for 2 h, to yield compound **28** as a pale yellow solid (11 mg, 33%, *E/Z* = 1.5/1); mp = 112-114 °C. ***Z* isomer**: ^{1}H NMR (300 MHz): δ 7.54 (d, *J* = 8.1 Hz, 4H), 7.29 (d, *J* = 8.1 Hz, 4H), 3.80 (q, *J* = 7.0 Hz, 4H), 1.35 (t, *J* = 7.0 Hz, 6H). ^{13}C NMR (75 MHz): δ 142.8, 138.8, 130.0, 129.9, 128.7, 125.1 (q, *J* = 3.9Hz), 66.5, 15.6. ***E* isomer**: ^{1}H NMR (300 MHz): δ 7.90 (d, *J* = 8.1 Hz, 4H), 7.67 (d, *J* = 8.1 Hz, 4H), 3.54 (q, *J* = 7.0 Hz, 4H), 1.14 (t, *J* = 7.0 Hz, 6H). ^{13}C NMR (75 MHz): δ 144.3, 137.9, 129.6 (q, *J* = 32.2 Hz), 129.5, 126.0, 125.0 (q, *J* = 3.8 Hz), 66.9, 15.2. IR (ATR): ν 1327, 1116 cm^{-1}. HRMS (ESI): *m/z* calcd for $C_{20}H_{19}F_6O_2$ $[M + H]^+$ 405.1284, found 405.1301.

Method B: Carbene complex **20** (200 mg, 0.51 mmol) and Pd(P^{t}Bu$_3$)$_2$ (13 mg, 0.026 mmol) were reacted for 24 h, to yield compound **28** as a pale yellow solid (66 mg, 64%, *E/Z* = 11/1).

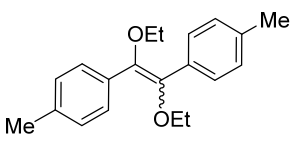

(*Z*)- and (*E*)-1,2-Diethoxy-1,2-bis(*m*-tolyl)ethylene (29). *Method A*. Carbene complex **21** (100 mg, 0.29 mmol), Pd catalyst (0.014 mmol) and Et$_3$N (40 μL, 0.29 mmol) were reacted for 16 h, to yield compound **29** as a yellow oil (40 mg, 94%, *E/Z* = 1/1.5). ***Z* isomer**: ^{1}H NMR (300 MHz): δ 7.57-6.93 (m, 16H, *Z* + *E*), 3.79 (q, *J* = 7.0 Hz, 4H), 2.23 (s, 6H), 1.33 (t, *J* = 7.0 Hz, 6H). ***E* isomer**: ^{1}H NMR (300 MHz): δ 7.56 (s, 2H), 7.53 (d, *J* = 7.8 Hz, 2H), 7.29 (dd, *J* = 7.8, 7.4 Hz, 2H), 7.11 (d, *J* = 7.4 Hz, 2H), 3.57 (q, *J* = 7.0 Hz, 4H), 2.40 (s, 6H), 1.16 (t, *J* = 7.0 Hz, 6H). ^{13}C NMR (75 MHz): δ 142.6, 137.3, 137.2, 135.3, 130.1, 130.0, 128.9, 128.2, 128.0, 127.8, 127.6, 127.0, 126.6, 125.4, 66.4, 65.8, 21.6, 21.3, 15.6, 15.2. IR (ATR): ν 1280, 1105 cm^{-1}. HRMS (ESI): *m/z* calcd for $C_{20}H_{25}O_2$ $[M + H]^+$ 297.1849, found 297.1860.

Method B: Carbene complex **21** (200 mg, 0.59 mmol) and Pd(P^{t}Bu$_3$)$_2$ (15 mg, 0.03 mmol) were reacted for 5 h, to yield compound **29** as a pale yellow oil (39 mg, 45%, *E/Z* = 10.8/1).

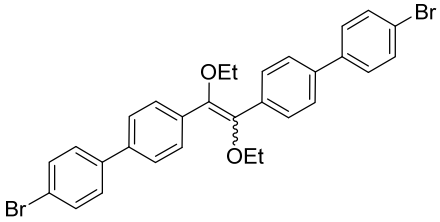

(*Z*)- and (*E*)-1,2-Bis[(*p*-bromophenyl)*p*-phenyl]-1,2-diethoxyethylene (30). *Method A*. Carbene complex **22** (100 mg, 0.21 mmol), Pd catalyst (0.011 mmol) and Et$_3$N (29 μL, 0.21 mmol) were

reacted for 16 h, to yield compound **30** as a pale yellow solid (19 mg, 32%, *E/Z* = 1/1.4); mp = 63-65 °C. ***Z* + *E* isomers:** ^{1}H NMR (300 MHz): δ 7.89-7.30 (m, 32H, *Z* + *E*) 3.88 (q, *J* = 7.0 Hz, 4H, *Z*), 3.66 (q, *J* = 7.0 Hz, 4H, *E*), 1.39 (t, *J* = 7.0 Hz, 6H, *Z*), 1.23 (t, *J* = 7.0 Hz, 6H, *E*). ^{13}C NMR (75 MHz): δ 144.4, 139.7, 138.9, 134.2, 132.1, 132.0, 131.9, 130.3, 130.0, 129.0, 128.9, 128.7, 128.6, 128.5, 126.9, 126.5, 126.4, 121.6, 66.7, 66.2, 15.7, 15.4. IR (ATR): ν 1480, 1263, 1115, 1073, 816 cm^{-1}. HRMS (ESI): *m/z* calcd for $C_{30}H_{27}Br_2O_2$ $[M + H]^+$ 579.0354, found 579.0359.

Method B: Carbene complex **22** (200 mg, 0.42 mmol) and Pd(P^{t}Bu$_3$)$_2$ (11 mg, 0.021 mmol) were reacted for 6 h, to yield compound **30** as a pale yellow solid (36 mg, 30%, *E/Z* = 2.2/1).

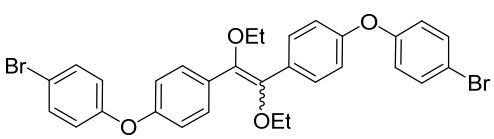

(*Z*)- and (*E*)-1,2-Bis[(*p*-bromophenyl ether)*p*-phenyl]-1,2-diethoxy ethylene (31). *Method A*. Carbene complex **23** (200 mg, 0.4 mmol), Pd catalyst (0.02 mmol) and Et_3N (56 μL, 0.4 mmol) were reacted for 16 h, to yield compound **31** as a yellow oil (33 mg, 28%, *E/Z* = 1/2.5). ***Z* isomer**: ^{1}H NMR (300 MHz): δ 7.44 (d, *J* = 8.9 Hz, 2H), 7.17 (d, *J* = 8.9 Hz, 2H), 6.88 (d, *J* = 8.9 Hz, 2H), 6.81 (d, *J* = 8.9 Hz, 2H), 3.83 (q, *J* = 7.1 Hz, 4H), 1.35 (t, *J* = 7.1 Hz, 6H). ***E* isomer**: ^{1}H NMR (300 MHz): δ 7.74 (d, *J* = 8.9 Hz, 2H), 7.47 (d, *J* = 8.9 Hz, 2H), 7.02 (d, *J* = 8.9 Hz, 2H), 6.96 (d, *J* = 8.9 Hz, 2H), 3.59 (q, *J* = 7.1 Hz, 4H), 1.18 (t, *J* = 7.1 Hz, 6H). ^{13}C NMR (75 MHz): δ 156.3, 156.1, 143.4, 133.1, 132.8, 131.7, 131.3, 130.1, 129.9, 128.8, 122.0, 120.8, 120.7, 118.9, 118.3, 118.2, 117.2, 115.9, 66.5, 66.1, 15.7, 15.3. IR (ATR): ν 1487, 1240 cm^{-1}. HRMS (ESI): *m/z* calcd for $C_{30}H_{27}O_4Br_2$ $[M + H]^+$ 609.0271, found 609.0304.

Method B. Carbene complex **23** (200 mg, 0.4 mmol) and Pd(P^{t}Bu$_3$)$_2$ (2.6 mg, 0.005 mmol) were reacted for 22 h, to yield compound **31** as a white solid (72 mg, 59%, *E/Z* = 6/1).

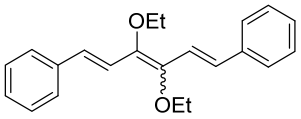

***(E,Z,E)- and (E,E,E)*-3,4-Diethoxy-1,6-diphenyl-1,3,5-hexatrienes, (32).**[3b] *Method B*. Carbene complex **25** (100 mg, 0.28 mmol) and Pd(P^{t}Bu$_3$)$_2$ (0.005 mmol) were reacted for 16 h, to yield compound **32** as a dark brown solid (23 mg, 51%, *E/Z* = 2/1). ***Z* + *E* isomers:** ^{1}H NMR (300 MHz): δ 7.42 (d, *J* = 7.6 Hz, 8H,), 7.31-7.16 (m, 12H), 7.07 (d, *J* = 16.1 Hz, 2H), 6.99 (d, *J* = 15.5 Hz, 2H), 6.81(d, *J* = 15.5 Hz, 2H), 6.72 (d, *J* = 16.1 Hz, 2H), 3.97 (q, *J* = 7.0 Hz, 4H), 3.84 (q, *J* = 7.0 Hz, 4H), 1.36 (t, *J* = 7.0 Hz, 6H), 1.34 (t, *J* = 7.0 Hz, 6H).

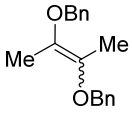

(*Z*)- and (*E*)- 1,2-Dibenzyloxy-1,2-dimethyethene, (34).[3b] *Method B*. Carbene complex **33** (50 mg, 0.15 mmol) and Pd(P^{t}Bu$_3$)$_2$ (0.002 mmol) were reacted for 22 h, to yield compound **34** as a mixture of isomers (14 mg, 70%, *E/Z* = 1/1.6). Compound **34** was unstable for further purification. ***Z* + *E* isomers:** ^{1}H NMR (300 MHz): δ 7.40-7.23 (m, 20H), 4.71 (s, 4H), 4.56 (s, 4H), 1.77 (s, 6H), 1.71 (s, 6H).

VII.6. References

(1) Gómez-Gallego, M.; Mancheño, M. J.; Sierra, M. A. *Acc. Chem. Res.* **2005**, *38*, 44.

(2) Selected general reviews in the chemistry of group 6 metal-carbenes: (a) Dötz, K. H.; Fischer, H.; Hofmann, P.; Kreissel, R.; Schubert, U.; Weiss K. *Transition Metal Carbene Complexes*, Verlag Chemie: Deerfield Beach, Florida, **1983**. (b) Dötz, K. H. *Angew. Chem. Int. Ed. Eng.* **1984**, *23*, 587. (c) Wulff, W. D. in *Comprehensive Organic Synthesis,* Trost B. M., Fleming I. Eds. Pergamon: Oxford, **1991**, *5*, 1065. (d) Schwindt, M. A.; Miller, J. R.; Hegedus, L. S. *J. Organomet. Chem.* **1991**, *413*, 143. (e) Rudler, H.; Audouin, M.; Chelain, E.; Denise, B.; Goumont, R.; Massoud, A.; Parlier, A.; Pacreau, A.; Rudler, M.; Yefsah, R.; Álvarez C.; Delgado-Reyes, F. *Chem. Soc. Rev.* **1991**, *20*, 503. (f) Grötjahn, D. B.; Dötz, K. H. *Synlett.* **1991**, 381. (g) Wulff, W. D. in *Comprehensive Organometallic Chemistry II,* Abel E. W.; Stone F. G. A.; Wilkinson G. Eds. Pergamon: Oxford. **1995**, *12*, 470. (h) Hegedus, L. S. in *Comprehensive Organometallic Chemistry II,* Abel E. W.; Stone F. G. A.; Wilkinson G. Eds. Pergamon: Oxford. **1995**, *12*, 549. (i) Harvey, D. F.; Sigano, D. M. *Chem. Rev.* **1996**, *96*, 271. (j) Hegedus, L. S. *Tetrahedron* **1997**, *53*, 4105. (k) Aumann, R.; Nienaber, H. *Adv. Organomet. Chem.* **1997**, *41*, 163. (l) Alcaide, B.; Casarrubios, L.; Domínguez, G.; Sierra, M. A. *Curr. Org. Chem.* **1998**, *2*, 551. (m) Sierra, M. A. *Chem. Rev.* **2000**, *100*, 3591. (n) De Meijere, A.; Schirmer, H.; Duetsch, M. *Angew. Chem., Int. Ed.* **2000**, *39*, 3964. (o) Barluenga, J.; Fañanás, F. J. *Tetrahedron* **2000**, *56*, 4597. (p) Barluenga, J.; Flórez, J.; Fañanás, F. J. *J. Organomet. Chem.* **2001**, *624*, 5. (q) Barluenga, J.; Santamaría, J.; Tomás, M. *Chem. Rev.* **2004**, *104*, 2259. (r) Herndon, J. W. *Coord. Chem. Rev*. **2006**, *250*, 1889. (s) Sierra, M. A.; Gómez-Gallego, M.; Martínez-Álvarez, R. *Chem. Eur. J.* **2007**, *13*, 736. (t) Sierra, M. A.; Fernández, I.; Cossío, F. P. *Chem. Commun.* **2008**, 4671. (u) Dötz, K. H.; Stendel, J. Jr. *Chem. Rev.* **2009**, *109*, 3227. (v) Fernández, I.; Cossío, F. P.; Sierra, M. A. *Acc. Chem. Res.* **2011**, *44*, 479.

(3) (a) Sierra, M. A.; Mancheño, M. J.; Sáez, E.; del Amo, J. C. *J. Am. Chem. Soc*. **1998**, *120*, 6812. (b) Sierra, M. A.; del Amo, J. C.; Mancheño, M. J.; Gómez-Gallego, M. *J. Am. Chem. Soc*. **2001**, *123*, 851.

(4) (a) Fernández, I.; Mancheño, M. J.; Vicente, R.; López, L. A.; Sierra, M. A. *Chem. Eur. J.* **2008**, *14*, 11222. (b) López-Alberca, M. P.; Fernández, I.; Mancheño, M. J.; Gómez-Gallego, M.; Casarrubios, L.; Sierra, M. A. *Eur. J. Org. Chem*. **2011**, 3293.

(5) Meana, I.; Toledo, A.; Albéniz, A. C.; Espinet, P. *Chem. Eur. J.* **2012**, *18*, 7658.

(6) Isolation and characterization of the mononuclear Pd-aminocarbene complex from the transmetalation of a tungsten(0) (Fischer) carbene with [PdBrPf$(MeCN)_2$] followed by reaction with PMe_3 has previously been reported, see: (a) Albéniz, A. C.; Espinet, P.; Manrique, R.; Pérez-Mateo, A. *Angew. Chem., Int. Ed.* **2002**, *41*, 2363. (b) Albéniz, A. C.; Espinet, P.; Manrique, R.; Pérez-Mateo, A. *Chem. Eur. J.* **2005**, *11*, 1565.

(7) (a) Barluenga, J.; López, L. A.; Löber, O.; Tomás, M.; García-Granda, S.; Álvarez-Rúa, C.; Borge, J. *Angew. Chem. Int. Ed*. **2001**, *40*, 3392. (b) Barluenga, J.; Barrio, P.; Vicente, R.; López, L. A.; Tomás, M. *J. Organomet. Chem*. **2004**, *689*, 3793.

(8) Fañanás-Mistral, M.; Aznar, F. *Organometallics* **2009**, *28*, 666.

(9) (a) López-Alberca, M. P.; Mancheño, M. J.; Fernández, I.; Gómez-Gallego, M.; Sierra, M. A.; Torres, R. *Org. Lett*. **2007**, *9*, 1757. (b) López-Alberca, M. P.; Mancheño, M. J.; Fernández, I.; Gómez-Gallego, M.; Sierra, M. A.; Torres, R. *Chem. Eur. J.* **2009**, *15*, 3595.

(10) Lage, M. L.; Curiel, D.; Fernández, I.; Mancheño, M. J.; Gómez-Gallego, M.; Molina, P.; Sierra, M. A. *Organometallics* **2011**, *30*, 1794.

(11) Facchetti, A.; Marks, T. J.; Huang, H.; Chen, Z. *PCT Int. Appl.* **2011**, WO 2011119374 A1 20110929.

(12) Representative recent examples: (a) Ohmura, T.; Oshima, K.; Taniguchi, H.; Suginome, M. *J. Am. Chem. Soc.* **2010**, *132*, 12194. (b) Tsvelikhovsky, D.; Buchwald, S. L. *J. Am. Chem. Soc.* **2010**, *132*, 14048. (c) Solé, D.; Fernández, I.; Sierra, M. A. *Chem. Eur. J.* **2012**, *18*, 6950.

(13) The *E/Z* stereochemistry of the self-dimerization products was determined from literature data. For methoxy-derivatives: (a) Fischer, E. O.; Heckl, B.; Dötz, K. H.; Müller, J.; Werner, H. *J. Organometal. Chem*., **1969**, *16*, P29. For ethoxy-derivatives: (b) Hansen, P.-E. *J. Chem. Soc. Perkins Trans. I* **1980**, *8*, 1627.

(14) The proposed mechanism for the oxygen oxidation of group 6 metal carbene complexes involves the stepwise addition of oxygen to the M=C bond, followed by the cycloreversion of the metalladioxetane thus formed, generating the corresponding ester and $(CO)_5Cr{=}O$. See, among others: (a) Gibert, M.; Ferrer, M.; Lluch, A.-M.; Sánchez-Baeza, F.; Messeguer, A. *J. Org. Chem.* **1999**, *64*, 1591. This process is easy, and it is the basis of the oxidative demetalation of group 6 metal-carbene complexes, a standard tool to remove the metal fragment. See the following, for example. (b) DMDO: Lluch, A.-M.; Jordi, L.; Sánchez-Baeza, F.; Ricart, S.; Camps, F.; Messeguer, A.; Moretó, J. M. *Tetrahedron Lett.* **1992**, *33*, 3021. (c) CAN: Luo, N.; Zheng, Z.; Yu, Z. *Org. Lett.* **2011**, *13*, 3384. (d) S/$NaBH_4$: Sandoval-Chávez, C.; López-Cortes, J. G.; Gutiérrez-Hernández, A. I.; Ortega-Alfaro, M. C.; Toscano, A.; Álvarez-Toledano, C. *J. Organomet. Chem.* **2009**, *694*, 3692. (e) SCO or SeCO: Zheng, Z.; Chen, J.; Luo, N.; Yu, Z.; Han, X. *Organometallics* **2006**, *25*, 5301. (f) TFMD: Barluenga, J.; Canteli, R.-M.; Flórez, J.; García-Granda, S.; Gutíerrez-Rodríguez, A. *J. Am. Chem. Soc.* **1994**, *116*, 6949. (g) PyNO: Capriati, V.; Florio, S.; Luisi, R.; Perna, F. M.; Barluenga, J. *J. Org. Chem.* **2005**, *70*, 5852. (h) I_2: Soderberg, B. C.; Bowden, B. A. *Organometallics* **1992**, *11*, 2220. (i) Electrochemical oxidation: Lloyd, M. K.; McClever, J. A.; Orchard, D. G.; Connor, J. A.; Hall, M. B.; Hillier, H.; Jones, E. M.; McEven, G. K. *J. Chem. Soc., Dalton Trans.* **1973**, 1743. Additionally, the recently reported Pd carbene complexes are extremely sensitive to water and oxygen.[5]

(15) Fischer, E. O.; Aumann, R. *Chem. Ber*. **1968**, *101*, 963.

(16) Fischer, E. O.; Dötz, K. H. *J. Organomet. Chem*. **1972**, *36*, C4.

(17) Fischer, E. O.; Roell, W.; Hoa Tran Huy, N.; Ackermann, K. *Chem. Ber*. **1982**, *115*, 2951.

(18) Lage, M. L.; Fernández, I.; Mancheño, M. J.; Sierra, M. A. *Inorg. Chem.* **2008**, *47*, 5253.

(19) Jayaprakash, K. N.; Hazra, D.; Hagen, K. S.; Samanta, U.; Bhadbhade, M. M.; Puranik, V. G.; Sarkar, A. *J. Organomet Chem.* **2001**, *617-618*, 709.

(20) Herrmann, W. A. *Synthetic Methods of Organometallic and Inorganic Chemistry, Thieme,* Stuttgart, New York, **1997**.

(21) Aumann, R.; Heinen, H. *Chem. Ber.* **1987**, *120*, 537.

(22) Hafner, A.; Hegedus, L. S.; DeWeck, G.; Hawkins, B.; Dötz, K. H. *J. Am. Chem. Soc.* **1988**, *110*, 8413.

(23) The reported *E/Z* ratios reflected the ratio of olefins obtained during the catalytic self-dimerization process. To discard, as proposed by a reviewer, the possibility of the Pd catalytic species reacting with the originally formed olefins and therefore affecting the final *E/Z* ratio, three separate experiments were carried out. Thus, a 1/1 *E/Z* mixture of olefins **17** (15 mg) was reacted in the presence of 1.3 mg of $Pd(P^tBu_3)_2$ in 0.4 mL of MeCN for 48 h. The resulting mixture contains a 1/1 *E/Z* mixture of olefins **17**. The olefins were recovered quantitatively. Two additional experiments were carried out with olefins (*Z*)-**11** and (*E*)-**26**. Both compounds were recovered unaltered under the reactions conditions used for **17**. These experiments prove that the obtained olefins are configurationally stable under the catalytic conditions used.

VIII. *DISCUSIÓN GENERAL*

En este apartado se discutirán los aspectos más relevantes de los distintos capítulos anteriormente tratados y se valorarán de forma crítica los resultados obtenidos y la consecución de los objetivos propuestos.

VIII.1. Síntesis, estructura y propiedades electrónicas de complejos alcoxi-biscarbeno de Fischer con conjugación-π extendida.

Estudios previos realizados en nuestro grupo de investigación sobre sistemas *push-pull* (D-π-A) basados en complejos alcoxi-carbeno α,β-insaturados de tipo Fischer proporcionaron un amplio conocimiento sobre la naturaleza electrónica de dichas especies.[56] Se demostró que estas especies presentan dos absorciones principales de naturaleza π-π* en sus correspondientes espectros de UV-vis, las bandas LF y MLCT, respectivamente. La primera transición se encuentra a mayor energía y se ve influenciada tanto por grupos π-dadores como π-aceptores. En cambio, la banda MLCT (que aparece en el visible y es responsable del color de los complejos) apenas se ve afectada por la presencia de sustituyentes con diferente naturaleza electrónica.

A la vista de estos resultados, diseñamos nuevos complejos *push-pull* de tipo Fischer de estructura general **23** con el objeto último de modular la posición de la banda MLCT en función del tipo de espaciador arilo que conecta ambos fragmentos carbénicos. Para ello se sintetizó y caracterizó la serie de complejos *push-pull* (A-π-D-π-A) **23** (Figura 37).[92]

[92] Chu, G. M.; Fernández, I.; Sierra, M. A *Chem. Eur. J.* **2013**, *19*, 5899.

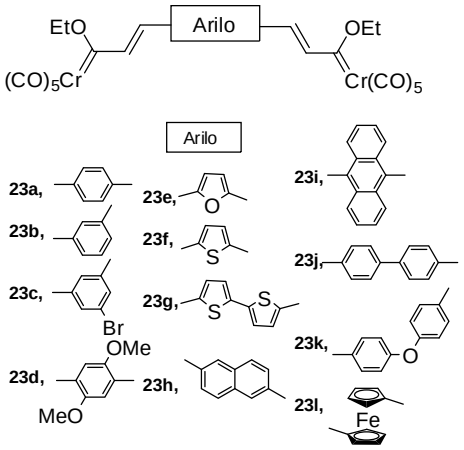

Figura 37. Complejos *push-pull* (A-π-D-π-A) estudiados.

Estos sistemas A-π-D-π-A presentan un efecto cooperativo entre los dos fragmentos metal-pentacarbonilo que, junto a la alta planaridad del sistema, amplifican la conjugación-π entre el espaciador y los dos fragmentos metálicos. Como resultado, se observa un desplazamiento batocrómico significativo en la posición de la banda MLCT con respecto a los análogos monocarbeno descritos previamente en nuestro grupo de investigación (Figura 38).[56]

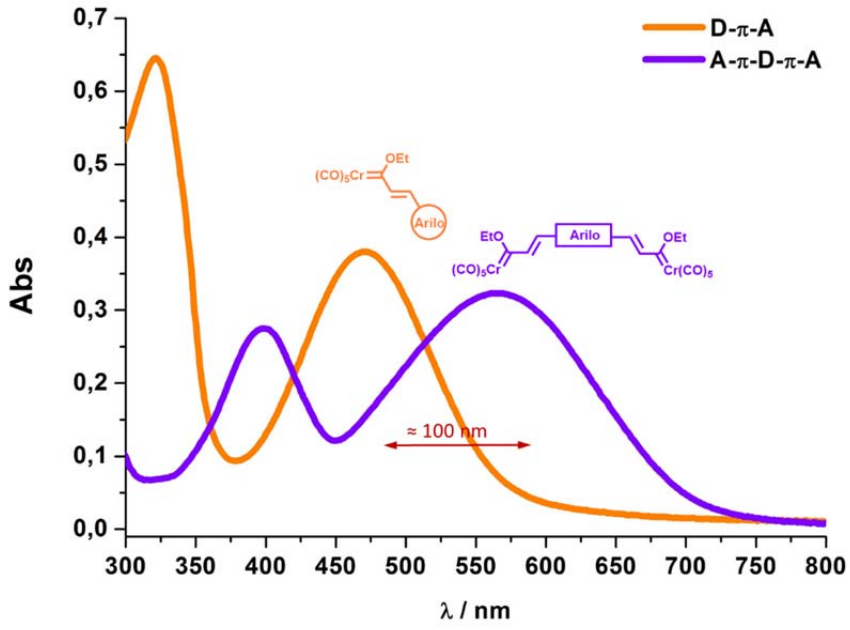

Figura 38. Comparación de espectros de absorción de los sistemas D-π-A y A-π-D-π-A basados en complejos metal-carbeno de tipo Fischer.

Los cálculos TD-DFT llevados a cabo indican que las bandas de absorción LF y MLCT presentan un marcado carácter π-π* y se pueden asignar a las transiciones HOMO-6 → LUMO y HOMO → LUMO, respectivamente (Figura 39).

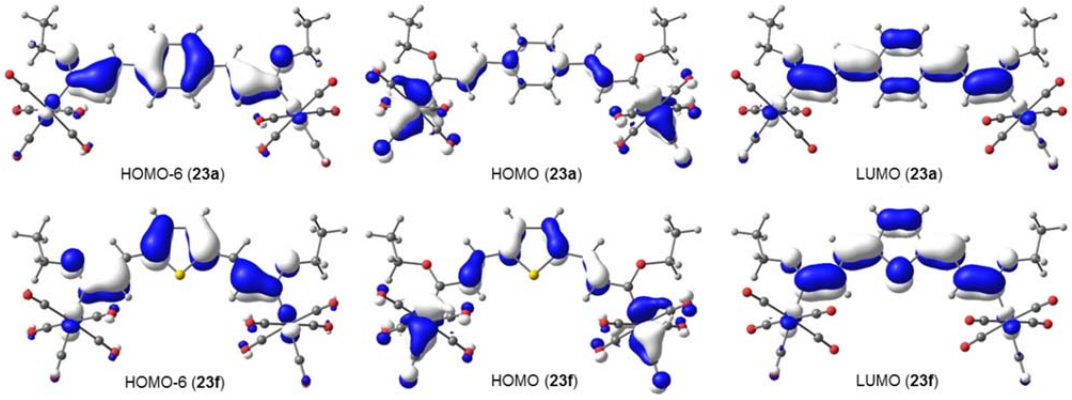

Figura 39. Orbitales moleculares calculados para los complejos **23a** y **23f**.

La amplificación de la conjugación-π en los sistemas *push-pull* **23** se refleja claramente en sus geometrías de equilibrio (Esquema 6). Así, la forma resonante **II** contribuye en mayor medida en aquellos complejos que exhiben mayor conjugación, es decir, en los complejos cuya banda MLCT se encuentra más desplazada batocrómicamente. Como consecuencia directa de la elevada contribución de dicha forma resonante se produce un acortamiento significativo de la distancia de los enlaces C1–C2 y C3–C4 y un alargamiento de los enlaces C2=C3 (como confirman tanto la estructura de rayos-X del complejo **23f** (Figura 40) como los valores calculados para los complejos **23a**,**b**,**e**,**f**).

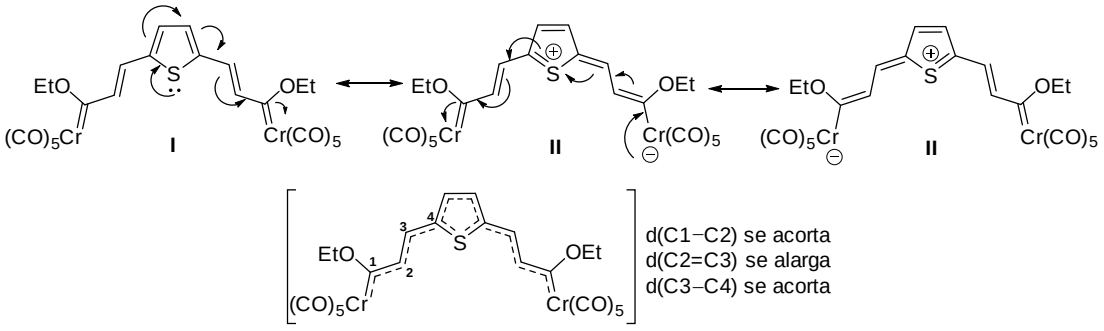

Esquema 1. Posibles formas resonantes del complejo **23f**.

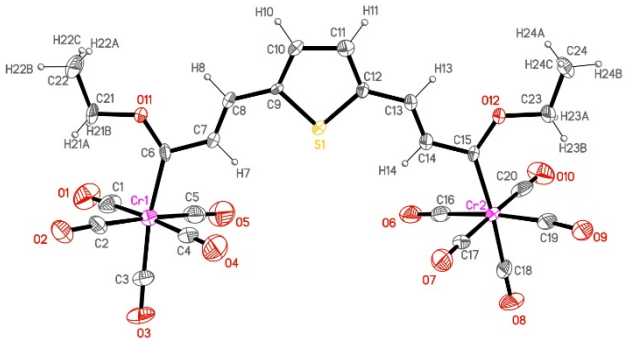

Figura 40. Estructura cristalina del biscarbeno **23f**.

Asimismo, se estudió la influencia de la naturaleza del metal sobre las propiedades electrónicas de los complejos **23**. Con este fin, se sintetizaron y caracterizaron los biscarbenos de la Figura 41. Así, la banda MLCT del complejo **23a** aparece a una mayor longitud de onda que la banda MLCT del complejo **23n**. Este resultado indica claramente que el biscarbeno de wolframio presenta una conjugación-π extendida menor que **23a**, lo que se puede atribuir a la menor capacidad π-aceptora del fragmento $W(CO)_5$. El valor intermedio encontrado para la posición de la banda MLCT del complejo mixto **23m** apoya la hipótesis del efecto cooperativo entre los dos fragmentos metal-pentacarbonilo mencionado anteriormente.

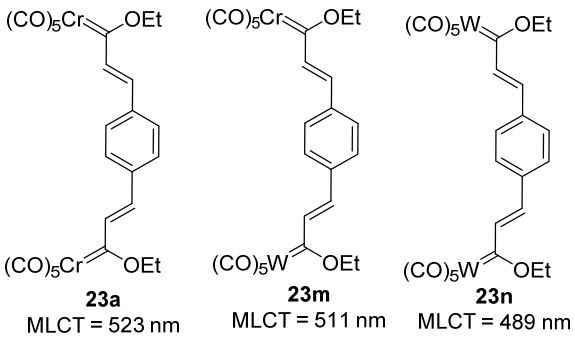

Figura 41. Complejos biscarbenos con distintos metales de transición estudiados.

Finalmente, la posición de la banda MLCT de los sistemas A-π-D-π-A de tipo Fischer es modulable a través de diversos cambios en el fragmento arilo. Así, un fragmento con mayor densidad electrónica provoca un desplazamiento batocrómico, mientras que un espaciador que interrumpe la conjugación entre los dos fragmentos metálicos provoca que la posición de la banda MLCT sea análoga a

la de un sistema *push-pull* mono-carbeno de tipo Fischer. De esta manera, no sólo hemos logrado el objetivo principal de modular la posición de la banda MLCT sino que además se ha obtenido el valor más alto (λ_{max} = 580 nm) de la posición de dicha banda en complejos metal-carbeno de tipo Fischer descrito hasta la fecha.

VIII.2. Moléculas BODIPY con propiedades fotofísicas modulables mediante conjugación-π con complejos metal-carbeno de tipo Fischer.

El diseño de nuevos sistemas metal-BODIPY donde el fragmento metálico se une tanto a la periferia como directamente al núcleo del BODIPY, tiene interés debido al gran número de modificaciones posibles que permiten, en principio, modular fácilmente las propiedades ópticas y electrónicas de estos compuestos.

A fin de estudiar la interacción electrónica entre el fluoróforo y el fragmento metálico se diseñaron nuevas díadas BODIPY-carbeno de tipo Fischer unidas por conjugación-π a través de un espaciador etileno (Figura 42). En estas especies, el fragmento metálico se encuentra, por tanto, directamente conjugado al núcleo del fluoróforo BODIPY.[93]

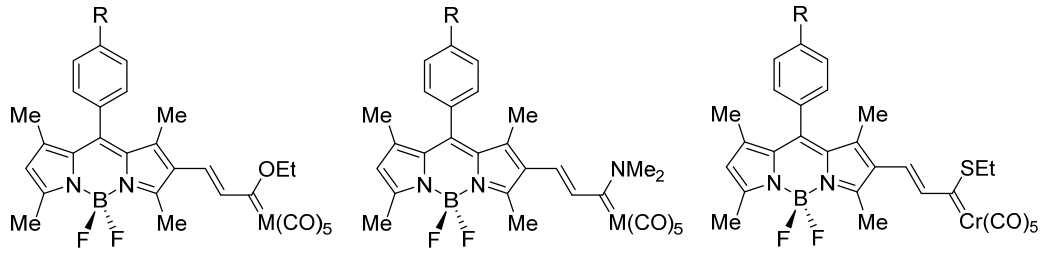

24a, M = Cr; R = H
24b, M = Cr; R = Me
24c, M = Cr; R = OMe
24d, M = W; R = H

25a, M = Cr; R = H
25b, M = Cr; R = Me
25c, M = W; R = H

26, R = H

Figura 42. Díadas BODIPY-metal-carbeno de tipo Fischer estudiadas.

Estos nuevos sistemas *push-pull* **24** (D-π-A) presentan una banda de absorción cuyo máximo aparece a λ_{max} = 570 nm, atribuible a la transición MLCT. Este fuerte desplazamiento batocrómico es aproximadamente de unos 100 nm

[93] Chu, G. M.; Guerrero-Martínez, A.; Fernández, I.; Sierra, M. A. *Chem. Eur. J.* **2014**, *20*, 1367.

con respecto a los complejos monocarbeno análogos ($\lambda_{max} \approx 475$ nm)[56] (Figura 43) y es comparable al observado en los sistemas A-π-D-π-A descritos en el capítulo VIII.1.[92] Por tanto, nos encontramos de nuevo ante sistemas con conjugación π-extendida con elevada planaridad (como se observa en la Figura 44). Cabe destacar que la modificación del sustituyente R sobre el anillo bencénico no modifica las propiedades de absorción de la díada ya que se sitúa perpendicularmente al plano de la díada metal-BODIPY.

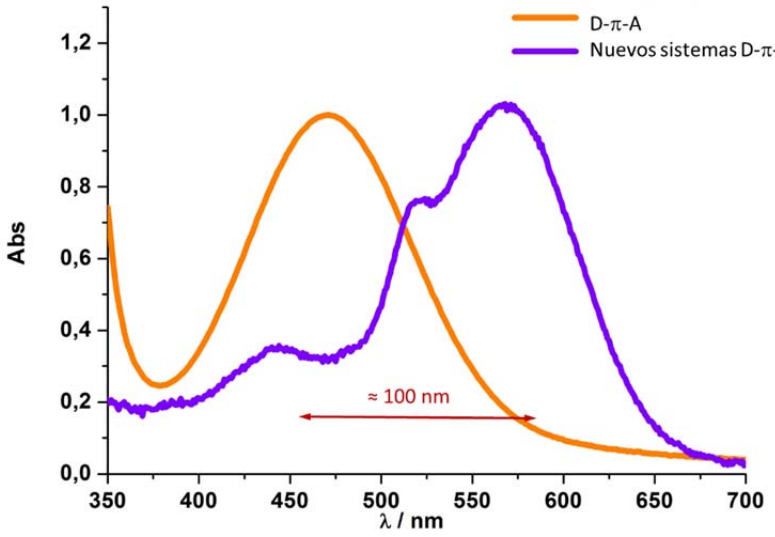

Figura 43. Comparación de espectros de absorción entre los sistemas D-π-A y las díadas **24**.

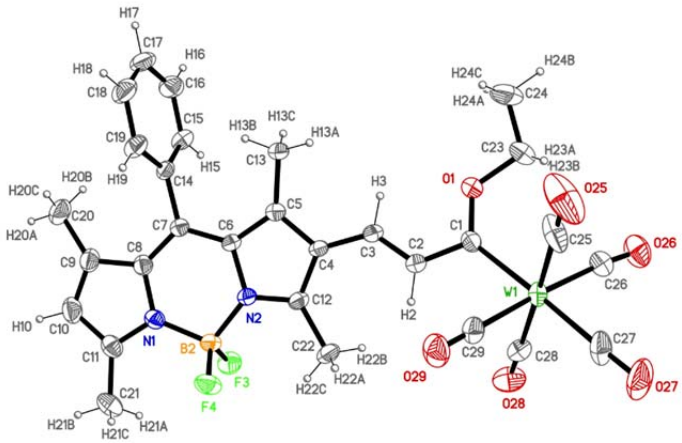

Figura 44. Estructura cristalina de la díada **24d**.

Los cálculos TD-DFT llevados a cabo para las díadas **24a**,**c** indican que la banda MLCT resulta de la promoción de un electrón desde el HOMO al LUMO, mientras que la banda LF corresponde a la transición HOMO-2 → LUMO. Ambas transiciones poseen un marcado carácter π-π* como se observa en la Figura 45.

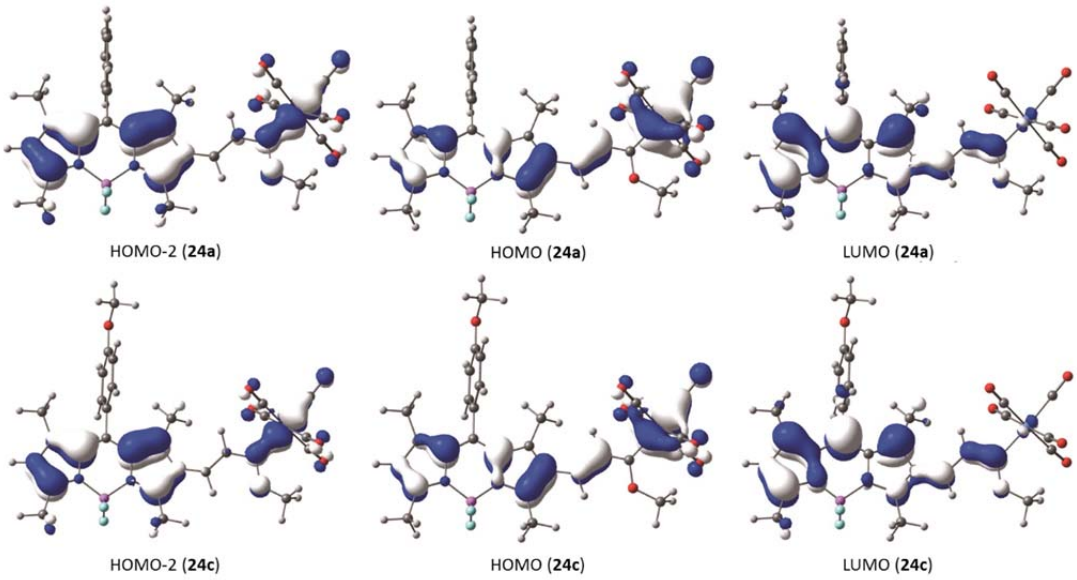

Figura 45. Orbitales moleculares calculados para los complejos **24a** y **24c**.

El efecto de la conjugación-π extendida se puede apreciar en las geometrías de equilibrio de las especies **24** (Esquema 7). Así, la forma resonante **I** describe fundamentalmente la situación de enlace en las díadas alcoxicarbeno, mientras que la forma resonante **II** es más representativa en los complejos aminocarbeno. Este hecho se hace evidente cuando se comparan los índices de enlace de Wiberg de C1–C2 y C2=C3 de las díadas **24** y **25** (1.21 y 1.61 frente a 1.12 y 1.71, respectivamente).

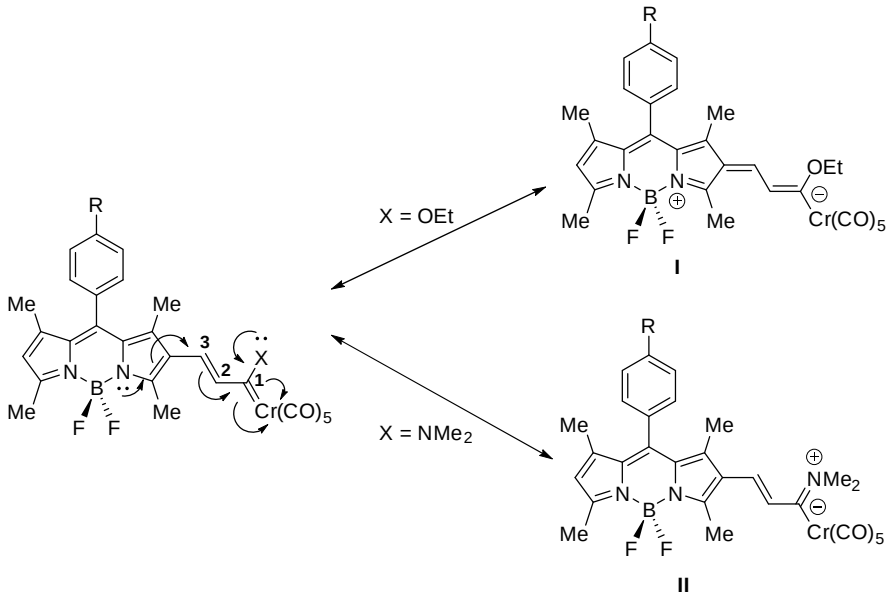

Esquema 7. Posibles formas resonantes de los complejos **24** y **25**.

Tanto los cálculos teóricos como la estructura de rayos-X para el complejo **24d** indican claramente que las díadas **24** se encuentran totalmente conjugadas y presentan una alta planaridad. En cambio, los complejos aminocarbeno **25** no presentan tal planaridad (Figura 46) y, como consecuencia, las propiedades fotofísicas son completamente diferentes. El mayor carácter π-dador del grupo amino con respecto al grupo alcoxi interrumpe la comunicación electrónica entre el fragmento BODIPY y la especie metálica, aislando de esta manera al fluoróforo. Así, las díadas **25** presentan propiedades fotofísicas características de las unidades BODIPY, mientras que en los complejos **24** se observa por el contrario una completa supresión de la fluorescencia (Figura 47).

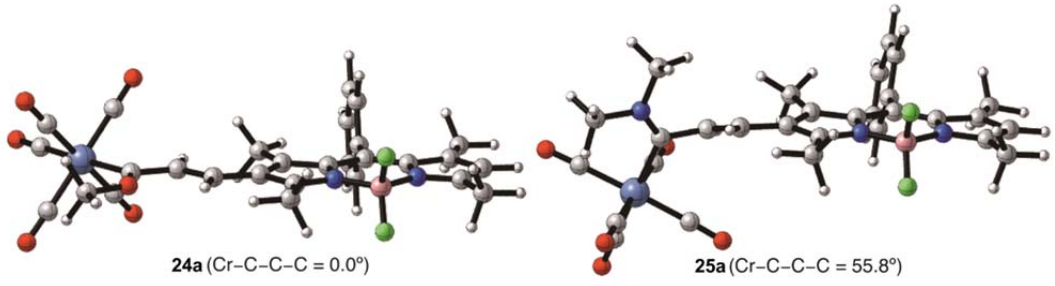

Figura 46. Geometrías optimizadas para los complejos **24a** y **25a**.

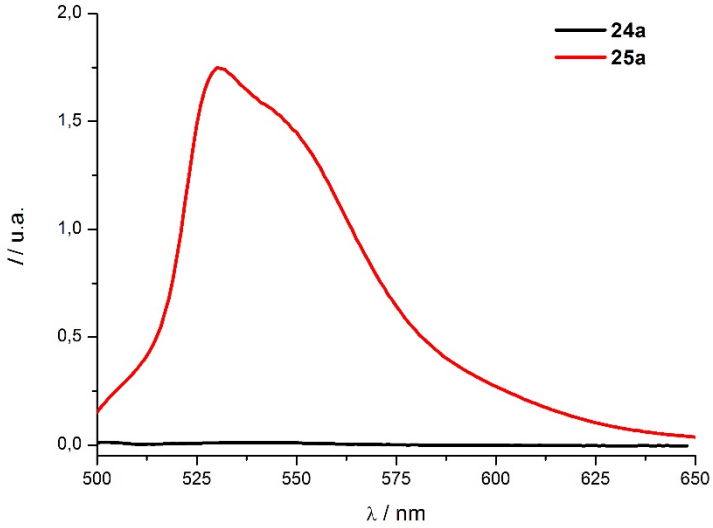

Figura 47. Espectro de emisión de las díadas **24a** y **25a**.

Adicionalmente, la modulación de las propiedades fotofísicas del BODIPY es posible mediante la modificación del carácter π-dador del heteroátomo unido directamente al carbono carbénico del complejo de Fischer. Así, se sintetizó y estudió la díada con un grupo -SEt **26** (Figura 42). Como cabía esperar, dicha díada mostró propiedades geométricas y fotofísicas intermedias entre las díadas **24** y **25** debido a que el átomo de azufre es menos π-dador que el nitrógeno y menos electronegativo que el oxígeno.

Por lo tanto, hemos logrado modular de manera eficaz las propiedades fotofísicas del fluoróforo BODIPY mediante la simple modificación de las propiedades electrónicas del heteroátomo del complejo metal-carbeno de tipo Fischer.

VIII.3. Nuevas díadas BODIPY-carbeno de Fischer con control de las propiedades de emisión mediante conjugación-π remota.

Teniendo en cuenta los resultados descritos anteriormente con propiedades fotofísicas modulables a través de la conjugación-π,[93] se diseñó una nueva familia de díadas metal-BODIPY. Para ello, se sintetizaron los complejos **26**

(Figura 48)[94] donde el complejo metal-carbeno se une al BODIPY a través de un grupo 4-aminofenilo situado en C8.

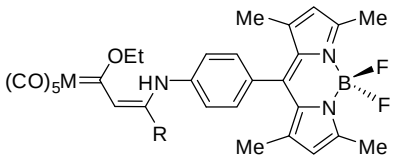

26a, M = Cr, R = Ph
26b, M = W, R = Ph
26c, M = Cr, R = ^{n}Bu
26d, M = Cr, R = 4-Me-C$_6$H$_4$
26e, M = Cr, R = 4-OMe-C$_6$H$_4$
26f, M = Cr, R = 4-NMe$_2$-C$_6$H$_4$
26g, M = Cr, R = 4-Br-C$_6$H$_4$
26h, M = Cr, R = 4-CF$_3$-C$_6$H$_4$
26i, M = Cr, R = Fc

Figura 48. Díadas BODIPY-carbeno de Fischer estudiadas.

Estos nuevos sistemas *push-pull* **26** presentan dos bandas de absorción principales: una en torno a 500 nm y otra, a 475 nm. Estas transiciones se pueden asignar en base a cálculos TD-DFT a la transición π-π* del BODIPY (HOMO → LUMO) y a la banda MLCT del complejo metálico (HOMO-1 → LUMO+1) (Figura 49).

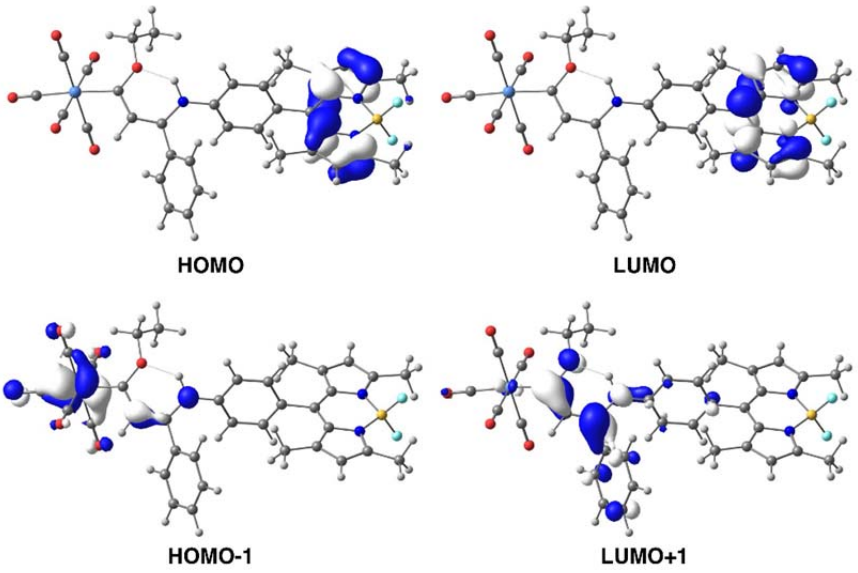

Figura 49. Orbitales moleculares calculados para la díada **26a**.

Las propiedades de absorción de las díadas son prácticamente la suma de las absorciones del fragmento BODIPY y del complejo metálico por separado. Esto

[94] Chu, G. M.; Guerrero-Martínez, A.; Ramírez de Arellano, C.; Fernández, I.; Sierra. M. A. *Enviado.*

es esperable ya que ambos cromóforos no son coplanares como indica la estructura de rayos-X de la díada **26b** (Figura 50). Por lo tanto, la unión del BODIPY con el fragmento metálico no altera significativamente las propiedades electrónicas del fluoróforo BODIPY.

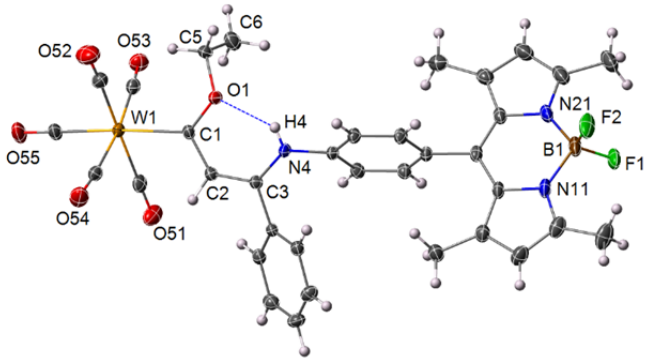

Figura 50. Estructura cristalina de la díada **26b**.

Por otro lado, la intensidad de la emisión de fluorescencia del éster **27**, generado mediante la oxidación de la díada **26a**, es mucho mayor que la del BODIPY **28** (Figura 51). Esto se debe a que el grupo carbonilo es capaz de aceptar densidad electrónica del par de electrones libre del átomo de nitrógeno de la anilina. Por tanto, dicho par de electrones se encuentra menos deslocalizado sobre el núcleo del BODIPY y, como consecuencia, la emisión de fluorescencia del sistema es mayor. Un efecto similar se debería observar en las díadas BODIPY-carbeno debido al gran carácter π-aceptor del fragmento metal-pentacarbonilo.[40] Sin embargo, en estos sistemas se observa una disminución significativa de la intensidad de emisión del BODIPY.

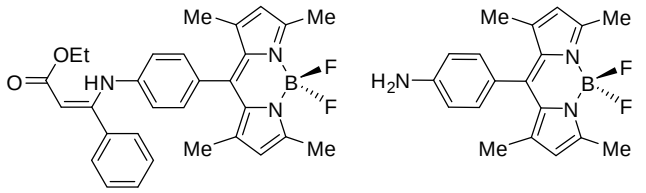

Figura 51. Estructura de la díada oxidada **27** y del BODIPY **28**.

Considerando el solapamiento existente entre la emisión del BODIPY y la absorción del complejo metal-carbeno de tipo Fischer y la distancia relativa entre los dos cromóforos (en torno a 10 Å), una interacción Dexter cobra fuerza como

mecanismo responsable de la reducción de la emisión de fluorescencia en las especies **26**.[70] Además, el cálculo de las energías relativas de los orbitales frontera de los cromóforos por separado indica una posible desactivación desde el LUMO del BODIPY excitado al LUMO del complejo metal-carbeno, lo que también apoya al mecanismo de desactivación Dexter (Figura 52). Sin embargo, tal desactivación no es posible si el aceptor es un grupo éster ya que el LUMO de éste se encuentra más alto en energía, lo que está de acuerdo con el hecho experimental observado.

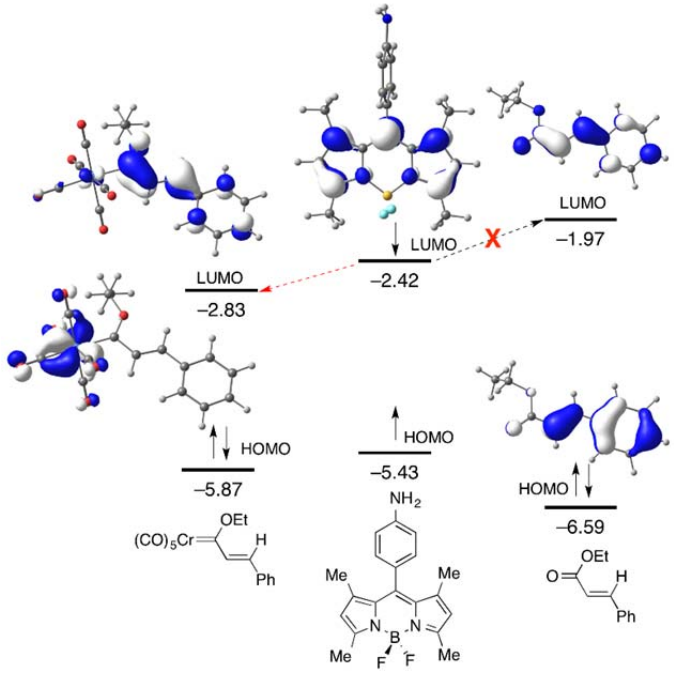

Figura 52. Orbitales frontera calculados para los cromóforos aislados.

A pesar de la baja emisión de las díadas **26** se aprecia una clara dependencia de la misma en función de la sustitución en la posición β del carbono carbénico (Figura 53). Así, los complejos con sustituyentes π-dadores sobre el anillo bencénico (**26e,f**) muestran una emisión mayor que aquellos con sustituyentes π-aceptores (**26g,h**), a excepción de **26i** donde la emisión se encuentra totalmente desactivada debido a un mecanismo PET inducido por el grupo ferrocenilo.[95]

[95] Este efecto ha sido observado previamente en sistemas análogos, véase: (a) Rao, M. R.; Kumar, K. V. P.; Ravikanth, M. *J. Organomet. Chem.* **2010**, *695*, 863. (b) Liu, J.-Y.; El-Khouly, M. E.; Fukuzumi, S.; Ng, D. K. P. *ChemPhysChem* **2012**, *13*, 2030.

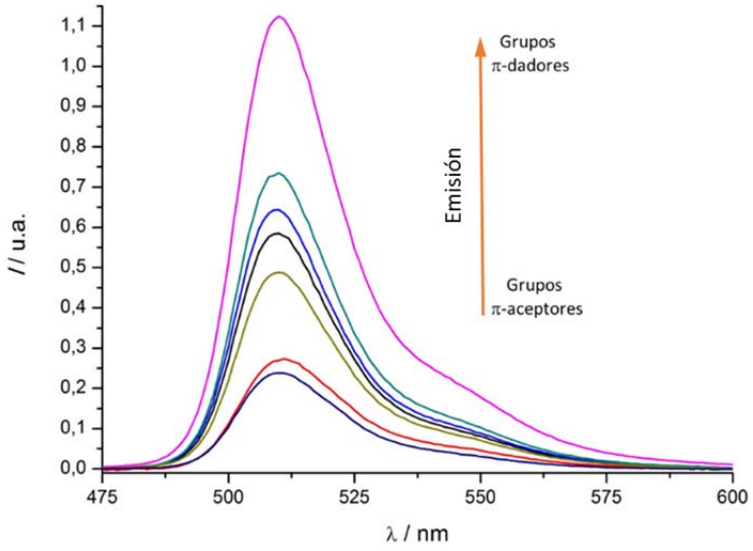

Figura 53. Comparación del espectro de emisión de las díadas **5** con diferentes sustituyentes en el grupo arilo.

Por otro lado, se han encontrado claras correlaciones lineales entre la intensidad de la emisión y los parámetros σ_p^+ de Hammet, así como con el desplazamiento químico de ^{13}C-RMN del carbono carbénico (Figura 54). Estas correlaciones confirman inequívocamente que la emisión del fluoróforo BODIPY en las díadas **26** se puede modular eficazmente mediante la conjugación-π ejercida por los correspondientes sustituyentes situados en posiciones remotas al fluoróforo BODIPY.

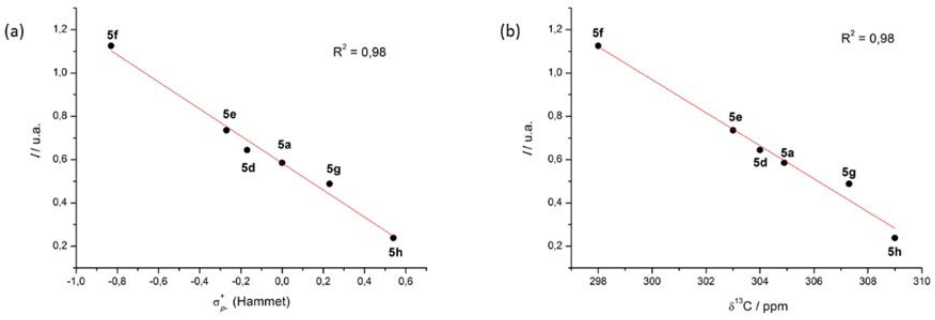

Figura 54. Representación gráfica de la intensidad de emisión frente al parámetro σ_p^+ (a) y al desplazamiento químico de ^{13}C-RMN del carbono carbénico (b).

La geometría de equilibrio de estas díadas se encuentra influenciada, por tanto, por la naturaleza de los sustituyentes del grupo R (Figura 48) y, a su vez, por el par de electrones libre del nitrógeno de la anilina unido al BODIPY en posición C8. Así, las formas resonantes **II** y **III** contribuyen en gran medida a la descripción de los complejos con grupos π-dadores **26e**,**f** (Esquema 8).En cambio, las díadas con grupos electroaceptores **26g**,**h**, junto a la especie con el resto butilo **26c**, se describen mejor mediante la forma resonante **IV**. En consecuencia, la emisión del BODIPY se encuentra más desactivada en las díadas que presentan grupos π-aceptores que en aquellas con grupos π-dadores.

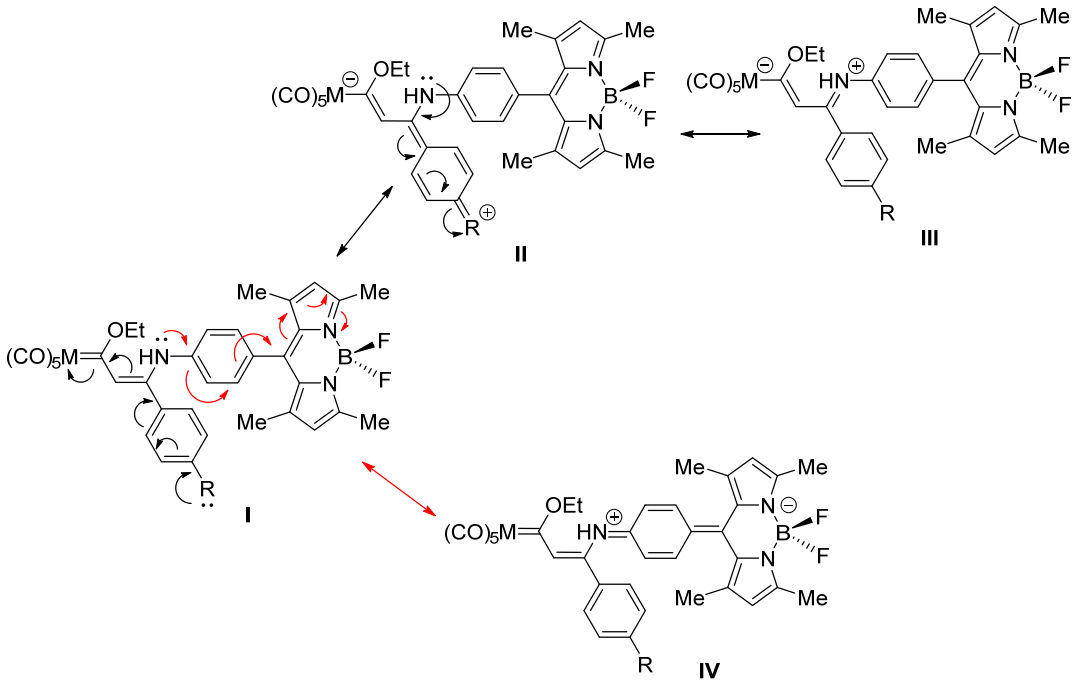

Esquema 8. Posibles formas resonantes de los complejos **26**.

Podemos concluir, por tanto, que se han logrado diseñar las primeras díadas metal-BODIPY donde el complejo metal-carbeno de tipo Fischer se encuentra unido a la periferia del BODIPY. Dichas especies presentan propiedades emisivas modulables a través de la conjugación-π remota del fragmento metálico y no de una conjugación-π directa con el fluoróforo BODIPY similar a la descrita en el capítulo VIII.2.

VIII.4. Complejos metal-BODIPY de Ir (III)y Rh (III) con desactivación de la fluorescencia.

Con el fin de evaluar el mecanismo de desactivación de la fluorescencia en sistemas metal-BODIPY no coplanares, se diseñaron, sintetizaron y caracterizaron nuevos complejos de rodio (III) e iridio (III) **30** y **32** mediante reacción de activación C-H/ciclometalación desde $[MCp^*Cl_2]_2$ y los cromóforos BODIPY **29** y **31**, respectivamente (Figura 55).[96]

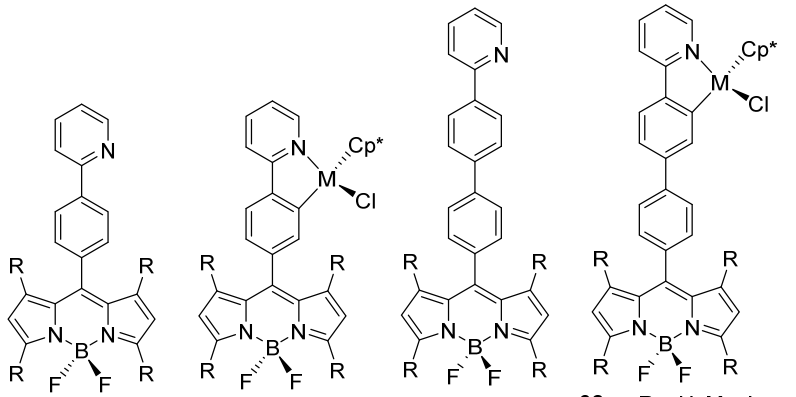

Figura 55. Especies BODIPY **29** y **31** y díadas metal-BODIPY **30** y **32** estudiadas.

Las estructuras de rayos-X de las díadas **30ba** y **33bb** (Figura 56) revelan que el ángulo diedro entre el núcleo del BODIPY y el grupo fenilo es prácticamente ortogonal (99.3° y 90.6°, respectivamente). En cambio, cálculos DFT sobre la díada sin grupos metilo **30aa** indican un valor del ángulo diedro de -52.5°. Esta sutil diferencia estructural en las moléculas BODIPY sin sustituir hace que dichos sistemas presenten una total desactivación de la emisión debida a la rotación libre del grupo arilo en posición C8 al BODIPY.

[96] Chu, G. M.; Fernández, I.; Guerrero-Martínez, A.; Ramírez de Arellano, C.; Sierra. M. A. En prensa: *Eur. J. Inorg. Chem.*

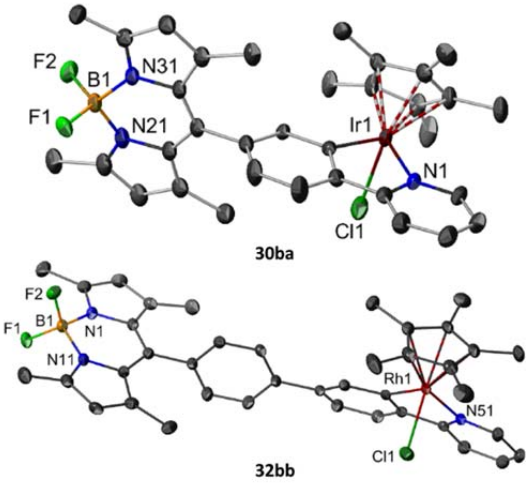

Figura 56. Representación cristalina de las díadas **30ba** y **32bb**.

Con respecto a las propiedades de absorción, la posición de la banda del BODIPY de los complejos **30** y **32** permanece prácticamente inalterada ($\lambda_{max} \approx 500$ nm) a pesar de la presencia del metalaciclo en la díada y de la inclusión de un grupo arilo adicional. Esto es consecuencia de la falta de conjugación-π directa entre el fluoróforo y el fragmento metálico, lo cual nos permite asignar inequívocamente la banda de absorción a una transición π-π* en la que solamente participa el fragmento BODIPY. Adicionalmente, cálculos TD-DFT confirman que dicha banda se debe a la promoción de un electrón desde el orbital HOMO-1 al orbital LUMO (ambos orbitales centrados casi exclusivamente en el fluoróforo, Figura 57).

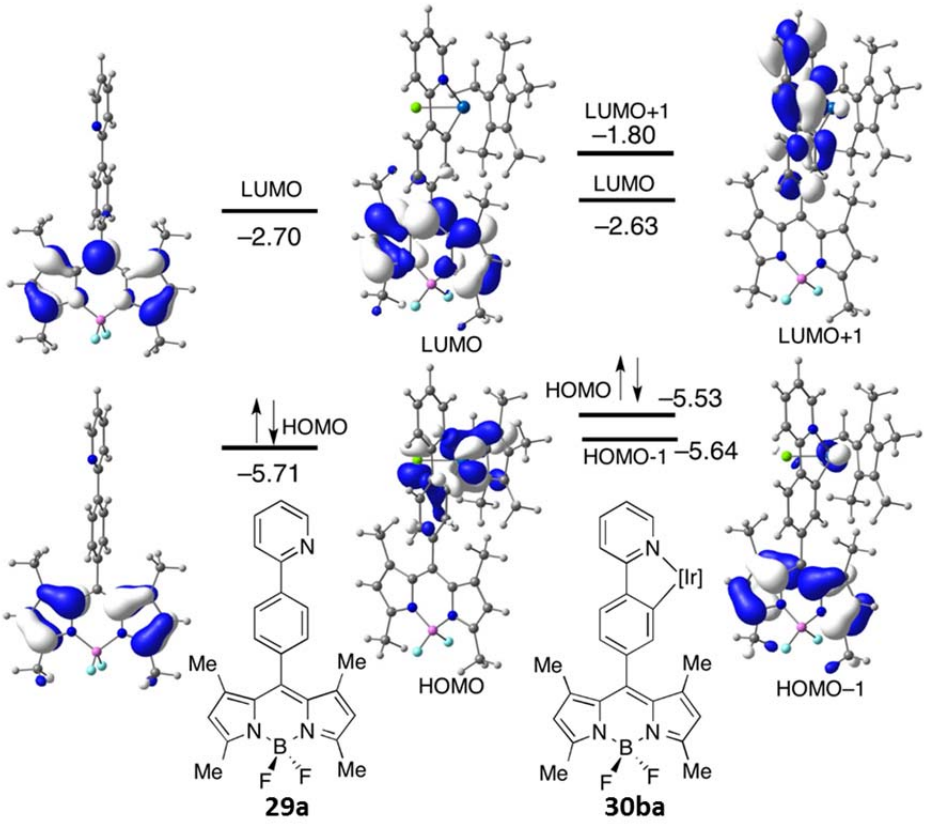

Figura 57. Orbitales moleculares calculados para los complejos **29a** y **30ba**.

Por otro lado, la presencia del metal provoca cambios muy significativos en la emisión de las díadas **30** y **32**. Así, el rendimiento cuántico de fluorescencia de los complejos metal-BODIPY **30ba** y **30bb** (0.001 y 0.014, respectivamente) disminuye drásticamente con respecto al BODIPY sin metalar **29b** (0.452). La presencia de un grupo arilo adicional influye ligeramente sobre el rendimiento cuántico de las especies **31b**, **32ba** y **32bb** (0.557, 0.062 y 0.125, respectivamente). Aunque la emisión se encuentra prácticamente desactivada, no se observa una completa supresión de la señal de fluorescencia debido a que el fragmento metálico se encuentra relativamente alejado del núcleo del BODIPY en los complejos **32**. Asimismo, se aprecia claramente que los complejos de iridio (III) **30ba** y **32ba** presentan una desactivación más eficiente con respecto a los complejos de rodio (III) **30bb** y **32bb**.

Los mecanismos de transferencia de energía Förster y la interacción de Dexter como responsables de la desactivación de la emisión de fluorescencia de las díadas **30b** y **32b** son muy improbables debido al prácticamente nulo

solapamiento entre la banda de emisión del dador y la banda de absorción del aceptor. En cambio, un mecanismo de transferencia electrónica fotoinducida constituye una alternativa razonable para explicar los hechos experimentales. Así, los cálculos DFT de las energías relativas de los orbitales frontera muestran que tras la fotoexcitación del BODIPY se puede producir una transferencia electrónica desde el fragmento metálico al fluoróforo en un mecanismo a-PET (Figura 58), responsable de la supresión de la fluorescencia observada experimentalmente.

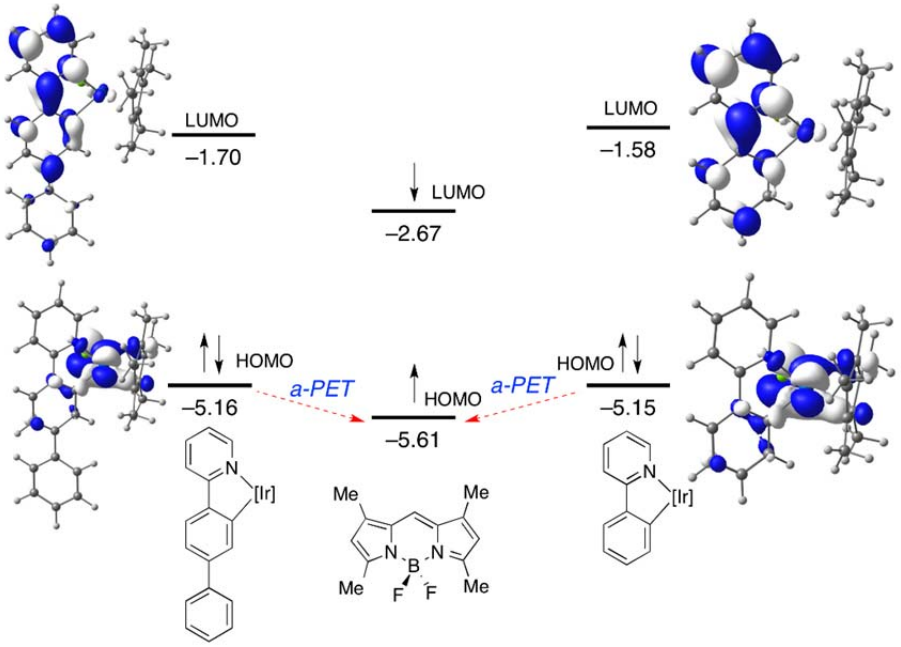

Figura 58. Mecanismo PET propuesto para las díadas **30** y **32**.

Por tanto, se ha realizado el estudio sistemático de complejos metal-BODIPY no coplanares, donde hemos controlado las propiedades de emisión mediante la modulación de la distancia entre el fragmento metálico y el fluoróforo BODIPY y la naturaleza del metal de transición. Estos factores son cruciales en el control de la eficiencia del mecanismo a-PET de las díadas metal-BODIPY **30** y **32**.

VIII.5. Control sobre la selectividad *E/Z* en la dimerización catalítica de complejos metal-carbeno de tipo Fischer.

Estudios experimentales y computacionales previos sobre la dimerización de complejos metal-carbeno de tipo Fischer catalizada por reactivos de paladio

(Esquema 9) confirmaron que el ligando unido al catalizador influye sobre la relación de isómeros *E/Z* del producto de reacción.[54]

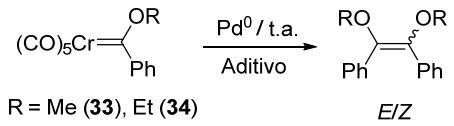

Esquema 9. Dimerización catalizada por paladio de los complejos **33** y **34**.

Con el objeto de controlar dicha relación *E/Z* y lograr procesos estereoselectivos se estudió el efecto de distintos aditivos sobre la relación de isómeros en los complejos metal-carbeno de tipo Fischer **33** y **34**.[97]

Así, en ausencia de aditivos se obtiene una relación de isómeros prácticamente equivalente para ambos complejos (relación *E/Z* 1/1.2 y 1.2/1 para los complejos **33** y **34**, respectivamente). De entre todos los aditivos ensayados (desde fosfinas mono- y bidentadas, fosfitos, arsina, bismutina, hasta carbenos *N*-heterocíclicos) para ambos complejos, únicamente la adición de fosfinas voluminosas (P^tBu_3) provocó un considerable aumento de la proporción del isómero *E* (hasta una relación *E/Z* 9.4/1 para el complejo **34**). Por otro lado, un ligero aumento en la proporción del isómero *Z* se consiguió mediante la aidición de PPh_3 (*E/Z* 1/4.4 para el complejo **33**).

Basándonos en estos resultados, decidimos evaluar el efecto de los ligandos unidos directamente al catalizador sobre la relación de isómeros. De esta manera, el complejo $Pd(P^tBu_3)_2$ aumentó significativamente la relación *E/Z* del proceso (hasta 15.7/1 para el complejo **34**) mientras que catalizadores con ligandos menos voluminosos como $Pd(PPh_3)_4$ provocaron una clara disminución (relación *E/Z* de 1/2.6).

Es importante destacar que la máxima relación *E/Z* para la especie $Pd(P^tBu_3)_2$ se obtuvo con cargas de catalizador del 5% mol. Tanto cargas superiores como cargas inferiores provocaron drásticas reducciones de dicha relación de isómeros.

[97] Chu, G. M.; Fernández, I.; Sierra, M. A. *J. Org. Chem.* **2013**, *78*, 865.

Estos resultados apuntan al uso de un complejo etoxicarbeno de tipo Fischer y un 5% del catalizador $Pd(P^tBu_3)_2$ como combinación óptima para aumentar la selectividad *E* en las reacciones de dimerización. Para confirmar esta hipótesis, dichas condiciones se emplearon en la dimerización de distintos complejos metal-carbeno (Esquema 10). En todos los casos, se observa un notable incremento en la producción del isómero *E*.

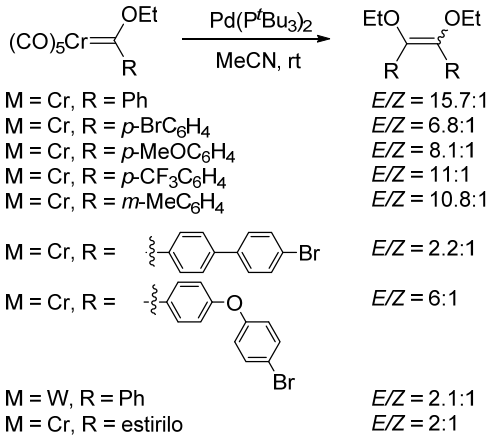

Esquema 10. Dimerización catalítica de diversos complejos metal-carbeno de tipo Fischer.

Por lo tanto, podemos concluir que la selectividad de la reacción de dimerización catalítica de complejos metal-carbeno de tipo Fischer se puede controlar eficazmente (hacia la producción del isómero *E*) mediante el uso del catalizador voluminoso $Pd(P^tBu_3)_2$ o a la adición de P^tBu_3 como aditivo. Este resultado podría ser de utilidad en la síntesis de polienos conjugados con potenciales aplicaciones en el campo de los materiales orgánicos.

IX. *CONCLUSIONES*

En el presente trabajo, hemos diseñado y sintetizado nuevos sistemas *push-pull* basados en metales de transición con propiedades fotofísicas modulables. Así, se ha llevado a cabo la síntesis de nuevos sistemas de tipo A-π-D-π-A cuyos grupos electroaceptores son complejos metal-carbeno de tipo Fischer. Estos complejos bis-carbeno presentan una comunicación-π amplificada que depende de la alta planaridad del sistema y del efecto cooperativo entre los dos fragmentos metal-pentacarbonilo. La amplificación de la conjugación-π se refleja en un desplazamiento batocrómico de la banda MLCT de más de 100 nm con respecto a los análogos D-π-A.

Asimismo, se han sintetizado por primera vez complejos organometálicos *push-pull* metal-BODIPY, de cromo y wolframio. Estos complejos presentan una extraordinaria conjugación-π extendida análoga a los sistemas A-π-D-π-A, descritos anteriormente. La modificación del heteroátomo (O, S, y N) unido directamente al carbono carbénico de los complejos de Fischer altera la conjugación-π existente entre la díada y, por tanto, sus propiedades fotofísicas. La desactivación de la emisión del fluoróforo se puede atribuir a un mecanismo Dexter.

Por otro lado, se han estudiado otras díadas metal-BODIPY basados en complejos metal-carbeno de tipo Fischer con conjugación-π remota. Estas díadas presentan propiedades fotofísicas modulables en función del sustituyente unido al carbeno α,β-insaturado. Así, grupos π-dadores provocan un aumento en la emisión del BODIPY mientras que grupos π-aceptores desactivan la fluorescencia. La disminución de la emisión se atribuye también a una interacción Dexter.

Además, se han caracterizado complejos metal-BODIPY de rodio e iridio sintetizados mediante reacciones de activación C-H/ciclometalación. En este caso la desactivación de la fluorescencia en estas díadas se produce principalmente como consecuencia de un mecanismo PET. Se ha demostrado que las propiedades emisivas dependen de la naturaleza del metal y de la distancia entre el fluoróforo y el fragmento metálico.

Además, en todos los casos anteriores se ha realizado un extenso estudio computacional sobre la estructura electrónica de los distintos complejos que ha permitido asignar adecuadamente las transiciones electrónicas asociadas a las bandas de absorción observadas experimentalmente. Dichos cálculos teóricos han contribuido enormemente a la hora de evaluar los distintos mecanismos de desactivación de la fluorescencia.

Por último, se han optimizado las condiciones de reacción de la dimerización catalizada por paladio de complejos metal-carbeno de tipo Fischer para obtener la mejor relación *E/Z*. La especie $Pd(P^tBu_3)_2$ (5% mol) se ha identificado como el catalizador óptimo para obtener mayoritariamente el isómero *E* en este tipo de reacciones.

X. *RESUMEN EN INGLÉS*

Synthesis, structure and electronic properties of new push-pull systems based on transition metal complexes.

The present work is aimed at designing novel organometallic push-pull species. To this end, different transition metal complexes, mainly based on Fischer type carbene complexes, have been synthesized and fully characterized. Their associated photophysical properties have been analysed in detail by means of experimental and computational tools.

In this regard, A-π-D-π-A push-pull systems (where A = Fischer carbene complex) with enhanced π-conjugation have been prepared (Chapter 1).[1] In addition, Fischer carbene complexes have been attached to the BODIPY core (Chapter 2)[2] or to its periphery (Chapter 3)[3] to modulate the photophysical properties of the fluorophore. Novel transition metal-BODIPY complexes having tunable emissive properties were prepared through *N*-directed C-H activation/cyclometallation reaction (Chapter 4).[4] Finally, a systematic investigation of the influence of the bulkiness of the ligands on the Pd-catalyzed self-dimerization reaction of alkoxychromium(0) (Fischer) carbene complexes has been carried out (Chapter 5).[5]

Chapter 1.

Chapter 1 describes the preparation of novel π-extended alkoxy Fischer bis(carbene) complexes A-π-D-π-A by the reaction of the corresponding dialdehydes with alkoxychromium(0) and alkoxytungsten(0) carbene complexes following the standard conditions reported by Aumann (Scheme 1).[6]

[1] Chu, G. M.; Fernández, I.; Sierra, M. A *Chem. Eur. J.* **2013**, *19*, 5899.
[2] Chu, G. M.; Guerrero-Martínez, A.; Fernández, I.; Sierra, M. A. *Chem. Eur. J.* **2014**, *20*, 1367.
[3] Chu, G. M.; Guerrero-Martínez, A.; Ramírez de Arellano, C.; Fernández, I.; Sierra. M. A. Submitted to: *Inorg. Chem.*
[4] Chu, G. M.; Fernández, I.; Guerrero-Martínez, A.; Ramírez de Arellano, C.; Sierra. M. A. Just accepted: *Eur. J. Inorg. Chem.*
[5] Chu, G. M.; Fernández, I.; Sierra, M. A. *J. Org. Chem.* **2013**, *78*, 865.
[6] Aumann, R.; Heinen, H. *Chem. Ber.* **1987**, *120*, 537.

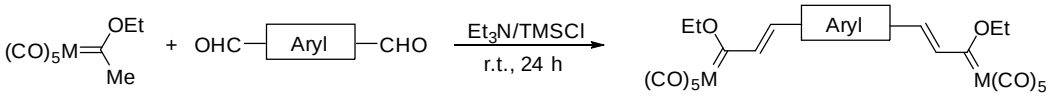

Scheme 1.

The UV/Vis spectra of these species display two main absorptions at approximately 350 and 550 nm attributable to ligand-field (LF) and metal-to-ligand charge transfer (MLCT) transitions, respectively. According to TD-DFT quantum chemical calculations at the B3LYP/def2-SVP level, these absorptions are ascribed to the HOMO-6 → LUMO (LF) and the HOMO → LUMO (MLCT) vertical transitions and possess a remarkable π-π* character. The planarity of the system and the cooperative effect of both pentacarbonyl metal moieties greatly enhance the conjugation between the tether and the metal carbene fragment, which is reflected in dramatic changes in the LF and MLCT absorptions. This behavior is markedly different to that observed for the monocarbene counterparts (Figure 1),[7] whose MLCT band remains unaltered regardless the nature of the substituent attached to the aryl fragment.

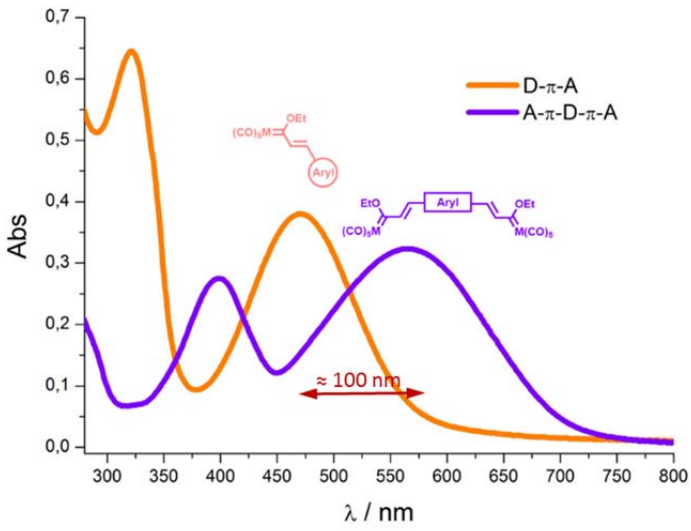

Figure 1.

This study shows that the MLCT absorption maxima can be efficiently tuned by means of subtle modifications of the electronic nature of the central aryl fragment connecting both metal moieties in the novel A-π-D-π-A systems. As a consequence of

[7] Lage, M. L.; Fernández, I.; Mancheño, M. J.; Sierra, M. A. *Inorg. Chem*. **2008**, *47*, 5253.

the extended π-conjugation, a strong correlation between the equilibrium geometries of these bis(carbene) complexes and their optical properties is observed. The experimental electrochemical data (the first oxidation potential, 1st E_{pa}) also correlates with the computed HOMO energies of the different complexes. The ability of tuning up the electronic properties of the compounds studied herein may be of future use in material chemistry.

Chapter 2.

The synthesis, structure, and photophysical properties of novel BODIPY–Fischer alkoxy-, thio- and aminocarbene dyads are described in the second chapter. Alkoxy- and thio-BODIPY–Fischer carbene complexes were prepared according to the reaction conditions reported by Aumann,[6] whereas aminocarbenes dyads were prepared from alkoxycarbene complexes by an aminolysis reaction at -100°C (Scheme 2).

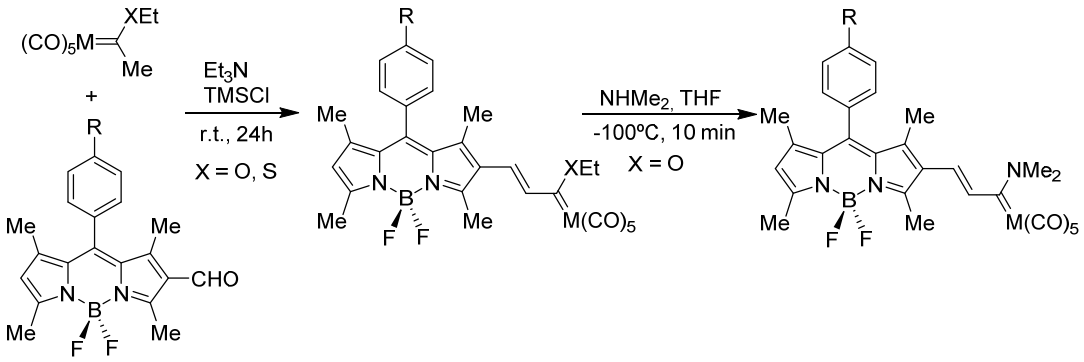

Scheme 2.

In these species, the BODIPY chromophore is directly attached to the carbene ligand by an ethylene spacer. The extension of the π-conjugation in these push-pull D-π-A systems is decisive in altering their equilibrium geometries, and consequently, modifies the corresponding photophysical properties of the BODIPY chromophore. Thus, when an alkoxycarbene complex is present in the BODIPY–metal carbene dyad, the π-conjugation is maximized. This is reflected in a significant bathochromic shift of the corresponding MLCT band, which is the result of the π-donor behavior of the BODIPY moiety.

In contrast, π-conjugation is strongly diminished when an aminocarbene complex is present in the dyad. As a consequence, the BODIPY moiety is mainly isolated in these compounds which exhibit a similar fluorescence than that observed for the parent formyl-BODIPY derivatives. In contrast, as the electronic structure of the BODIPY fragment is strongly altered by π-conjugation with the alkoxycarbene moiety, these complexes exhibit a complete suppression of the fluorescence associated with the BODIPY chromophore (Figure 2).

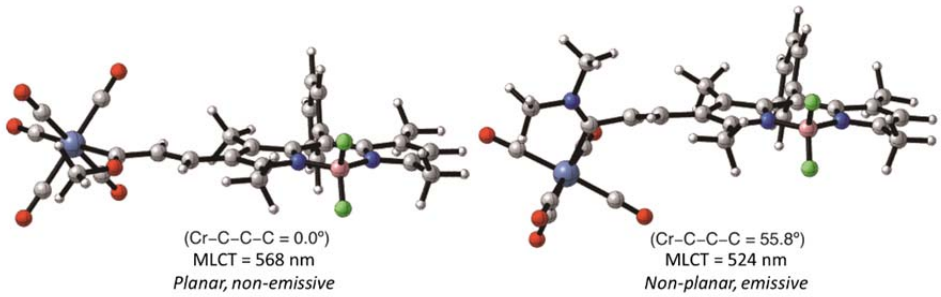

Figure 2.

An intermediate situation is found in BODIPY–thiocarbene complex dyads owing to the lower electronegativity (compared to oxygen) and π-donor ability (compared to nitrogen) of the sulfur atom, which confirms the importance of π-conjugation in controlling the properties of the BODIPY units. From our joint experimental–computational study, it becomes obvious that the photophysical properties of the BODIPY chromophore can be modified, in principle at will, by means of direct π-conjugation with Fischer carbene complexes. It is expected that the present study will be of future use in materials chemistry owing to the ease of tuning the photophysical properties of BODIPY units by subtle modifications on the metal-carbene moiety.

Chapter 3.

In this chapter, the synthesis, structure and complete characterization of novel mono- and bimetallic dyads joining Fischer carbene complexes and BODIPY chromophores are described. These complexes attached to a BODIPY moiety through a

p-aminophenyl group linked at the C8 carbon atom of the BODIPY core were prepared according to Scheme 3.

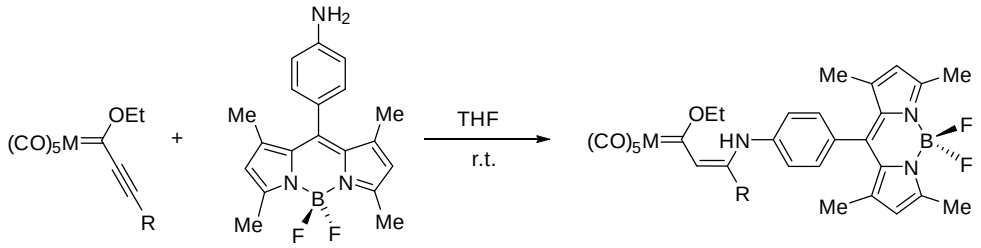

Scheme 3.

It is found that the metal fragment does not alter significantly the absorption properties of the BODIPY. In all cases, the UV-Vis spectra of the novel organometallic dyads are characterized by three main absorptions in the range of 350-550 nm, where the more intense band (located at $\lambda_{max} \approx 500$ nm) can be assigned to the typical π-π^* transition involving the BODIPY fragment. Despite that, the fluorescence emission properties of the BODIPY moiety is dramatically reduced by the corresponding pentacarbonyl-metal fragment. This is very likely the result of a Dexter-type energy transfer mechanism, as inferred by the noticeable influence on the emission intensity of substituents placed at the 4-position of the aryl group attached to the β-carbon atom of the carbene complexes (Figure 3).

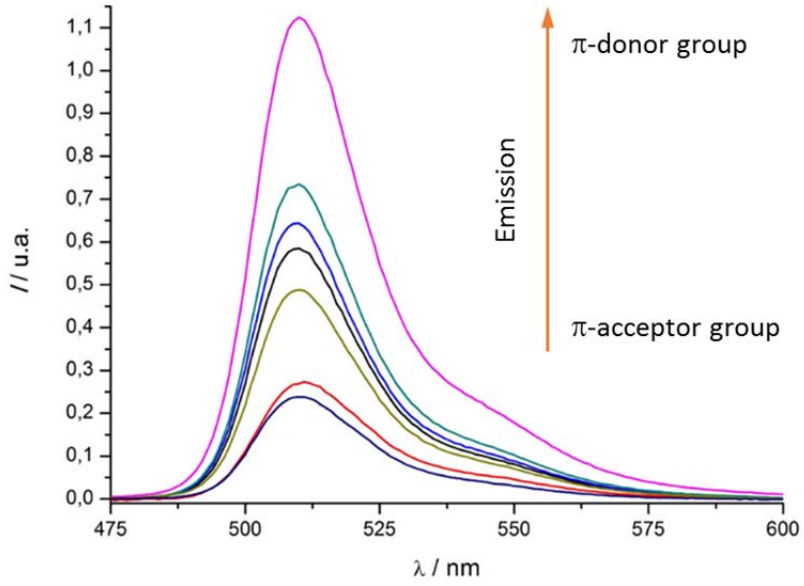

Figure 3.

Further support to this finding is provided by DFT-calculations and by the good linear relationships observed when plotting the emission intensity versus the Hammett-parameters and ^{13}C-NMR chemical shifts of the carbene carbon atom. Therefore, it can be concluded that the emissive properties of the BODIPY core can be controlled by means of π-conjugation even by remote substituents placed at the C8 position.

Chapter 4.

An efficient synthetic methodology based on *N*-directed C–H bond activation/cyclometallation reaction, which allows the efficient access to novel BODIPY dyads containing irida- and rhodacycles in their structures, has been developed (Scheme 4).

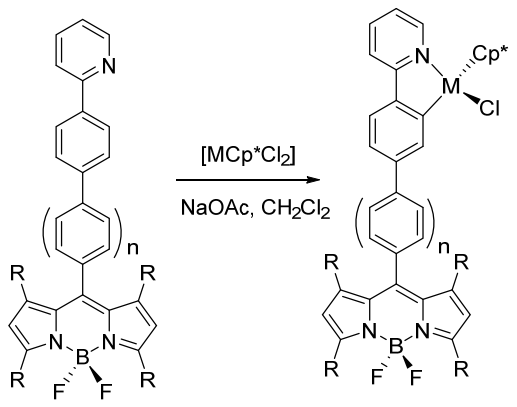

Scheme 4.

This simple synthetic procedure makes it possible to produce organometallic BODIPYs differing in the nature of the transition metal fragment, the distance between the fluorophore and the transition metal, as well as the substitution of the pyrrole framework. It is found that the organometallic moiety has little influence on the extinction coefficient and the position of the wavelength of the BODIPY absorption maxima. On the contrary, the distance between the metal and the BODIPY influences the emissive properties of irida- and rhoda-BODIPYs. Thus, dyads having the metal-center and the BODIPY separated by a phenyl ring are non-emissive, while a noticeable emission is observed when the metal and the BODIPY are separated by two phenyl groups (Figure 4).

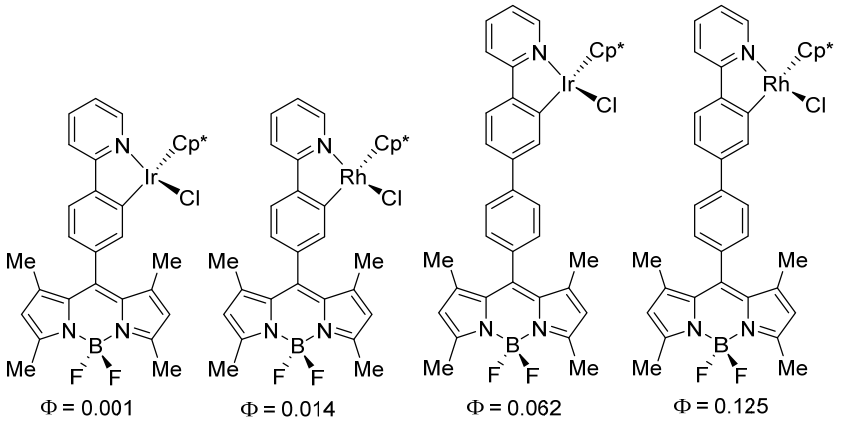

Figure 4.

As the overlap between the emission of the donor fragment and the absorption of the acceptor moiety is almost negligible, energy-transfer by Förster or Dexter mechanisms can be ruled out as responsible for the observed fluorescence quenching. According to DFT calculations, the observed complete suppression of the intense BODIPY fluorescence can be attributed to an acceptor-excited PET-quenching mechanism as a result of the donation of electron density from the transition metal fragment to the photoexcited acceptor BODIPY moiety. The efficiency of the PET depends on both the distance between the chromophores in the dyad and the nature of the transition metal fragment, which opens doors to the preparation of new BODIPY derivatives having tailored photophysical properties.

Chapter 5.

Lastly, a systematic investigation of the factors (i.e., additives, catalyst) controlling the Pd-catalyzed self-dimerization reaction of alkoxychromium(0) (Fischer) carbene complexes was carried out (Scheme 5).

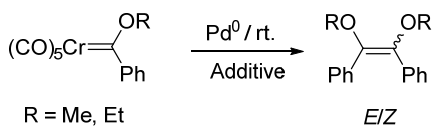

Scheme 5.

The use of $Pd(P^tBu_3)_2$ and chromium(0) ethoxycarbene complexes is identified as the optimal combination to obtain good to excellent *E* selectivities (Scheme 6).

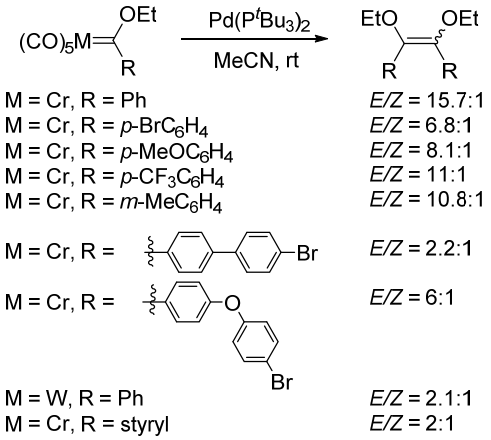

Scheme 6.

This catalyst might allow the control of the geometry in the synthesis of polyconjugated olefins, one of the main emerging applications of these catalytic reactions.

XI. *ANEXO*

CHEMISTRY
A EUROPEAN JOURNAL

FULL PAPER

DOI: 10.1002/chem.201204512

Synthesis, Structure, and Electronic Properties of Extended π-Conjugated Group 6 Fischer Alkoxy–Bis(carbene) Complexes

Gong M. Chu, Israel Fernández,* and Miguel A. Sierra*[a]

Abstract: The synthesis, structure and electronic properties of novel Group 6 Fischer alkoxy–bis(carbene) complexes are reported. The UV/Vis spectra of these species display two main absorptions at approximately 350 and 550 nm attributable to a ligand-field (LF) and metal-to-ligand charge-transfer (MLCT) transitions, respectively. The planarity of the system and the cooperative effect of both pentacarbonyl metal moieties greatly enhance the conjugation between the group at the end of the spacer and the metal carbene fragment provoking dramatic changes in the LF and MLCT absorptions. This is in contrast to related push–pull Fischer monocarbenes, where the position of the MLCT band remains mostly unaltered regardless the substituent attached to the donor fragment. In addition, the MLCT maxima can be tuned with subtle modifications of the electronic nature of the central aryl fragment in the novel A–π-D–π-A (A = acceptor, D = donor) systems. DFT and time-dependent (TD) DFT quantum chemical calculations at the B3LYP/def2-SVP level have also been performed to determine the minimum-energy molecular structure of this family of compounds and to analyse the nature of the vertical one-electron excitations associated to the observed UV/Vis absorptions as well as to rationalise their electrochemical behaviour. The ability of tuning up the electronic properties of the compounds studied herein may be of future use in material chemistry.

Keywords: carbenes · conjugation · DFT calculations · electrochemistry · UV/Vis spectroscopy

Introduction

Fischer carbene complexes are attractive synthetic intermediates that are able to carry out a wide variety of organic transformations under mild reaction conditions.[1] Representative examples of the rich and versatile chemistry of this family of organometallic complexes are the useful Dötz benzannulation reaction,[2] which produces substituted phenols by reaction of the carbene with alkynes and carbon monoxide, different cycloaddition reactions,[3] the catalytic transmetalation to late transition metals,[4] which enhances the reactivity of the carbene complexes and the photochemical transformations[1h,5] (mainly the photocarbonylation reaction[6] but also photo-dyotropic rearrangements[7]).

Although these species have been mainly applied to organic and organometallic synthesis, nowadays their applications have been extended to other fields like bioorganometallics,[8] sugar-derived metal--carbene gelators,[9] and materials chemistry.[10] In the latter field, the well-known electron-withdrawing ability of the pentacarbonyl(metal) carbene moiety, which behaves similar to a Lewis acid complexed carbonyl function,[11] has been used in new push–pull molecules with interesting non-linear optical (NLO) properties. The good NLO behaviour of these complexes has been attributed to the polarisation of the π-electron system of the spacer connecting the carbene complex and the donor fragment produced by the strong electron-accepting character of the $(CO)_5M{=}C$ group.[10b]

On the other hand, we have studied the electronic structure of α,β-unsaturated Fischer carbenes **1**, where the $(CO)_5Cr{=}C$ group is connected to aryl groups, which have different substituents, through the simplest π-spacer moiety (i.e., HC=CH, Scheme 1).[12] It was found that π-donor groups lead to significant red shifts of the ligand-field (LF) band whereas π-acceptor groups provoke the opposite effect (λ_{max} ranging from 307 to 360 nm). However, this effect is not observed in the corresponding metal–ligand charge-transfer (MLCT) band, whose absorption maximum remains practically constant (λ_{max} ranging from 468 to 484 nm) and, therefore, it does not depend on the electronic nature of the substituent. Moreover, the corresponding Cr–C bond lengths remain nearly constant as well, indicating that π conjugation between the metal fragment and the

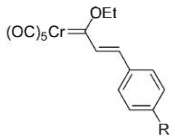

1: R = H, Me, OMe, Cl, CN
furyl, styryl, Fc

Scheme 1. α,β-Unsaturated Fischer carbenes studied previously (see Ref. [12]).

[a] G. M. Chu, Dr. I. Fernández, Prof. Dr. M. A. Sierra
Departamento de Química Orgánica
Facultad de Química, Universidad Complutense
28040 Madrid (Spain)
Fax: (+34) 913944310
E-mail: israel@quim.ucm.es
sierraor@quim.ucm.es

Supporting information for this article (containing copies of the ^1H NMR and ^{13}C NMR spectra of the new species prepared, Figure 1S as well as Cartesian coordinates and total energies of all computed stationary points) is available on the WWW under http://dx.doi.org/10.1002/chem.201204512.

ChemPubSoc Europe

DOI: 10.1002/chem.201303952

CHEMISTRY A European Journal Full Paper

BODIPY Chromophores

Tuning the Photophysical Properties of BODIPY Molecules by π-Conjugation with Fischer Carbene Complexes**

Gong Ming Chu,[a] Andrés Guerrero-Martínez,[b] Israel Fernández,*[a] and Miguel Ángel Sierra*[a]

Abstract: The synthesis, structure, and photophysical properties of novel BODIPY–Fischer alkoxy-, thio-, and aminocarbene dyads are reported. The BODIPY chromophore is directly attached to the carbene ligand by an ethylenic spacer, thus forming donor–bridge–acceptor π-extended systems. The extension of the π-conjugation is decisive in the equilibrium geometries of the dyads and is clearly reflected in the corresponding absorption and emission spectra. Whereas the BODIPY fragment is mainly isolated in aminocarbene complexes, it is fully conjugated in alkoxycarbene derivatives. The former thus exhibit the characteristic photophysical properties of BODIPY units, whereas complete suppression of the BODIPY fluorescence emission is observed in the latter, as a direct consequence of the strong electron-accepting character of the $(CO)_5M{=}C$ moiety. As the π-acceptor character of the metal–carbene group can be modified, the electronic properties of the conjugated BODIPY can be tuned. Density functional calculations have been carried out to gain insight into the photophysical properties.

Introduction

Since the synthesis of the first 4,4-difluoro-4-borata-3a-azonia-4a-aza-*s*-indacene in 1968 by Treibs and Kreuzer,[1] boradiazaindacenes (BODIPYs) have become highly useful molecular entities in fields such as materials science or medicinal chemistry.[2] This is mainly due to the fascinating optical properties associated with this family of compounds. Thus, their excellent thermal and photochemical stabilities, high fluorescence quantum yields, negligible triplet-state formation, and intense absorption profiles have transformed BODIPY species into quite attractive materials with applications in, for instance, biomolecules labeling, ion sensing and signaling, energy transfer cassettes, or light harvesting systems.[2] For these reasons, it is not surprising that numerous synthetic methods have been developed to produce new BODIPY derivatives with interesting and tunable photophysical properties.[2,3] In this sense, the attachment of BODIPY units to a transition-metal center to prepare a dyad is highly attractive. The great number of possible modifications (that is, variation of the transition metal and/or its coordination sphere) that can be effected in these systems may, in principle, allow the properties of the BODIPY–transition-metal dyad to be tuned. However, in most of the reported dyads the metal centers were attached onto the peripheral moieties of the BODIPY fragment[4–6] rather than to its π-conjugated core.[7,8] As a result, the impact of the transition-metal fragment on the properties associated with the BODIPY chromophore is not that remarkable.

At this point, we turned our attraction to Group 6 Fischer carbene complexes because of their exceptional properties as electron-withdrawing groups.[9] The π-acceptor ability of these species has resulted not only in their wide use in organic synthesis (that is, Fischer carbene complexes behaving similarly to a Lewis acid complexed carbonyl function),[10] but also in their emerging role as building blocks in the field of new materials.[11]

As the modification of the electronic properties of the carbene ligand has proved to be relatively easy,[9] we hypothesized that the direct attachment by π-conjugation of a Group 6 Fischer carbene complex to the π-core of BODIPY could have a significant impact on the photophysical properties of the BODIPY moiety. Herein we report the successful accomplishment of such hypothesis, which allows the preparation of new organometallic compound–BODIPY dyads possessing tunable photophysical properties.

[a] G. M. Chu, Dr. I. Fernández, Prof. Dr. M. Á. Sierra
Departamento de Química Orgánica
Facultad de Quimica, Universidad Complutense de Madrid
28040 Madrid (Spain)
Fax: (+34) 913944310
E-mail: israel@quim.ucm.es
sierraor@quim.ucm.es

[b] Dr. A. Guerrero-Martínez
Departamento de Química Física I
Facultad de Ciencias Químicas, Universidad Complutense de Madrid
28040 Madrid (Spain)

[**] BODIPY=boradiazaindacene

Supporting information for this article (including NMR spectra of isolated compounds, excitation spectra, Cartesian coordinates, and total energies of all of the stationary points discussed in the text) is available on the WWW under http://dx.doi.org/10.1002/chem.201303952.

FULL PAPER WILEY-VCH

Fluorescence Quenching in BODIPYs Having Ir- and Rh-Tethered Complexes

Gong M. Chu,[a,d] Israel Fernández,*[a,d] Andrés Guerrero-Martínez,[b] Carmen Ramírez de Arellano,[c,d] and Miguel A. Sierra*[a,d]

Dedicated to Prof. José Gimeno on the occasion of his retirement.

Abstract: The effect of Rh- and Ir-centers on the optical properties of the BODIPY core is studied. To this end, novel metal complexes-tethered to BODIPY have been prepared through an easy and versatile procedure using *N*-directed C–H activation reactions. The organometallic moiety has a tremendous influence on the emissive properties of the BODIPY fragment. A Photoinduced Electron Transfer (PET) mechanism is suggested as the main mechanism responsible for the suppression of the BODIPY fluorescence emission in the newly formed dyads. The efficiency of the PET depends on both the distance between the chromophores in the dyad and the nature of the transition metal (Rh vs Ir).

Introduction

The 4,4-difluoro-4-bora-3a,4a-diaza-*s*-indacene (BODIPY)[1] core is arguably one of the most versatile organic luminophore having useful applications in different fields ranging from sensors to medicinal chemistry. The chemistry of BODIPY derivatives and their applications have been profusely reviewed.[2] The importance of BODIPYs is due to their photophysical properties that include intense visible absorption, relatively sharp fluorescence combined with high quantum yield and good thermal and photochemical stabilities (including reasonable stability to physiological conditions). As a consequence, a significant number of synthetic methodologies have been developed allowing the access to BODIPY derivatives with tunable properties.[2c]

One additional feature of the BODIPY motif is its susceptibility to experience drastic changes in its emission properties derived from subtle changes in its structure. Therefore, attaching a transition metal complex to a BODIPY core is particularly attractive, in terms of manipulation of the photophysical properties of this system. In fact, the properties of transition metal complex–BODIPY dyads can be drastically changed by modifying either the nature of the transition metal or the surrounding ligands. Obviously, the distance between the metal center and the BODIPY is an additional variable to play with. Therefore, it is not strange that several metal–BODIPY systems have been prepared,[3] spanning from discrete organometallic structures to complex metal-organic frameworks (MOFs). Nevertheless, the versatile and efficient C–H activation/cyclometallation[4] sequence has not been reported to prepare transition metal complex–BODIPY dyads so far.

Work from our laboratories has shown that the attachment of a group 6 metal (Fischer) carbene complex to the pyrrole unit of the BODIPY core is able to modulate the emission of the fluorophore by controlling the planarity and π-conjugation of the system.[3b] Thus, whereas alkoxy-carbene complexes **1** containing a planar dyad are non-emissive, non-planar complexes **2** are emissive. Interestingly, the related thio-carbene complexes **3** show an intermediate emission behavior, in concordance with the intermediate angle between the BODIPY and the metal-carbene center compared to **1** and **2** (Figure 1).

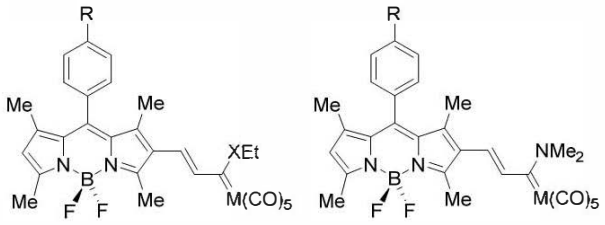

1 M = Cr, W; X = O
3 M = Cr; X = S

2 M = Cr, W

Figure 1. BODIPY-metal (Fischer) carbene complexes previously studied.

Following these results we devised the possibility of tethering a metal center to the BODIPY core by using a preformed all-organic fluorophore and placing the metal moiety using a C–H activation/cyclometallation sequence in an adequate tether.[5] In this way, by modifying the distance between the two components of the dyad, the influence of the transition metal fragment on the emission properties of the dyad will be studied. Different to the usual work in which the proximity of the metal to the BODIPY is used to quench the fluorescence of the emissive system (probe-off state),[3h] in this approach the existence of fluorescence will be used as a probe for studying the effect of the metal on the luminescence of the boron fluorophore.

[a] G. M. Chu, Dr. I. Fernández, Prof. M. A. Sierra
Dpto, de Química Orgánica I
Facultad de Química
Universidad Complutense, 28040-Madrid (Spain)
E-mail: (IF) Israel@ucm.es
(MAS) sierraor@ucm.es
[b] Dr. A. Guerrero-Martínez
Dpto, de Química Física I
Facultad de Química
Universidad Complutense, 28040-Madrid (Spain)
[c] Prof. C. Ramírez de Arellano
Dpto. de Química Orgánica,
Universidad de Valencia, E-46100,
Valencia (Spain).
[d] Centro de Innovación en Química Avanzada (ORFEO-CINQA)

Supporting information for this article is given via a link at the end of the document.

JOC The Journal of Organic Chemistry

Article

pubs.acs.org/joc

Control over the *E*/*Z* Selectivity of the Catalytic Dimerization of Group 6 (Fischer) Metal Carbene Complexes

Gong M. Chu, Israel Fernández,* and Miguel A. Sierra*

Departamento de Química Orgánica, Facultad de Ciencias Químicas, Universidad Complutense, 28040 Madrid, Spain

Supporting Information

ABSTRACT: The systematic investigation of the effect of different catalysts and additives in the reaction of self-dimerization of alkoxychromium(0) (Fischer) carbene complexes resulted in the selection of $Pd(P^tBu_3)_2$ to effect this transformation with good to excellent *E* selectivities and acceptable to excellent chemical yields. This catalyst will allow the control of the geometry in the synthesis of polyconjugated olefins, one emerging application of these catalytic reactions.

INTRODUCTION

Transmetalation processes from group 6 Fischer metal carbene complexes to late transition metals (Pd, Pt, Cu, Ni, Rh, Au, etc.) lead to new carbene complexes, exhibiting exceedingly different chemical behavior with respect to the starting metal complex.[1] Thus, the new carbene complexes may show an enhanced reactivity compared to the precursor complex[2] or they may undergo different reaction pathways, opening doors to the synthesis of new classes of compounds (Scheme 1). This

Scheme 1. Effect of Transmetalation in the Reactivity of Group 6 Metal Carbene Complexes

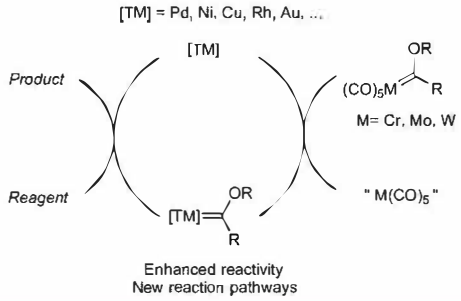

fascinating process has been profusely exploited since our original report on the self-dimerization of chromium(0) and tungsten(0) carbene complexes promoted by Pd catalysts.[3]

The reaction mechanism for this transformation, which has been proposed on the basis of experimental and theoretical studies,[3,4] is summarized in Scheme 2. Accordingly, a transmetalation reaction of the carbene ligand from complex **1** to the palladium(0) catalyst leads to a new Pd−carbene complex such as **3**, through a heterobimetallic intermediate **2** that evolves to **3** by extrusion of the $[M(CO)_5]$ (M = Cr, W) fragment, mediated by coordination of the solvent. Subsequent transmetalation from a new molecule of the carbene complex **1** leads to the Pd(0) bis-carbene complex **4**, which produces a mixture of the *Z*/*E* olefins **5** with concomitant regeneration of the catalyst.

The key intermediates in this catalytic cycle are the mono-carbene complexes **3** and bis-carbene complexes **4**. Very recently,[5] Albéniz and Espinet isolated the first Pd alkoxycarbene **7** from the reaction of the W(0) Fischer carbene complex **6** and $[PdCl_2(NCMe)_2]$.[6] In addition, related Cu(I)[7]

Scheme 2. Catalytic Cycle for the Self-Dimerization of Group 6 Carbene (Fischer) Complexes in the Presence of Pd Catalysts

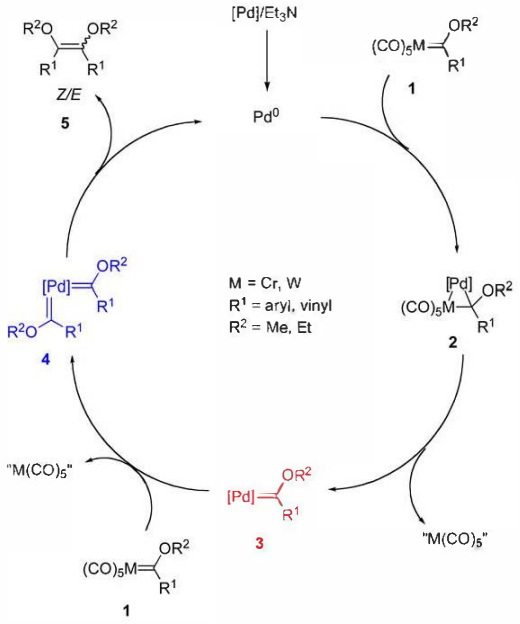

Received: September 27, 2012
Published: January 4, 2013